Multi-Mode Quasi-Static Loading and Interface Reduction to Model Joint Nonlinearity

by

Aabhas Singh

A dissertation submitted in partial fulfillment of the requirements for the degree of

DOCTOR OF PHILOSOPHY

(Engineering Mechanics)

at the

UNIVERSITY OF WISCONSIN - MADISON

2021

Date of Final Oral Examination: June 17, 2021

This dissertation is approved by the following members of the Final Oral Committee:

Matthew S. Allen	Professor	Engineering Mechanics
Ramathasan Thevamaran	Assistant Professor	Engineering Mechanics
Melih Eriten	Associate Professor	Mechanical Engineering
Michael Zinn	Associate Professor	Mechanical Engineering
Robert J. Kuether	Member Of Technical Staff	Sandia National Laboratories

ABSTRACT

Nearly all engineering structures are constructed from multiple parts joined by bolts, rivets or other fasteners. Although these joints facilitate construction, they introduce uncertainty into the stiffness and damping associated with the joint, and even nonlinearity. Research has shown that the presence of joints causes the effective natural frequency and damping of modes of vibration of a structure to vary with excitation amplitude. To realize this effect accurately, finite element models of these structures require high-fidelity modeling of the interface, resulting in computationally expensive simulations. To circumvent this issue, reduction techniques are used to create Reduced Order Models (ROMs) that capture the dynamics of the full model. The industry standard approach is to use multi-point constraints (MPC) and/or spring element(s) to reduce the number of degrees of freedom (DOF) that need to be joined at the contact interfaces (spiders). Scalability becomes an issue when multiple joints are present in a system, each requiring a specifically tuned model to capture the dynamics. Furthermore, experimental tests have shown that at large enough amplitudes, one mode influences the vibration of the other, i.e. the modes exhibit coupling due to the nonlinearity in the joints. Typically this has been neglected in structures, since simulating the response requires costly dynamic analyses. This dissertation presents three contributions to the joints community that address these challenges with reduced order modeling and modal coupling of jointed structures.

The first contribution presents two rich experimental data-sets that can be used to update numerical models. The first set provides nonlinear data on a new benchmark structure. This data is then used to tune various full and reduced order models such that these models exhibit the same characteristics as the structure. The experimental data collected in the second data-set presents a first study of modal coupling, indicating that some degree of modal coupling is present and observable.

The second contribution of this dissertation investigates uncertainty in the industry stan-

dard approach. Variations in the size of the contact area and the formulation for the MPC are compared against experimental data obtained from a new benchmark structure. This is contrasted against a novel approach that captures nonlinear effects of joints in a reduced space characterized by the deformation of the interface. This retains the flexibility of the interface by using joint models on non-physical deformation shapes, whereas spiders are done on physical coordinates. This novel method has shown to be effective and efficient at modeling multiple modes of a numerical structure.

The last contribution is a novel extension of Quasi-static Modal Analysis (QSMA) to numerically simulate modal coupling. Typical methods are done on a mode-by-mode basis, thus neglecting any interactions between modes. This novel approach explores an alternative where quasi-static forces are applied in the shapes of two or more modes of vibration simultaneously, and the resulting load-displacement curves are used to deduce the effect of other modes on the effective frequency and damping of the mode in question. The quasi-static approach produced reasonable albeit highly conservative bounds on the observed coupled dynamics of a 2D structure and gave insight into the coupling of a structure for which a dynamic analysis is infeasible.

ACKNOWLEDGEMENTS

The views expressed in the article do not necessarily represent the views of the U.S. Department of Energy or the United States Government. Sandia National Laboratories is a multimission laboratory managed and operated by National Technology & Engineering Solutions of Sandia, LLC, a wholly owned subsidiary of Honeywell International Inc., for the U.S. Department of Energy's National Nuclear Security Administration under contract DE-NA0003525. **SAND2021-7546T**

I would like to give a big thanks to my advisor, Prof. Matt Allen for his guidance and immeasurable patience as I learned my way through joint modeling. With his help, I have become a better researcher and more knowledgeable about how to do research while still having fun (Sheepshead).

I am also very thankful for Rob Kuether. Not only is he an exceptional mentor, he is someone who is just as excited for me when there is good news, and even more supportive when there is bad news. Both him and Prof. Matt Allen are people I would be honored to call friends.

I would also like to thank my family and friends for reminding me that I can enjoy weekends and life is more than research. From happy hours with research colleagues and kayaking with my favorite person to flying cross country for family celebrations, these people have made these college years something I will never forget.

Lastly, this dissertation is solely dedicated to my mother. Everything I am and have done is due to her support and love. No words can convey the gratitude I have for her and how much her being in this world has impacted me as a person. Thank you mom.

DISSERTATION

This dissertation consists of an extended summary (**Chapter I**) and the following appended papers (**Chapter II**):

Paper I A. Singh, M. Scapolan, Y. Saito, M. S. Allen, D. Roettgen, B. Pacini, and R. J. Kuether,"Experimental Characterization of a New Benchmark Structure for Prediction of Damping Nonlinearity," in Nonlinear Dynamics, Vol. 1, Conference Proceedings of the Society for Experimental Mechanics Series, (Orlando, FL), pp. 57–78, Springer International Publishing, 2019.

Paper II B. J. Moldenhauer, A. Singh, P. Thoenen, D. R. Roettgen, B. R. Pacini, R. J. Kuether, and M. S. Allen, "Influences of Modal Coupling on Experimentally Extracted Nonlinear Modal Models," in Nonlinear Structures and Systems, Vol. 1, Conference Proceedings of the Society for Experimental Mechanics Series, (Orlando, FL), pp. 189–204, Springer International Publishing, Jan. 2019.

Paper III A. Singh, M. S. Allen, and R. J. Kuether, "Spider Configurations for Models with Discrete Iwan Elements," *Mechanical Systems and Signal Processing*, (submitted, 2021).

Paper IV A. Singh, M. S. Allen, and R. J. Kuether, "Substructure Interface Reduction Techniques to Capture Nonlinearities in Bolted Structures," in Proceedings of the ASME 2020 International Design Engineering Technical Conferences & Computers and Information in Engineering Conference, IDETC/CIE 2020, (St. Louis, Missouri), Aug. 2020.

Paper V A. Singh, M. S. Allen, and R. J. Kuether, "Multi-mode Quasi-static Excitation for Systems with Nonlinear Joints," *Mechanical Systems and Signal Processing*, (in review, 2021).

The included papers were prepared in collaboration with co-authors. The author of this dissertation was responsible for most of the major progress of work for **Papers III, IV, and V**, i.e. conducting numerical simulations, and writing the papers. For **Papers I, and II**, the author contributed equally in the testing and documentation, and contributed the major progress for numerical analysis. **Papers I and II** emphasize experimental techniques, whereas the remainder emphasize numerical analysis.

TABLE OF CONTENTS

Chapter I

Executive Summary

1 INTRODUCTION AND MOTIVATION

Mechanical structures are subject to various types of loads during their lifetime including pressures, forces, and thermal loads among others. One method to gain insight into the effect of these loads is experimental testing. An example of this is the flight tests done for the F-16 [1] in 1983. Totaling 177.2 flight hours, these 118 maneuver tests resulted in upgrades to the flight control system that optimize aircraft handling during various missions. However, considering that an hour flight for the F-16 costs approximately $8,278 USD [2], the test of the control system cost an astonishing $1,466,862 USD. When evaluating other aspects of the aircraft, total costs for instrumented field testing can become insurmountable. To mitigate costs, finite element analysis (FEA) can be used to model the structure to predict the response due to various environments. To limit the physical testing required, FEA is essential for virtual testing and design. As with the F-16, these models can be used to provide insight into optimizing the design of these structures.

While FEA can produce highly accurate results for a single elastic part that behaves linearly, significant challenges arise when the structure is composed of multiple parts (i.e. an assembly) or behaves nonlinearly, often resulting in computationally expensive or infeasible simulations to obtain a meaningful response. Nonlinear behavior can be classified in various ways: constitutive material nonlinearity [3], geometric nonlinearity with large deformations [4, 5, 6], fluid-structure interactions [7, 8], or frictional contact nonlinearity [9, 10, 11] among others. In some cases, nonlinearities can be exploited for design improvements, e.g. nonlinear vibration absorbers [12, 13, 14]. In other cases, these nonlinearities could cause a harmless (although jarring) brake squeal [15] due to friction, up to system failures [16, 17]. While these

nonlinearites may occur in combination, this dissertation will focus on cases where friction at a bolted joint that connects two or more parts is the sole source of nonlinearity during vibrational loading; that is, this work assumes the material is linear elastic and does not have thin members undergoing large deformations.

Although bolted joints facilitate in the construction of engineering structures by joining smaller components in an assembly, they are also known to be a major source of energy dissipation and, hence, damping in the structure [18]. To avoid this effect, engineers over-design structures with conservative estimates such that the stiffness and damping of the joint are constant, i.e. a linear assumption. However, in aerospace structures, such conservative estimates are infeasible. Rather, engineers rely on the passive energy dissipation of bolted joints to reduce vibration amplitudes [19, 20]. Consider the GE F110 engine used in the F-16 as shown in Fig. 1. The efficiency of the engine is strongly tied to the very small gap between the turbine blades and the engine casing. During flight, the engine is subjected to large vibrations, which, if not mitigated, could cause erosion on the turbine blades due to the casing making contact with the blades. The numerous joints throughout the casing assist to dampen and reduce the vibration amplitude through energy dissipation such that the engine can be made more efficient.

Figure 1: GE F110 engine for the F-16 (image courtesy of Prof. Matt Allen)

In jointed structures, energy dissipation is typically caused when the contact interface between components slips as the structure is loaded, also leading to stiffness loss. Consequently, the dissipation and stiffness of a joint has been shown to change with excitation amplitude [18,21,22]. This phenomenon is shown on a numeric model of the S4 Beam structure in Fig. 2 where the contact interface is predominantly stuck (red) at load step 10, but begins to slip (green) as it is loaded such that there is a prominent region of slip at the extremities of contact by load step 50 [23].

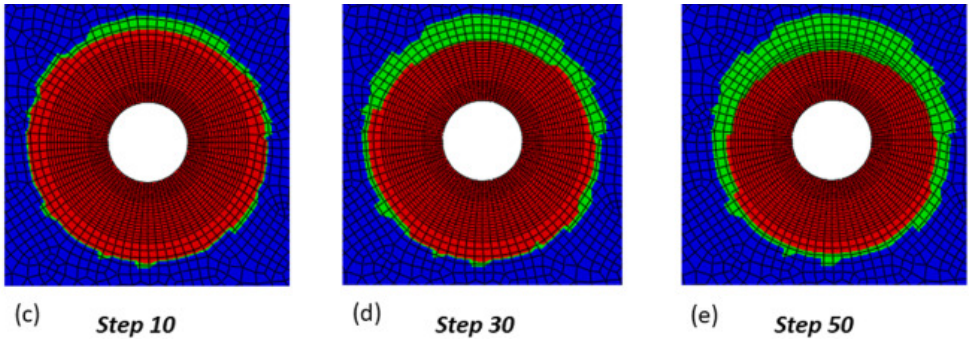

Figure 2: Contact interface at three increasing load steps of a 3D cantilever beam structure as shown in [23]

During experimental testing of the S4 Beam structure (Fig. 3a), Singh et al. observed that at higher vibration excitation amplitudes, the damping of the response tends to increase substantially, whereas the natural frequencies can be seen to decrease slightly [24]. This is shown in Fig. 3b, where the blue time response is a 100N excitation and the red time response is a 500N excitation at the same point. However, time responses are not an efficient method of showing the change in frequency and damping for each mode with respect to amplitude. A common practice is to treat the system as effectively linear for a segment of time to get the frequency and damping at that amplitude. Figure 4 shows the frequency and amplitude fit to the 100N data in Fig. 3, where each time/amplitude segment is treated linearly (flat) and joined to form the amplitude dependent frequency and damping curves.

Refer to the specifics of the methods in Section 1.3.1.

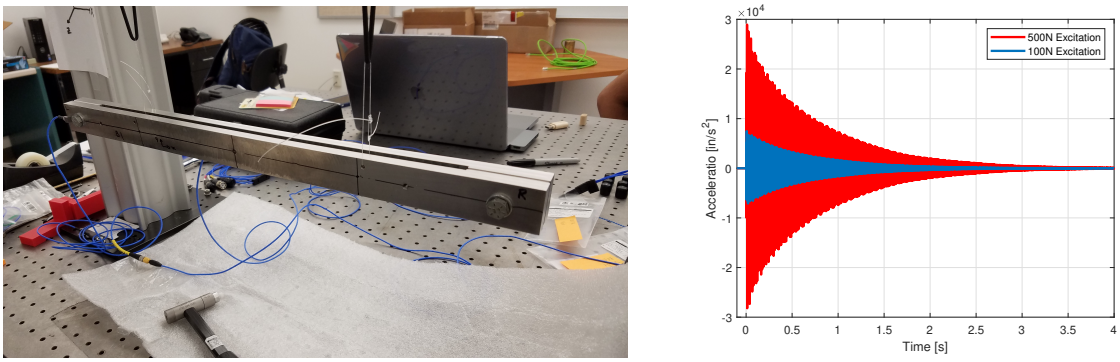

(a) **(b)**

Figure 3: (a) S4 Beam bolted structure, (b) Response of a low-level and high-level excitation

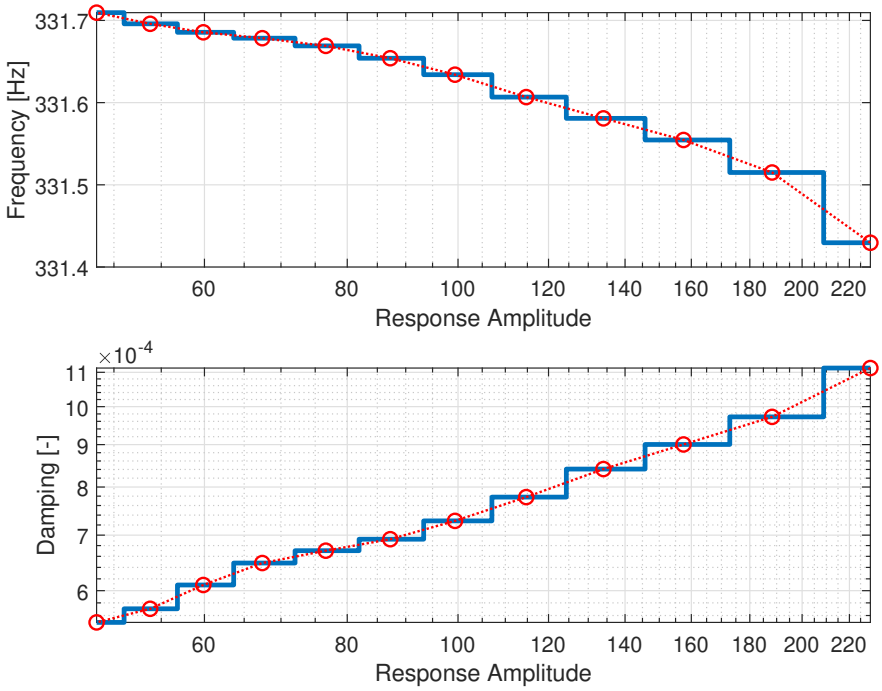

Figure 4: Change in frequency and damping with respect to amplitude

This nonlinearity can be described in one of two ways: microslip, and macroslip [25].

A joint is in the microslip regime when slip occurs at the extremities of the contact patch and the remainder of the patch remains stuck. In this regime the nonlinearity tends to be weak and the response is typically quasi-linear and yet significant energy can be dissipated causing the effective modal damping to increase significantly and the modal natural frequency to decrease with an increase in vibration amplitude as shown above in Fig. 4. [26, 27, 28]. In contrast, as the load on the structure is increased, macroslip may occur in which the joint loses in-plane stiffness and the entire interface slips, causing a change in geometry of the system. If the slip in the joints is large enough, complicated phenomena such as multi-harmonic responses, modal coupling and even quasi-periodic responses or chaos can occur. However, in most cases the joint is considered to have failed if macroslip is reached so this dissertation will focus on modeling joints in the microslip regime.

Considerable effort from the community has gone into understanding this behavior through experimentally characterizing benchmark structures with joints [24, 29, 30, 31, 32, 18, 33], numerical methods to model and simulate joint behavior [34, 35, 36, 37, 38, 39, 40], and nonlinear system identification of joint parameters [41, 42, 43]. These works reveal that there are three important challenges associated with numerically modeling this nonlinearity, specifically:
(1) simulating the nonlinear response efficiently and accurately
(2) developing a constitutive model to represent the local behavior of the joint
(3) modeling the interactions between modes of vibration (modal coupling).

The subsequent subsections briefly discuss the state of the art in each of these areas. Section 2 addresses the scope of the dissertation and provides a brief overview of the appended papers. Section 3 provides concluding remarks and suggestions for future work to further the progress presented in this dissertation.

1.1 Methods to Simulate the Vibration of Jointed Structures

The first challenge of modeling joint nonlinearity is to simulate it efficiently and accurately. A common method for modeling jointed structures is to neglect the nonlinear effects of the joints by approximating the structure interface connections as linear with fully stuck joints, such applied loads do not exceed stress limitations of the structure. These conservative approximations often lead to over-designed structures, where weight may become an issue. For example, this method is infeasible in the aerospace industry where minimizing the weight of the structure is crucial to reducing the cost of fuel. A study of commercial airliners found that for every 100 kg of mass added to the aircraft, about 2.5 kg more in jet fuel was consumed per hour in flight [44]. During flight, a structure experiences random loading that induces stress. If the structure is over-designed the effect of loading will be lower. Whereas for a structure with joints, there is inherent passive energy dissipation. Therefore if engineers can accurately estimate the structure's ability to dissipate energy, then they can design lighter air-crafts and reduce costs. Given the importance of joints, there are two modeling methods considered in this dissertation: full order modeling and reduced order modeling with whole-joint models.

The first option is to model the structure in detail. However, when incorporating joints into a model, significant mesh refinement is necessary at the contact interfaces to capture the localized slip [21,45,23] as shown in Fig. 5. As the number of joints increases, high-resolution modeling of these interfaces becomes computationally expensive or even infeasible. This was illustrated by Jewel et al. [23] who demonstrated that when the mesh was adequately refined and the solver (Abaqus) was tuned to accurately solve the contact mechanics problem, tens of hours were required to obtain accurate solutions for the static response of a structure with only two joints. Dynamic analysis of the same jointed structure could take days to weeks for a few cycles of loading, and thousands of cycles would be needed if one wished to model a time response similar to what might be recorded in an experiment. To mitigate the

computational costs of time integration, various alternative methods have been developed to produce accurate results when compared to a dynamic analysis.

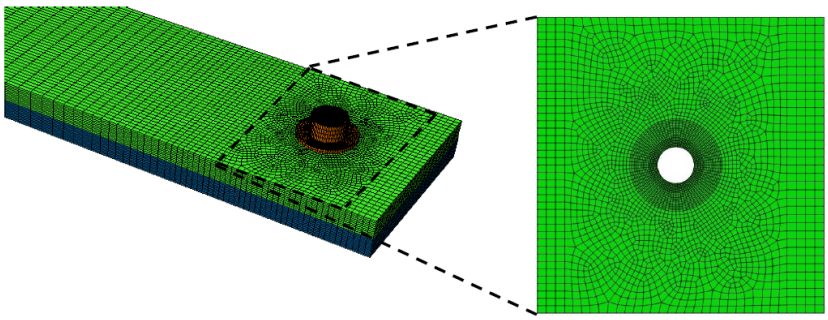

Figure 5: Mesh refinement near a bolt hole required to accurately model the energy dissipation of the joint. This structure was studied by Jewell et al. [46]. Figure is from Lacayo [47]

A few different classes of methods have been proposed that can extend the concept of a mode to nonlinear systems, and hence describe phenomena such as the amplitude dependent frequency and damping that are observed in structures with bolted joints. One of the most well known is the nonlinear normal mode (NNM) definition of Vakakis & Kerschen [48,49,50], which defines an NNM as a periodic response of a conservative nonlinear system. This has proven quite effective for understanding the dynamics of conservative nonlinear systems such as structures exhibiting geometric nonlinearity [51]. Krack extended this concept to damped systems by adding an artificial negative damping term to counter-act the actual damping in the system, calling the resulting method the extended periodic motion concept (EPMC) [52]. Using this method, one can extend existing methods for computing NNMs [50] to damped systems. Other methods such as numerical continuation, shooting methods, and manifold methods [53, 54, 55, 56] can also be applied to damped systems. Shooting methods typically integrate the equations of motion over one vibration cycle and iterate on the initial conditions until the steady-state response has been obtained [50]. In contrast, Harmonic Balance (HB) methods, which have been extended to address systems with frictional contact, [57, 58, 45], represent the response as a Fourier series and solve a nonlinear system of algebraic equations

to obtain the Fourier Coefficients at each frequency/amplitude.

1.1.1 Quasi-Static Modal Analysis

The methods used in this dissertation (**Papers III, IV, and V**) are derived from the averaging method [59], which integrates the nonlinear equations over one cycle of vibration to find the quasi-linear system that best approximates the nonlinear response [41]. A quasi-linear system is a linear system whose parameters, i.e. natural frequency and damping, are amplitude dependent; at a fixed amplitude the response is assumed to be well approximated as linear. Within this framework, methods [60,35,36] have recently been developed that can compute the frequency and damping of a structure as a function of vibration amplitude from a single quasi-static load-displacement curve. Festjens et al. [60] introduced a quasi-static framework for jointed systems where a structure is forced to the shape of a mode of interest and the elastic energy and energy dissipated are used to compute the effective frequency and damping. A variant of this method, called quasi-static modal analysis (QSMA), was introduced by Allen and Lacayo [35] which simplified the approach in [60] slightly and uses the static load-displacement curve in modal coordinates to compute the effective natural frequency and damping ratio, allowing one to more easily diagnose problems with the contact simulations. It has been shown that QSMA can accurately compute the nonlinear frequency and damping of simple joined structures on a **mode-by-mode basis** in orders of magnitude less time than would be required to compute the dynamic response [35] and the method has subsequently been applied to various systems [23, 61, 38]. For example, in one case study for the S4 Beam structure with 350,000 elements and two contact interfaces shown in Fig. 6, the modal behavior was extracted using QSMA in 8 to 48 hours; the authors judged dynamic analysis to be infeasible, although Najera-Flores and Kuether [62] later performed a 1.0 second dynamic analysis on a similar model, requiring 20 days on 112 processors.

A brief overview of the QSMA approach by Lacayo and Allen [35] is detailed below.

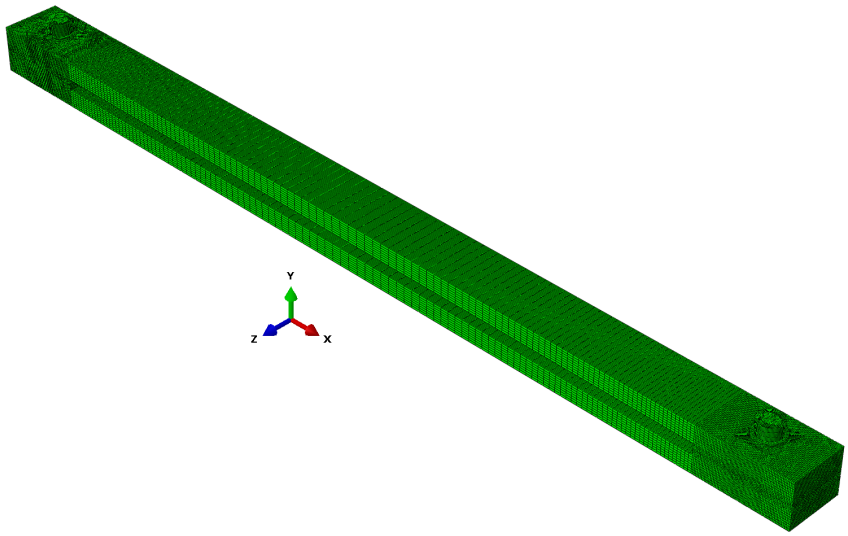

Figure 6: Finite element model of the S4 Beam built in Abaqus

Refer to [35, 63, 34, 23] for additional details and limitations. The FE discretized equations of motion for an undamped multi-degree of freedom (MDOF) system are given by Eq. 1, where $\mathbf{M}$ is the mass matrix, $\mathbf{K}$ is the stiffness matrix, $\mathbf{F}_{ext}$ is the external forcing, $\mathbf{F}_J(\mathbf{u}, \boldsymbol{\theta})$ is the force localized at the joint, which is a function of the preload applied to the joint, and $\mathbf{u}$ is the physical displacement. To determine whether the nodes of the joint are slipping or stuck, an internal variable, $\boldsymbol{\theta}$, is used to track the state of the slider elements the comprise the joint model in the previous timestep to determine the force and displacement of the nodes at the next timestep.

$$\mathbf{M}\ddot{\mathbf{u}} + \mathbf{K}\mathbf{u} + \mathbf{F}_J(\mathbf{u}, \boldsymbol{\theta}) = \mathbf{F}_{ext} \tag{1}$$

If the displacements are small relative to an equilibrium position, the joint force can be linearized about the equilibrium state by computing the Jacobian of the force with respect to each coordinate of $\mathbf{u}$. This is often done when a preload or clamping force is applied to the system prior to dynamic loading, resulting in the following tangent stiffness matrix for

the joint forces.

$$\mathbf{K}_0 = \left.\frac{\partial \mathbf{F}_J}{\partial \mathbf{u}}\right|_{\mathbf{u}_0} \tag{2}$$

The linearized modes of vibration can be computed about this equilibrium by solving the following eigenvalue problem where ω_r and $\boldsymbol{\phi}_r$ are the respective eigenvalue and eigenvector for the rth mode.

$$\left(\mathbf{K} + \mathbf{K}_0 - \omega_r^2 \mathbf{M}\right) \boldsymbol{\phi}_r = \mathbf{0} \tag{3}$$

A quasi-static distributed force is then applied such that replicates the inertial loading experienced during vibration in the rth mode. The following equation is then solved quasi-statically

$$\mathbf{K}\mathbf{u} + \mathbf{F}_J(\mathbf{u}, \boldsymbol{\theta}) = \mathbf{M}\boldsymbol{\phi}_r \alpha \tag{4}$$

where α represents a scalar amplitude for the applied body load. For the purposes of this paper, α is linearly increased from 0 to a maximum amplitude level of interest. The maximum value of alpha is determined by Eq. 5 where ω_r is the natural frequency of the rth mode, h is the thickness of the structure, γ is a scale factor, and ϕ_{max} is the absolute maximum of the rth mode shape.

$$\alpha_{max} = \frac{\gamma \omega_r^2 \mathrm{sgn}(\phi_{r,max}) h}{\phi_{max}} \tag{5}$$

It is important to note that the loading does not account for changes in the mode shapes, but the resulting static response may depend on all of the modes, i.e., modes other than the mode in question may be statically excited. After solving Eq. 4 one obtains the static

response as a function of the scalar amplitude levels, $\mathbf{u}(\alpha)$, from which the modal amplitude, natural frequency ($\omega(\alpha)$), and damping ratio ($\zeta(\alpha)$) can be written as function of α as shown in Eq. 12-17 in [35]. Once these are obtained, one can plot the frequency and damping as a function of modal amplitude. Note that one can compute the amplitude of every mode from $\mathbf{u}(\alpha)$, and this has been used to detect modal coupling in previous works, but the response is typically dominated by the mode that is excited (i.e., mode r in Eq. 4).

1.1.2 Reduced Order Modeling

Even with quasi-static methods, full order finite element models can take tens of hours to simulate a response for a model with a single bolt [23]. Extrapolating this method to realistic systems with 100s to 1000s of joints and to cases where the dynamic response must be computed over many cycles (whereas Jewell et al. modeled only a quarter vibration cycle), it is clear that modeling the contact in detail is not feasible for larger structures. Furthermore, Berger found that there is a trade-off between the finite element model resolution of the contact interface versus the computational cost of simulating the model [64]. This motivates the use of reduced order models (ROMs) to decrease the computational burden by approximating the full-order model at a set of reduction nodes between the mechanical interfaces. The approximation requires that these components remain linear and that the only source of nonlinearity within in the joined system is at the contact interface [65]. For this work, the Hurty/Craig Bampton (HCB) reduction method will be used [66]. For details, refer to **Papers III and IV** and references [66, 67, 68, 65] among others. Furthermore, this dissertation uses two techniques that further reduce the interface: multi-point constraint approach and the novel System-Level Characteristic Constraint (S-CC) reduction approach. A brief overview of the HCB method, spidering, and S-CC reduction are given below.

1.1.2.1 Hurty/Craig Bampton Method

For the HCB method, the system as given in Eq. 1 is partitioned between the boundary and

internal DOFs as

$$\begin{bmatrix} \mathbf{M}_{ii} & \mathbf{M}_{ib} \\ \mathbf{M}_{bi} & \mathbf{M}_{bb} \end{bmatrix} \begin{Bmatrix} \ddot{\mathbf{u}}_i \\ \ddot{\mathbf{u}}_b \end{Bmatrix} + \begin{bmatrix} \mathbf{K}_{ii} & \mathbf{K}_{ib} \\ \mathbf{K}_{bi} & \mathbf{K}_{bb} \end{bmatrix} \begin{Bmatrix} \mathbf{u}_i \\ \mathbf{u}_b \end{Bmatrix} + \begin{Bmatrix} 0 \\ \mathbf{F}_{j,b(\mathbf{u}_b)} \end{Bmatrix} = \begin{Bmatrix} 0 \\ \mathbf{F}_b \end{Bmatrix} \tag{6}$$

where subscripts b and i represent the boundary and interior DOF respectively. Note that only the boundary DOF are assumed to be forced either externally or internally through the joint. The interface is described by static constraint modes. The interior is described by vibration modes (fixed-interface modes) and the static constraint modes. These are combined to capture the dynamics of the assembled structure. As a result, a small number of fixed interface modes, Φ, are computed and that basis is augmented with constraint modes, Ψ, as detailed [69], to obtain the HCB transformation matrix,

$$\begin{Bmatrix} \mathbf{u}_i \\ \mathbf{u}_b \end{Bmatrix} = \mathbf{T}^{\mathrm{HCB}} \begin{Bmatrix} \mathbf{q}_i \\ \mathbf{u}_b \end{Bmatrix} = \begin{bmatrix} \mathbf{\Phi} & \mathbf{\Psi} \\ \mathbf{0} & \mathbf{I} \end{bmatrix} \begin{Bmatrix} \mathbf{q}_i \\ \mathbf{u}_b \end{Bmatrix} \tag{7}$$

This transformation then reduces the equations of motion to the following where the bar above the mass and stiffness terms indicates the transformed HCB model. This results in a significant reduction in the size of the model since the removed internal DOF (u_i) is much greater than the retained modal DOF (q_i).

$$\begin{bmatrix} \mathbf{I} & \bar{\mathbf{M}}_{ib} \\ \bar{\mathbf{M}}_{bi} & \bar{\mathbf{M}}_{bb} \end{bmatrix} \begin{Bmatrix} \ddot{\mathbf{q}}_i \\ \ddot{\mathbf{u}}_b \end{Bmatrix} + \begin{bmatrix} \Lambda_{ii} & \mathbf{0} \\ \mathbf{0} & \bar{\mathbf{K}}_{bb} \end{bmatrix} \begin{Bmatrix} \mathbf{q}_i \\ \mathbf{u}_b \end{Bmatrix} + \begin{Bmatrix} 0 \\ \mathbf{F}_{j,b}(\mathbf{u}_b) \end{Bmatrix} = \begin{Bmatrix} 0 \\ \mathbf{F}_b \end{Bmatrix} \tag{8}$$

The ROM can be used to analyze the dynamic response of a structure more efficiently than the full finite element model, depending on the number of boundary DOF that must be retained in the nonlinear internal force vector.

1.1.2.2 MPC Spidering

Once a HCB model retaining the boundary (interface) DOF is made, the industry standard practice is to spider the interface. Referred to as a whole-joint model, this approach reduces the interface using multi-point-constraints (MPCs) to constrain the displacement and rotation of the interface nodes to a single node [70]. In this dissertation (**Paper III**), two types of MPCs are examined: RBAR and RBE3 (using NASTRAN's naming convention). RBAR MPCs are rigid beam elements consisting of infinitely rigid beams that constrain a set of nodes to a single 6-DOF node [71]. RBARs have six constraint equations where the translations of the reduced node are consistent with the rotations (three equations) and the rotations are equal at both ends of the rigid bar (3 equations).

On the other hand, RBE3 elements consist of averaging type elements that constrain the average displacement and rotation of a set of nodes to a single 6-DOF node. Unlike the RBAR element, the RBE3 element applies a distributed force to the constrained set of nodes while not adding additional stiffness to those nodes. The distributed forces are determined the six constraint equations where the translation of the single node is the sum of the translations of the set of nodes, and the rotations of the single node are are the weighted average of the nodal translations of set of nodes [72].

Figure 7 depicts an example of the MPC spidering approach on the S4 Beam. Note that separate virtual and spidered HCB reduction nodes are required given that spidered nodes can not be used as both a spidered node and a node for a joint model per the implementation of the HCB Method for Abaqus [73] and Sandia National Laboratories Sierra Structural Dynamics code [71]. The nodes are shown expanded for visualization, but in fact are all coincident. Linear springs or nonlinear hysteretic models can then be used to connect these nodes to capture the linear/nonlinear dynamics of the system [74, 75].

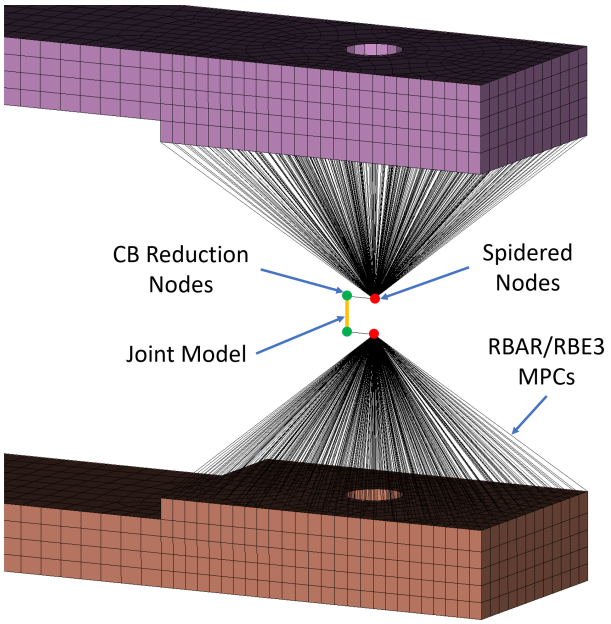

Figure 7: Section of a model where two interfaces are reduced to a single node and connected by a joint model. This structure was studied by Singh et al. [61] and is covered in appended Paper III

1.1.2.3 Alternative to MPC Spidering: S-CC Reduction

Consider the F-16 engine casing shown in Fig. 1. If spidering were done on this structure, spidered joints would be at every connection to join sub-components together, each with its own linear spring constants and nonlinear parameters that require updating, often leading to heavy computational costs.

This can become a cumbersome task and can lead to deficiencies in the model where the joint is oversimplified to mitigate that computational cost. An alternative to MPC spidering each joint is to perform an eigen-analysis on the interface DOF to get deformation shapes. These interface deformation shapes can be used to reduce the interface to non-physical DOF, while maintaining flexibility at the interface and spanning all the possible joints in the structure. Unlike the MPC approach where a joint model is required at each physical joint, joint models can be applied to interface deformation shapes. For details, refer to **Paper IV**.

1.2 A Brief Overview of Joint Models

Developing a constitutive model to represent joint nonlinearity can be divided into three areas of research: structural dynamics, contact mechanics, and tribology. Structural dynamics aims to understand the effects of the joint on the global behavior of the structure, a macroscale approach. Contact mechanics is used to address the mesoscale problem of the contact pressure variation over the interface, leading to fretting, wear, and slip in joints [76]. Lastly, tribology is used to address the imperfections of the contact interface from design tolerances to wear from repeated cycles of loading. Although there have been efforts to develop a multi-scale model to capture the effect of each area of research on joint nonlinearity, most constitutive joint models are used to capture the behavior to the mesoscale.

There are a number of approaches proposed for representing this behavior that can be characterized in two sets: (1) velocity based models and (2) state based models. Velocity based models are common for macroslip formulations, whereas state based models are common for microslip formulations [11]. Velocity based approaches utilize forms similar to Coulomb Friction [77], viscous friction, and stiction [11]. A simple approach is to join two coincident contact interfaces with linear spring elements [78] or Coulomb friction elements [79, 58, 45] as shown in Fig. 7. However, linear spring elements are able to capture the resonant frequencies at a single excitation level but fall short of capturing the damping effects and any dependency of these modal parameters on excitation amplitude. Others seek to add nonlinear elements with polynomial stiffness and damping in parallel with linear springs or to better estimate the frequency and damping trends [80]. Conversely, state based models require state variables to record the state at discrete time steps [81, 20, 82]. An example of this is the Jenkin's element [20, 82]. The Jenkins element consists of a linear spring and a slider in series that can describe both microslip and macroslip. Another option is zero-thickness continuum elements which were first used for soil mechanics and civil engineering [83]. These elements assume an elastic material model but utilize stick-slip Jenkins

elements tangential to the contact interface to capture frictional behavior [84, 85, 86]. The two most common state based models used today are the Iwan element and the Bouc-Wen Hysteresis model. The Iwan element utilizes a large number of springs and sliders in parallel and can be characterized by four or five parameters [87, 88, 35, 89], whereas the Bouc-Wen model parameterizes the state velocity and joint force [90, 91, 92, 93, 94]. For a review of friction models, refer to [95] that compares the ability of each friction model to correlate a reduced order model to experimental data.

1.2.1 Iwan Model

The work presented in **Papers III and IV** use Segalman's Four Parameter Iwan Model to characterize the energy dissipation due to joints [88]. A brief overview is presented below.

Using his four parameter Iwan model formulation, Segalman found both analytical solutions for contact and empirical evidence that showed that joints exhibit power-law energy dissipation versus force (or vibration amplitude) [88]. An Iwan element is a collection of slider or Jenkins elements in parallel as shown in Fig. 8, in which the slip force[1]for each slider is governed by several parameters, i.e. the friction coefficient, normal force, etc.... Segalman's model recognizes that the net effect of all of these parameters must be to produce power-law dissipation versus vibration amplitude, which is governed by only two of the four parameters in the Iwan model. The other two parameters control the transition to macroslip when the joint slips completely.

The four parameter Iwan model can be represented by the parameters F_s,K_T,χ,and β as defined below:

F_S: The force necessary to cause macroslip

K_T: The tangential stiffness of the Jenkins elements (i.e. the joint stiffness when no slip occurs)

χ: The exponent that describes the slope of the energy dissipation curve

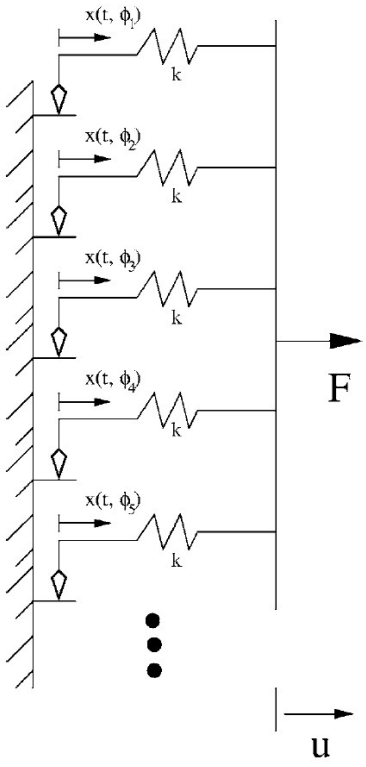

Figure 8: Collection of springs and sliders (Jenkins elements) that comprise an Iwan Model [88]

β: The parameter that relates the level of energy dissipation and the shape of the energy dissipation curve as the macroslip force is approached

When the excitation amplitude is small, the Iwan model exhibits a tangential stiffness (K_T) that is equivalent to a linear model with springs connecting the joints. For an in-depth discussion of the Iwan element, refer to Segalman's original paper on Iwan elements [88]. The Iwan model has been implemented on various structures [96, 61] at discrete joints using the Whole Joint Model framework. However, when there are thousands of joints, each joint will require an Iwan element, each with its own set of parameters, resulting in a large number of unknowns. Segalman thus applied the Iwan model in modal space rather than at each physical discrete joint to decrease the number of unknowns, hence referred to as a modal Iwan approach [97, 98]. In this approach, the nonlinearity of each mode is characterized

by fitting a single DOF unit mass oscillator at the mode that exhibits nonlinearity. The oscillator has a four parameter Iwan element in parallel with a linear spring and a damper (dashpot). Therefore the number of unknowns is dictated by the number of modes one wishes to characterize, rather than the number of joints. This overcomes the issue where each joint needs to be explicitly modeled, e.g. a turbine with 1000's of joints can be reduced to a single modal joint model. While this may seem efficient, this requires that the modes remain uncoupled. Therefore, by its modal nature, the modal Iwan is incapable of capturing modal coupling.

1.3 Methods to Simulate Modal Coupling

The third challenge is incorporating modal coupling into the model. For a linear system, the modes of a structure are independent of amplitude and a modal filter [99] can be used to separate a multi-modal response into the contributions from the individual modes. If the modal frequencies are sufficiently distinct then a temporal filter could be used instead. For a weakly nonlinear response, it is often observed that the nonlinearity primarily affects damping and does not alter the mode shapes significantly; thus, the linear modes are assumed to remain uncoupled and can be used to decouple the nonlinear system, as long as the criteria outlined by Eriten et al. [41] are satisfied (e.g. modal frequencies are not integer multiples of one another). However, the modes may not always satisfy these conditions. Coupling occurs when the excitation of one mode causes a transfer of energy that perturbs another mode [100]. Recent studies on experimental structures have shown that the interactions between modes are not always negligible and hence one may obtain large errors in the predicted damping if they are not considered [63, 101, 102]. However, realizing the modal coupling experimentally is not a trivial task. Current methods require modal filtering a time response, which in turn cannot capture the interactions. As a result, the direct time fitting method was developed.

---

[1] If all sliders have the same friction coefficient then the slip force is defined by the normal force for each slider.

1.3.1 Experimentally Determining Modal Coupling

When a time response is obtained from experimental tests, signal processing methods are necessary to realize the change in frequency and damping with respect to amplitude from a MDOF time response. Foremost, a method is required that does not depend on modally filtering the dynamic time histories from a transient response. The widely used Hilbert method [103, 63] assumes that a modal filter can decouple the response from a time signal to modal single degree of freedom (SDOF) systems. This dissertation uses the direct time fitting method, initially proposed by Goyder [104] and expanded upon by Moldenhauer et al. [105].

The method introduced by Goyder [104], fits a damped sine to the modally filtered SDOF response to obtain the modal parameters as a function of amplitude. This is done by splitting the time history into short intervals. Within each interval, it is assumed that the frequency and damping are constant. Each segment can be represented as a damped sine given by Eq. 9 where $y_f(t)$ is the fit of the response of the segment, ζ and ω_n are the damping and natural frequency, and A and B are amplitudes.

$$y_f(t) = e^{-2\zeta\omega_n t}[A\cos\left(\sqrt{1-\zeta^2}\omega_n t\right) - B\sin\left(\sqrt{1-\zeta^2}\omega_n t\right)] \tag{9}$$

These can be written in terms of auxiliary variables $\alpha = \sqrt{1-\zeta^2}\omega_n t$ and $\beta = 2\zeta\omega_n t$. Values for frequency and damping may be found by solving these equations to get

$$\omega_n = \sqrt{\alpha^2+\beta^2} \tag{10}$$

$$\zeta = \frac{\beta}{\sqrt{\alpha^2+\beta^2}} \tag{11}$$

The modal parameters can be found in two stages. First, estimate values for α and β and then find the amplitudes, A and B, through a least squares process. This is done until the mean squared error between the fit and response is minimized and repeated for each segment

of the time history.

Moldenhauer et al. extend this by fitting a multi-harmonic response simultaneously as a summation of damped sines at the harmonics of the system. Equation 12 is an extension of Eq. 9 in that manner, where i represents the ith harmonic

$$y_f(t) = \sum_{i}^{N} e^{-2\zeta_i \omega_{n,i} t} [A_i \cos\left(\sqrt{1-\zeta_i^2}\omega_{n,i} t\right) - B_i \sin\left(\sqrt{1-\zeta_i^2}\omega_{n,i} t\right)] \tag{12}$$

The workflow for this method is shown below in Fig 9 corresponding to the following steps

1. Segment time history into intervals with assumed constant frequency and damping
2. Fit a multi-harmonic damped sine to the segment
3. Return the fit for each mode present in the response
4. Generate the amplitude dependent damping and frequency curves for each mode

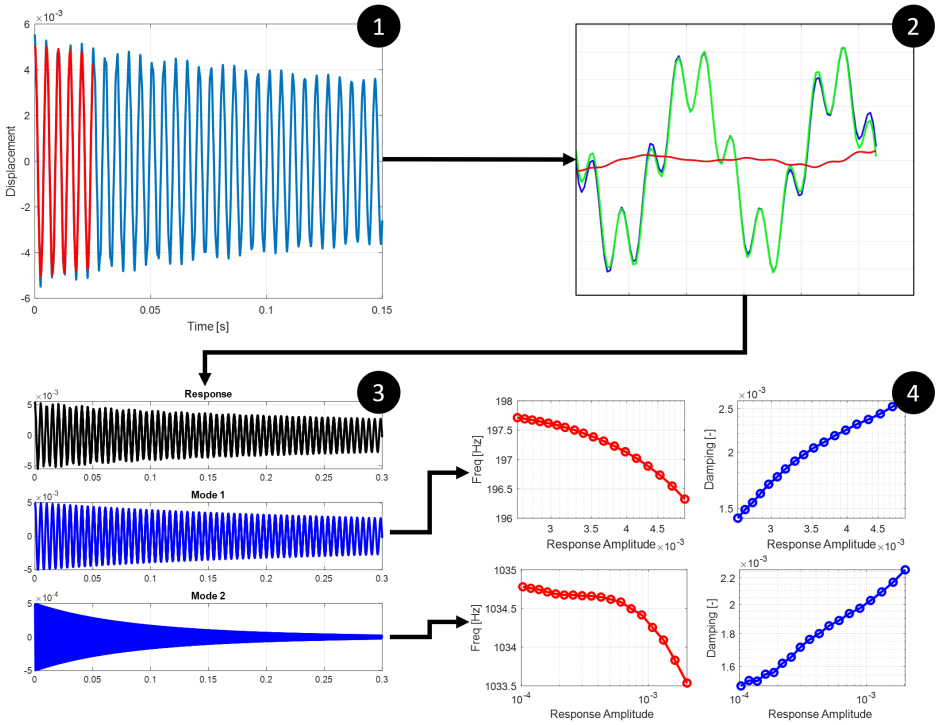

Figure 9: Workflow for direct time fitting of multi-harmonic signals

1.3.2 Numerically Determining Modal Coupling

Many works have studied nonlinearity and the coupling that it can induce between modes. For example, the NNM framework in [49, 106] captures internal resonance branches, which are a manifestation of coupling in an undamped nonlinear system. Vakakis has studied this extensively in the context of vibration absorbers and the one-way transfer of energy (see, e.g. [107]) and the International Conference on Nonlinear Vibrations, Localization and Energy Transfer is dedicated, in part, to this topic. Most works on modal interactions focus on cases in which the frequencies of the two modes in question are integer multiples of one another, in which case a super-harmonic resonance can occur and modal coupling is known to be significant [59]. This work is concerned with a different phenomenon, in which a typically weaker nonlinearity causes coupling between two modes whose frequencies are not integer related, such that the effective frequency and damping of one mode is influenced by the other mode. Such was the case in the measurements for the S4 Beam, as reported by Wall et al. [102].

While experimentally capturing modal coupling is feasible, numerically modeling the coupling is computationally expensive, especially when seeking to model the contact between the structures in detail as is the focus of this work. A dynamic transient analysis can produce a response that is consistent with the mesh and the friction law that was assumed at the interface, but this comes at a large computational cost. On the other hand, the QSMA method in [35] is computationally efficient, but requires that the joints remain weakly nonlinear such that modal coupling is negligible. The work in **Paper V** presents an extension of the quasi-static framework in [35] to predict modal coupling without having to run a dynamic analysis. Termed Multi-Mode QSMA (MM-QSMA), this method statically loads the structure in the shape of two or more modes simultaneously. The loading is defined such that other modes are excited in addition to the mode of interest, whose motion is suspected to change the response of the mode of interest. For details, refer to **Paper V**.

2 SCOPE OF THE DISSERTATION

An overview of the research conducted in the appended papers is shown in Fig. 10. The publications can be segmented into three categories, each of which aim to address joint nonlinearity:

1. Experimental Characterization
2. Reduced Order Modeling
3. Numerically Simulating Modal Coupling

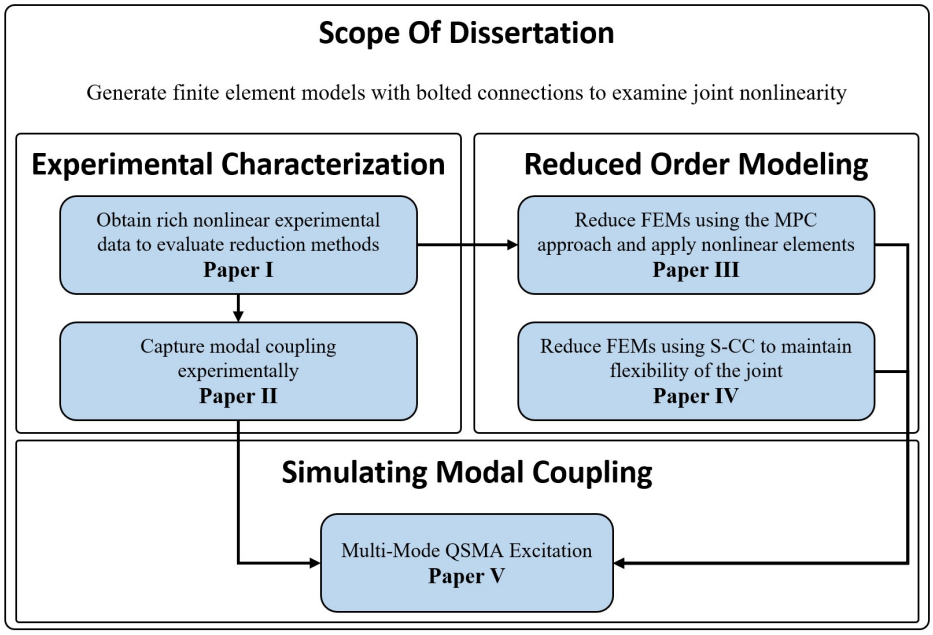

Figure 10: Layout of the appended papers in Chapter II of the dissertation

The objective of this work is to understand the effect of interface reduction on the ability to capture the nonlinear dynamics of the structure on a macro-level. **Papers I and II** highlight methods to obtain linear and nonlinear experimental time histories that will serve as the truth data for all subsequent chapters. Utilizing this data, **Paper III** examines the influence of the type of MPC on the ability to capture nonlinearity. In previous work by Lacayo and Allen [35], they observed pareto fronts which showed that there was a trade off

where either the frequency error or damping error between numerical/experimental results could be minimized, but not both. This study expands on that by varying the MPC from rigid bars to averaging constraints and adjusting the contact area to better evaluate the solution space that could minimize frequency and damping error. **Paper IV** seeks to develop a methodology that transitions from the traditional MPC approach to a continuous flexible interface and inherently extend linear reduction techniques to nonlinear problems. This paper begins to address the concern of the uncertainty in the type of MPC with the spidered models (**Paper III**), by reducing the model to a set of DOF in the modal domain while maintaining the flexibility of the interface (no rigid or averaging constraints). Lastly, **Paper V** introduces a novel approach to quantify the interactions between modes of vibration for jointed structures. The work done to this point is shown in Chapter II with a brief description of each paper given below.

2.1 Paper I: Experimental Characterization of Joint Nonlinearity

This work sought to characterize a new benchmark structure and to provide a rich data set against which simulations may be compared when seeking to predict damping nonlinearities. The S4 beam as shown in Fig. 11, consisting of two C beams bolted together at the ends, was tested and the first six elastic modes, all below 800 Hz were characterized both linearly and nonlinearly.

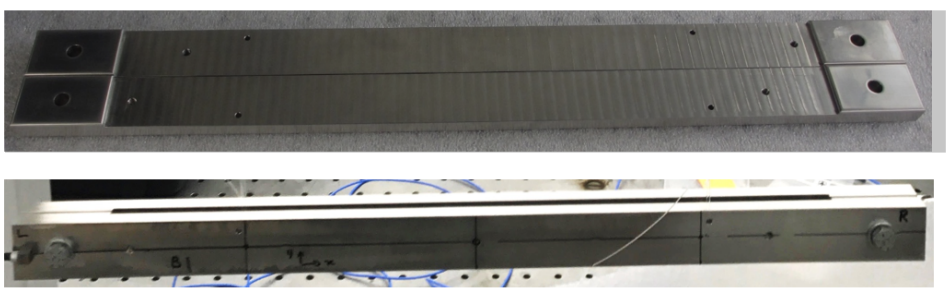

Figure 11: The benchmark structure, S4 Beam

The pressure distributions were characterized and qualitatively correlated to variations in the linear natural frequencies and in the nonlinearity observed. As in other studies, those modes that exhibited shearing of the joint depicted strongest nonlinearity with respect to damping. In general, none of the modes showed large stiffness nonlinearities even though the damping of some modes changed by a factor of five or more. Four configurations of beams were tested: hertzian contact, flat-on-flat interface contact, flat-on-curved interface contact, and hertzian contact with a washer. Between the four configurations of beams, the beams that had flat interfaces depicted the largest damping nonlinearity, whereas the curved beams with a washer depicted the least damping nonlinearity. This data was then used to investigate the ability of reduction techniques to capture nonlinearity.

2.2 Paper II: Experimental Measurement of Modal Coupling

This collaborative work sought to experimentally characterize a structure and establish a dataset that depicted modal coupling. To acquire this experimental data, a Cylinder-Plate-Beam structure was manufactured and instrumented. Low-level shaker testing was done to identify baseline linear modal parameters such as natural frequency, damping ratio, and mass normalized mode shapes. For nonlinear data, windowed sinusoidal excitations were completed at various excitation levels on each mode individually and on pairs of modes simultaneously. Amplitude dependent natural frequency and damping ratio curves were extracted for each mode. For the isolated modes excited at various shaker levels, the curves were found to overlay, implying that while each is nonlinear, the corresponding response is consistent over the observed range and is independent of initial excitation. However, when two bending modes were excited simultaneously, the curves for each deviate from the isolated baseline as the relative excitation of the other increases. Such a relationship was not observed with either of these modes when a drum was also excited. Conversely, the drum mode was observed to vastly deviate from its isolated baseline when bending modes were

excited. The experimental data collected presents a first study of modal coupling, indicating that some degree of modal coupling is present and observable. While the previous data set is useful in evaluating the capability of reproducing amplitude dependent curves for frequency and damping, this data set is useful in evaluating the ability of the models to capture the interactions between modes. Future work would be to use these measurements to tune a model of the Cylinder-Plate-Beam.

2.3 Paper III: Spider Configurations for Reduced Order Models

This work explored the ability for MPC reduction techniques to correlate to the experimental results for the S4 Beam. High fidelity models were created using RBAR and RBE3 spidered joints to understand the effects of the area of influence for the joint (i.e. using full and reduced contact interface areas as shown in Fig 12).

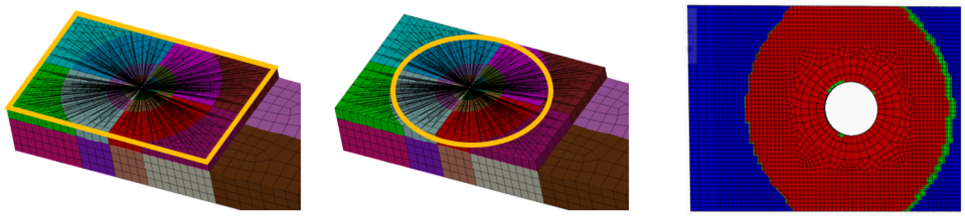

Figure 12: (Left) The full contact area, (Middle) the reduced contact area, (Right) An Abaqus simulation to yield the reduce contact area

The viability of the models was studied by evaluating their ability to reproduce the linear natural frequencies of the assembly (i.e. by updating linear springs at the interface) and their ability to capture the amplitude dependent frequency and damping caused by the joints (i.e. by updating the parameters of nonlinear Iwan elements at the interfaces). The linear updating exercise showed that all models were quite similar, although the models with spiders constructed with rigid bar elements captured the second mode more accurately. This was significant because the second mode was sensitive to shearing of the joint due to

bending of the beam, a phenomenon that is often observed in lap joints. Quasi-static modal analysis was then used to update the parameters of the nonlinear Iwan elements, using the joint stiffnesses found in the linear updating step. Although the models captured the linear modes quite similarly, they produced widely varying results for the nonlinear damping and for the change in frequency with vibration amplitude. The model with a full interface spidered with RBAR elements resulted in the excellent correlation between the experimental nonlinear frequency and damping curves, perhaps the best that has been observed in this type of study to date, whereas both models that used the RBE3 spiders gave very poor results. In some instances, the models were able to capture the change in frequency and damping to some degree, but that required sacrificing the linear agreement. The preliminary conclusion of this work is that the method of spidering the interface does indeed matter for this type of modeling. Furthermore, there is a trade-off between linear and nonlinear correlation; therefore, one could not solely use the stiffnesses from linear updating to ensure that the nonlinearity is captured correctly.

2.4 Paper IV: Substructure Interface Reduction utilizing S-CC Reduction

This work explored a new way of representing the linear and nonlinear properties of joints using the S-CC reduction technique. Traditionally high-fidelity models were created using rigid bar (RBAR) and averaging constraints (RBE3) spidered joints to understand the joint behavior as shown in **Paper III**. This paper studied reduction techniques that maintained the flexibility of the interface to an even greater degree than the RBE3 spidering approach, while reducing the number of interface DOF. This paper explored the extension of linear S-CC reduction to nonlinear analyses (nSCC) against the traditional spidering approach with RBAR MPCs. This was done on a 2D Beam case study with known quasi-static curves to gauge the effectiveness of these NLROMs. The viability of both methods were evaluated on their ability to reproduce the linear natural frequencies of the beam, as well as the amplitude

dependent frequency and damping curves using QSMA with Iwan joints. The RBAR model failed to create a set of curves that could represent the true nonlinear response for both frequency and damping for any of the 3 modes of interest even after a thorough exploration of the parameter space. In contrast, the extension of S-CC to nonlinear (nSCC) allowed for tuning of the Iwan parameters and excellent correlation for the 3 modes of interest. The preliminary conclusion of this work is a novel technique extended from a linear reduction method to capture joint nonlinearity. This method shows promise in capturing coupling between the linear modes of vibration.

2.5 Paper V: Multi-mode Quasi-static Excitation for Systems with Nonlinear Joints

This paper explored a new method for evaluating the effect of mode coupling on the natural frequency and damping that is observed in each mode in a structure with nonlinearities due to a bolted joint. In contrast to prior works, in this paper the structure was excited quasi-statically in the shape of two modes simultaneously. The viability of this approach was first studied on a 2D beam structure, quantifying the static coupling between the modes and comparing it to the coupling observed in a few dynamic responses. Then this approach was examined on a 3D structure to statically quantify modal coupling where a dynamic response was impractical. The slip induced at the interfaces was examined in both cases to understand the effect that simultaneously exciting two modes has on the interface [35]. The results were found to form conservative (sometimes highly conservative) bounds on the damping and effective natural frequency that were observed in the dynamic response. In a dynamic response, the phase of the modes would change continuously with time unless their natural frequencies were integer multiples, whereas the phasing is constant when statically excited. Although the coupling is over-predicted, considering the huge difference in the cost of MM-QSMA versus the dynamic response, the bounding boxes are still highly useful even

if they are sometimes overly conservative.

3 CONCLUDING REMARKS AND FUTURE WORK

The work completed to date has sought to advance numerical modeling of joints. Rich experimental data-sets were developed to gauge the numerical models and provide insight into the effects of joint nonlinearity on the vibration of a structure. Considerable progress has been achieved to understand how reduction techniques affect linear and nonlinear correlation. As a result of this work, limitations to the industry standard MPC approach were discovered and a novel reduction method was proposed as an alternative to spidering. Lastly, this work presents the first computationally efficient method to model modal coupling in jointed structures. It has been shown that not only does this method form a bounding box on the nonlinearity seen dynamically, it can capture the unequal transfer of energy between modes of vibration seen in experiments and dynamically.

While significant work has been done to advance numerical modeling, the models examined in this dissertation were assessed a posteriori, that is, they were calibrated to measurements at a single excitation level. While this is a common procedure for model correlation, ideally the calibrated model would be able to predict the dynamic behavior a priori. Therefore, further work needs to be done to evaluate the ability of these tuned models to predict responses at various other excitation levels. Furthermore, the academic structures used in this work to evaluate the reduced order models are typically smaller and feature fewer types of motion than industrial structures. An example of the latter is ribs in mechanical morphing wing structures which feature hinge joints in addition to the types of joints modeled in this dissertation [108]. Therefore, to evaluate their robustness, these methods should be applied to capture the nonlinear behavior in industrial applications.

In this dissertation, modal coupling was observed experimentally on the Cylinder-Plate-Beam structure through the use of sine-beat excitation in **Paper II**. While effort has gone

into characterizing the structure experimentally, modeling efforts, particularly reduced order models, are few and far between. Therefore, it would be of interest to see if reduced order models can capture the nonlinearity for a single mode, and if MM-QSMA can capture the effects of coupling on a full order FEM.

While reduced order models can capture the dynamics of the full order model, the question remains as to whether these reduced order models can capture modal coupling. To date, modal coupling has been observed experimentally or through simulations of full order models, and while MM-QSMA is an excellent method to decrease the computational burden, a single coupled quasi-static response could take upwards of 8 hours to simulate for the S4 Beam. Extending that to larger structures (Cylinder-Plate-Beam) and even industrial structures, MM-QSMA can become costly. As a result, further research is needed to evaluate the ability of this novel method in conjunction with reduced order models to numerically capture modal coupling.

REFERENCES

[1] S. D. Ishmael and D. R. McMonagle, "AFTI/F-16 Flight Test Results and Lessons," Technical Memorandum 84920, NASA, Edwards, California, Oct. 1983.

[2] Niall McCarthy, "The Hourly Cost Of Operating The U.S. Military's Fighter Fleet," *Forbes Magazine*, Aug. 2016.

[3] C. S. Desai, "Constitutive modeling of materials and contacts using the disturbed state concept: Part 1 – Background and analysis," *Computers & Structures*, vol. 146, pp. 214–233, Jan. 2015.

[4] Chris Ian Van Damme, Matt S. Allen, and Joesphka J. Hollkamp, "Updating Geometrically Nonlinear Reduced Order Models using Nonlinear Modes and Harmonic Balance," *AIAA Journal (Accepted Feb. 2020)*, Feb. 2020.

[5] S. M. Spottswood, J. J. Hollkamp, and T. G. Eason, "Reduced-order models for a shallow curved beam under combined loading," *AIAA Journal*, vol. 48, no. 1, pp. 47–55, 2010. Number: 1.

[6] M. Crisfield, *Nonlinear finite element analysis of solids and structures. Volume 1: Essentials*. Other Information: DN: From review by Murli M. Gupta, George Washington Univ., in Applied Mechanics Review, Vol. 45, No. 4 (Apr 1992); PBD: 1991, New York: John Wiley and Sons, 1991.

[7] A. J. Culler and J. J. McNamara, "Coupled Flow-Thermal-Structural Analysis for Response Prediction of Hypersonic Vehicle Skin Panels," Apr. 2010.

[8] R. Kamakoti and W. Shyy, "Fluid–structure interaction for aeroelastic applications," *Progress in Aerospace Sciences*, vol. 40, pp. 535–558, Nov. 2004.

[9] R. Lacayo, L. Pesaresi, J. Gross, D. Fochler, J. Armand, L. Salles, C. W. Schwingshackl, M. S. Allen, and M. R. Brake, "Nonlinear modelling of structures with bolted joints: a comparison of two approaches based on a time-domain and frequency-domain solver," *Mechanical Systems and Signal Processing*, 2017.

[10] A. A. Ferri, "Friction damping and isolation systems," *Journal of Mechanical Design, Transactions of the ASME*, vol. 117 B, pp. 196–206, 1995.

[11] M. R. W. Brake, ed., *The Mechanics of Jointed Structures: Recent Research and Open Challenges for Developing Predictive Models for Structural Dynamics*. Springer International Publishing, 2018.

[12] A. F. Vakakis, O. V. Gendelman, L. A. Bergman, D. M. McFarland, G. Kerschen, and Y. S. Lee, *Nonlinear Targeted Energy Transfer in Mechanical and Structural Systems*. Solid Mechanics and Its Applications, Springer Netherlands, 2009.

[13] B. J. Olson and S. W. Shaw, "Vibration absorbers for a rotating flexible structure with cyclic symmetry: Nonlinear path design," *Nonlinear Dynamics*, vol. 60, no. 1-2, pp. 149–182, 2010. Number: 1-2.

[14] R. Viguie and G. Kerschen, "The Nonlinear Tuned Vibration Absorber," Feb. 2013.

[15] S. K. Rhee, P. H. S. Tsang, and Y. S. Wang, "Friction-induced noise and vibration of disc brakes," *Wear*, vol. 133, pp. 39–45, Sept. 1989.

[16] R. S. Birch and M. Alves, "Dynamic failure of structural joint systems," *Thin-Walled Structures*, vol. 36, pp. 137–154, Feb. 2000.

[17] "Death of a Drone," *Popular Mechanics*, vol. 189, p. 16, June 2012.

[18] L. Gaul and J. Lenz, "Nonlinear dynamics of structures assembled by bolted joints," *Acta Mechanica*, vol. 125, no. 1-4, pp. 169–181, 1997. Number: 1-4.

[19] E. E. Ungar, "The status of engineering knowledge concerning the damping of built-up structures," *Journal of Sound and Vibration*, vol. 26, pp. 141–154, Jan. 1973. Number: 1.

[20] L. Gaul and R. Nitsche, "The Role of Friction in Mechanical Joints," *Applied Mechanics Reviews*, vol. 54, pp. 93–106, Mar. 2001. Publisher: American Society of Mechanical Engineers Digital Collection.

[21] D. J. Segalman, D. L. Gregory, M. J. Starr, B. R. Resor, M. D. Jew, J. P. Lauffer,

and N. M. Ames, "Handbook on Dynamics of Jointed Structures," tech. rep., Sandia National Laboratories, Albuquerque, NM 87185, 2009.

[22] C. Hartwigsen, Y. Song, D. McFarland, L. Bergman, and A. Vakakis, "Experimental study of non-linear effects in a typical shear lap joint configuration," *Journal of Sound and Vibration*, vol. 277, pp. 327–351, Oct. 2004. Number: 1-2.

[23] E. Jewell, M. S. Allen, I. Zare, and M. Wall, "Application of Quasi-Static Modal Analysis to a Finite Element Model and Experimental Correlation," *Journal of Sound and Vibration*, vol. 479, no. 4 August, p. 115376, 2020. Number: 4 August.

[24] A. Singh, M. Scapolan, Y. Saito, M. S. Allen, D. Roettgen, B. Pacini, and R. J. Kuether, "Experimental Characterization of a New Benchmark Structure for Prediction of Damping Nonlinearity," in *Nonlinear Dynamics, Volume 1* (G. Kerschen, ed.), Conference Proceedings of the Society for Experimental Mechanics Series, (Cham), pp. 57–78, Springer International Publishing, 2019.

[25] M. Groper, "Microslip and macroslip in bolted joints," *Experimental Mechanics*, vol. 25, pp. 171–174, June 1985.

[26] R. A. Ibrahim and C. L. Pettit, "Uncertainties and dynamic problems of bolted joints and other fasteners," *Journal of Sound and Vibration*, vol. 279, no. 3-5, pp. 857–936, 2005. Number: 3-5.

[27] B. Deaner, M. S. Allen, M. J. Starr, D. J. Segalman, and H. Sumali, "Application of Viscous and Iwan Modal Damping Models to Experimental Measurements From Bolted Structures," *ASME Journal of Vibrations and Acoustics*, vol. 137, p. 12, 2015.

[28] D. R. Roettgen and M. S. Allen, "Experimental Dynamic Substructuring of a Catalytic Converter System using the Transmission Simulator Method," 2015.

[29] M. Wall, A. Matthew S., and Z. Iman, "Predicting S4 Beam Joint Nonlinearity Using Quasi-Static Modal Analysis," *IMAC XXXVII*.

[30] S. Cooper, M. Rosatello, A. Mathis, M. R. Brake, M. S. Allen, A. Ferri, D. R. Roettgen,

B. R. Pacini, and R. L. Mayes, "Effect of Far-Field Structure on Joint Properties," 2017.

[31] M. S. Bonney, B. A. Robertson, M. Mignolet, F. Schempp, and M. R. Brake, "Experimental Determination of Frictional Interface Models," in *Dynamics of Coupled Structures, Volume 4* (M. Allen, R. L. Mayes, and D. Rixen, eds.), Conference Proceedings of the Society for Experimental Mechanics Series, (Cham), pp. 473–490, Springer International Publishing, 2016.

[32] T. Dossogne, T. Jerome, D. Lancereau, S. Smith, M. Brake, B. Pacini, P. Reuss, and C. Schwingshackl, "Experimental Assessment of the Influence of Interface Geometries on Structural Dynamic Response," pp. 255–261, Apr. 2017.

[33] A. Zmitrowicz, "A vibration analysis of a turbine blade system damped by dry friction forces," *International Journal of Mechanical Sciences*, vol. 23, pp. 741–761, Jan. 1981.

[34] M. S. Allen, R. Lacayo, and M. R. Brake, "Quasi-static Modal Analysis based on Implicit Condensation for Structures with Nonlinear Joints," in *International Seminar on Modal Analysis (ISMA)*, (Leuven, Belgium), Sept. 2016.

[35] R. M. Lacayo and M. S. Allen, "Updating Structural Models Containing Nonlinear Iwan Joints Using Quasi-Static Modal Analysis," *Mechanical Systems and Signal Processing*, vol. 118, no. 1 March 2019, pp. 133–157, 2019. Number: 1 March 2019.

[36] N. N. Balaji and M. R. W. Brake, "A quasi-static non-linear modal analysis procedure extending Rayleigh quotient stationarity for non-conservative dynamical systems," *Computers & Structures*, vol. 230, p. 106184, Apr. 2020.

[37] Aabhas Singh, Matthew S. Allen, and Robert J. Kuether, "Substructure Interface Reduction with Iwan Elements to Capture Nonlinearity," (Houston, Texas), Feb. 2020.

[38] I. Zare and M. S. Allen, "Adapting a contact-mechanics algorithm to predict damping in bolted joints using quasi-static modal analysis," *International Journal of Mechanical Sciences*, vol. 189, Jan. 2021.

[39] E. P. Petrov, K. Y. Sanliturk, and D. J. Ewins, "A new method for dynamic analysis

of mistuned bladed disks based on the exact relationship between tuned and mistuned systems," *Journal of Engineering for Gas Turbines and Power*, vol. 124, no. 3, pp. 586–597, 2002. Number: 3.

[40] S. Bograd, P. Reuss, A. Schmidt, L. Gaul, and M. Mayer, "Modeling the dynamics of mechanical joints," *Mechanical Systems and Signal Processing*, vol. 25, no. 8, pp. 2801–2826, 2011. Number: 8.

[41] M. Eriten, M. Kurt, G. Luo, D. Michael McFarland, L. A. Bergman, and A. F. Vakakis, "Nonlinear system identification of frictional effects in a beam with a bolted joint connection," *Mechanical Systems and Signal Processing*, vol. 39, no. 1-2, pp. 245–264, 2013. Number: 1-2.

[42] J. Paduart, L. Lauwers, J. Swevers, K. Smolders, J. Schoukens, and R. Pintelon, "Identification of nonlinear systems using Polynomial Nonlinear State Space models," *Automatica*, vol. 46, pp. 647–656, Apr. 2010.

[43] M. Scheel, G. Kleyman, A. Tatar, M. R. W. Brake, S. Peter, J.-P. Noël, M. S. Allen, and M. Krack, "Experimental assessment of polynomial nonlinear state-space and nonlinear-mode models for near-resonant vibrations," *Mechanical Systems and Signal Processing*, vol. 143, p. 106796, Sept. 2020.

[44] E. Turgut, "An analysis of the effects of non-payload fuel consumption for a wide-bodied aircraft," *ANADOLU UNIVERSITY JOURNAL OF SCIENCE AND TECHNOLOGY A - Applied Sciences and Engineering*, vol. 18, pp. 59–59, Mar. 2017.

[45] E. P. Petrov and D. J. Ewins, "Analytical Formulation of Friction Interface Elements for Analysis of Nonlinear Multi-Harmonic Vibrations of Bladed Disks," *Journal of Turbomachinery*, vol. 125, no. 2, pp. 364–371, 2003. Number: 2.

[46] E. Jewell, M. S. Allen, and R. Lacayo, "Predicting damping of a cantilever beam with a bolted joint using quasi-static modal analysis," in *Proceedings of the ASME 2017 International Design Engineering Technical Conference & 13th International Confer-*

ence on Multibody Systems, Nonlinear Dynamics, and Control IDETC/ MSNDC 2017, Aug. 2017.

[47] R. M. Lacayo, *An Investigation on Iwan Models for Capturing the Amplitude-Dependent Behavior of Structures with Bolted Joints*. PhD thesis, University of Wisconsin-Madison, 2017.

[48] R. M. Rosenberg, "Normal modes of nonlinear dual-mode systems," *Journal of Applied Mechanics*, vol. 27, pp. 263–268, 1960.

[49] G. Kerschen, M. Peeters, J. C. Golinval, and A. F. Vakakis, "Nonlinear normal modes. Part I. A useful framework for the structural dynamicist," *Mechanical Systems and Signal Processing*, vol. 23, no. 1, pp. 170–94, 2009. Number: 1.

[50] M. Peeters, R. Viguié, G. Sérandour, G. Kerschen, and J. C. Golinval, "Nonlinear normal modes, Part II: Toward a practical computation using numerical continuation techniques," *Mechanical Systems and Signal Processing*, vol. 23, no. 1, pp. 195–216, 2009. Number: 1.

[51] R. J. Kuether, M. R. Brake, and M. S. Allen, "Evaluating Convergence of Reduced Order Models Using Nonlinear Normal Modes," Feb. 2014.

[52] M. Krack, "Nonlinear modal analysis of nonconservative systems: Extension of the periodic motion concept," *Computers & Structures*, vol. 154, pp. 59–71, July 2015.

[53] L. Renson, G. Kerschen, and B. Cochelin, "Numerical computation of nonlinear normal modes in mechanical engineering," *Journal of Sound and Vibration*, vol. 364, pp. 177–206, Mar. 2016.

[54] G. Kerschen, "Computation of Nonlinear Normal Modes through Shooting and Pseudo-Arclength Computation," in *Modal Analysis of Nonlinear Mechanical Systems* (G. Kerschen, ed.), CISM International Centre for Mechanical Sciences, pp. 215–250, Vienna: Springer, 2014.

[55] R. Arquier, S. Bellizzi, R. Bouc, and B. Cochelin, "Two methods for the computation of

nonlinear modes of vibrating systems at large amplitudes," *Computers and Structures*, vol. 84, no. 24-25, pp. 1565–1576, 2006. Number: 24-25.

[56] G. Haller and S. Ponsioen, "Nonlinear normal modes and spectral submanifolds: existence, uniqueness and use in model reduction," *Nonlinear Dynamics*, vol. 86, pp. 1493–1534, Nov. 2016.

[57] M. Krack and J. Groß, *Harmonic Balance for Nonlinear Vibration Problems*. Mathematical Engineering, Springer International Publishing, 2019.

[58] C. W. Schwingshackl, D. D. Maio, I. Sever, and J. S. Green, "Modeling and validation of the nonlinear dynamic behavior of bolted flange joints," *Journal of Engineering for Gas Turbines and Power*, vol. 135, no. 12, 2013. Number: 12.

[59] A. H. Nayfeh, *Introduction to perturbation techniques*. New York: Wiley, 1981.

[60] H. Festjens, G. Chevallier, and J.-L. Dion, "A numerical tool for the design of assembled structures under dynamic loads," *International Journal of Mechanical Sciences*, vol. 75, pp. 170–177, 2013.

[61] A. Singh, M. Wall, M. S. Allen, and R. J. Kuether, "Spider Configurations for Models with Discrete Iwan Elements," in *Nonlinear Structures and Systems, Volume 1*, Conference Proceedings of the Society for Experimental Mechanics Series, (Orlando, FL), pp. 25–38, Springer International Publishing, Jan. 2019.

[62] D. A. Najera-Flores and R. J. Kuether, "A Study of Whole Joint Model Calibration Using Quasi-Static Modal Analysis," *Journal of Vibration and Acoustics*, vol. 142, June 2020.

[63] R. Lacayo, B. Deaner, and M. S. Allen, "A Numerical Study on the Limitations of Modal Iwan Models for Impulsive Excitations," *Journal of Sound and Vibration*, vol. 390, pp. 118–140, 2017.

[64] E. J. Berger, "Friction modeling for dynamic system simulation," *Applied Mechanics Reviews*, vol. 55, pp. 535–577, Nov. 2002. Publisher: American Society of Mechanical

Engineers Digital Collection.

[65] R. J. Kuether, P. B. Coffin, and A. R. Brink, "On Hurty/Craig-Bampton Substructuring With Interface Reduction on Contacting Surfaces," in *Proceedings of ASME 2017 International Design Engineering Technical Conferences and Computers and Information in Engineering Conference*, American Society of Mechanical Engineers Digital Collection, Nov. 2017.

[66] R. R. J. Craig and M. C. C. Bampton, "Coupling of Substructures Using Component Mode Synthesis," *AIAA Journal*, vol. 6, no. 7, pp. 1313–1319, 1968. Number: 7.

[67] W. C. Hurty, "Dynamic analysis of structural systems using component modes," *AIAA Journal*, vol. 3, pp. 678–685, Apr. 1965. Number: 4.

[68] R. J. Kuether and M. S. Allen, "Craig-Bamptom Substructuring for Geometrically Nonlinear Subcomponents," Feb. 2014.

[69] D. Krattiger, L. Wu, M. Zacharczuk, M. Buck, R. J. Kuether, M. S. Allen, P. Tiso, and M. R. W. Brake, "Interface Reduction for Hurty/Craig-Bampton Substructured Models: Review and Improvement," *Mechanical Systems and Signal Processing*, vol. 114, pp. 579–605, Jan. 2019.

[70] D. J. Segalman, "Modelling joint friction in structural dynamics," *Structural Control and Health Monitoring*, vol. 13, pp. 430–453, Jan. 2006. Number: 1.

[71] Sierra Structural Dynamics Development Team, "Sierra/SD – User's Manual – 4.56," Tech. Rep. SAND2020-3028, Sandia National Laboratories, Albuquerque, NM, Apr. 2020.

[72] SIERRA Solid Mechanics Team, "Sierra/SolidMechanics 4.56.2 User's Guide," Tech. Rep. SAND2020-5362, Sandia National Laboratories, Albuquerque, NM, May 2020.

[73] Dassault Systèmes, "Abaqus Analysis User's Manual Version 6.14," 2014.

[74] M. Griebel, J. Wilson, A. Johnson, B. Erickson, A. Doan, C. Flanigan, P. Bremner, J. Sills, and E. Bruno, "Orion E-STA Nonlinear Dynamic Correlation and Coupled

Loads Analysis," in *38th International Modal Analysis Conference (IMAC XXXVIII)*, (Houston, Texas), Feb. 2020.

[75] M. S. Allen, J. Schoneman, W. C. M. Scott, and J. W. Sills, "Application of Quasi-Static Modal Analysis to an Orion Multi-Purpose Crew Vehicle Test," in *38th International Modal Analysis Conference (IMAC XXXVIII)*, (Houston, TX), Feb. 2020.

[76] J. T. M. D. Hossen, M. Hadfield, and C. A. Brebbia, *Surface Effects and Contact Mechanics including Tribology XII: Computational Methods and Experiments*. WIT Press, Apr. 2015. Google-Books-ID: 60ycBwAAQBAJ.

[77] C. A. Coulomb, *Théorie des machines simples en ayant égard au frottement de leurs parties et à la roideur des cordages*. Bachelier, 1821. Google-Books-ID: XmQJAAAAIAAJ.

[78] Y. Luan, Z.-Q. Guan, G.-D. Cheng, and S. Liu, "A simplified nonlinear dynamic model for the analysis of pipe structures with bolted flange joints," *Journal of Sound and Vibration*, vol. 331, pp. 325–344, Jan. 2012.

[79] P. R. Dahl, "Solid Friction Damping of Mechanical Vibrations," *AIAA Journal*, vol. 14, no. 12, pp. 1675–1682, 1976. Publisher: American Institute of Aeronautics and Astronautics _eprint: https://doi.org/10.2514/3.61511.

[80] M. Böswald, M. Link, and S. Meyer, "EXPERIMENTAL AND ANALYTICAL INVESTIGATIONS OF NON-LINEAR CYLINDRICAL CASING JOINTS USING BASE EXCITATION TESTING," 2003.

[81] C. Canudas de Wit, H. Olsson, K. Astrom, and P. Lischinsky, "A new model for control of systems with friction," *IEEE Transactions on Automatic Control*, vol. 40, pp. 419–425, Mar. 1995. Conference Name: IEEE Transactions on Automatic Control.

[82] G. M. Jenkins, "Analysis of the stress-strain relationships in reactor grade graphite," *British Journal of Applied Physics*, vol. 13, pp. 30–32, Jan. 1962. Publisher: IOP Publishing.

[83] R. E. Goodman, R. L. Taylor, and T. L. Brekke, "A Model for the Mechanics of Jointed Rock," *Journal of the Soil Mechanics and Foundations Division*, vol. 94, no. 3, pp. 637–659, 1968. Publisher: ASCE.

[84] J. Geisler and K. Willner, "Modeling of jointed structures using zero thickness interface elements," *PAMM*, vol. 7, no. 1, pp. 4050009–4050010, 2007. _eprint: https://onlinelibrary.wiley.com/doi/pdf/10.1002/pamm.200700227.

[85] D. Süß and K. Willner, "Investigation of a jointed friction oscillator using the Multiharmonic Balance Method," *Mechanical Systems and Signal Processing*, vol. 52-53, pp. 73–87, Feb. 2015.

[86] J. C. J. Schellekens and R. D. Borst, "On the numerical integration of interface elements," *International Journal for Numerical Methods in Engineering*, vol. 36, no. 1, pp. 43–66, 1993. _eprint: https://onlinelibrary.wiley.com/doi/pdf/10.1002/nme.1620360104.

[87] W. D. Iwan, "ON DEFINING EQUIVALENT SYSTEMS FOR CERTAIN ORDINARY NONLINEAR DIFFERENTIAL EQUATIONS," *International Journal of Non-Linear Mechanics*, vol. 4, no. 4, pp. 325–334, 1969. Number: 4.

[88] D. J. Segalman, "A Four-Parameter Iwan Model for Lap-Type Joints," *Journal of Applied Mechanics*, vol. 72, pp. 752–760, Sept. 2005. Number: 5.

[89] D. J. Segalman and M. J. Starr, "Iwan models and their provenance," 2012.

[90] D. Shetty, M. S. Allen, and J. D. Schoneman, "Application of the Bouc-Wen Model to Bolted Joint Dynamics," (Houston, TX), Springer International Publishing, Feb. 2020.

[91] R. Bouc, "Forced Vibration of Mechanical Systems with Hysteresis," 1967. Library Catalog: www.semanticscholar.org.

[92] Y.-K. Wen, "Method for Random Vibration of Hysteretic Systems," *Journal of the Engineering Mechanics Division*, vol. 102, no. 2, pp. 249–263, 1976. Publisher: ASCE.

[93] M. Ismail, F. Ikhouane, and J. Rodellar, "The Hysteresis Bouc-Wen Model, a Survey,"

Archives of Computational Methods in Engineering, vol. 16, pp. 161–188, June 2009.

[94] M. Oldfield, H. Ouyang, and J. E. Mottershead, "Simplified models of bolted joints under harmonic loading," *Computers & Structures*, vol. 84, pp. 25–33, Dec. 2005.

[95] Justin H Porter, Nidish N Balaji, C R Little, and Matthew R W Brake, "Quantitative Assessment of the Model Form Error of Friction Models Across Different Interface Discretizations for Jointed Structures," *Mechanical Systems and Signal Processing*, 2021.

[96] M. S. Allen and R. L. Mayes, "Estimating the Degree of Nonlinearity in Transient Responses with Zeroed Early-Time Fast Fourier Transforms," *Mechanical Systems and Signal Processing*, vol. 24, pp. 2049–2064, 2010.

[97] B. J. Deaner, M. S. Allen, M. J. Starr, and D. J. Segalman, "Investigation of Modal Iwan Models for Structures with Bolted Joints," in *Topics in Experimental Dynamic Substructuring, Volume 2*, Conference Proceedings of the Society for Experimental Mechanics Series, (New York, NY), pp. 9–25, Springer, 2014.

[98] D. J. Segalman, "A Modal Approach to Modeling Spatially Distributed Vibration Energy Dissipation," tech. rep., Sandia National Laboratories,, Albuquerque, New Mexico, 2010. SAND2010-4763.

[99] Q. Zhang, R. J. Allemang, and D. L. Brown, "Modal Filter: Concept and Applications," pp. 487–496, 1990.

[100] A. Mathis and D. Quinn, "Analysis of Systems with Generalized Light Damping with Emphasis on Mode Coupling," in *Proceedings of the ASME 2017 International Design Engineering Technical Conferences & Computers and Information in Engineering Conference IDETC/CIE 2017*, (Cleveland, Ohio), Aug. 2017.

[101] B. J. Moldenhauer, A. Singh, P. Thoenen, D. R. Roettgen, B. R. Pacini, R. J. Kuether, and M. S. Allen, "Influences of Modal Coupling on Experimentally Extracted Nonlinear Modal Models," in *Nonlinear Structures and Systems, Volume 1* (G. Kerschen,

M. R. W. Brake, and L. Renson, eds.), Conference Proceedings of the Society for Experimental Mechanics Series, (Orlando, FL), pp. 189–204, Springer International Publishing, Jan. 2019.

[102] Mitchell P. Wall, Matthew S. Allen, and Robert J. Kuether, "Observations of Modal Coupling due to Bolted Joints in an Experimental Benchmark Structure," *Mechanical Systems and Signal Processing*, 2020.

[103] M. Feldman, "Hilbert transform in vibration analysis," *Mechanical Systems and Signal Processing*, vol. 25, no. 3, pp. 735–802, 2011. Number: 3.

[104] H. G. D. Goyder and D. P. T. Lancereau, "Methods for the Measurement of Non-Linear Damping and Frequency in Built-Up Structures," American Society of Mechanical Engineers Digital Collection, Nov. 2017.

[105] B. Moldenhauer, A. Singh, M. S. Allen, and D. Roettgen, "Extensions to a method for characterizing instantaneous frequency and damping of nonlinear systems," in *Proceedings of 39th International Modal Analysis Conference (XXXIX)*, (Orlando, FL), Feb. 2021.

[106] R. J. Kuether, L. Renson, T. Detroux, C. Grappasonni, G. Kerschen, and M. S. Allen, "Nonlinear Normal Modes, Modal Interactions and Isolated Resonance Curves," *Journal of Sound and Vibration*, vol. 351, no. 299-310, 2015. Number: 299-310.

[107] A. F. Vakakis, D. M. McFarland, L. Bergman, L. I. Manevitch, and O. Gendelman, "Isolated Resonance Captures and Resonance Capture Cascades Leading to Single- or Multi-Mode Passive Energy Pumping in Damped Coupled Oscillators," *Journal of Vibration and Acoustics*, vol. 126, no. 2, pp. 235–244, 2004. Number: 2.

[108] Aabhas Singh, Kayla M. Wielgus, Ignazio Dimino, Robert J. Kuether, and Matthew S. Allen, "Nonlinear Dynamic Analysis of a Finger-Like Mechanism for Morphing Wings," in *Proceedings of 39th International Modal Analysis Conference (XXXIX)*, Feb. 2021.

Chapter II

Appended Papers I - V

Experimental Characterization of a new Benchmark Structure for Prediction of Damping Nonlinearity

Aabhas Singh	University of Wisconsin - Madison
Matteo Scapolan	Politecnico di Torino
Yuta Saito	University of Illinois at Urbana–Champaign
Matthew S. Allen	University of Wisconsin - Madison
Daniel Roettgen	Sandia National Laboratories
Ben Pacini	Sandia National Laboratories
Robert J. Kuether	Sandia National Laboratories

ABSTRACT

Spacecraft, airplanes, automobiles, machines and civil structures are all constructed from multiple parts joined by bolts, rivets or other fasteners and these joints lead to large uncertainties in the structural stiffness, damping and can even introduce nonlinearity. Even with the best available simulation tools, it is still difficult to predict the effective stiffness and damping of bolted interfaces, and so these parameters are often assumed and updated after tests have been performed. Damping estimates are critical to limit the resonant vibration response of a structure and thus prevent failure. Even so, it remains poorly understood and available methods for modeling damping are inaccurate and computationally expensive. A new benchmark structure has been created that is designed so as to be predictable with current simulation tools. This paper presents a thorough experimental characterization of this new benchmark structure using the Hilbert transform method applied to modally filtered time data. The nonlinear frequency and damping of each mode is characterized for various levels of bolt preload and excitation amplitude. The interfaces of the bolted structure are also characterized in detail by measuring the contact pressure distribution using pressure sensitive film. The resulting data presents a set of well characterized tests that can be used to validate numerical methods that seek to predict the nonlinear behavior of bolted interfaces.

1 INTRODUCTION

The finite element method has developed to the point that one can now create remarkably accurate and predictive models of parts even with complicated and intricate geometry. However, this is only true so long as they are constructed of a single piece of metal. Interfaces between parts of different materials or the same material lead to large uncertainties. Airplanes, automobiles, machines and civil structures are all constructed from multiple parts joined by bolts, rivets or other fasteners and these joints introduce large uncertainties in the structural stiffness, damping and nonlinearity. Even with the best available simulation tools, it is still difficult to predict the effective stiffness and damping of bolted interfaces, and so often these parameters are assumed and updated after tests have been performed. Damping is critical to limit the resonant response of a structure and thus prevent failure, and yet it remains poorly understood and available methods for modeling damping are inaccurate and computationally expensive.

In recent years, test methods have been developed that can accurately describe the nonlinear stiffness and damping of structures with joints, and these have been used to tune models to measurements up to moderately large amplitudes. Recent experimental works by Roettgen et al. [1], and Deaner et al. [2] show that the modes of a structure with joints can remain uncoupled. This characteristic has been used to test several structures to update the corresponding finite element models to describe the nonlinear effects of the joints. Free response time histories have been used for this purpose to allow quick comparisons between these experimental data and simulations from models using some recently developed signal processing and analysis techniques. The amplitude dependent natural frequencies and damping ratios estimated with the Hilbert transform from experimental data, allowing the models to be calibrated using the analysis proposed by Allen et al., [3] and Festjens et al. [4]. Lacayo [5] has successfully demonstrated this workflow using the Brake-Reuss (BRB) beam. Previous work towards understanding the characteristics of the joint nonlinearity

in the structural dynamic response has proved successful in correlating Iwan models to the nonlinear characteristics of the Brake – Reuss Beam. This benchmark structure has a square cross-section with a three-bolt lap joint at the center [6]. The work in this paper aims to characterize a beam with a simpler two – bolt joint assembly in an effort to create simpler interfaces to investigate the joints influence on the nonlinear stiffness and damping. This new benchmark structure, termed the "S4 Beam", features two bolted interfaces at the ends of two c - shaped beams, designed to model the nonlinear effects of joint bending and shearing in bolted structures. The beam structure is depicted below in Figure 1

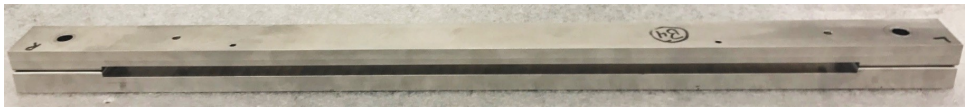

Figure 1: The unbolted S4 Beam

Prior to the characterization the joint, a comprehensive test sequence is developed to understand the effects of bolt torque level, excitation level, and joint interface curvature on the nonlinear dynamics of the structure. Similarly to the BRB, the Hilbert Transform is used on the free response data to detect the degree of nonlinearity [7]. In addition to the nonlinearity, the joint is characterized by measuring the pressure distribution along the surface of the interface through pressure film measurements taken at various torque levels.

2 THEORETICAL BACKGROUND

Experimental modal analysis of a structure is used to identify the linear modal parameters (i.e. shapes, frequencies and damping) of a linear, time invariant system. However, if the system is nonlinear, then nonlinear techniques are needed to characterize the degree of nonlinearity for each mode of the system. In this research, the nonlinearity is characterized numerically using the Hilbert transform. Below is a summary of the Hilbert transform as described by Allen and Roettgen [1].

The Hilbert transform has been widely used for nonlinearity detection for single degree of freedom (SDOF) systems. However, given that the physical measurements ($\ddot{x}(t)$) from accelerometers commonly used in modal testing incorporate coupling when multiple modes are excited for a given input, the measurements are transformed into the modal domain ($\ddot{q}(t)$) using a modal filter to result in modal SDOF systems as described in Kerschen et al. [8]. and as shown in Equation 1.

$$\ddot{x}(t) = \Phi\ddot{q}(t) \longrightarrow \ddot{q}(t) = \Phi^{\dagger}\ddot{x}(t) \tag{1}$$

If the modes can be sufficiently uncoupled, then the envelope of the modal signal for the rth mode can be described as a sum of the decaying harmonic function and its Hilbert transform as given by Equation 2.

$$Q_r(t) = q_r(t) + i\tilde{q}_r(t) \tag{2}$$

where $\tilde{q}_r(t)$ is the Hilbert transform of the signal and $Q_r(t) = A(t)\exp(i\psi t)$. $A(t)$ denotes the magnitude of the envelope as given by $A(t) = \sqrt{q_r(t)^2 + \tilde{q}_r(t)^2}$ and $\psi(t)$ represents the instantaneous phase of the modal response as given by $\psi(t) = \tan^{-1}\frac{\tilde{q}(t)}{q(t)})$ [9]. Equation2 is depicted in terms of modal displacement amplitude, but can also be applied to modal velocity and acceleration amplitude as governed by

$$|q_r| = \frac{|\dot{q}_r|}{\omega_r} = \frac{|\ddot{q}_r|}{\omega_r^2} \tag{3}$$

The objective is to describe the nonlinear damping and stiffness as a function of peak velocity

amplitude such that type of nonlinearity can be described with the increase in amplitude. As a result, the instantaneous damped natural frequency can be described as the time derivative of the instantaneous phase and the instantaneous damping can be calculated from the time derivative of the amplitude as shown below

$$\omega_{r_{damped}} = \frac{d\psi(t)}{dt}$$

$$-\omega_r \zeta_r = \frac{dA(t)}{dt}$$

where ω_r is the natural frequency as governed by $\omega_r = \omega_{r_{damped}}/\sqrt{1-\zeta^2}$. However, given that experimental data yields discrete points, the data is fit with a spline with 50 points (knots). An in-depth discussion of the derivation of the Hilbert transform can be found in Feldman [10].

3 EXPERIMENTAL METHODOLOGY

The work presented in this paper was conducted on two C-shaped beams manufactured with Stainless Steel type ANSI 304. The two beams before and after assembly with two bolted connections at the ends are shown in Figure 2 Each beam is 20 inches long, with two 2" x 1.25" contact surfaces. Each beam is 0.5" tall at the contact surface, and 0.38" elsewhere. All dimensions on the beam were manufactured with a 0.005" tolerance. Two different sets of beams were manufactured with variable surface conditions at the bolted interfaces: (1) convex interface with a center to edge drop of 0.005" to 0.008", and (2) flat interface as shown below. All contact surfaces were polished to a minimum surface finish of

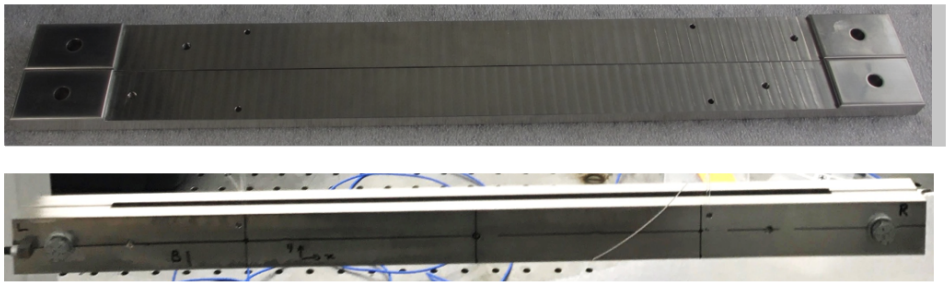

Figure 2: Two separate beam halves of the S4 Beam (top) and the assembled beam (bottom)

$Ra = 8$. Prior to modal testing, four configurations of beams were assembled as indicated

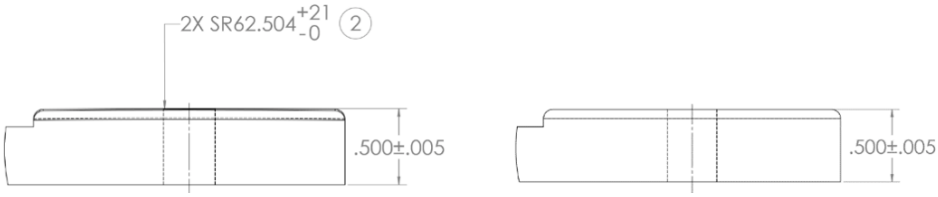

Figure 3: Drawing of the convex (left) and flat (right) interfaces

in Figure 4. B1-B2 features an interface of two convex surfaces in contact. This contact was modified slightly by placing thin stainless-steel washers at the interface for B1-B2W, in an effort to move the contact pressure distribution further away from the bolt holes. In B1-B6, the contact was such that a convex surface is mated with a flat surface. The flat-flat surface case is examined with B5-B6. All beams were assembled by 5/16"-24 bolts and nuts, and type – A washers.

3.1 Impact Hammer Testing

Modal testing of the S4 Beam was accomplished by hanging the assembly using bungee cords and fishing line to emulate "free–free" boundary conditions with as little impact on the dynamics of the system as possible. Discrete points along the beams were excited by an impact hammer to obtain the linear mode shapes (at low impact amplitudes) and nonlinear time histories (at higher amplitudes) for the nonlinear system parameter identification. The

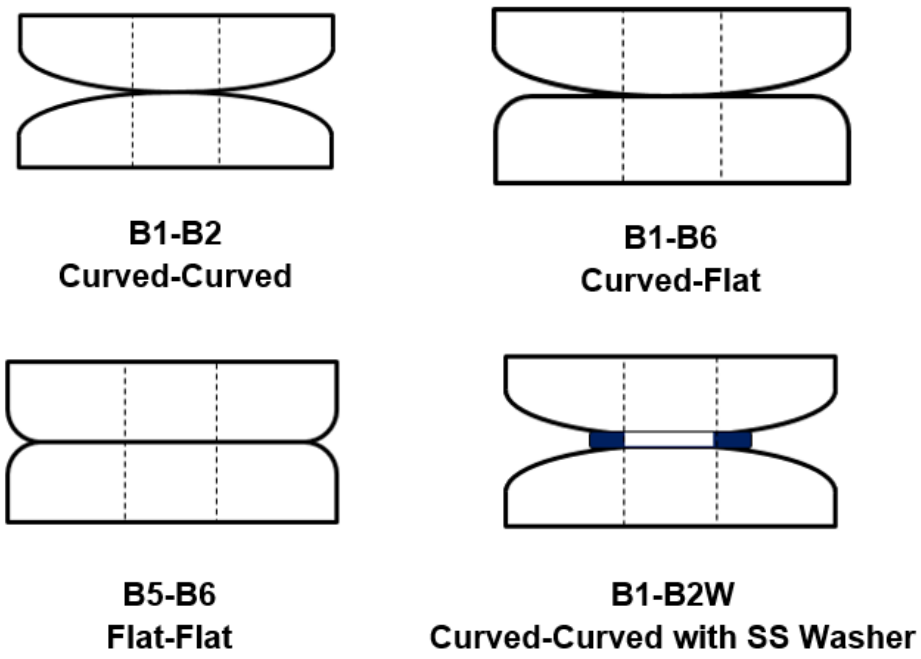

Figure 4: Combinations of beams and their corresponding contact surfaces

bolted beams were tested at three torque levels: 10.2 N-m, 16.9 N-m, and 25.1 N-m to evaluate the effect of preload, and four input forces 10 N, 100 N, 250 N, and 500 N to assess the effect of input force on the joint nonlinearity. The experiment was then repeated for the four combinations of beams.

Prior to commencing testing at all torque and impact levels, the optimal setup was found to minimize the cable damping, and hence the number of accelerometers necessary to capture the desired mode shapes. This optimization process was carried out by progressively increasing the number of accelerometers and checking experimental natural frequencies and modal damping. Small variations with respect to a setup with a minimum number of accelerometers indicated that the added sensors did not significantly influence the structure. Cables were taped to the beam, as it was found that it mitigated additional damping to the system in these conditions. In this phase, prior to nonlinear data collection, the interest was not in the mode shapes, but rather in the natural frequencies and damping ratios, so that

the setup with a minimum number of sensors was used as a reference to evaluate structural effects (mass and damping) of the accelerometers on the beam.

The first six elastic mode shapes for B1-B2 are reported in Figure 5 and were considered the target modes when defining the accelerometer placement.

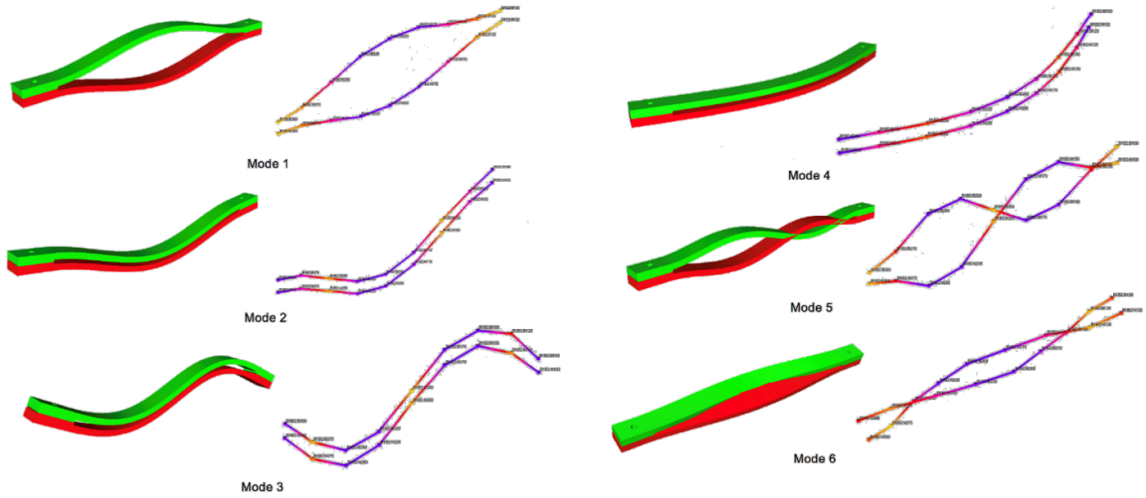

Figure 5: Linear elastic mode shapes of the S4 Beam

Figure 6 depicts the optimal sensor setup for B1-B2, which was then replicated for the three other combinations. Accelerometer locations were chosen to obtain completely observable modes in the bandwidth of interest. Input locations were similarly selected such that for each mode there was at least one point efficiently exciting the mode. As a result, the final setup consisted of ten accelerometers, with nine tri-axial and one uniaxial, for a total of 28 output channels. Additional optimization was done using a roving hammer test to evaluate the ideal input locations as depicted in Appendix A. To capture the first six elastic modes, the test bandwidth was limited to 800 Hz based on the preliminary modal simulation of the finite element model. The data acquisition was performed by Siemens LMS Test Lab and LMS SCADAS system.

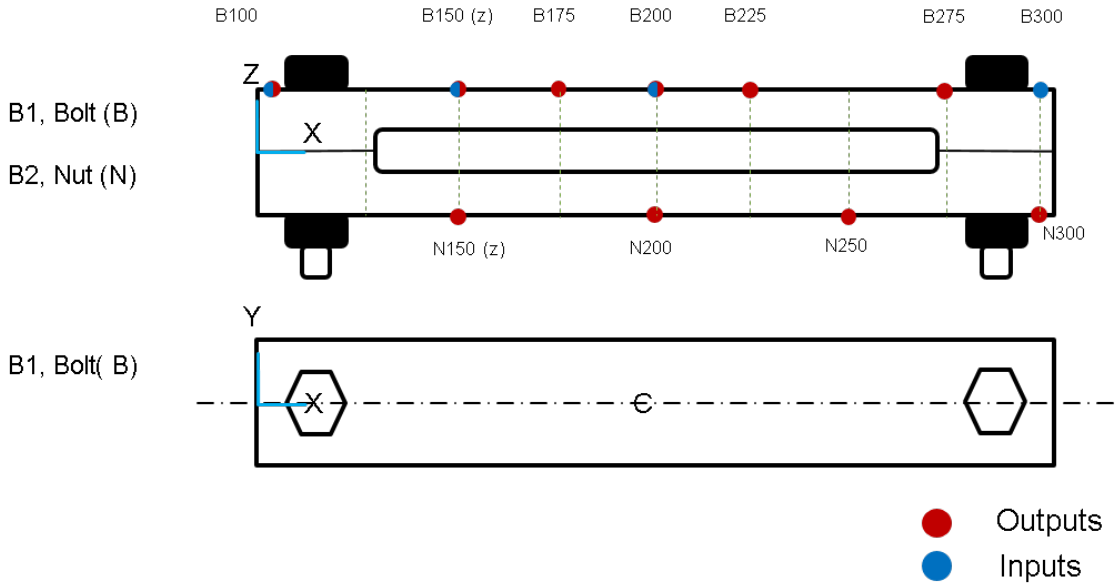

Figure 6: Optimal test setup

3.2 Joint Profile Testing

In order to capture the change in the joint characteristics due to the change in torque, the two contact areas of the beams were characterized with normal contact pressure measurements using Fujifilm Prescale pressure films. Three film types were used to capture different pressure ranges for all torque levels as depicted in Table 1. The films were placed between the two contacting surfaces as the beams were fastened with two bolts up to the prescribed torque level. Following the preload, the beams were held together for two minutes before loosening the bolts and removing the pressure film. The experiment was repeated for all three torque levels and all beam sets.

Table 1: Film types and corresponding pressure ranges

Film Type	Pressure Range [MPa]
Low	2.41-9.65
Medium	9.65 – 48.95
High	48.95 – 127.55

4 EXPERIMENTAL RESULTS

Three types of data were collected during the experiments: (1) joint pressure distributions, (2) frequency response functions (FRFs), and (3) time histories. The pressure film results were used to qualify the influence of the pre-stress on the joint interface due to the torque. The FRFs were used to determine the linear mode shapes and linear modal parameters, whereas the time histories were used to determine the nonlinear characteristics of the beam. For the subsequent discussion, beam sets B1-B2 and B5-B6 were mainly analyzed with respect to pressure distribution, torque level, and impact level.

4.1 Interface Characterization

The pressure film measurements of the three torque cases for different contact surface combinations are summarized below in Figures 7 to 9. The B1-B2 (convex-convex) case had a high concentration of pressure at the proximity of the through hole and showed small changes in pressure areas across the film due to the change in torque levels. As an intermediate between a spherical interface and a flat interface, the B1-B6 (convex-flat) case was similar to the previous case with a concentration of pressure near the hole, but with a larger contact area. In contrast, the B5-B6 (flat-flat) case showed a significant amount of pressure saturation with low to medium pressure readings across most of the film. This suggests that the B1-B2 (convex-convex) should have the smallest contact area, whereas B5-B6 (flat-flat) should have the largest. The pressure readings and contact area decreased for all contact surface combinations as the value of the preload torque was decreased on the joint. It is worth pointing out that the B5-B6 (flat-flat) showed the most dramatic reduction in pressure readings compared to the other cases.

To understand the correlation between the pressure readings across the joint and the structural response of the assembly, the change in the linear natural frequency with respect to varying torque levels was examined for the three contact surface combinations. Table 2

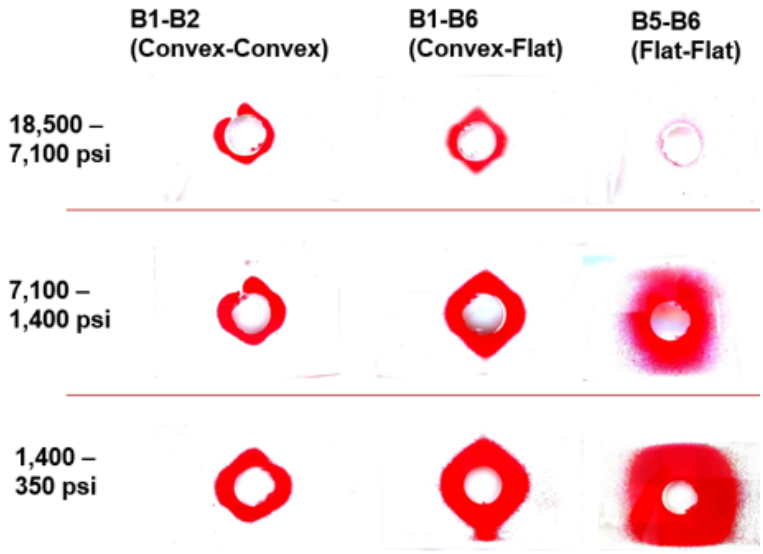

Figure 7: Pressure film measurement at 25.1 N-m torque

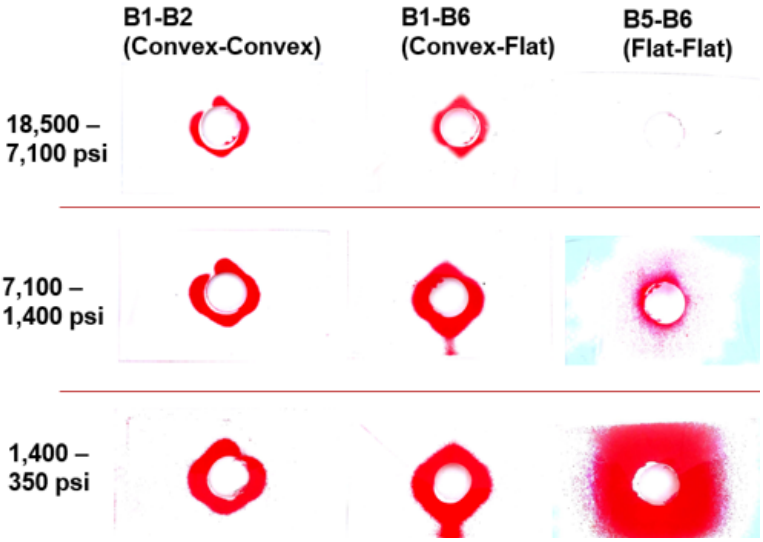

Figure 8: Pressure film measurement at 16.9 N-m torque

summarizes the linear natural frequency of the first six modes for the three contact surface combinations at varying torque levels.

Modes 2, 3, and 4 show similar linear natural frequency values for any torque level or contact surface combination, concluding that the stiffness of these modes is not affected by the joint. Since the ends of the beams deflect parallel to each other at the joints, the influence

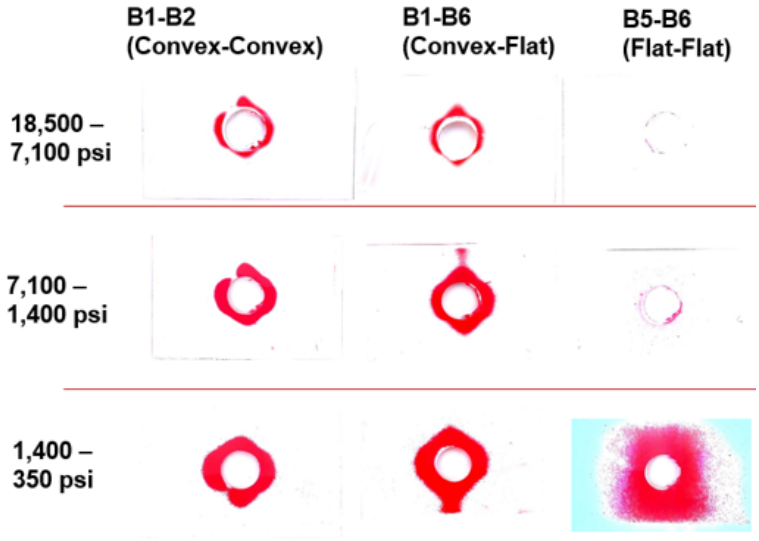

Figure 9: Pressure film measurement at 10.2 N-m torque

of the joint characteristics to the structural response of the assembly due to varying contact conditions is mitigated. However, Mode 2 is a possible exception to this rule, since bending in this shape induces a shear stress onto the bolted interfaces.

In contrast, for the mode shapes with tensile loads or breathing of the joint, and with shearing of joints (Modes 1, 5, and 6), the structural response of the assembly demonstrated a strong correlation to the varying joint characteristics. Figure 10 shows the plot of the natural frequencies of Modes 1 and 5 as the torque is varied. It seems reasonable that both of these modes show identical trends since they have tensile loads at the joints and exhibit joint breathing. In addition, for a constant torque level, Mode 6 for the flat – flat configuration (B5-B6) depicts a frequency shift of 150 Hz in comparison to B1-B2 as a result of the flat interface.

These observations follow the results of the pressure film measurements in Figures 7 - 9, where B5-B6 (flat-flat) case has a larger contact area at all torque levels compared to the other two cases. At 10.2 N-m torque, B1-B2 (convex-convex) case shows a similar contact area to the B1-B6 (convex- flat) case, but a higher pressure reading since the pressure is

Table 2: Linear natural frequencies (Hz) of the assembly vs bolt torque

Mode	B1-B2 (convex-convex)			B1-B6 (convex-flat)			B5-B6 (flat-flat)			Mode Type
	10.2	16.9	25.1	10.2	16.9	25.1	10.2	16.9	25.1	
	[N-m]	[N-m]	[N-m]	[N-m]	[N-m]	[N-m]	[N-m]	[N-m]	[N-m]	
1	235.2	237.3	239.7	233.9	237.8	240.3	253	256.4	258.6	1st out of phase bending - Z
2	327.8	328.5	329.1	326.4	327.3	327.8	330.3	331	331.8	1st in phase bending - Z
3	483.7	483.7	483.7	481.6	481.6	481.8	478.7	478.5	478.5	2nd in phase bending - Z
4	570.5	570.6	570.7	568.8	568.7	569.3	568	567.6	567.4	1st in phase bending - Y
5	641.4	647.1	653.6	638.1	648.2	655.4	693.2	703.5	710	2nd – out of phase bending - Z
6	655.6	672.2	686.5	655	682.2	696.8	823.4	841.4	854.8	1st – out of phase bending - Y

concentrated near the bolt, resulting in stiffer joint. As the torque is increased, the contact area of the B1-B6 (convex-flat) case exceeds the B1-B2 (convex-convex) case, and therefore a higher stiffness at these torque levels. It is also interesting to note that the natural frequency is measurably sensitive to the bolt torque even for B1-B2 and B1-B6, even though the contact pressure distributions shown previously suggested that the contact area changed very little for these structures.

Figure 11 shows the case of Mode 6, which involves rotational shearing at the joints. Mode 6 follows an almost identical trend to the previous comparison where the B5-B6 (flat-flat) case has a significantly higher natural frequency across the torque level compared to the other contact surface combinations and B1-B6 (convex-flat) has a higher natural frequency

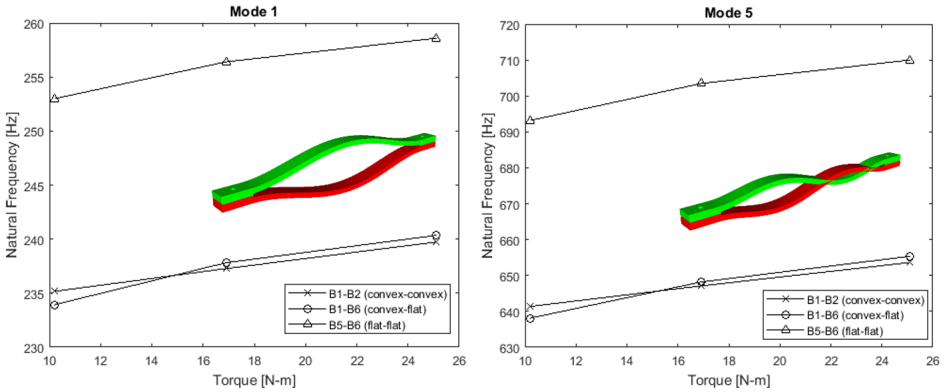

Figure 10: Linear natural frequency of Modes 1 (left) and Mode 5 (right)

at 16.9 N-m and 25.1 N-m torque levels.

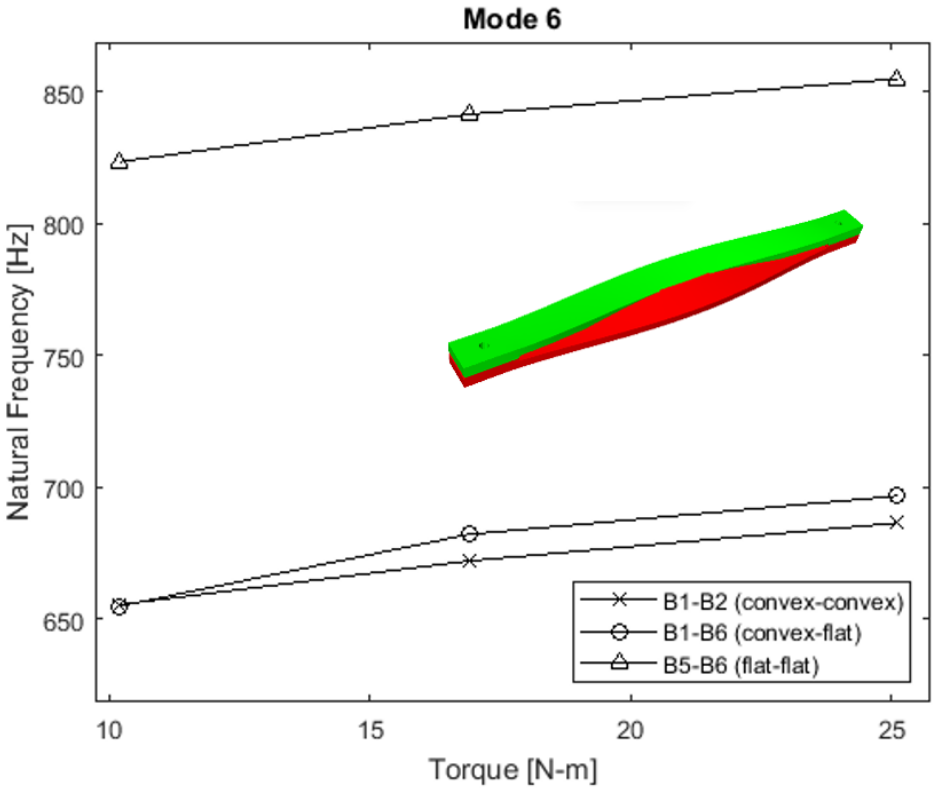

Figure 11: Linear natural frequency of Mode 6

To evaluate the repeatability and accuracy of the linear analysis, the most linear case

where the structure is assembled with the largest torque (25.1 Nm) and impacted at the lowest excitation level is examined. A larger torque should produce less slipping along the contact interface, therefore less friction and nonlinearity. The linear resonance frequencies for the two extreme configurations (convex–convex, flat–flat), are depicted below in Table 3 with the percent variation from the average value for the natural frequency. The variation in frequency was computed through multiple measurements to ensure that the beam had repeatable results within a single test setup.

Table 3: Natural frequencies (Hz) and percent variation at a 25.1 Nm torque

Mode	**B1-B2**	**B5-B6**
1	239.1 (+1.92%)	258.0 (+1.98%)
2	328.6 (0.34%)	331.7 (+0.42%)
3	483.5 (-0.02%)	478.5 (-0.04%)
4	570.7 (+0.05%)	567.7 (-0.05%)
5	652.4 (+1.94%)	708.3 (+2.16%)
6	683.8 (+4.73%)	851.8 (+3.14%)

Though the repeatability resulted in frequency disparities, all remained within 5% variance. Next, the Hilbert transform can be used on the decoupled modes to identify the nonlinearities in select modes.

4.2 Nonlinearity Detection and Analysis

FRFs are used to qualitatively determine which modes exhibited nonlinearity. To do this, the FRFs were compared between each beam combination and between different torque levels and different force amplitudes. This comparison is only qualitative, since the amplitude-varying, and hence time varying modal properties are all convolved into a single FRF. In the following subsection, the time histories will be used to quantitatively identify the non-

linearities in those modes that exhibited significant nonlinearity. Within the first six linear elastic modes, three modes of interest were chosen based on the behavior of the joint as well as the degree of nonlinearity in response to a larger excitation. Figure 12 depicts the cumulative summation of all FRFs for the four levels of excitation at the middle torque level (16.9 Nm) for the B1-B2 (convex-convex) beam, and Figure 13 shows the results for the B5-B6 (flat-flat) beam.

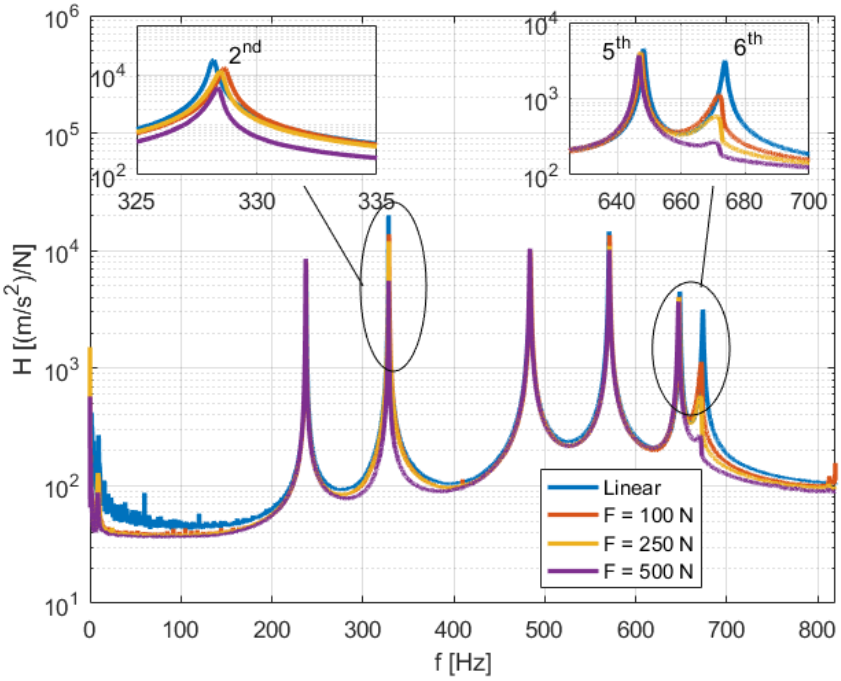

Figure 12: Amplitude and force variation for B1-B2 for 16.9 Nm Torque

As evident by both beam configurations, mode six exhibits a large degree of damping nonlinearity as depicted by the widening of the peak and drop in amplitude. Therefore, it is a mode of interest to identify this damping nonlinearity using the Hilbert transform algorithm. To help explain why each mode does or does not exhibit significant nonlinearity, Table 4 describes the effect that each mode shape is expected to have on the joint.

The Hilbert transform analysis results for the fundamental mode of the system are not

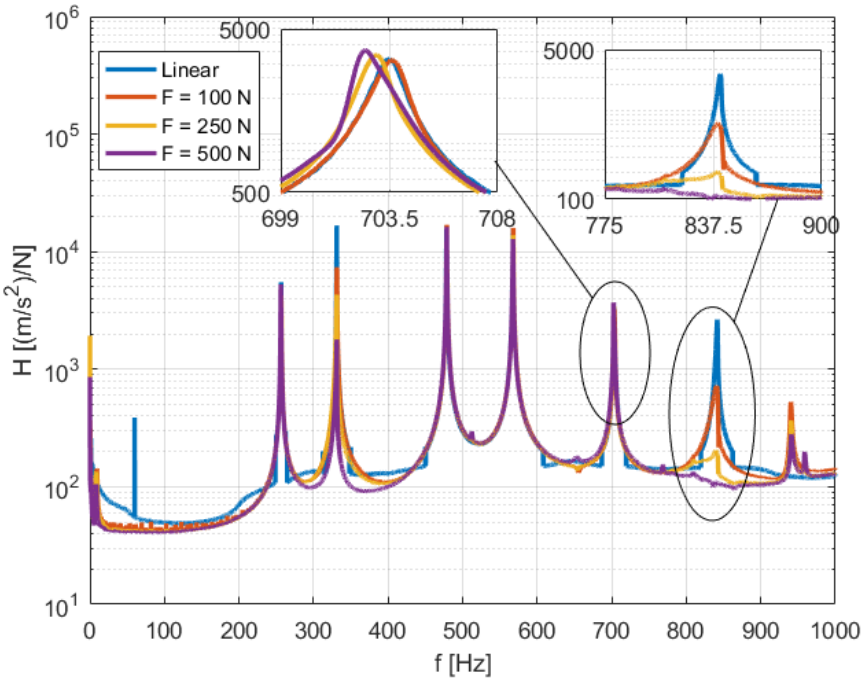

Figure 13: Amplitude and force variation for B5-B6 for 16.9 Nm Torque

Table 4: Beam motion and joint behavior

Mode	Description	Joint Behavior
1	1st out of phase bending - Z	Opening/closing of the joint
2	1st in phase bending - Z	Shearing of the joint
3	2nd in phase bending - Z	None
4	1st in phase bending - Y	None
5	2nd – out of phase bending - Z	Opening/closing of the joint
6	1st – out of phase bending - Y	Rotational shearing of the joint

shown here. It exhibits the breathing of the joint which results in a weak stiffness nonlinearity, with no significant change in damping due to micro-slip.

Modes 2 and 6 are further analyzed in this section since both modes produce shearing at the joint and hence produce damping nonlinearity. Therefore, to evaluate the degree of nonlinearity of each mode with respect to the lowest torque, the Hilbert transform was used

to find the damping and frequency variation as a function of peak velocity amplitude. The frequency variation is depicted as a percent change from the linear natural frequency. Prior to examining additional trends for torque, impact, and configuration of the beams, the results for mode six are depicted in detail in Figures 4.8 and 4.9 for the two different configurations at the lowest torque. Given that multiple points can efficiently excite each mode, these results are based on the analysis of the data at B200Y, the center of the beam. The horizontal axis in each of these plots is the peak amplitude, here defined as the amplitude at the point on the beam that has the largest motion for the mode of interest. In each response, the system is expected to behave linearly, although the measured signals become noisy at very low amplitudes leading to spurious oscillations in the measurements. At higher amplitudes the nonlinearity is evident.

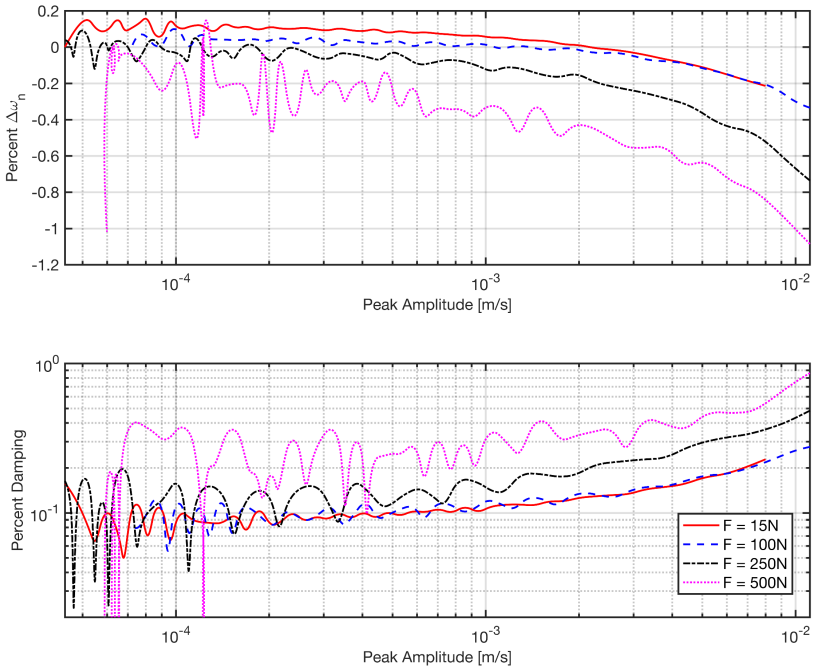

Figure 14: Natural frequency and damping versus amplitude for Mode 6 at 10.2 Nm torque for B1-B2 using B200Y as the drive point

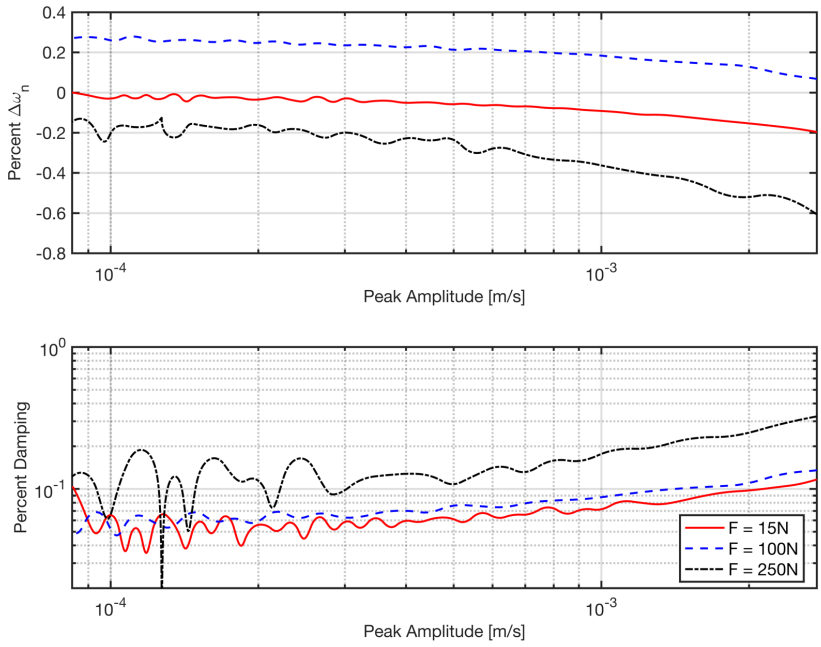

Figure 15: Natural frequency and damping versus amplitude for Mode 6 at 10.2 Nm torque for B5-B6 using B200Y as the drive point

The results show that B5-B6 did not always return to the same linear natural frequency when larger forces were applied. This suggests that some change has occurred at the interface due to the vibration, and potentially calls the measurements into question. This is surprising because the joints were "broken in" prior to the tests by tapping the beam many times with a rubber mallet. No result is shown for mode six at an impulse of 500 N for B5-B6. This is because the mode became so heavily damped that Hilbert transform analysis was no longer possible. The smoothness of the damping versus amplitude curves at low force levels suggests that the nonlinearity is weak and the joints are in a state of micro-slip. However, at greater excitation levels the modal behavior does not follow the same trend, suggesting either that macro-slip has occurred or that this mode has become coupled to other modes in the structure. The remainder of the analysis presented below shows only those cases that seem to be dominated by micro-slip, because only those cases have the weak modal coupling

necessary for the Hilbert transform analysis to be valid.

The following four figures examine modes two and six for both configurations of beams at various drive points. A single drive point is capable of exciting multiple modes, which can then induce additional modal coupling. However, the results in [6] suggest that the curve with the lowest damping should be a good estimate for the damping due to that mode alone. Table 5 gives the drive points used for each mode in this analysis.

Table 5: Drive point used for each mode

Mode	**Drive Point**	**Description**
2	B100 – Z	Left end of beam
	B200 – Z	Center of beam
	B300 – Z	Right end of beam
6	B100 – Y	Left end of beam
	B200 – Y	Center of beam

Neglecting the scatter in the data at low amplitudes, the different drive points produced relatively similar trends. For modeling purposes, the results of the center drive point, B200-Z and B200–Y should be used for both modes for both configurations. The other drive points either do not excite the beam well or introduce additional modal coupling. To understand the percent variation of the damping and frequency, Table 6 depicts the maximum deviation for the two modes of interest.

In both cases for mode six, the percent damping of the mode increased extensively, depicting a large damping nonlinearity for the mode with much smaller stiffness nonlinearity. In addition, the force varying Hilbert transform curves for mode six for the largest torque (25.1 Nm) are also shown below.

Even at the largest torque with the stiffest joint, mode six exhibits large stiffness and damping nonlinearities. At 500N, mode six seems to exhibit macro-slip as seen by the erratic

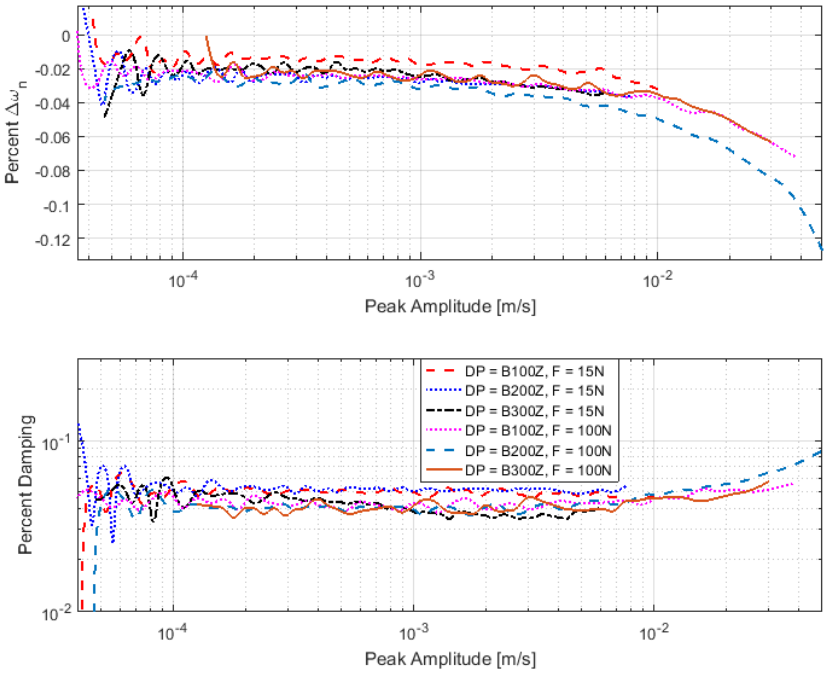

Figure 16: Natural Frequency and damping versus amplitude for Mode 2 at 10.2 Nm torque for B1-B2

Table 6: Drive point used for each mode

Beam	Mode	Max Freq. Change	Max Damping Change	Type of NL
B1-B2	2	-0.14%	148%	Damping NL
	6	-0.33%	582%	Damping NL
B5-B6	2	-0.08%	95%	Damping NL
	6	-0.26%	316%[1]	Damping NL

deviating trend from the other impulse levels, and so that data should be used appropriately.

In an effort to classify the linearity of the four configurations, the variance of frequency and damping for each beam set was analyzed at an intermediate force (100 N) and both the lowest and highest torque to lightly excite the nonlinearity. Figure 22 depicts the results of this comparison.

Between the four beam sets, the convex beam set and the convex – flat set are classified

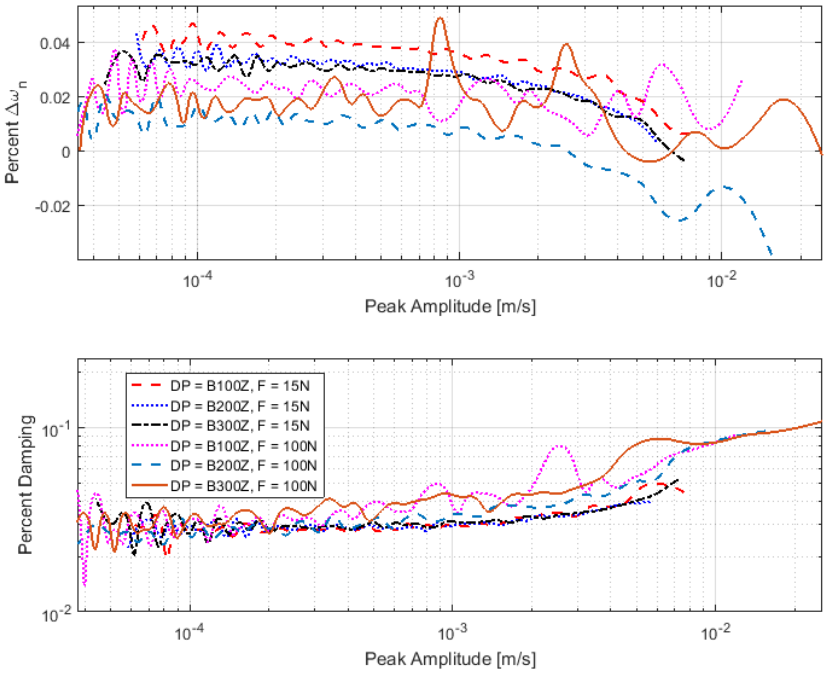

Figure 17: Nat. Freq. and Damping versus amplitude for Mode 2 at 10.2 Nm torque for B5-B6

in the same "family" due to similar modal frequencies, whereas the other two sets are in the same "family" of beams. The washer configuration and flat–flat configuration had similar resonant frequencies, whereas the convex–flat and convex beams had similar resonances. In terms of damping for the lowest torque, the beams can be classified from relatively linear to significantly nonlinear based on the damping variance as given: (1) convex–convex with washer (B1-B2W), (2) convex–convex (B1-B2), (3) convex–flat (B1-B6), and (4) flat–flat (B5-B6). However, at the higher torque, the beams show variable trends with respect damping, yielding it difficult to classify the beams. Even though the slip is restricted at the higher torque, the pressure in the contact surface increases, requiring the same energy dissipation as with lower torque; therefore, additional torque does little to impact the nonlinearity in the joint.

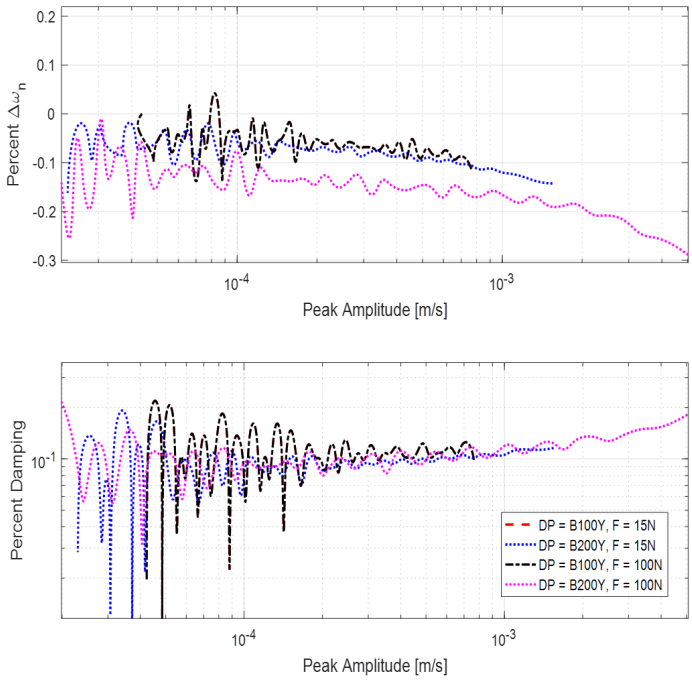

Figure 18: Nat. Freq. and Damping versus amplitude for Mode 6 at 10.2 Nm torque for B1-B2

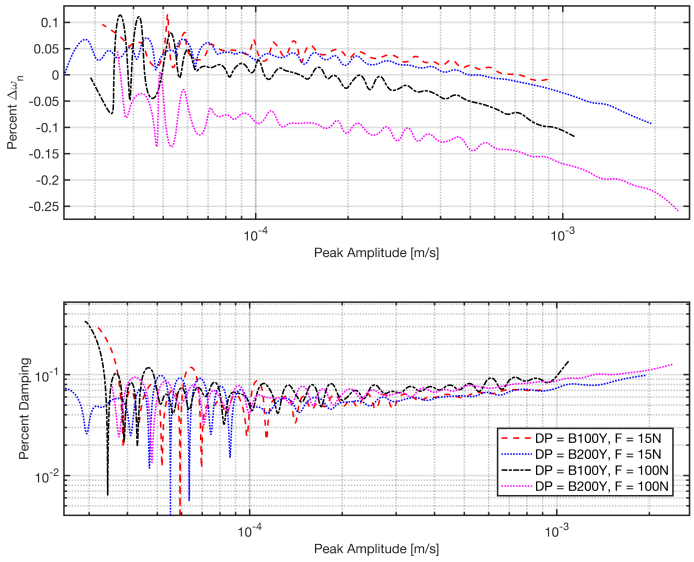

Figure 19: Nat. Freq. and Damping versus amplitude for Mode 6 at 10.2 Nm torque for B5-B6

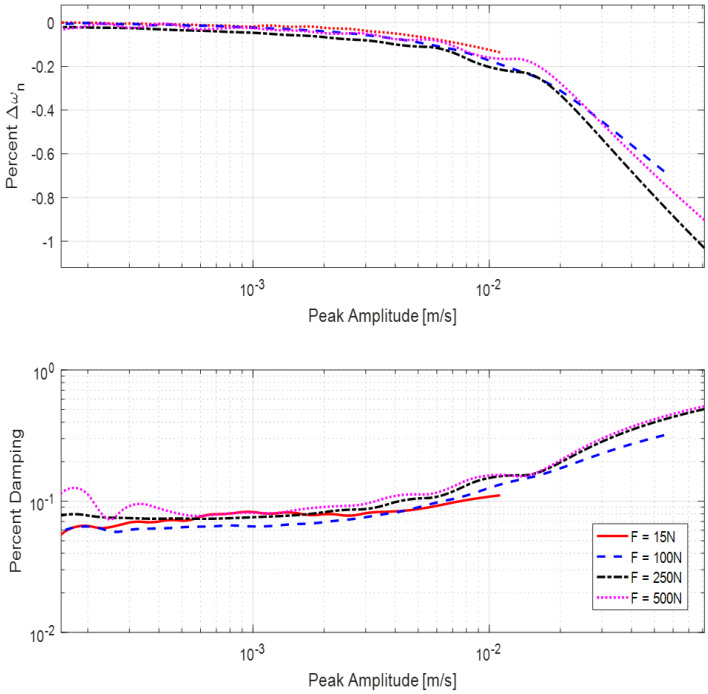

Figure 20: Nat. freq. and damping versus amplitude for Mode 6 at 25.1 Nm torque for B1-B2

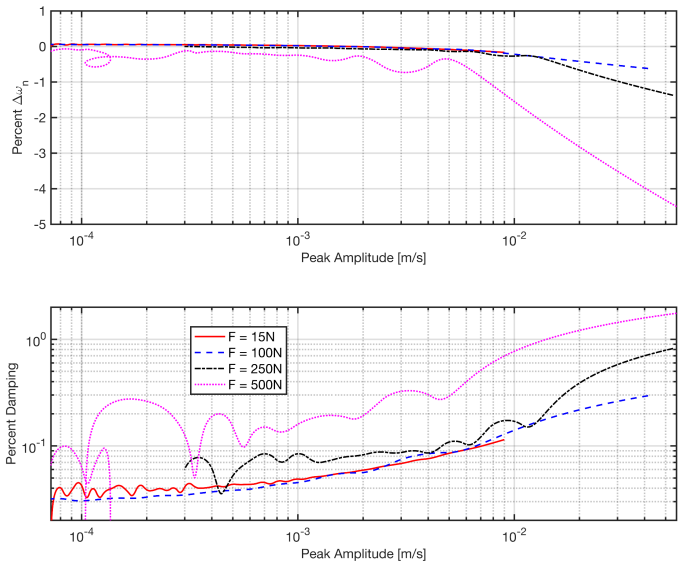

Figure 21: Nat. freq. and damping versus amplitude for Mode 6 at 25.1 Nm torque for B5-B6

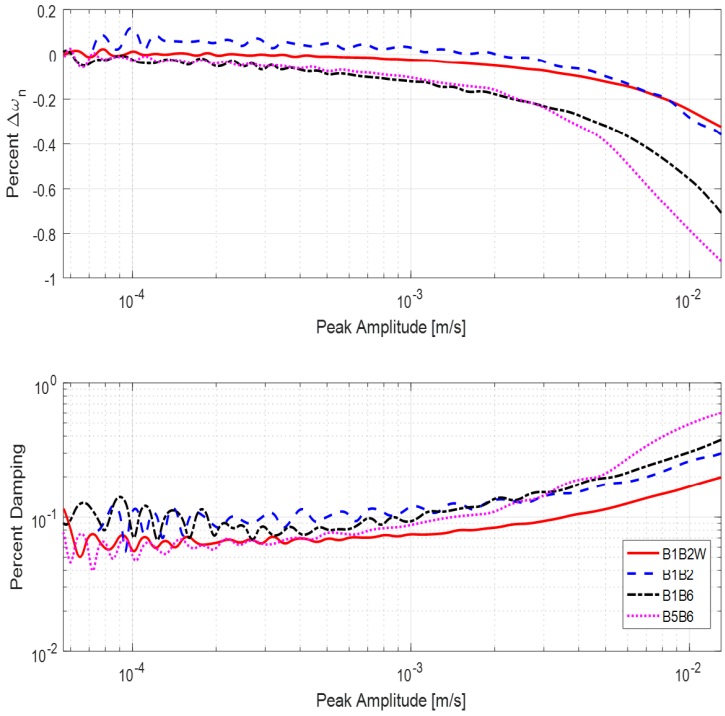

Figure 22: Comparison of frequency and damping across the different beam combinations for an intermediate force level and the lowest torque

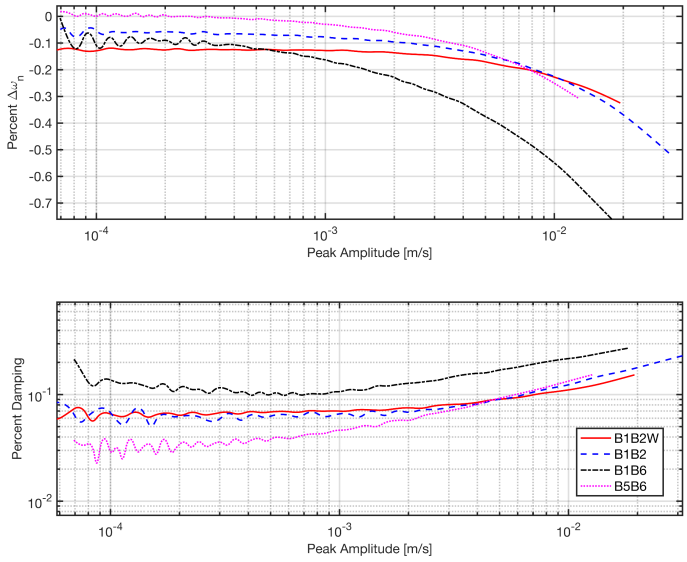

Figure 23: Comparison of frequency and damping across the different beam combinations for an intermediate force level and the highest torque

5 CONCLUSION

This work sought to characterize a new benchmark structure and to provide a rich data set against which simulations may be compared when seeking to predict damping nonlinearities. The S4 beam, consisting of two C beams bolted together at the ends, was tested and the first six elastic modes, all below 800 Hz were characterized both linearly and nonlinearly. The pressure distributions were characterized and qualitatively correlated to variations in the linear natural frequencies and in the nonlinearity observed. As in other studies, those modes that exhibited shearing of the joint yielded as the strongest nonlinearity with respect to damping. In general, none of the modes showed large stiffness nonlinearities even though the damping of some modes changed by a factor of five or more. Between the four configurations of beams, the beams that had flat interfaces depicted the largest damping nonlinearity with a 316% increase in damping for the second largest impact excitation level, the highest that could be reliably characterized. On the other hand, the curved beams with a washer depicted the least damping nonlinearity. Although the testing was judged successful, throughout the process of nonlinear model identification, some lessons were learned that could improve the results in future testing. Most importantly, the sample rate chosen was barely adequate, and while the LMS system was not able to take longer time records in FFT mode, throughput mode should have been used so that the modal hammer impacts could be captured more accurately and then it might have been possible to use alternate identification methods such as the Restoring Force Surface Method as an additional method to characterize the joint [8]. Furthermore, a shaker or automatic hammer could provide additional accuracy when compared to a modal hammer. Lastly, it was sometimes noted that if the modal filtered response was not a SDOF system with a single mode, the results of the Hilbert transform for frequency and damping were erratic, impeding the proper fit of the data. Perhaps the modal filter used for this system could have been improved by testing at even lower levels than was used here (i.e. perhaps using higher sensitivity sensors) to extract the

mode shapes more accurately. In any event, this beam provides a significant data set that can now be used to validate numerical predictions of damping. Given that the beam exhibits modes with all degrees of damping nonlinearities, the beam should provide a good test case for numerical methods.

ACKNOWLEDGEMENTS

This research was conducted at the 2017 Nonlinear Mechanics and Dynamics (NOMAD) Research Institute supported by Sandia National Laboratories. Sandia National Laboratories is a multi-mission laboratory managed and operated by National Technology and Engineering Solutions of Sandia, LLC., a wholly owned subsidiary of Honeywell International, Inc., for the U.S. Department of Energy's National Nuclear Security Administration under contract DE-NA-0003525.

REFERENCES

[1] D. R. Roettgen and M. S. Allen, "Nonlinear characterization of a bolted, industrial structure using a modal framework," *Mechanical Systems and Signal Processing*, vol. 84, pp. 152–170, 2017.

[2] B. Deaner, M. S. Allen, M. J. Starr, D. J. Segalman, and H. Sumali, "Application of Viscous and Iwan Modal Damping Models to Experimental Measurements From Bolted Structures," *ASME Journal of Vibrations and Acoustics*, vol. 137, p. 12, 2015.

[3] M. S. Allen, R. Lacayo, and M. R. Brake, "Quasi-static Modal Analysis based on Implicit Condensation for Structures with Nonlinear Joints," Sept. 2016.

[4] H. Festjens, G. Chevallier, and J.-L. Dion, "A numerical tool for the design of assembled structures under dynamic loads," *International Journal of Mechanical Sciences*, vol. 75, pp. 170–177, 2013.

[5] R. M. Lacayo, *AN INVESTIGATION ON IWAN MODELS FOR CAPTURING*

THE AMPLITUDE-DEPENDENT BEHAVIOR OF STRUCTURES WITH BOLTED JOINTS. PhD thesis.

[6] M. S. Bonney, B. A. Robertson, M. Mignolet, F. Schempp, and M. R. Brake, "Experimental Determination of Frictional Interface Models," in *Dynamics of Coupled Structures, Volume 4* (M. Allen, R. L. Mayes, and D. Rixen, eds.), Conference Proceedings of the Society for Experimental Mechanics Series, (Cham), pp. 473–490, Springer International Publishing, 2016.

[7] T. Dossogne, T. Jerome, D. Lancereau, S. Smith, M. Brake, B. Pacini, P. Reuss, and C. Schwingshackl, "Experimental Assessment of the Influence of Interface Geometries on Structural Dynamic Response," pp. 255–261, Apr. 2017.

[8] G. Kerschen, K. Worden, A. F. Vakakis, and J.-C. Golinval, "Past, present and future of nonlinear system identification in structural dynamics," *Mechanical Systems and Signal Processing*, vol. 20, pp. 505–592, 2006.

[9] R. Lacayo, B. Deaner, and M. S. Allen, "A Numerical Study on the Limitations of Modal Iwan Models for Impulsive Excitations," *Journal of Sound and Vibration*, vol. 390, pp. 118–140, 2017.

[10] M. Feldman, "Hilbert transform in vibration analysis," *Mechanical Systems and Signal Processing*, vol. 25, no. 3, pp. 735–802, 2011. Number: 3.

Influences of modal coupling on experimentally extracted nonlinear modal models

Benjamin Moldenhauer	University of Wisconsin - Madison
Aabhas Singh	University of Wisconsin - Madison
Phil Thoenen	University of Southern California
Matthew S. Allen	University of Wisconsin - Madison
Daniel Roettgen	Sandia National Laboratories
Ben Pacini	Sandia National Laboratories
Robert J. Kuether	Sandia National Laboratories

ABSTRACT

Research has shown that mechanical structures can be modeled as a combination of weakly nonlinear uncoupled modal models. These modal models can take many forms such as a basic cubic stiffness and damping force model, or a modal Iwan model. This method relies on two assumptions: 1) the mode shapes of the structure are not amplitude dependent, and 2) the modes of the structure do not couple or interact in the amplitude range of interest. Recently, a hypothesis was proposed that when multiple modes are excited that exercise the same nonlinear joint, the modes begin to couple. This hypothesis is tested on a physical system using a series of narrow-band excitation techniques via a modal shaker and broad-band excitation from a modal hammer. The resulting amplitude dependent stiffness and damping from the various excitation types are used to characterize the degree of modal coupling. Significant modal coupling is observed between three of the low order modes of a cylindrical structure with a beam connected to a plate on its end, which exhibits nonlinearity due to micro-slip in bolted joints.

1 INTRODUCTION

Mechanical structures with jointed interfaces are common in modeling and design due to ease of assembly and the difficulty in producing single part structures. These jointed interfaces introduce nonlinearity to structural dynamic response in the form of frictional energy dissipation caused by microslip in low pressure contact regions. This behavior affects the frequency and damping characteristics observed in the mechanical response of the global system, which is difficult to model and requires advanced computational and experimental techniques to characterize. Modal analysis is the most utilized approach for non-destructive experimental testing to determine natural frequencies and damping ratios of built-up systems. For linear analysis, it is proven that the modes of vibration are amplitude independent and can be superimposed due to their orthogonality properties. For pseudo – nonlinear modal analysis, it is assumed that the nonlinearity primarily affects damping and does not alter the mode shapes; thus, the linear modes are assumed to remain uncoupled and can be used to decouple nonlinear data, as shown by Eriten et. al. [1]. However, recent studies have demonstrated that the coupling between modes is nonnegligible and can lead to inaccurate nonlinear models [2]. This work drives to challenge the uncoupled mode assumption by experimentally measuring modal coupling behavior in a controlled testing environment. Multimodal structural response is passed through a modal filter to approximate a single degree of freedom response, which is then analyzed with the Hilbert Transform, as described by Feldman [3], to extract the amplitude dependent natural frequency and damping ratio for each mode. These modal characteristics serve as the metrics for evaluating the influence of modal coupling. The structure of interest is the Cylinder–Plate–Beam (CPB) benchmark structure, which consists of an aluminum cylinder with an end plate and a cantilever beam, as shown in Figure 1. The small joint interface between the plate and beam is presumed to be essentially bonded, as the beam is attached via two steel bolts and an adhesive. Thus, most nonlinearity in the system is assumed to be frictional damping in the large, continuous

interface between the plate and cylinder flange.

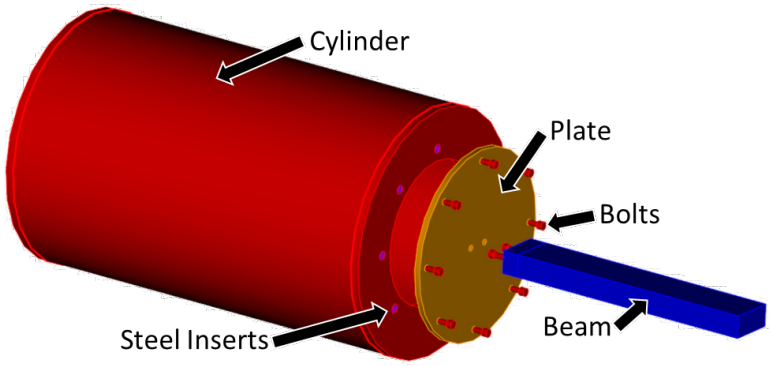

Figure 1: A schematic of the Cylinder – Plate – Beam (CPB)

To capture the modal coupling within this system, the first three elastic modes, the soft and stiff cantilever beam modes and the first drum mode of the end plate, are excited both independently and simultaneously. In this work, windowed sinusoids from a modal shaker [4] and modal hammer impacts are used to excite these CPB modes. By comparing the nonlinear response from each, the degree of coupling can be quantified, as detailed in the results that follow.

2 EXPERIMENTAL THEORETICAL BACKGROUND

2.1 Pseudo - Modal Models

Linear motion in structural dynamics implies that the response of the system is linearly proportional to the excitation amplitude and the modal frequency and damping is constant with respect to response amplitude. A typical linear system can be denoted by Equation 1 where M, C, and K are the mass, damping and stiffness matrices, respectively, F is the physical input force vector, and x(t) is the physical motion of the system.

$$[\mathbf{M}]\ddot{\mathbf{x}}(t) + [\mathbf{C}]\dot{\mathbf{x}}(t) + [\mathbf{K}]\mathbf{x}(t) = \{\mathbf{F}\} \tag{1}$$

A modal filter can transform the physical motion to a set of single degree of freedom (SDOF) modal systems as shown in Equations 2 and 3, where q(t) is the modal response as described in [5], [6], and [7]. The modal filter consists of the system linear mass normalized mode shapes.

$$\ddot{x}(t) = \Phi\ddot{q}(t) \longrightarrow \ddot{q}(t) = \Phi^{\dagger}\ddot{x}(t) \tag{2}$$

$$\ddot{q}_r(t) + 2\zeta_r\omega_r\dot{q}_r(t) + \omega_r^2 q_r(t) = \Phi^T\{F\} \tag{3}$$

A nonlinear pseudo–modal model introduces a nonlinear term into Equation 3 as shown in the following equation.

$$\ddot{q}_r(t) + 2\zeta_r\omega_r\dot{q}_r(t) + \omega_r^2 q_r(t) + F_{nl}(\dot{q}_r, q_r) = \Phi^T\{F\} \tag{4}$$

This model assumes:

(1) The mode shapes of the structure are amplitude independent

(2) Mode shapes do not couple or interact, and no energy is transferred between modal DOF

Using these assumptions, the linear mode shapes can decouple nonlinear response of the system into a modal response. However, if significant interactions between modes are introduced, i.e. modal coupling, these assumptions fail and cannot accurately capture the

nonlinear behavior of the system. The nonlinear terms added to the linear equations of motion (EOM) could incorporate additional stiffness and damping that are functions of the response of other modes.

2.2 Hilbert Analysis

Linear modal analysis is used to capture the modal parameters (i.e. mode shapes, frequencies, and damping) of a time invariant system. However, for systems that depict nonlinearities, Hilbert Analysis is widely used to depict the amplitude dependent frequency and damping behavior [8], [9], [10] of a SDOF response. If the modes can be sufficiently uncoupled to yield SDOF modal equations for the rth mode, the response envelope can be described as a sum of the decaying harmonic response and its Hilbert transform as governed by

$$Q_r(t) = q_r(t) + i\tilde{q}_r(t) \tag{5}$$

where $\tilde{q}_r(t)$ is the Hilbert transform of the signal and $Q_r(t) = A(t)\exp(i\psi t)$. $A(t)$ denotes the magnitude of the envelope, and $\psi(t)$ represents the instantaneous phase of the modal response. Using that equation, the nonlinear amplitude dependency can be described through the modal damping and stiffness as a function of amplitude. As a result, the instantaneous damped natural frequency and the instantaneous damping ratio can be described as derivatives of the phase and amplitude, respectively, where $\omega_r = \omega_{r_{damped}}/\sqrt{1-\zeta^2}$.

$$\omega_{r_{damped}} = \frac{d\psi(t)}{dt} \tag{6}$$

$$-\omega_r\zeta_r = \frac{dA(t)}{dt} \tag{7}$$

An extended overview of the Hilbert transformation and its application to modal analysis can be found in Feldman [3]. In this work, the Hilbert transformation is used to determine the amplitude dependent modal parameter behavior of experimental system response from windowed sinusoid shaker testing and modal hammer impacts.

3 EXPERIMENTAL METHODOLOGY

3.1 Test Structure

The Cylinder – Plate – Beam (CPB) structure, depicted in Figure 2, is manufactured from 6061-T6 aluminum and anodized for aesthetic reasons. The structure consists of an 18” long, 11” diameter hollow cylinder in which eight steel inserts are press-fit into the flange on each end. The interior of the cylinder was lined with foam to mitigate any acoustic resonances of the cylinder that could interfere with the recorded responses. An 8.5” diameter x 0.25” thick plate is attached to the cylinder flange using eight steel bolts, threaded into the steel inserts to a torque of 50 in-lbs. A 1” x 2” x 12” beam is bolted to the plate using two bolts as well as bonded with dental cement to minimize contact nonlinearities at this particular interface. The intent of this was to localize any nonlinear behavior in the response to the large contact area between the plate and cylinder flange.

Figure 2: A side view of the Cylinder – Plate – Beam (CPB)

Twenty-six accelerometers, eighteen triaxial and eight uniaxial, are placed on the struc-

ture according to engineering judgement, as shown in Figure 3. Accelerometers on flat faces were attached with superglue while those on the curved wall of the cylinder were mounted with dental cement to better bond to the non-flat surface. Point 341, on the cylinder flange and in the axial direction, was selected as the shaker drive point since the first three modes of the CPB, the target modes, could all be easily excited from this location. The accelerometer response data was recorded in LMS Test.Lab^{TM} software with an 88 channel LMS SCADAS frontend. In order to achieve a fine time domain resolution, a bandwidth of 12800 Hz was used with 65536 frequency lines, leading to a time sample increment of 39.0625 μs.

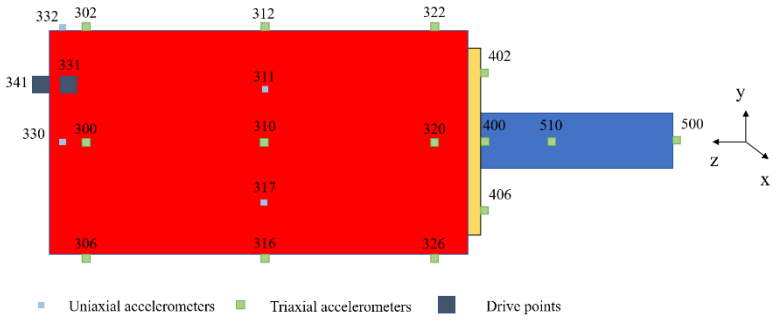

Figure 3: CPB Accelerometer Layout. Green denotes triaxial, blue are uniaxial, and black are uniaxial accels underneath a force transducer to serve as shaker drive points.

3.2 Linear Testing

To collect the linear modal parameters for the CPB, low level burst random excitation from the shaker was utilized to avoid exciting any nonlinearity in the cantilevered beam modes and drum mode of the end plate. The resultant linear FRFs, a composite of which is shown below in Figure 4, were curve fit using the Algorithm of Mode Isolation (AMI) [11] in MATLAB, producing the natural frequencies and damping ratios contained in Table 1, and mass normalized mode shapes, representations of which are given in Figure 5.

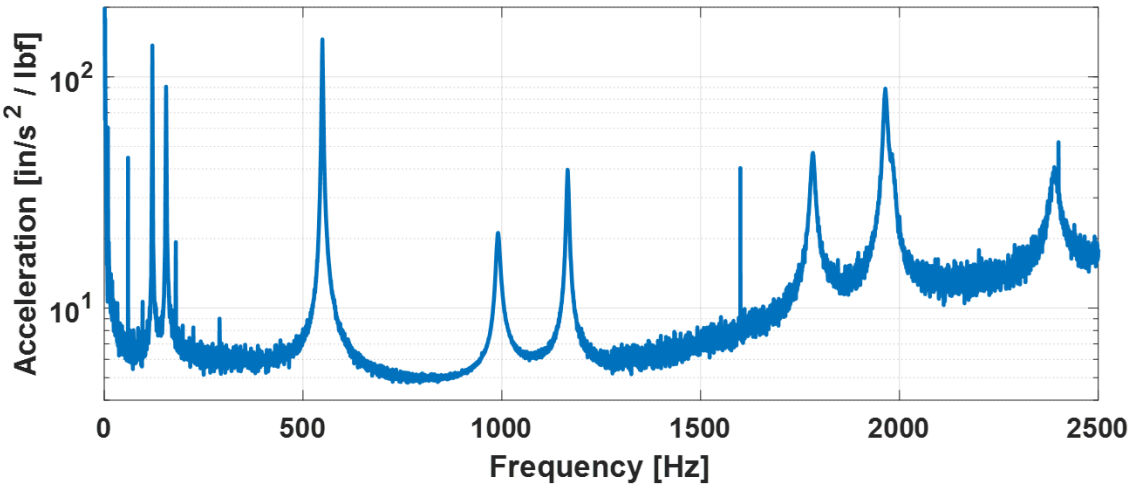

Figure 4: Composite FRF from a low level burst random shaker test of the CPB

Table 1: Experimental natural frequencies and damping ratios

	Mode 1	**Mode 2**	**Mode 3**
Natural Frequency [Hz]	121.2	155.7	548.8
Damping Ratio [%]	0.206	0.325	0.247

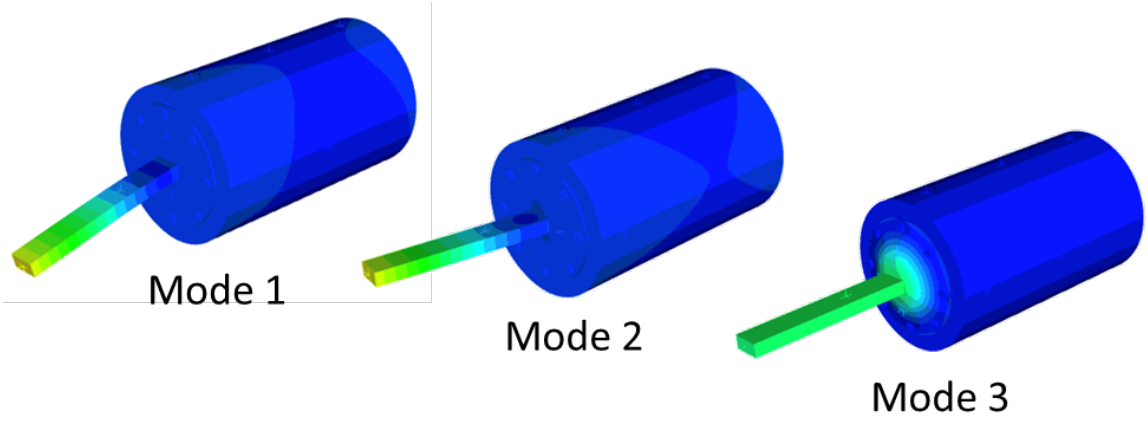

Figure 5: The first three elastic modes of the CPB

3.3 Nonlinear Shaker Testing

To obtain nonlinear response data, the shaker was used to excite the CPB via the setup shown in Figure 6. The aluminum stinger connecting the shaker to the CPB was set to have

a free length of 1.5” to maximize separation between the CPB and the shaker while keeping the first stinger buckling mode above the frequency range of interest.

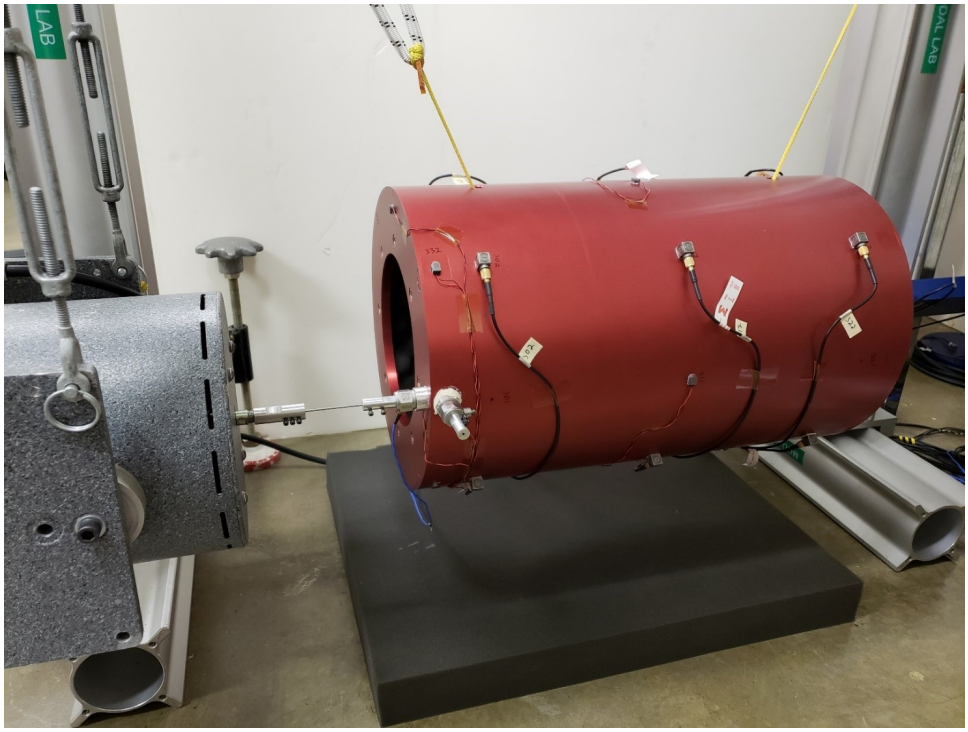

Figure 6: Experimental Setup, showing the shaker, CPB, and the stinger connecting them

To excite the CPB, the shaker was supplied with signal traces to create windowed sinusoidal inputs, or a sine beat [12]. These signals are a sine wave of specified frequency and sample rate passed through a Blackman-Harris window [13], resulting in a signal of definable width in the frequency domain. For example, the signal used to excite the first mode is shown in Figure 7. The time trace on the left shows the widowed sine wave, while its FFT on the right shows that the frequency content contained in the signal is centered at the natural frequency and has a maximum width of 60 Hz. A 30 Hz roll off to either side of the natural frequency was chosen to produce a peak wide enough to continually excite the mode as the natural frequency shifts due to nonlinear effects, while narrow enough to only significantly excite the mode of interest.

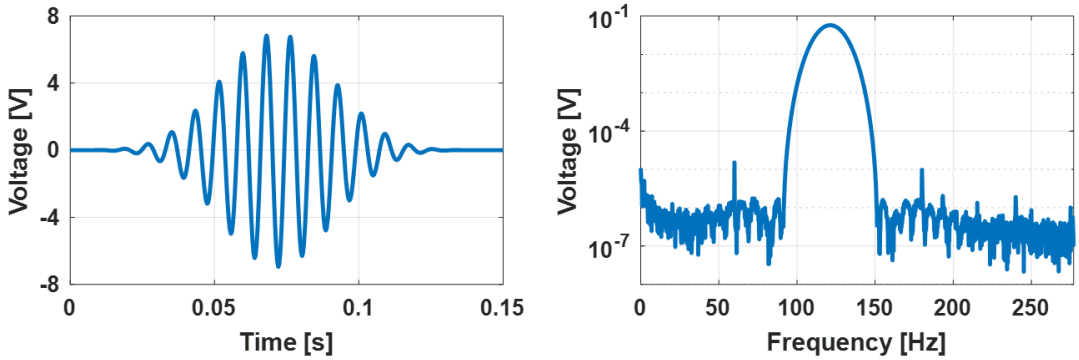

Figure 7: Voltage signal sent to produce a windowed sine centered on mode 1

The goal of this work is to study whether the test specimen exhibits a different nonlinear response when a single mode is excited versus when multiple modes are excited. To excite two modes simultaneously, the same process was completed on each mode, with the windowed signals then added and superimposed. To exemplify this, the signal created to excite mode 1 and mode 2 is shown in Figure 8.

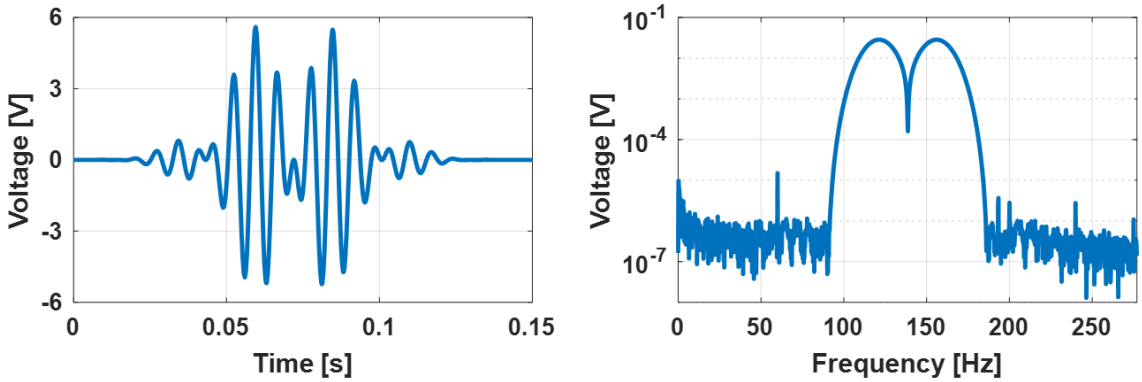

Figure 8: Voltage trace used to simultaneously excite modes 1 and 2

Windowed sine excitations were defined for each mode individually and for each pairing between the first three modes, or modes 1 & 2, 1 & 3, and 2 & 3. For the individual modes, peak voltages of 7.0, 5.6, 3.5, and 1.4 volts were used. A maximum of 7 volts was set due to the shaker amplifier at predetermined settings being unable to accept above this

level without clipping the signal. The subdivisions below 7V were set to provide several intermediary excitation levels to compare the response from each. The mode pairs were performed with various combinations of these voltage levels, as shown in Table 2. This was done to collect data with modes at different relative excitation levels, which could cause varying degrees of modal coupling.

Table 2: Test Matrix showing all the test cases and voltages used

Mode 1	**Mode 2**	**Mode 3**	**Modes 1 & 2**	**Modes 1 & 3**	**Modes 2 & 3**
1.4 V	1.4 V	1.4 V	1.4 V 1.4 V	1.4 V 1.4 V	1.4 V 1.4 V
3.5 V	3.5 V	3.5 V	3.5 V 1.4 V	3.5 V 1.4 V	3.5 V 1.4 V
5.6 V	5.6 V	5.6 V	1.4 V 3.5 V	1.4 V 3.5 V	1.4 V 3.5 V
7.0 V	7.0 V	7.0 V	3.5 V 3.5 V	3.5 V 3.5 V	3.5 V 3.5 V
			5.6 V 1.4 V	5.6 V 1.4 V	5.6 V 1.4 V
			1.4 V 5.6 V	1.4 V 5.6 V	1.4 V 5.6 V

3.4 Shaker Experimental Results

After performing all the necessary windowed sine excitations, the recorded time responses from the accelerometers were imported into MATLAB. This physical domain data was transferred to the modal domain by a modal filter, using the mass normalized mode shapes from the linear tests. This produces an approximately SDOF response for each mode, which can then be analyzed via the Hilbert Transform to acquire the amplitude dependent natural frequency and damping ratio. For the isolated modes 2 and 3, excited at various voltage levels, the Hilbert curves for damping ratio and natural frequency versus modal velocity amplitude are shown in Figure 9; mode 1 results closely resemble mode 2 and are consigned to Appendix A, Figure A1, for brevity.

In these figures, the horizonal black line represents the linear modal value, as determined

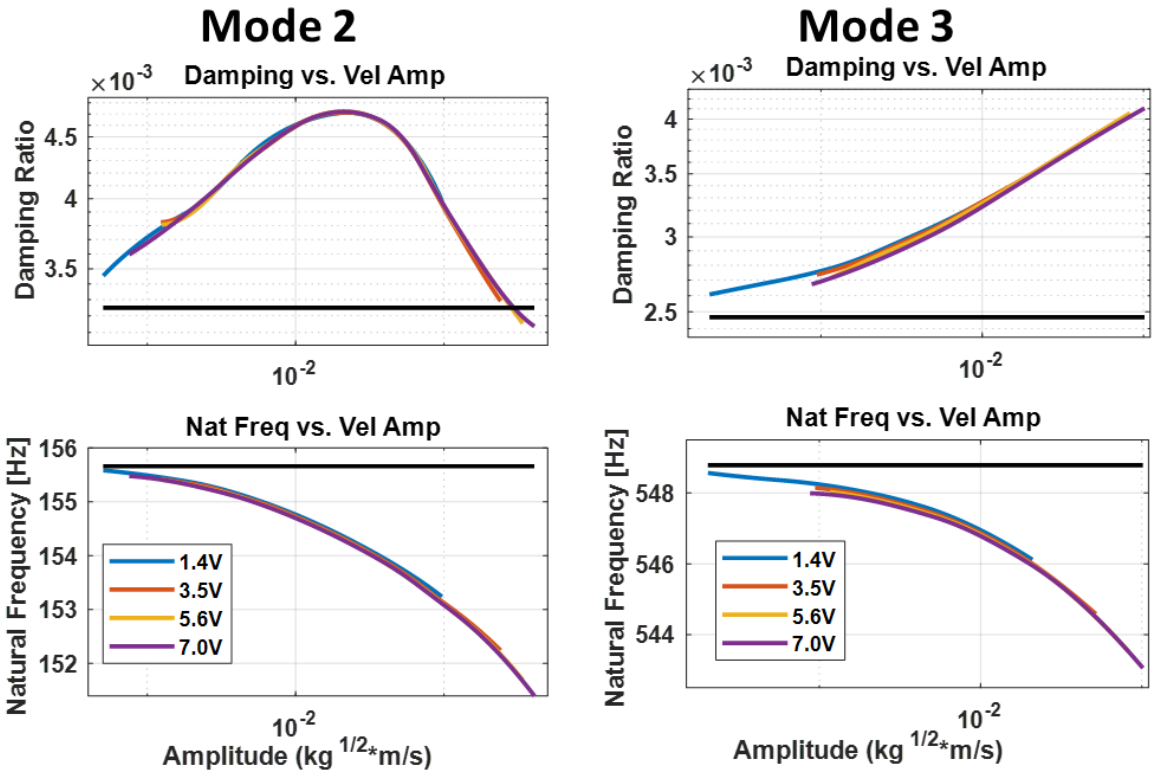

Figure 9: Damping Ratio & Natural Frequency vs. Velocity Amplitude for (Left) Mode 2 and (Right) Mode 3 at various excitation levels. The horizontal black line represents the linear value

from curve fitting a low level burst random test performed immediately prior to the windowed sinusoid tests. This value was found to agree with results from a curve fit of an additional low level burst random performed immediately after the windowed sines, signifying that the linear system did not significantly change during the test. At low amplitude, the Hilbert curves converge toward the expected linear value, while as amplitude increases, the natural frequency gradually decreases for all three modes. For mode 3, damping is observed to continually increase, while modes 1 and 2 experience an initial increase and then decrease in damping value, which may be indicative of macro-scale slip in the joint. However, all three modes follow their same trend in frequency and damping over all four excitation levels, in that the curves overlay. This signifies that, while the modes exhibit clearly nonlinear

attributes, these effects are consistent and repeated excitations at various levels do not alter the system characteristics.

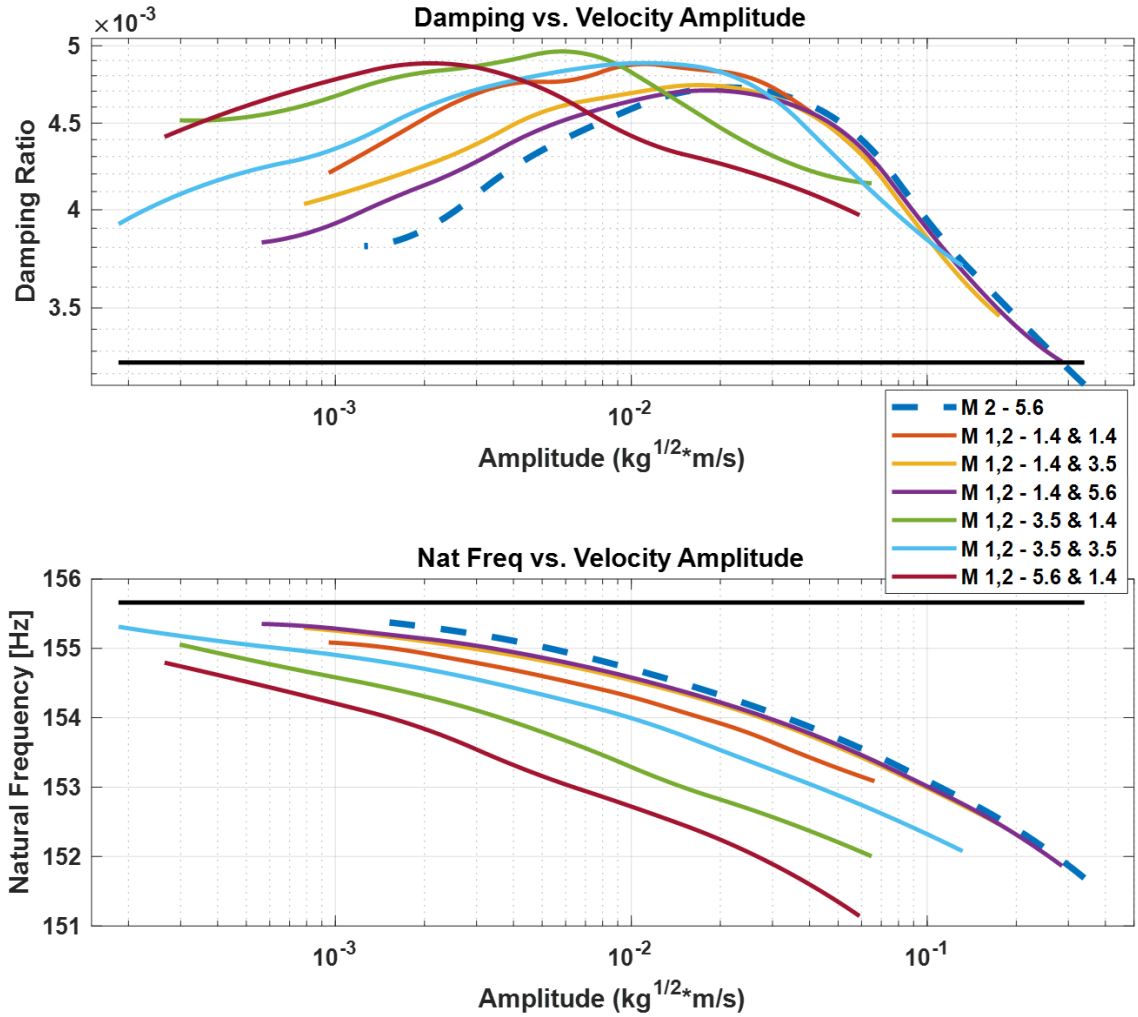

Figure 10: Mode 2 response when modes 1 and 2 are excited simultaneously

When exciting two modes simultaneously, the modally filtered response results in two SDOF responses that can be analyzed with the Hilbert Transform. Figure 10 shows the response of mode 2 when it is excited together with mode 1. The dashed line represents the response of an isolated mode 2, while the other lines represent the various combinations of mode 1 and 2 excitation. In the legend, the numbers are the voltage level of the mode

with respect to the order given at the beginning of the entry. As the excitation of mode 1 increases relative to the mode 2 excitation, the Hilbert curves deviate further from the isolated baseline. The decrease in natural frequency becomes much more prominent and the damping curves seem to shift to the left, where the damping is increasing at lower amplitudes. These changes can be interpreted as follows: mode 2 has a certain damping nonlinearity when it is excited in isolation, which comes about because a larger fraction of the joint area slips as mode 2's amplitude increases. When mode 1 is also excited, this apparently puts the joints into a state of slip that is greater than what they would experience if mode 2 was excited alone, and so mode 2's apparent stiffness decreases and its damping increases. A similar trend is visible in the mode 1 response when mode 2 is excited, as shown in Figure A2. Specifically, when mode 2 is excited to a higher level than mode 1, the mode 1 response deviates away from the isolated baseline.

Figure 11 shows the mode 2 response when mode 3 is also excited. This case does not show any significant change in natural frequency while also displaying a very slight decrease in damping for all the mode pair levels. This reveals that modes 2 and 3 are not significantly coupled, and perhaps arises because these modes exercise the joints in a way such that they do not influence the stiffness/damping of the other mode. Mode 1 also does not exhibit any reaction to mode 3 excitation, as shown in Figure A3. These results indicate that modes 1 and 2, the first two cantilevered beam modes of the CPB, have some degree of modal coupling, while both seem to be independent of Mode 3, the drum mode of the plate.

Seemingly contrary to the previous statement, large deviations in the mode 3 response are observed when mode 2 is simultaneously excited, as seen in Figure 12. Any degree of mode 2 excitation causes the mode 3 response to deviate from its isolated state, again given by the dashed line. Also, the various cases with the same mode 2 voltage level are grouped together, as in all three 1.4V and both 3.5V cases show very similar responses. A comparable scenario is observed when mode 1 is also excited, as shown in Figure A4. As the mode 1 or 2

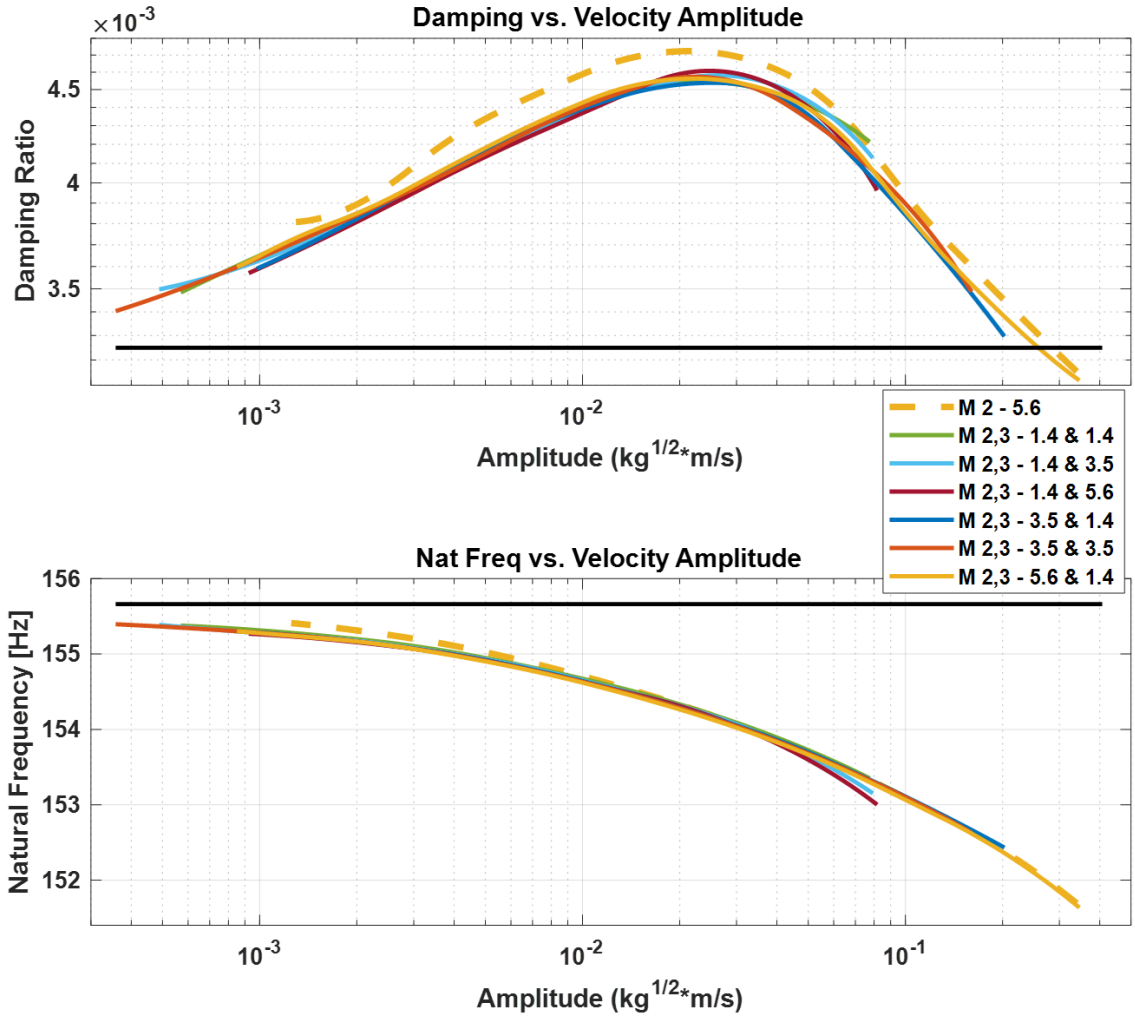

Figure 11: Mode 2 response when modes 2 and 3 are excited simultaneously

excitation increases, the mode 3 response exhibits consistently decreasing natural frequency and increasing damping.

Thus, while modes 1 and 2 both affect the response of the other, mode 3 seems to have little to no effect on modes 1 and 2, while mode 3 is greatly affected by modes 1 and 2. This would indicate that there is some degree of modal coupling present between all three modes, but to varying degrees. An explanation for this could simply be the dynamics of the physical motion associated with each mode. As seen in Figure 5, modes 1 and 2 are first cantilever beam modes acting in perpendicular directions, but with the same mass. For both modes to

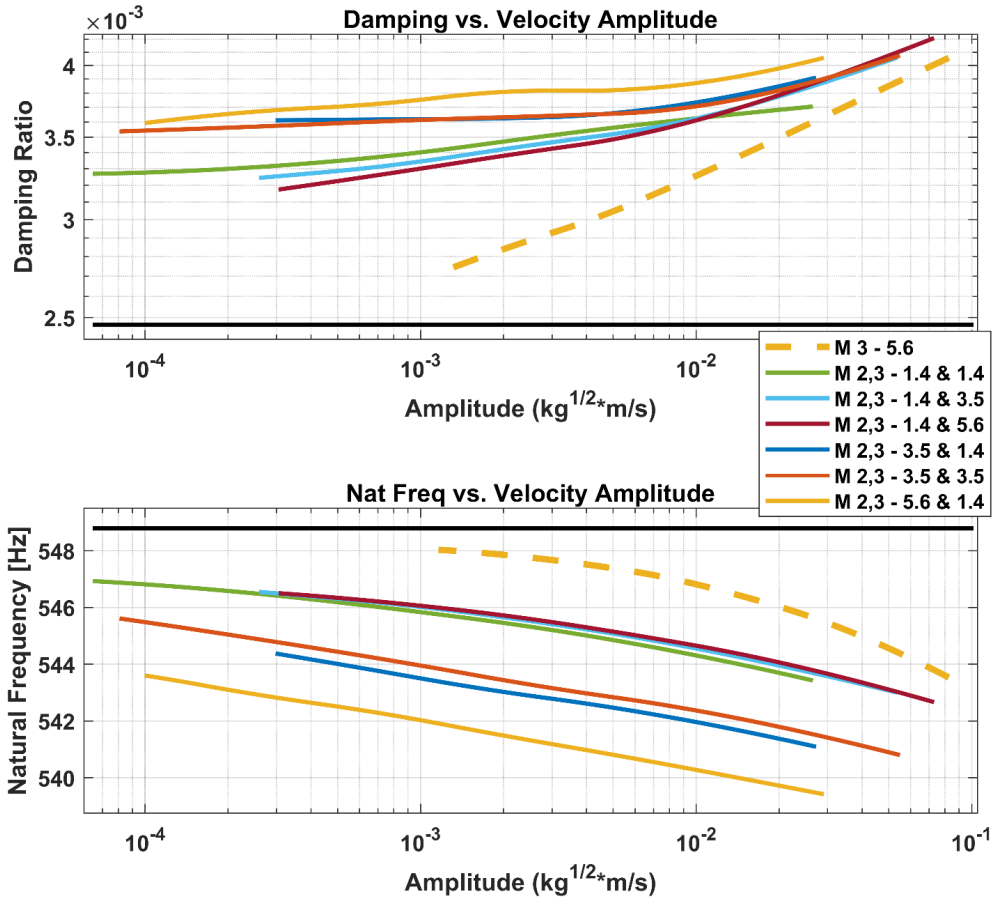

Figure 12: Mode 3 response when modes 2 and 3 are excited simultaneously

be simultaneously excited, each must act against the inertia associated with the other. This will produce some degree of diagonal motion, changing how to beam contacts the plate at the root, thus slightly altering the characteristics of the modes. For mode 3, it likely doesn't affect the beam modes because the beam is rooted at the center of the plate. This location is a nodal point in the plate drum mode shape; the cantilevered motion of modes 1 and 2 are unperturbed by the root of the beam translating axially. However, it is the transverse motion of the beam in modes 1 and 2 that causes the drastic shifts in mode 3. As the beam oscillates, the plate flexes and warps under it, distorting the shape of the drum mode and thus how the plate contacts the cylinder flange. This range of dynamic interaction could be

the cause of the modal coupling observed in the experimental data shown above.

3.5 Nonlinear Hammer Testing

Immediately following the shaker testing, a modal hammer was used to excite the CPB under the same boundary conditions, i.e. the same environment and with the shaker still attached. The CPB was impacted beside the shaker drive point to directly compare with the shaker results and at the tip of the beam in all three directions to directly excite each mode. As with the shaker data, the physical response was passed through a modal filter before preforming Hilbert analysis. Figure B1 contains plots of typical hammer input, physical response, and modal response in the time and frequency domain. The resultant Hilbert curves for mode 2 due to the various impact cases are shown in Figure 13, where the dashed line shows the response due to a windowed sinusoidal excitation from the shaker. In terms of natural frequency, all the impact responses overlay with the shaker results throughout the entire amplitude range. For damping, the impact excitation responses generally show the same curve profile as found in the shaker data, but at a lower magnitude. When impacting at the end of the beam, the damping converges toward the linear damping found in the low level burst random shaker data. Also, as the impact force level increases at the point near the shaker drive point, the damping curves seem to converge toward what is observed in the shaker response curve. The data for mode 1 again displays similar results to mode 2 and is shown in Figure B2.

The Hilbert response curves for mode 3 are shown below in Figure 14. In this case, only the very low force level impacts match the shaker results for natural frequency and show similar, or lower damping levels. As the excitation level increases, the response deviates further from the linear values and the shaker response curve. This agrees with what was observed in the shaker data when mode 3 was excited simultaneously with modes 1 or 2. The same is true here, as the broadband frequency content imparted by the modal hammer

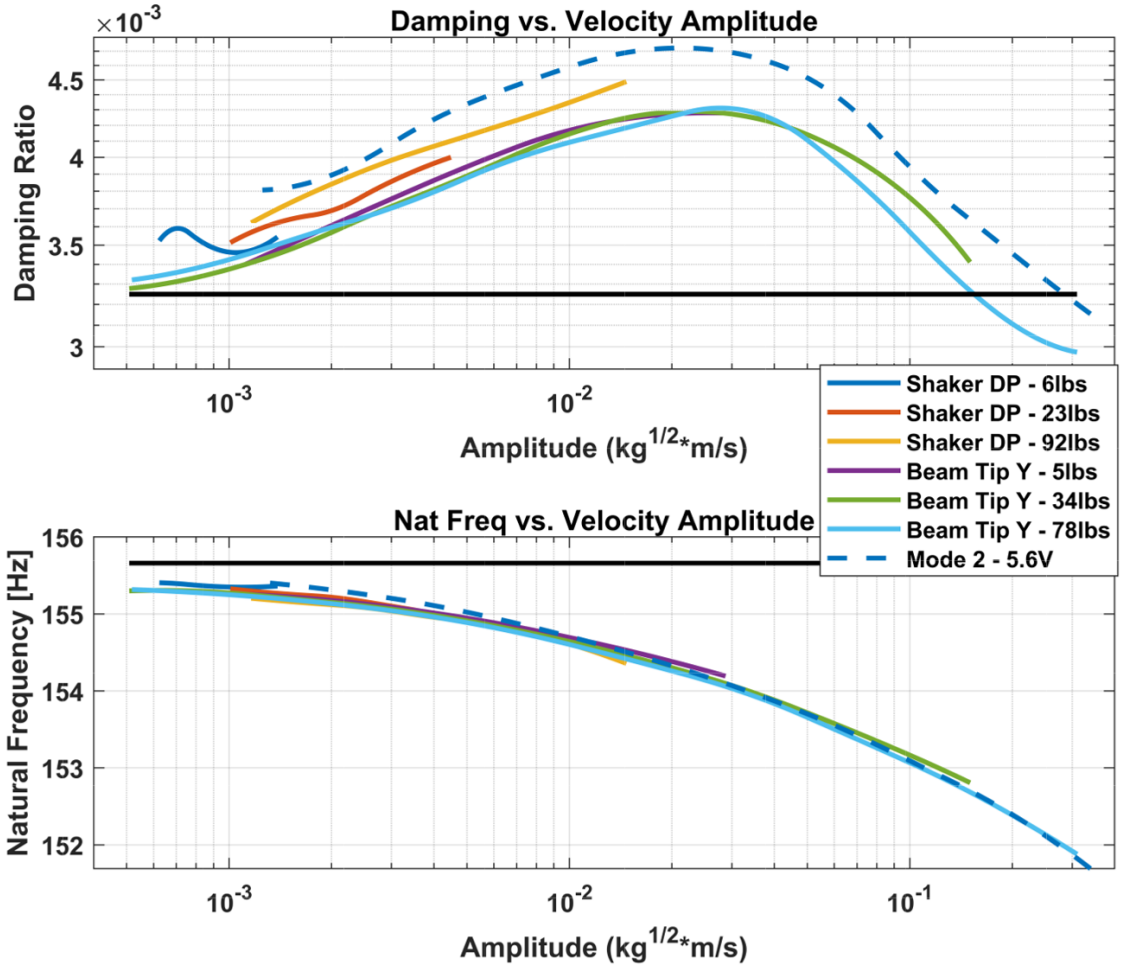

Figure 13: Mode 2 response to various impact locations and force levels

excites all modes up to several thousand Hertz, depending on the force level.

These results strongly correlate to those found from the shaker excitation. This shows that the effects of modal coupling can be observed under different excitation techniques, and thus, cannot be avoided by simply choosing a different excitation method.

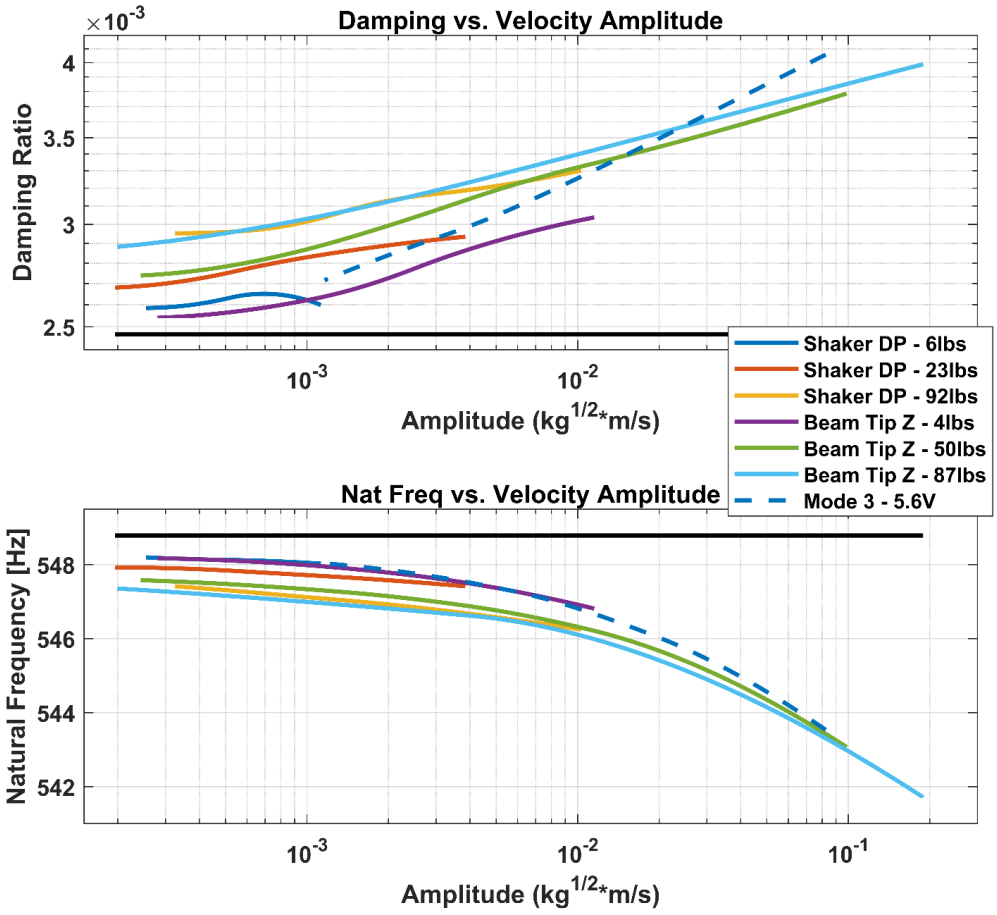

Figure 14: Mode 3 response to various impact locations and force levels

4 CONCLUSION

The purpose of this work was to experimentally characterize a structure and establish a dataset that depicted modal coupling. To acquire this experimental data, a new Cylinder-Plate-Beam structure was manufactured and instrumented. Low-level shaker testing was done to identify baseline linear modal parameters, such as natural frequency, damping ratio, and mass normalized mode shapes. For nonlinear data, windowed sinusoidal excitations were completed at various excitation levels on each mode individually and on pairs of modes simultaneously. Modal hammer testing was also done at several locations and force levels to collect impact excitation response. After passing the physical response from each test case through a modal filter and preforming Hilbert Analysis on the single degree-of-freedom modal responses, amplitude dependent natural frequency and damping ratio curves were found for each mode. For the isolated modes excited at various shaker levels, the curves were found to overlay, implying that while each is nonlinear, the corresponding response is consistent over the observed range and is independent of initial excitation. However, when Modes 1 and 2 are excited simultaneously, the Hilbert curves for each deviate from the isolated baseline as the relative excitation of the other increases. Such a relationship was not observed with either of these modes when Mode 3 was also excited. Conversely, Mode 3 was observed to vastly deviate from its isolated baseline when Modes 1 or 2 were also excited. Similar trends were also observed in the nonlinear modal hammer impact responses. Thus, the experimental data collected indicates that some degree of modal coupling is present and observable between the first three modes of the structure. Future work will seek to further understand these results by better quantifying the degree to which each mode was excited in the coupled responses and to understand what types of models can be used to capture the observed coupling. We have also begun to create a high-fidelity model that characterizes the interface using whole joint elements to represent each bolt. It also may be possible to create a model that reproduces the experimental data by using Restoring Force

Surface Analysis Method [14, 15] to fit quadratic/cubic stiffness and damping models to the measurements. Experimentally, additional mode pairings that include higher order modes could be examined. Expanding beyond pairs, groups of three or more modes could be excited simultaneously with windowed sinusoids. .

ACKNOWLEDGEMENTS

This research was conducted at the 2018 Nonlinear Mechanics and Dynamics (NOMAD) Research Institute supported by Sandia National Laboratories. Sandia National Laboratories is a multi-mission laboratory managed and operated by National Technology and Engineering Solutions of Sandia, LLC., a wholly owned subsidiary of Honeywell International, Inc., for the U.S. Department of Energy's National Nuclear Security Administration under contract DE-NA-0003525. The authors would also like to thank Bill Flynn from Siemens Industry Software NV for supplying the data acquisition and testing systems used to collect the experimental measurements presented throughout this work.

REFERENCES

[1] M. Eriten, M. Kurt, G. Luo, D. Michael McFarland, L. A. Bergman, and A. F. Vakakis, "Nonlinear system identification of frictional effects in a beam with a bolted joint connection," *Mechanical Systems and Signal Processing*, vol. 39, no. 1-2, pp. 245–264, 2013. Number: 1-2.

[2] R. Lacayo, B. Deaner, and M. S. Allen, "A Numerical Study on the Limitations of Modal Iwan Models for Impulsive Excitations," *Journal of Sound and Vibration*, vol. 390, pp. 118–140, 2017.

[3] M. Feldman, "Non-linear system vibration analysis using Hilbert transform–I. Free vibration analysis method 'Freevib'," *Mechanical Systems and Signal Processing*, vol. 8, no. 2, pp. 119–127, 1994. Number: 2.

[4] B. R. Pacini, R. L. Mayes, B. C. Owens, and R. Schultz, "Nonlinear Finite Element Model Updating, Part I: Experimental Techniques and Nonlinear Modal Model Parameter Extraction," (Garden Grove, CA), 2017.

[5] A. W. Phillips and R. J. Allemang, "Single Degree-of-Freedom Modal Parameter Estimation Methods," pp. 253–260, Feb. 1996.

[6] J. H. Ginsberg, *Engineering Dynamics*. Cambridge, MA: Cambridge University Press, 3rd ed., 2005.

[7] G. Kerschen, K. Worden, A. F. Vakakis, and J.-C. Golinval, "Past, present and future of nonlinear system identification in structural dynamics," *Mechanical Systems and Signal Processing*, vol. 20, pp. 505–592, 2006.

[8] A. Singh, M. Scapolan, Y. Saito, M. S. Allen, D. Roettgen, B. Pacini, and R. J. Kuether, "Experimental Characterization of a New Benchmark Structure for Prediction of Damping Nonlinearity," in *Nonlinear Dynamics, Volume 1* (G. Kerschen, ed.), Conference Proceedings of the Society for Experimental Mechanics Series, (Cham), pp. 57–78, Springer International Publishing, 2019.

[9] J. N. Yang, Y. Lei, S. Pan, and N. Huang, "System identification of linear structures based on Hilbert-Huang spectral analysis. Part 1: Normal modes," *Earthquake Engineering and Structural Dynamics*, vol. 32, no. 9, pp. 1443–1467, 2003. Number: 9.

[10] M. Feldman, "Time-varying vibration decomposition and analysis based on the Hilbert transform," *Journal of Sound and Vibration*, vol. 295, no. 3-5, pp. 518–30, 2006. Number: 3-5.

[11] M. S. Allen and J. H. Ginsberg, "Global, Hybrid, MIMO Implementation of the Algorithm of Mode Isolation," 2005.

[12] E. G. Fischer, "Sine Beat Vibration Testing Related to Earthquake Resonance Spectra," *Shock and Vibration Bulletin*, vol. 42, pp. 1–8, Jan. 1972.

[13] F. Harris, "On the use of windows for harmonic analysis with the discrete fourier trans-

form," in *Proceedings of the IEEE*, 1978.

[14] K. Worden, J. R. Wright, M. A. Al-Hadid, and K. S. Mohammad, "Experimental Identification of Multi Degree-of-freedom Nonlinear Systems using Restoring Force Methods," *The International Journal of Analytical and Experimental Modal Analysis*, vol. 9, no. 1, pp. 35–55, 1994. Number: 1.

[15] M. Allen, H. Sumali, and D. S. Epp, "Restoring Force Surface Analysis of Nonlinear Vibration Data from Micro-Cantilever Beams," Nov. 2006.

APPENDIX A - ADDITIONAL SHAKER HILBERT PLOTS

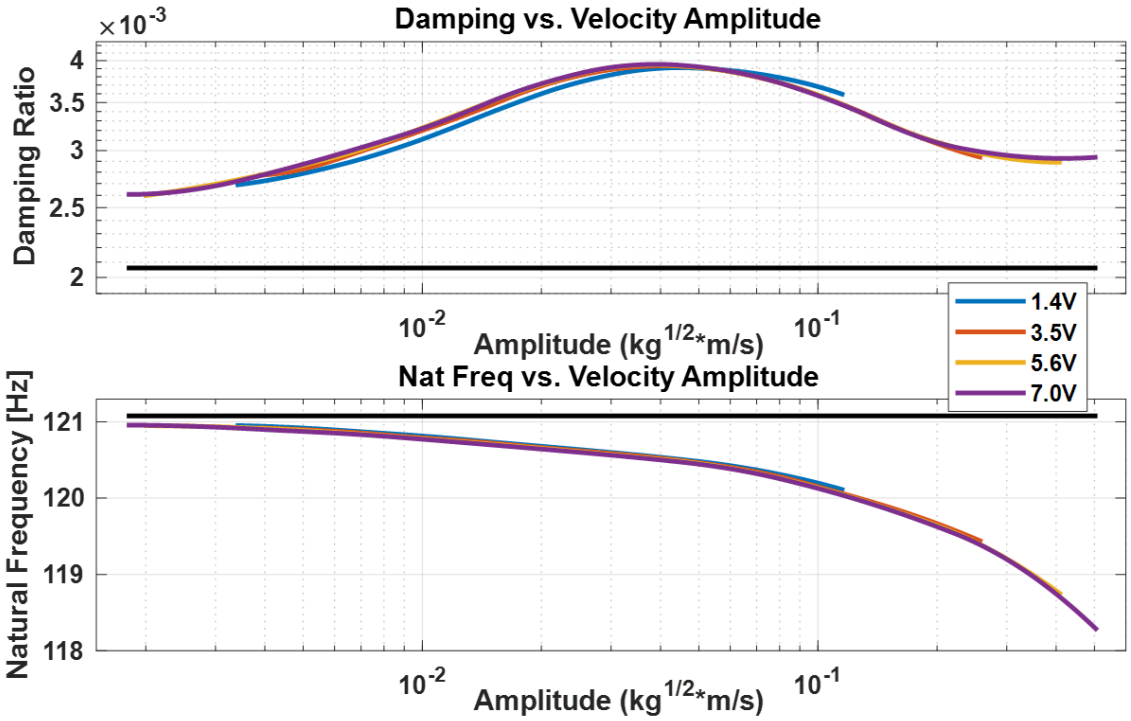

Figure A1: Mode 1 response at various excitation levels

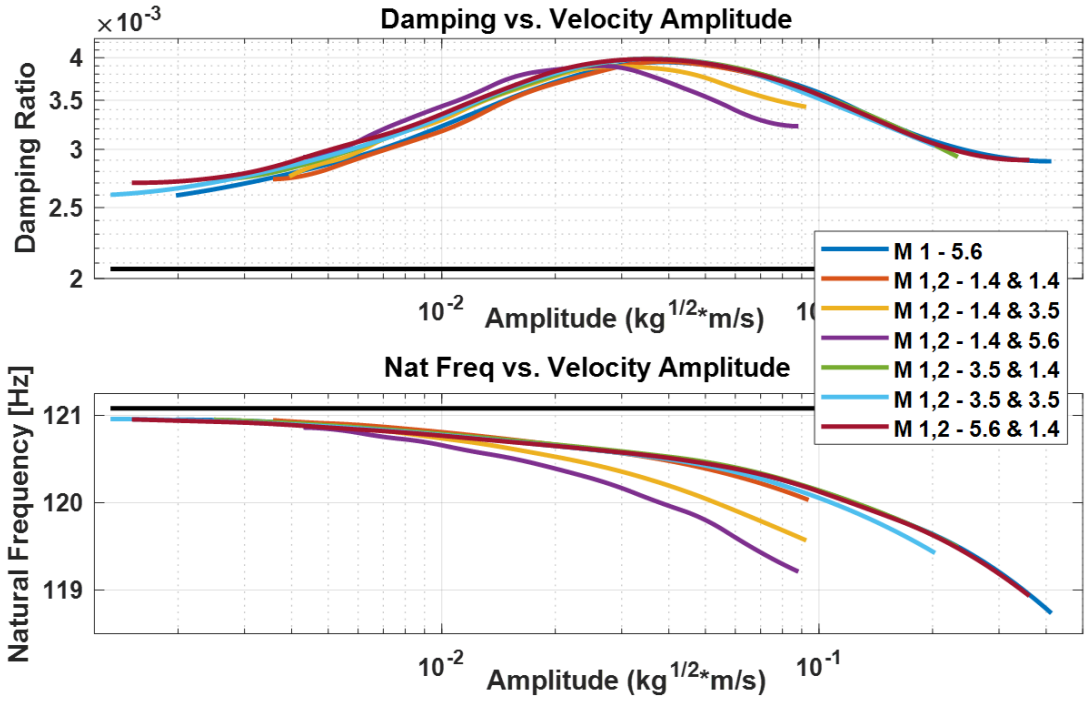

Figure A2: Mode 1 response when modes 1 and 2 are excited simultaneously

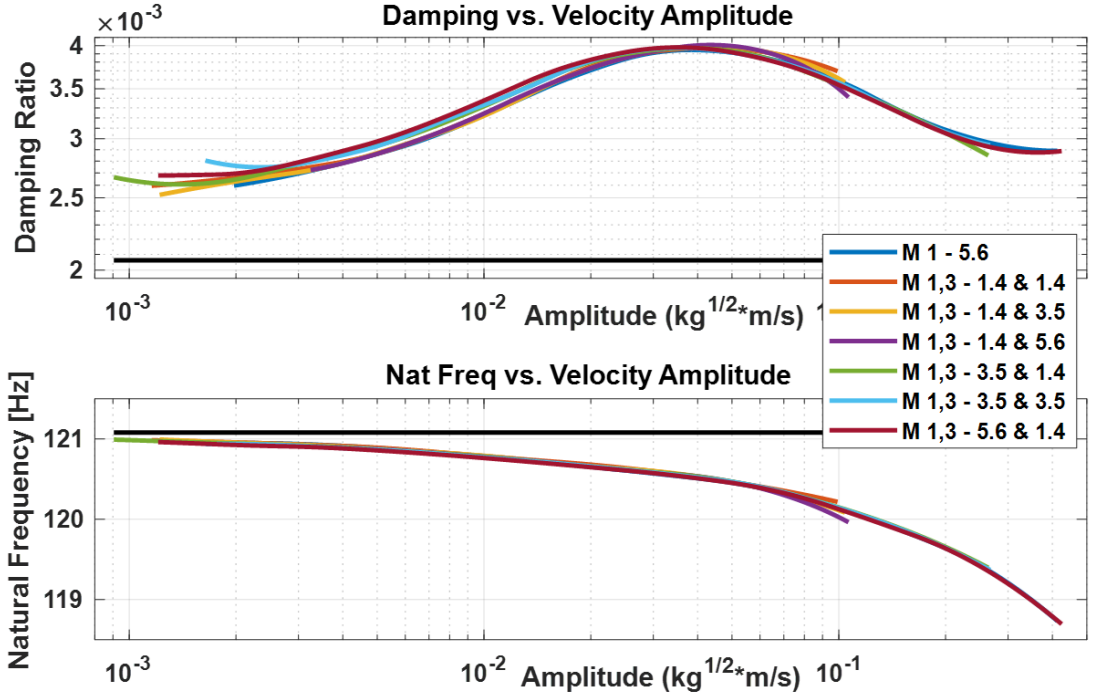

Figure A3: Mode 1 response when modes 1 and 3 are excited simultaneously

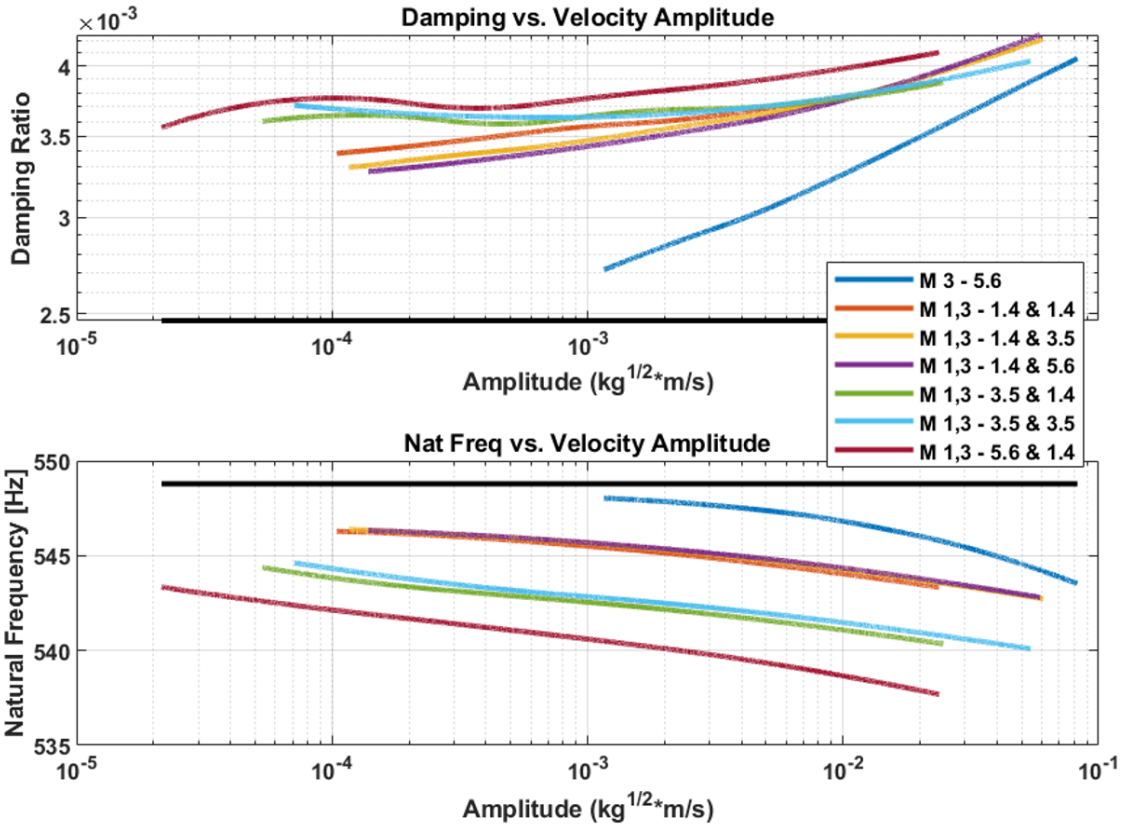

Figure A4: Mode 3 response when modes 1 and 3 are excited simultaneously

APPENDIX B - ADDITIONAL HAMMER DATA PLOTS

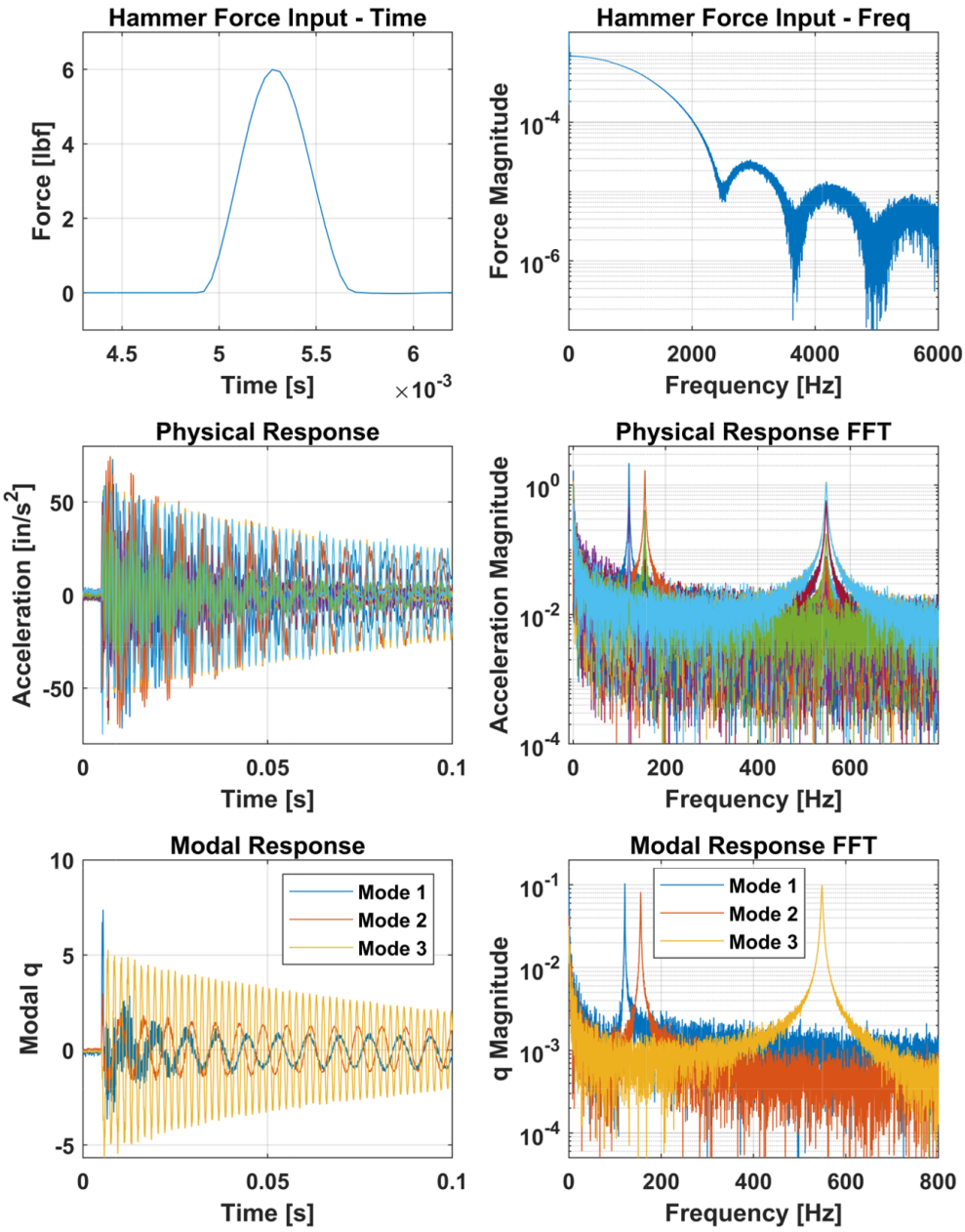

Figure B1: Example of hammer, physical, and modal response in time and frequency domains

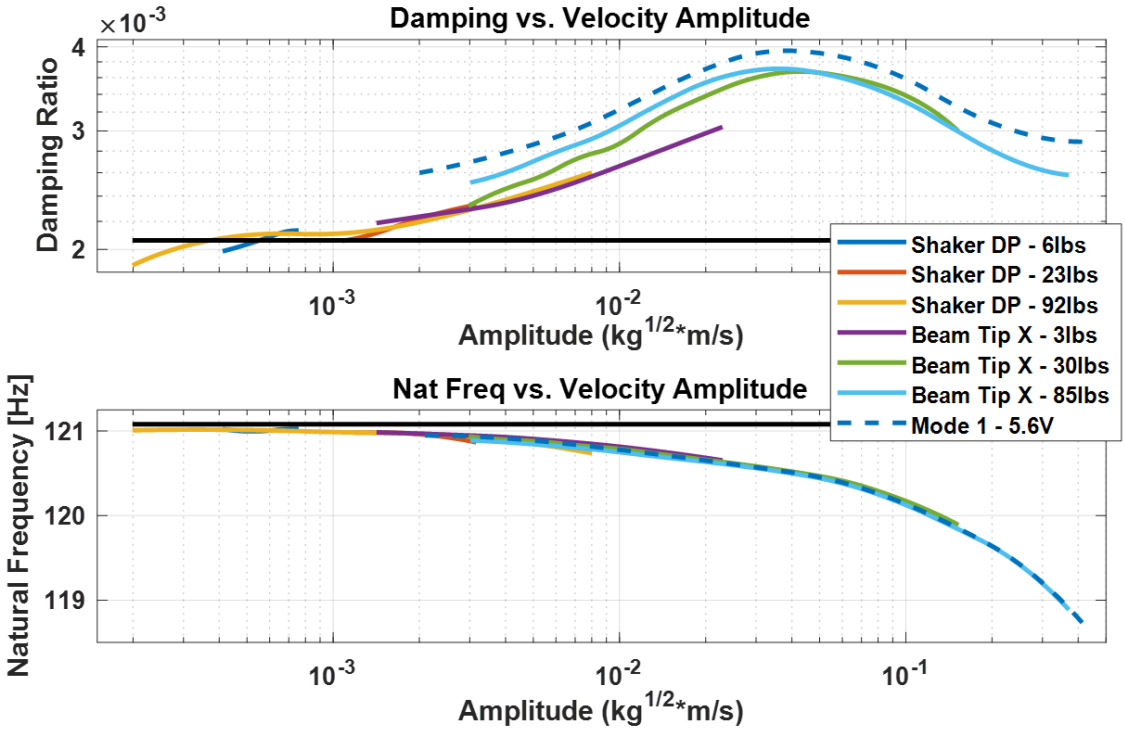

Figure B2: Mode 1 response to various impact locations and levels

Spider Configurations for Models with Discrete Iwan Elements

Aabhas Singh — University of Wisconsin - Madison

Matthew S. Allen — University of Wisconsin - Madison

Robert J. Kuether — Sandia National Laboratories

ABSTRACT

Lacayo et al. (Mechanical Systems and Signal Processing, 118, p. 133-157, 2019) recently proposed a fast model updating approach for finite element models that include Iwan models to represent mechanical joints. The joints are defined by using RBE3 averaging constraints or RBAR rigid constraints to tie the contact surface nodes to a single node on each side, and these nodes are then connected with discrete Iwan elements to capture tangential frictional forces that contribute to the nonlinear behavior of the mechanical interfaces between bolted joints. Linear spring elements are used in the remaining directions to capture the joint stiffness. The finite element model is reduced using a Hurty/Craig-Bampton approach such that the physical interface nodes are preserved, and the Quasi-Static Modal Analysis approach is used to quickly predict the effective natural frequency and damping ratio as a function of vibration amplitude for each mode of interest. Model updating is then used to iteratively update the model such that it reproduces the correct natural frequency and damping at each amplitude level of interest. In this paper, Lacayo's updating approach is applied to the S4 Beam (Singh et al., IMAC XXXVI, 2018) giving special attention to the size and type of the multi-point constraints used to connect the structures, and their effect on the linear and nonlinear modal characteristics.

1 INTRODUCTION

Mechanical structures with complicated geometry can be accurately modeled with finite element techniques if the structure is monolithic and manufactured from a single piece of material. However, even with additive manufacturing, most structures cannot be manufactured as such, and therefore mechanical interfaces are introduced between sub-assemblies often joined with bolts, rivets, or welds. These joints introduce uncertainty and significant challenges in modeling the physics involved with frictional contact and the effective stiffness

and damping within the joint [1]. While joints in general can introduce strong nonlinearity, resulting in complicated phenomena such as modal coupling, response at higher harmonics, and even chaos, in many structures of practical interest the nonlinearity is weak and is observed experimentally as a slight decrease in the effective natural frequency and a large increase in damping of some of the structure's vibration modes as vibrational amplitude increases [2–5].

Commercial finite element analysis or multi-body dynamics software are capanle of solving contact problems with coulomb friction [6, 7], although significant mesh refinement is necessary near the interface in order to obtain an accurate model, which can be computationally prohibitive [8]. Full order modeling approaches may include high fidelity thread and joint models [9, 10], models with thin-layer and zero-thickness elements at the contact interface [11, 12], among others. For these cases dynamic analyses are often computationally infeasible, whereas static analyses are dependent on the solver settings used. This was illustrated recently by Jewel et. al [8] who found that tens of hours were required to obtain accurate solutions for the static response of a structure with only one or two joints when the joint was meshed with adequate refinement and the solver settings were tuned to accurately solve the contact problem. It would be extremely expensive to perform dynamic simulations with such a model, and even more so for realistic structures with hundreds of joints. Solution to this are harmonic balance methods and quasi-static methods that realize the nonlinear effects [13–16], although they are still computationally expensive for large high fidelity models. As a result, a coarse mesh and model reduction methods are used to reduce the interface to nodes that can be connected using linear springs or nonlinear joint models to describe the global behavior at a fraction of the cost of a full fidelity analysis.

This can be done through various dynamic substructuring methods [17,18], although this paper will focus on the Component Mode Synthesis (CMS) modal domain method. For CMS approaches, each sub-component in the model is reduced on the basis of its respective normal

modes and then connected via linear or nonlinear elements. The first CMS approach was developed by Hurty [19] using fixed interface modes (FIM) as the basis for reduction. Craig et al. augmented FIMs with static constraint modes to further reduce each sub-component [20], yielding the commonly used Hurty/Craig-Bampton (HCB) method. Although, additional CMS methods exist [21–24], this work utilizes the HCB method.

Using a HCB reduction, a full model is reduced to a subset of modes to describe the global behavior and a set of DOF at the interface of each sub-component. However, for larger interfaces, this can be computationally expensive since an element must be placed at each DOF to connect the sub-components. Therefore, a secondary reduction is done to reduce each interface down to a single node using multi-point-constraints (MPCs). This whole-joint approach, introduced by Segalman [25–27], describes the effect of the interface on the global behavior by first "spidering" the interface to a single node, then joining those nodes with a linear or nonlinear hysteretic element, and lastly simulating the response using a numerical method. In some cases, nonlinear hysteretic models are used in place of linear springs when using this whole-joint approach. These models represent the nonlinearity through constitutive equations between the degrees of freedom of a single set of nodes. When introduced into a reduced order model (ROM), such as a Hurty/Craig-Bampton (HCB) reduced model, they can capture nonlinear behavior while maintaining tractable computational cost. An example of the whole-joint model is the four parameter Iwan joint introduced by Segalman in 2005 [25, 28], which was derived based on analytical solutions to contact problems and empirical data to best capture the energy dissipation observed in joints. These joint models can often be used to capture the amplitude dependent frequency or damping measured in experiments, so long as the joints remain in the micro-slip regime.

The parameters of a whole-joint model such as an Iwan element cannot currently be predicted from first principles, so measurements must be taken and model updating used to update the joint parameters until the model reproduces the measured response. The Hilbert

Transform can be used to extract the frequency and damping as a function of amplitude from transient response measurements [29]. Then the recently developed Quasi-Static Modal Analysis (QSMA) approach [30], [15] can be used to quickly compute these quantities. Lacayo et al. [15] recently demonstrated this workflow to update a reduced model of the Brake-Reuss (BRB) beam. Similarly, this paper investigates the model updating procedure and applicability of the four parameter Iwan joint with a new benchmark structure studied at Sandia's Nonlinear Mechanics and Dynamics Institute in 2017 that is shown in Figure 1.

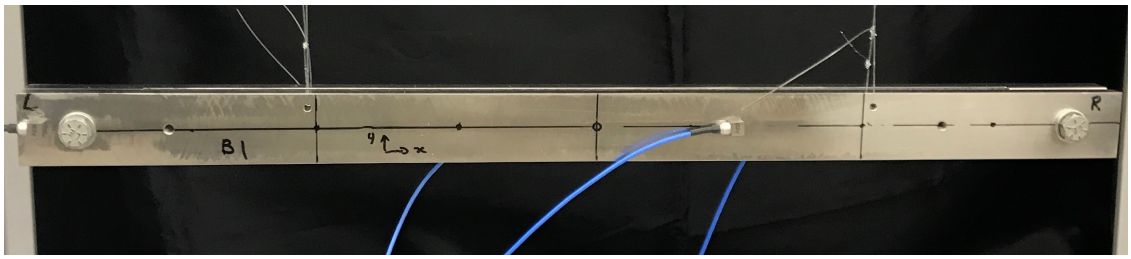

Figure 1: The S4 Beam (C-Beam) side view

The S4 Beam was studied experimentally by Singh et al. [4] and that data is used to calibrate the ROMs in this work. First, an HCB model is made for each beam and linear springs are inserted and updated to match the measured linear frequencies. Then, Iwan joints are inserted in place of some of the springs and QSMA is used to compute and iterate on the amplitude dependent damping and frequency in an effort to reproduce the experimentally measured frequency and damping. The experimental structure showed a high degree of nonlinearity in the first in-phase bending mode (Mode 2), so the goal is to use the methodology to calibrate the model to capture this mode. In doing so, prior works have shown that a pareto front is often observed, a case in which the model cannot be updated to capture both the stiffness and damping. This work explores this issue by creating models with various types of spiders, or various ways to define the Multi-Point Constraints (MPCs) used to reduce the contact surfaces to a single node.

2 THEORETICAL BACKGROUND

2.1 Hurty/Craig Bampton Reduction

To incorporate the high geometric detail of the structures of interest and reduce computational costs, Reduced Order Models (ROMs) are used to approximate the full-order model at a set of reduction nodes between the mechanical interfaces. The approximation requires that these components remain linear and that the only source of nonlinearity within in the joined system is at the contact interface [31]. For this work, the Hurty/Craig Bampton (HCB) reduction method will be used [20].

The FE discretized equations of motion (EOM) for an N degree-of-freedom (DOF) undamped system can be written as

$$\mathbf{M}\ddot{\mathbf{u}} + \mathbf{K}\mathbf{u} + \mathbf{F}_J(\mathbf{u}, \theta) = \mathbf{F}_{ext} \tag{1}$$

where $\mathbf{M}$, $\mathbf{K}$ are the N $\times$ N mass and stiffness matrices respectively, $\mathbf{F}_{ext}$ is a N $\times$ 1 vector of the externally applied loads, and $\mathbf{u}$ is a N $\times$ 1 vector of the physical displacement with $\ddot{\mathbf{u}}$ as the acceleration. $\mathbf{F}_J(\mathbf{u}, \boldsymbol{\theta})$ is a N $\times$ 1 vector of the force localized to the joint. $\boldsymbol{\theta}$ is an internal variable used to track the state of the slider elements in the joint model to determine the force and displacement of the following time-step from the previous one.

The system can be equivalently written with matrices partitioned between the boundary (interface) and internal DOFs as

$$\begin{bmatrix} \mathbf{M}_{ii} & \mathbf{M}_{ib} \\ \mathbf{M}_{bi} & \mathbf{M}_{bb} \end{bmatrix} \begin{Bmatrix} \ddot{\mathbf{u}}_i \\ \ddot{\mathbf{u}}_b \end{Bmatrix} + \begin{bmatrix} \mathbf{K}_{ii} & \mathbf{K}_{ib} \\ \mathbf{K}_{bi} & \mathbf{K}_{bb} \end{bmatrix} \begin{Bmatrix} \mathbf{u}_i \\ \mathbf{u}_b \end{Bmatrix} + \begin{Bmatrix} 0 \\ \mathbf{F}_{j,b}(\mathbf{u}_b, \theta_b) \end{Bmatrix} = \begin{Bmatrix} 0 \\ \mathbf{F}_b \end{Bmatrix} \tag{2}$$

where subscripts b and i represent the boundary and internal DOF respectively. It is assumed

that only the boundary DOF are forced either externally or internally through the joint. As detailed in [32], the basis to transform from physical space to a reduced set consists of fixed interface modes[1], Φ, and constraint modes [2], Ψ, to obtain the HCB transformation matrix in Eq. 3 where $\mathbf{q}_i$ are the modal DOF associated with the fixed interface modes.

$$\begin{Bmatrix} \mathbf{u}_i \\ \mathbf{u}_b \end{Bmatrix} = \mathbf{T}^{\text{HCB}} \begin{Bmatrix} \mathbf{q}_i \\ \mathbf{u}_b \end{Bmatrix} = \begin{bmatrix} \mathbf{\Phi} & \mathbf{\Psi} \\ \mathbf{0} & \mathbf{I} \end{bmatrix} \begin{Bmatrix} \mathbf{q}_i \\ \mathbf{u}_b \end{Bmatrix} \tag{3}$$

Then, one can use this transformation matrix to reduce the EOM to that shown in 4 where the interface DOF are preserved.

$$\begin{bmatrix} \mathbf{I} & \bar{\mathbf{M}}_{ib} \\ \bar{\mathbf{M}}_{bi} & \bar{\mathbf{M}}_{bb} \end{bmatrix} \begin{Bmatrix} \ddot{\mathbf{q}}_i \\ \ddot{\mathbf{u}}_b \end{Bmatrix} + \begin{bmatrix} \Lambda_{ii} & \mathbf{0} \\ \mathbf{0} & \bar{\mathbf{K}}_{bb} \end{bmatrix} \begin{Bmatrix} \mathbf{q}_i \\ \mathbf{u}_b \end{Bmatrix} + \begin{Bmatrix} 0 \\ \mathbf{F}_{j,b}(\mathbf{u}_b, \theta_b) \end{Bmatrix} = \begin{Bmatrix} 0 \\ \mathbf{F}_b \end{Bmatrix} \tag{4}$$

2.2 Spidering using Multi-Point Constraints

The HCB reduced model has a basis of fixed interface modes and the interface DOF. A second reduction is done on the interface using multi-point-constraints (MPCs) to constrain the displacement and rotation of the interface nodes to a single node. In this study, two types of MPCs are examined: RBAR and RBE3 (using NASTRAN's naming convention). RBAR MPCs are rigid beams psuedo-elements consisting of infinitely rigid beams that constrain a set of nodes to a single 6-DOF node [7]. RBARs have six constraint equations where the translations of the reduced node are consistent with the rotations (three equations) and the rotations are equal at both ends of the rigid bar (3 equations).

On the other hand, RBE3 elements consist of averaging type elements that constrain

---

[1]Fixed interface modes are normal modes obtained by fixing the interface between two subcomponents

[2]Constraint modes are obtained by deflecting a single DOF by a unit displacement while fixing the other DOF

the average displacement and rotation of a set of nodes to a single 6-DOF node. Unlike the RBAR element, the RBE3 element applies a distributed force to the constrained set of nodes while not adding additional stiffness to those nodes. The distributed forces are determined the six constraint equations where the translation of the single node is the sum of the translations of the set of nodes, and the rotations of the single node are are the weighted average of the nodal translations of set of nodes [33].

Figure 2 shows an example of the MPC spidering approach on the S4 Beam. As part of this process, the degrees of freedom belonging to the spidered node set will be specified as the boundary set that is retained after the reduction, and the algorithm assigns a constraint-type formulation on these boundary nodes. Note that separate spider nodes and HCB reduction nodes are required given that spidered nodes can not be used as both a MPC node and HCB reduced node set per the implementation of the HCB Method for Abaqus [6] and Sandia National Laboratories Sierra Structural Dynamics code [7]. In order to mirror the translation and rotation of the spidered nodes, the CB reduction nodes are attached to the spidered nodes with a stiff spring. The nodes are shown expanded for visualization, but in fact are all coincident.

The spiders reduce an area of nodes of each interface surface to a single node that can be used to connect the two surfaces. Linear springs or nonlinear hysteretic models can be used to connect these nodes to capture the linear/nonlinear dynamics of the system.

2.3 Whole joint Model

Segalman's 4-parameter Iwan element can be readily used as a whole joint model to model the change in frequency and damping for a mode of vibration. It was developed as part of a large research effort at Sandia National Laboratories that considered both analytical solutions for contact and empirical evidence that showed that joints exhibit power-law energy dissipation versus vibration amplitude [25]. An Iwan element is simply a collection of slider

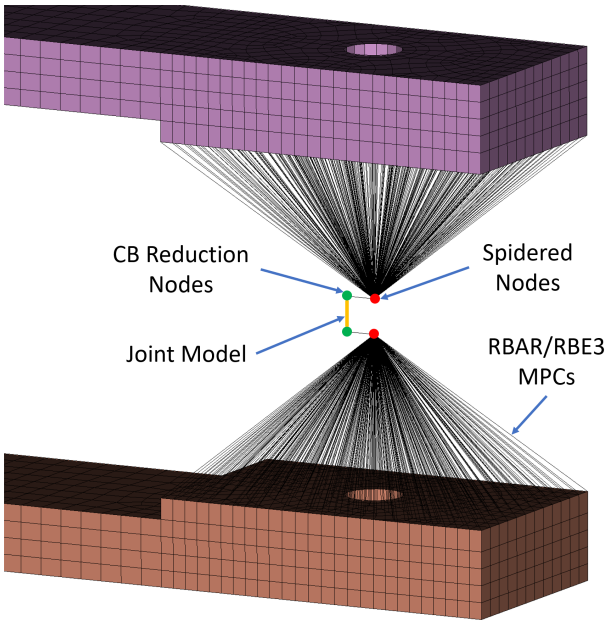

Figure 2: Spidered Joint depicting the MPCs, reduction nodes and the joint model that connects both interfaces

or Jenkins elements in parallel, in which the slip force[3] for each slider is chosen to create an element that exhibits power-law energy dissipation. This approach simplifies joint modeling significantly; typical joint models consider every point in the interface to be independent and governed by several parameters, i.e. the friction coefficient, normal force, etc.... The computational cost significantly increases when one multiplies these unknowns by the number of contact elements there may be hundreds or thousands of free parameters. Segalman's model recognizes that the net effect of all of these parameters must be to produce power-law dissipation versus vibration amplitude, which is governed by only two of the four parameters in the Iwan model. The other two parameters control the transition to macro-slip when the joint slips completely. Macro-slip is typically not observed in engineered joints if they are tightened properly, except perhaps under extreme loading. The four parameter Iwan model can be represented by four parameters: F_s, K_T,χ and β given in Table 1. For an in-depth discussion of the Iwan element, refer to [25].

[3]If all sliders have the same friction coefficient then the slip force is defined by the normal force for each slider.

Table 1: Definition of Iwan Parameters (physical description)

F_s	The force necessary to cause macroslip
K_T	The tangential stiffness of the Jenkins elements (i.e. the joint stiffness when no slip occurs)
χ	The exponent that describes the slope of the energy dissipation curve
β	The ratio of the number of Jenkins elements that slip before micro-slip and then at macroslip

For the nonlinear analysis, the Iwan joint replaces a linear spring between two spiders, and the corresponding spring constant becomes the K_T parameter of the Iwan element.

2.4 Nonlinear Model Updating

Quasi-Static Modal Analysis (QSMA) was originally proposed by Festjens et. al [30] as a method that replaces a dynamic simulation of a joint with a quasi-static problem that can be solved to estimate the effective natural frequency and damping of a single mode due to the joints in the structure. A quasi-static distributed force is applied that replicates the inertial loading experienced during vibration in that mode and coupling between the vibration modes is ignored. Lacayo and Allen further extended QSMA, developing an even faster algorithm for the case where the joints are represented by Iwan elements [15]. A brief overview of that QSMA approach by Lacayo and Allen is detailed below. Refer to [8, 15, 34, 35] for additional details and limitations.

The joint force in Eq. 1 is linearized about an equilibrium state by evaluating the Jacobian of the force with respect to each coordinate of $\mathbf{u}$. This can be done by a preload or by joining the interface nodes with linear springs, resulting in the tangent stiffness matrix for the joint forces given in Eq. 5.

$$\mathbf{K}_0 = \left.\frac{\partial \mathbf{F}_J}{\partial \mathbf{u}}\right|_{\mathbf{u}_0} \tag{5}$$

The natural frequencies and modes are computed about this equilibrium by solving the following eigenvalue problem where ω_r and $\boldsymbol{\phi}_r$ are the respective eigenvalue and eigenvector for the rth mode.

$$\left(\mathbf{K} + \mathbf{K}_0 - \omega_r^2 \mathbf{M}\right) \boldsymbol{\phi}_r = \mathbf{0} \tag{6}$$

A quasi-static distributed force is then applied such that replicates the inertial loading experienced during vibration in the rth mode. The following equation is then solved statically

$$\mathbf{K}\mathbf{u} + \mathbf{F}_J(\mathbf{u}, \boldsymbol{\theta}) = \mathbf{M}\boldsymbol{\phi}_r \alpha \tag{7}$$

where α represents a scalar amplitude for the applied body load. For the purposes of this paper, α is linearly increased from 0 to a maximum amplitude level of interest. Given that all three variables are functions of amplitude, the damping and natural frequency can be plotted in terms of modal velocity amplitude and this is the convention that will be used in this work.

3 EXPERIMENTAL EXAMPLE: S4 BEAM

This paper applies the spidering approach to compute the linear and nonlinear characteristics of the S4 Beam experimental structure as modeled in Figure 3 [4]. For experiment measurements, refer to [4, 36]. Section 3.1 describes the geometry and the modeling procedure to construct a HCB ROM and material property calibration of the structure using a single beam. Section 3.2 and 4 discuss the linear and nonlinear updating methodology and procedure, respectively.

3.1 Overview of Finite Element Model

The model incorporates two C shaped beams that are held together by bolts and washers at each end. A single beam is 50.8 cm (20 in) long and 3.18 cm wide (1.25 in). At each end, the beam is 1.27 cm (0.5 in) thick with a 5.08 x 3.18 cm (2 x 1.25 in) contact interface that is nominally flat. The steel bolts and washers were modeled as one entity and tied to the top and bottom of the beam, but the contact interfaces between the beams were left free to slide or penetrate relative to each other. Lastly, the full order model of the structure was coarsely meshed, only containing 16,312 HEX elements. Since the model will be further reduced and tuned to experiments, a high-fidelity model is not required.

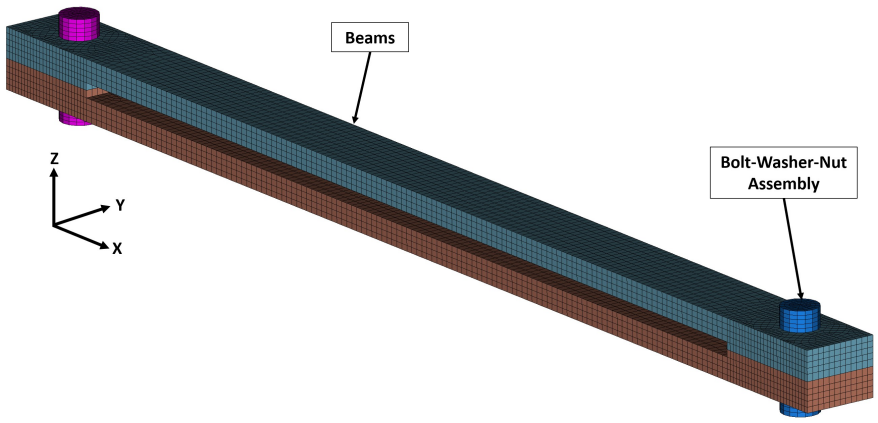

Figure 3: Finite element model of the S4B depicting the coordinate system. The beam is segmented into blocks with nodes corresponding to measurement points

The FEM was reduced by creating a HCB model in which only the spider DOF were retained as interface (boundary) nodes to create a compact and efficient model. The resulting model had 24 interface DOF (a six DOF CB reduction node at each of the four interfaces) and 30 fixed interface modes to capture the global behavior, resulting in a ROM of 54 DOF, a reduction by a factor of 302.

The spiders were defined over two different areas: the full interface and a reduced in-

terface, both of which are shown in Fig. 4a and Fig. 4b. The full interface consists of all nodes on the flat portion where contact is possible, whereas the reduced interface consists of an estimate of relative contact patch nodes that was found to be in contact in a nonlinear contact simulation performed in Abaqus [8]. The result of this contact simulation is also shown in Figure 4. Note that this simulation approximates the surfaces as perfectly smooth and flat, and there is some evidence that the surfaces are not truly flat, as reported in [4,36]. Nevertheless, these models are in line with the typical approach detailed in Section 2.2, considering the information that might be available during the design of a structure. For each of the interface areas, two models were created, one using RBAR elements and one using RBE3s as the type of MPC, resulting in a total of four candidate HCB models.

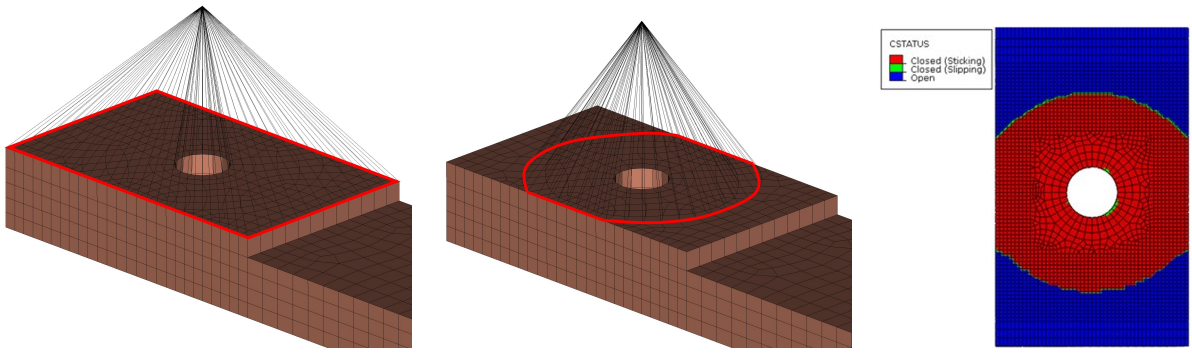

(a) **(b)** **(c)**

Figure 4: (A) Full contact area, (B) Reduced contact area, (C) Abaqus Contact Simulation from [8]

Prior to calibrating the whole-joint models with linear springs, a FEM of each single beam was calibrated against experiment data by adjusting the material properties for each beam to ensure minimal uncertainty for the frequencies of the assembled system against the experimental structure. Table 2 lists the adjusted material properties for each entity in the model. The densities of the model were calibrated by measuring the mass of the experimental beams and bolts, and dividing by the volume of the FEM to ensure that the

FEM has correct mass. These material properties were used for the four candidate HCB models.

Table 2: Adjusted material properties for each sub-component of the S4 Beam system

Property	**Top Beam**	**Bottom Beam**	**Bolt-Nut-Washer Assembly**
Density	7.83e-3 kg/cm^3 (7.33e-4 $slinch/in^3$)	7.83e-3 kg/cm^3 (7.33e-4 $slinch/in^3$)	5.26e-3 kg/cm^3 (4.92e-4 $slinch/in^3$)
Elastic Modulus	187.8 GPa (27.2e6 psi)	194.8 GPa (28.3e6 psi)	204.8 GPa (29.7e6 psi)
Poisson Ratio	0.29	0.29	0.29

3.2 Whole-joint Spring Calibration of the Assembled ROM

To match frequencies and mode shapes of the HCB reduced systems to the experimental data, six linear springs were placed between the reduced nodes at each interface corresponding to three translational DOF and three rotational DOF as shown in Fig. 2. This work assumed that the spring stiffnesses on either end of the beam are identical for each DOF. MATLAB's fmincon function using the interior point algorithm [37,38] was used to optimize each model with the objective function given in Eq. 8. The stiffnesses were lower bounded

such that a negative stiffness was not possible. Table 3 depicts the percent error natural frequencies of the assembly after optimization and Table 4 lists the spring stiffnesses for each of the cases.

$$ObjectiveFunction = \sum_{i=1}^{N} \left(\frac{\omega_{model,i} - \omega_{test,i}}{\omega_{test,i}} \right)^2 \tag{8}$$

Table 3: Natural frequency errors for each of the candidate models. The four candidate models contain different spider areas (full vs. reduced) and different constraint elements (RBAR vs. RBE3).

Mode	Test Freq. [Hz]	Full RBAR	Full RBE3	Reduced RBAR	Reduced RBE3	Mode Shape
1	258.0	0.64%	0.22%	0.47%	0.18%	
2	331.7	-0.00%	-0.02%	-0.00%	-0.55%	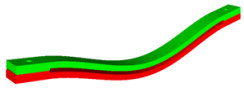
3	478.6	0.59%	0.43%	0.52%	0.40%	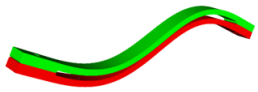
4	567.7	-0.50%	-0.54%	-0.53%	-0.54%	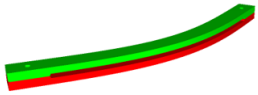
5	708.3	-0.57%	-0.19%	-0.41%	-0.15%	
6	851.5	0.00%	0.00%	0.00%	-0.00%	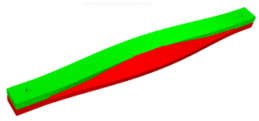

The S4 Beam has several different types of mode shapes, and each is influenced by

Table 4: Linear spring stiffnesses for each candidate model.

Spring	Full RBAR MPC	Full RBE3 MPC	Reduced RBAR MPC	Reduced RBE3 MPC
$T_x[\frac{lb}{in}]$	5.53e6	4.28e8	9.98e6	3.24e10
$T_y[\frac{lb}{in}]$	9.74e8	2.43e8	7.12e7	2.99e5
$T_z[\frac{lb}{in}]$	9.49e7	1.23e8	4.07e8	1.83e10
$R_x[\frac{in-lb}{rad}]$	3.81e8	5.22e6	7.86e8	5.23e10
$R_y[\frac{in-lb}{rad}]$	3.45e5	5.56e5	4.80e5	1.70e6
$R_z[\frac{in-lb}{rad}]$	2.03e6	3.84e6	3.47e6	7.75e7

different springs depending on how the joint is loaded. The mode shapes shown in Table 3 can be used to deduce these differences. For example, Modes 1 and 5 involve opening of the joint and hence are most sensitive to the Z-direction translational stiffness, whereas Mode 4 is completely insensitive to the joint stiffness.

While the overall agreement was similar for each candidate model, a few differences are noted between the results obtained using RBE3 and RBAR elements. Most notably, the models with RBE3s had slightly larger errors for Mode 2 than the RBAR models; this mode is sensitive to the axial stiffness of the joint (T_x), loading it in the fashion of the lap joints that have been studied in many prior works [15, 27]. Each model has similar error for Mode 4, a mode that is not influenced by the joint interface. Therefore, there is some error present between the material property calibration of the piece-parts and the fully assembled structure. Although this does not influence the joint characteristics, it is important to understand that model calibration to experiment measurements has some inherent uncertainty.

In comparing the results with the reduced and full interfaces, one can see that the reduced interface typically required higher spring stiffnesses than the full interface (e.g. consider R_y in Table 4). This result makes sense, as reducing the interface area effectively decreases the stiffness of the joint region, and so the spring constants must be increased to compensate. Furthermore, RBAR models require softer springs since there is stiffness present in the rigid

bar MPC.

To get a sense of the sensitivity of the natural frequencies to the spring constants and what ranges for these stiffnesses might be reasonable, Figure 5 depicts the percent error in each natural frequency of the full interface with RBAR MPC model against the experimental frequencies as each design variable changes relative to the values in Table 4. Each stiffness was varied by 3 to 4 orders of magnitude higher and lower of the nominal value, while the other five springs were held at their nominal value. The scaling is hence referred to as γ.

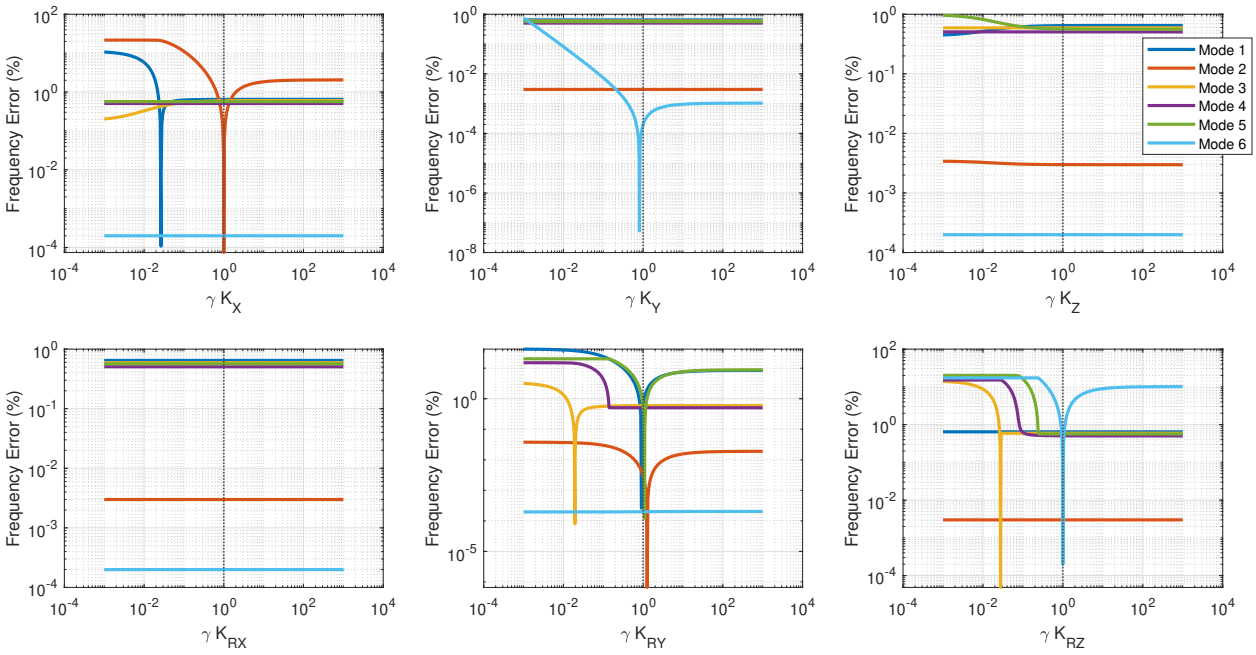

Figure 5: Frequency error for each mode as each spring stiffness is varied separately for the Full Interface RBAR HCB model.

It is apparent that no value of the X-direction rotational spring stiffness (K_{RX}) can better correlate either model since the joints and modes do not exercise this rotation within the frequency range of interest. In the instances of X-direction translational, Y-direction rotational, and Z-direction rotational stiffnesses for the full interface RBAR MPC model,

the optimal stiffness for one mode does not correspond to the optimal stiffness of the others. For example, the X-direction translational spring has a nominal stiffness that minimizes the error for Mode 2, whereas a $\gamma = 0.026$ scaling on the stiffness (T_x) minimizes Mode 1 error at the cost of a Mode 2 error of 21%. This is repeated for the reduced interface RBE3 MPC model as shown in Fig 6.

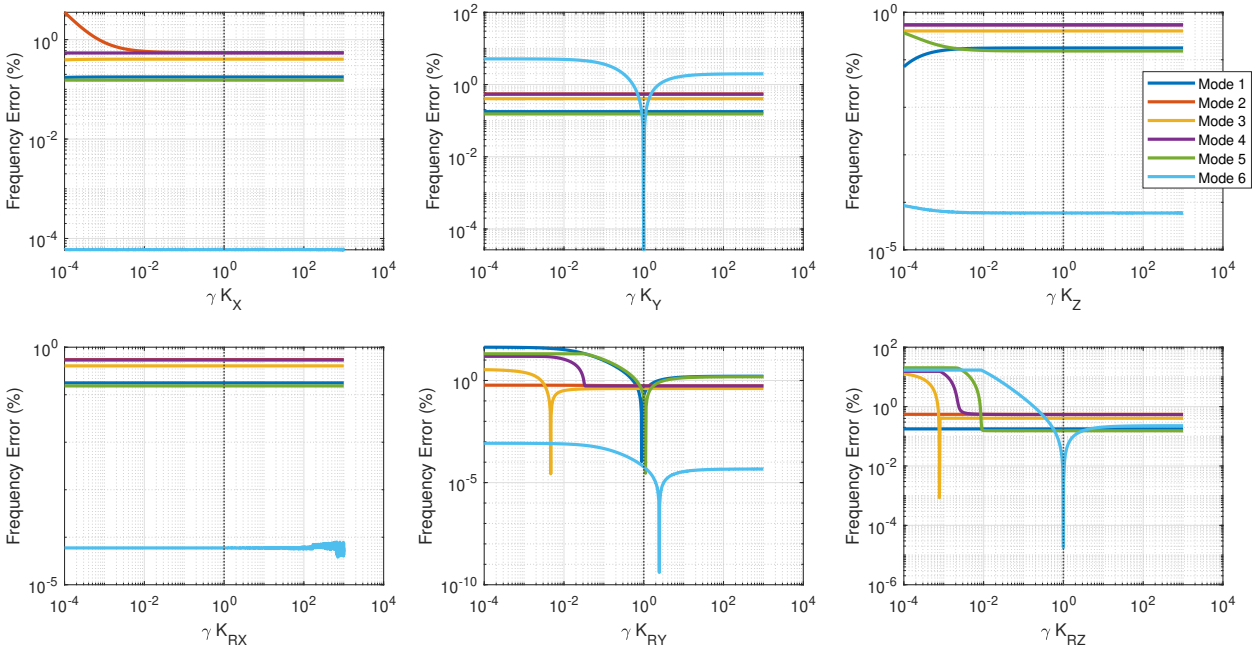

Figure 6: Frequency error for each mode as each spring stiffness is varied separately for the Reduced Interface RBE3 HCB model.

A similar result is seen for the reduced interface RBE3 MPC model, where there exists optimal K_T scaling for one mode that is sub-optimal for another, whereas no adjustment of the x-direction and z-direction translational springs can produce lower frequency errors. For the stiffnesses that exhibit troughs, there is very little freedom to vary the spring stiffness parameters in nonlinear updating in order to improve nonlinear correlation if preserving linear frequencies was desired. This introduces the concept of a trade-off between linear

updating where the linear optima may not have suitable stiffnesses for nonlinear updating. This is explored further in the following section.

4 NONLINEAR MODEL UPDATING

In order to investigate the ability of each candidate model to correlate to nonlinear experiment data, Iwan elements are placed in parallel to the linear springs at each interface. In the results that follow, Mode 2 was correlated to measurements at an impact level of 250 N (56.2 lbf) and a torque on each bolt of 25.1 N-m (18.5 ft-lb). This is done by placing an Iwan element in the X translation direction that affects the shearing of the joint and is assumed to cause the nonlinearity observed in this mode. The nominal tangential stiffness (K_T) of the joint is the linear stiffness (K_X) obtained from linear updating for each model. The optimal set of parameters for each model was found in two ways: a Monte Carlo simulation (MCS) and MATLAB's Global Search function (GS). The MCS is done to establish the parameter space for the slip force (F_S), χ, and β, without varying the tangential stiffness as to preserve the linear correlation. The GS optimization is done to find a global optimum with K_T allowed to vary, using MATLAB's fmincon function repeatedly [39].

4.1 Nonlinear Optimization Function

In both methods, the optimization function minimizes the frequency and damping error with respect to amplitude against measurements. However, due to end effects present in the measurements, the nonlinear fits could be skewed. Therefore, only a portion of the response that depicts power law behavior for damping is used to fit the nonlinear models measurements [27, 40]. The experiment responses and fit region are shown in Fig. 7.

The cost function evaluates the root mean square percent error (rmspe) between the quasi-static simulated response to the measurement for both frequency (ε_ω) and damping (ε_ζ). The total error (ε_{Total}) is then defined as the sum of the root of the squares of these

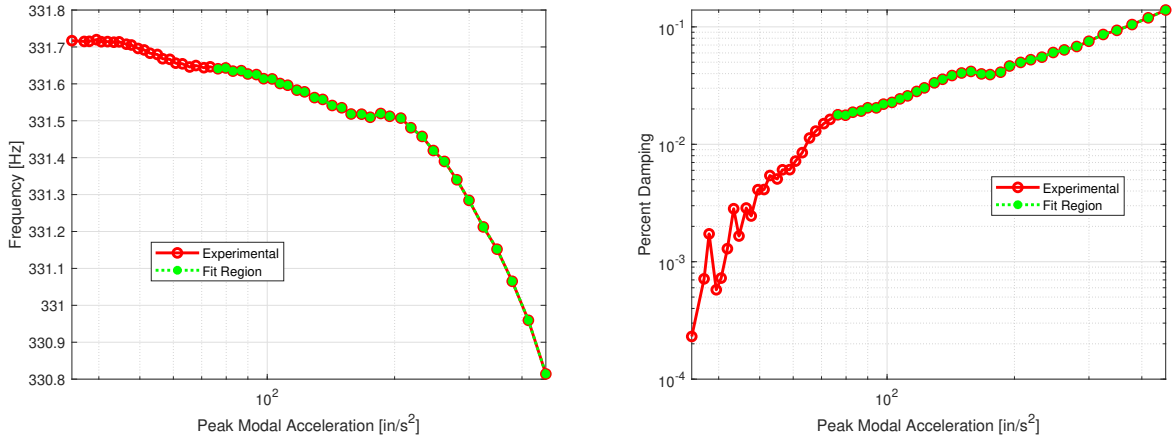

(a) **(b)**

Figure 7: Measurement of (a) Frequency vs. Modal Acceleration, (b) Percent Damping vs. Modal Acceleration for Mode 2

errors as given in Eq. 9c.

$$\varepsilon_\omega = RMS\left(\frac{\omega_{model} - \omega_{exp}}{\omega_{exp}}\right) \tag{9a}$$

$$\varepsilon_\zeta = RMS\left(\frac{\zeta_{model} - \zeta_{exp}}{\zeta_{exp}}\right) \tag{9b}$$

$$\varepsilon_{Total} = \sqrt{\varepsilon_\omega^2 + \varepsilon_\zeta^2} \tag{9c}$$

4.2 Monte Carlo Simulations

The objective of the Monte Carlo optimization was to determine the parameter space for the Iwan parameters about the linear solution, i.e. a nominal tangential stiffness. An initial 1000 iteration MCS simulation was done to determine the appropriate bounds of F_S, χ, and β. Afterwards, a 100,000 iteration MCS was done on each model where F_S was randomly distributed between 50 to 500 lbf, χ between -0.9 to 0.9, and β between 1e-3 and 3. The computation time parallelized to 12 cores was approximately 6 minutes for each model for

QSMA on the ROM with Iwan elements. Figure 8 shows the percent frequency and damping error for each MCS run of each model as defined by Eq. 9a and 9b.

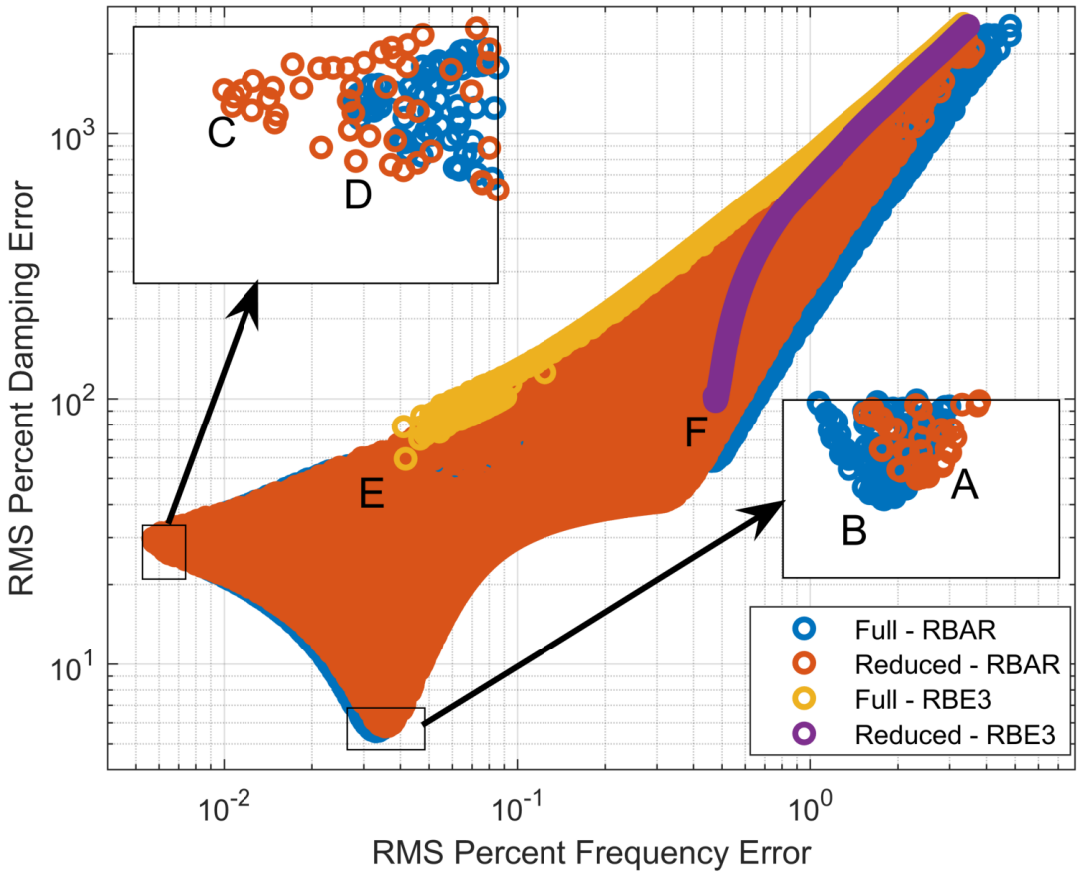

Figure 8: Plot of errors of frequency and damping for Mode 2 for 100,000 random Iwan parameter iterations. This is repeated for each of the four candidate models.

Both the RBAR models exhibit Pareto fronts where one can minimize frequency error or damping error, but not both. Furthermore, both models have very similar boundaries, indicating that the type of MPC influences the correlation, rather than the area for contact. The RBE3 models have much higher errors for frequency and damping and do not exhibit a pareto front. Six solutions of the four 100,000 iterations are of particular interest and are shown in Fig. 9. Solutions A and B optimize for damping, while allowing some frequency

error for the full and reduced interface RBAR models respectively, whereas solutions C and D optimize for frequency. Solutions E and F are the optimal solutions for the full and reduced RBE3 models respectively. Each solution in Fig. 9 contains three subplots where they show the change in damping, the change in frequency, and the normalized change in frequency to the low level frequency. Since models may have an offset from the low level frequency of measurements, the latter provides insight into the differences between the change in frequency of the measurement to the change in frequency of the model. The parameters and errors in frequency and damping for each solution are shown in Table 5.

Table 5

Solution	**Model**	F_S	K_T	χ	β	ε_ω (%)	ε_ζ (%)	ε_{Total} (%)
A	Full - RBAR	93.73	5.53e06	-0.05	1.83	0.034	5.59	5.59
B	Red - RBAR	96.74	9.98e06	-0.15	0.74	0.035	5.82	5.82
C	Full - RBAR	78.88	5.53e06	0.32	1.91	0.006	28.73	28.73
D	Red - RBAR	79.17	9.98e06	0.20	0.82	0.0057	29.82	29.82
E	Full - RBE3	76.62	4.28e08	-0.89	2.33e-3	0.0426	57.61	57.61
F	Red - RBE3	73.89	3.24e10	-0.81	0.11	0.477	98.04	98.04

Both RBAR models have excellent correlation to the frequency and damping seen experimentally, regardless when optimizing for frequency or damping. However, it is clear that optimizing for damping (Fig. 9A, Fig. 9C) rather than frequency, reduced total errors for the model in Table 5. For RBE3 models, Table 5 shows large errors in both frequency and damping. In fact, a reason for this lies with the order of magnitude of the tangential stiffness. Although the slip force is similar for all candidate models, the RBE3 tangential stiffness is much higher than the RBAR models. Naturally, this is due to the stiffness provided by the MPC. To allow for a better fit and compensate for the stiffness, the optimization aims to push χ to the lower bound, resulting in poor fits to measurements. These fits maintain

linear correlation between the model and the experiments, whereas the subsequent section optimizes for the nonlinear solution by allowing the tangential stiffness to vary by a factor of γ, and hence the linear correlation.

4.3 Global Search Optimization

After determining the parameter space for the Iwan elements, the candidate models were optimized using a global search optimization in an effort to obtain a global optima. The computational cost for each model varied from 1 minute for the Full - RBAR to 4 minutes for Reduced - RBE3 with 1,000 trial points. γ was allowed to vary from 1e-4 to 1e2. Table 6 lists the updated parameters and errors for each model, and Fig. 10 shows each solution when compared to measurements.

Table 6: Iwan parameters and errors for each candidate model using Global Search Optimization

Model	F_S	γ	K_T	χ	β	ε_ω (%)	ε_ζ (%)	ε_{Total} (%)
Full - RBAR	81.50	0.994	5.50E+06	-0.05	2.37	0.043	5.58	5.58
Full - RBE3	72.39	0.016	6.90E+06	-0.10	2.05	1.54	5.62	5.82
Red - RBAR	80.27	0.643	6.42E+06	-0.07	1.97	0.62	5.60	5.63
Red - RBE3	130.53	2.30E-04	7.45E+06	-0.11	0.22	1.96	5.66	5.99

It is apparent in Fig. 10 that all models have a qualitatively excellent fit to damping and the frequency shift. All models required a decrease in the tangential stiffness to obtain a better correlation, where the RBE3 models had the largest reduction by 0.016 for the Full - RBE3 model, and 2.3e-4 for the Reduced - RBE3 model. As a result, the tangential stiffness for each model is on the order of magnitude of 10^6, with the tangential stiffness of RBE3 ROMs stiffer than the RBAR ROMs.

While the nonlinear correlation is remarkably good, there is inherently a trade-off between

linear and nonlinear correlation. Table 7 lists the frequency errors of Mode 2 for each candidate model during the linear updating step (Section 3.2) where the linear frequency errors are minimized, and the frequency errors during the nonlinear updating step (using GS) where the error in the nonlinear correlation is minimized.

Table 7: Mode 2 linear updating frequency percent error and nonlinear updating frequency percent error for all candidate models.

Model	**Linear Updating Freq. Error (%)**	**Nonlinear Updating Freq. Error (%)**
Full RBAR	-0.00	-0.01
Full RBE3	-0.02	-1.51
Red RBAR	-0.00	-0.59
Red RBE3	-0.55	-1.93

Immediately it is apparent that having good nonlinear correlation requires that the joint stiffness is reduced, and hence introduces additional frequency error. Since only one stiffness (K_x) is reduced, one can reference the stiffness variation study in Figs. 5 and 6, to gain further insight into this trade-off between linear and nonlinear correlation. The reduced interface RBE3 model requires such a large stiffness adjustment factor of 2.3e-4, that the linear correlation error is sufficiently large for Mode 2. Per Fig. 6, although there is a large range of γK_x that does not introduce further error, the large reduction in K_x necessary for nonlinear correlation is enough to cause an error of -1.93%. However, previous studies have examined an alternative of adding a post-slip stiffness to maintain the nominal joint stiffness, but reduce the stiffness in the Iwan element.

A study done by Porter et al. [41] assessed various friction models for bolted interfaces, in which the authors found that adding a post-slip stiffness reduced the frequency and damping error for a HCB ROM of the Brake-Reuß Beam [5]. A post-slip stiffness is a

spring that is placed in parallel to the Iwan element to join the interfaces together. This is done to lower the tangential stiffness, while retaining linear frequency accuracy such that $K_{PostSlip} + K_T = K_{Joint}$. In essence, this transfers some of the energy from the Iwan element to the post-slip spring, thus reducing the effect of the Iwan element. While this is very useful for other models, for the four candidate S4 Beam models a post-slip stiffness increases error in both frequency and damping and therefore was not employed here.

5 CONCLUSION

This paper explored the applicability of linear and nonlinear model updating to the nonlinear benchmark structure, S4 Beam. Coarse meshed models were created using RBAR and RBE3 spidered joints to understand the effects of the area of influence for the joint (i.e. using full and reduced contact interface areas) and the type of multi-point-constraint, resulting in four candidate models. The viability of the models was studied by evaluating two criteria: (1) ability to reproduce the linear natural frequencies of the assembly by updating linear springs at the interface and (2) ability to capture the amplitude dependent frequency and damping caused by the joints by updating the parameters of nonlinear Iwan elements at the interfaces.

The linear updating exercise showed that all models were quite similar, although the models with spiders constructed with rigid bar elements (RBAR) had lower tangential stiffnesses that affect Mode 2. This is significant since nonlinear updating required a softer tangential spring for a better correlation. Spring variance studies were done that showed that the optimal stiffness that minimizes the error for one mode does not necessarily correspond to the optimal stiffness for another mode.

Quasi-static modal analysis was then used to update the parameters of the nonlinear Iwan elements, using the joint stiffnesses found in the linear updating step. Although the models captured the linear modes quite similarly, they produced a widely varying results

for the nonlinear damping and for the change in frequency with vibration amplitude. The model with RBAR elements, regardless of contact area, resulted in the excellent correlation between the experimental nonlinear frequency and damping curves, whereas both RBE3 models resulted in a poor correlation. The tangential stiffness was varied to obtain a better nonlinear correlation at the cost of a higher linear frequency error. As a result, the stiffness of the RBE3 models was decreased to the same order of magnitude of the RBAR models, resulting in a higher linear frequency error for the RBE3 models. It is important to consider both linear updating and nonlinear updating simultaneously to minimize the linear frequency error and the nonlinear frequency and damping error.

In the case of the S4 Beam, a lower tangential stiffness is beneficial for both linear and nonlinear updating, indicating that the RBAR models are optimal for this structure. However, there is uncertainty if this is true for all structures. Future work seeks to apply the spidering approach detailed in this paper to other structures to develop best practices for spidering.

REFERENCES

[1] R. A. Ibrahim and C. L. Pettit, "Uncertainties and dynamic problems of bolted joints and other fasteners," *Journal of Sound and Vibration*, vol. 279, no. 3-5, pp. 857–936, 2005. Number: 3-5.

[2] D. Di Maio, "Identification of Dynamic Nonlinearities of Bolted Structures Using Strain Analysis," 2016.

[3] C. Hartwigsen, Y. Song, D. McFarland, L. Bergman, and A. Vakakis, "Experimental study of non-linear effects in a typical shear lap joint configuration," *Journal of Sound and Vibration*, vol. 277, pp. 327–351, Oct. 2004. Number: 1-2.

[4] A. Singh, M. Scapolan, Y. Saito, M. S. Allen, D. Roettgen, B. Pacini, and R. J. Kuether, "Experimental Characterization of a New Benchmark Structure for Prediction of Damp-

ing Nonlinearity," in *Nonlinear Dynamics, Volume 1* (G. Kerschen, ed.), Conference Proceedings of the Society for Experimental Mechanics Series, (Cham), pp. 57–78, Springer International Publishing, 2019.

[5] T. Dossogne, T. Jerome, D. Lancereau, S. Smith, M. Brake, B. Pacini, P. Reuss, and C. Schwingshackl, "Experimental Assessment of the Influence of Interface Geometries on Structural Dynamic Response," pp. 255–261, Apr. 2017.

[6] Dassault Systèmes, "Abaqus Analysis User's Manual Version 6.14," 2014.

[7] Sierra Structural Dynamics Development Team, "Sierra/SD – User's Manual – 4.56," Tech. Rep. SAND2020-3028, Sandia National Laboratories, Albuquerque, NM, Apr. 2020.

[8] E. Jewell, M. S. Allen, I. Zare, and M. Wall, "Application of Quasi-Static Modal Analysis to a Finite Element Model and Experimental Correlation," *Journal of Sound and Vibration*, vol. 479, no. 4 August, p. 115376, 2020. Number: 4 August.

[9] P. Gray and C. McCarthy, "A global bolted joint model for finite element analysis of load distributions in multi-bolt composite joints," *Composites: Part B*, vol. 41, pp. 317–325, 2010.

[10] J. Kim, J.-C. Yoon, and B.-S. Kang, "Finite element analysis and modeling of structure with bolted joints," *Applied Mathematical Modelling*, vol. 31, no. 5, pp. 895–911, 2007. Number: 5.

[11] R. E. Goodman, R. L. Taylor, and T. L. Brekke, "A Model for the Mechanics of Jointed Rock," *Journal of the Soil Mechanics and Foundations Division*, vol. 94, no. 3, pp. 637–659, 1968. Publisher: ASCE.

[12] D. Süß and K. Willner, "Investigation of a jointed friction oscillator using the Multiharmonic Balance Method," *Mechanical Systems and Signal Processing*, vol. 52-53, pp. 73–87, Feb. 2015.

[13] E. P. Petrov and D. J. Ewins, "Analytical Formulation of Friction Interface Elements

for Analysis of Nonlinear Multi-Harmonic Vibrations of Bladed Disks," *Journal of Turbomachinery*, vol. 125, no. 2, pp. 364–371, 2003. Number: 2.

[14] S. Bograd, P. Reuss, A. Schmidt, L. Gaul, and M. Mayer, "Modeling the dynamics of mechanical joints," *Mechanical Systems and Signal Processing*, vol. 25, no. 8, pp. 2801–2826, 2011. Number: 8.

[15] R. M. Lacayo and M. S. Allen, "Updating Structural Models Containing Nonlinear Iwan Joints Using Quasi-Static Modal Analysis," *Mechanical Systems and Signal Processing*, vol. 118, no. 1 March 2019, pp. 133–157, 2019. Number: 1 March 2019.

[16] N. N. Balaji and M. R. W. Brake, "A quasi-static non-linear modal analysis procedure extending Rayleigh quotient stationarity for non-conservative dynamical systems," *Computers & Structures*, vol. 230, p. 106184, Apr. 2020.

[17] M. S. Allen and R. J. Kuether, "Substructuring with Nonlinear Subcomponents: A Nonlinear Normal Mode Perspective," Jan. 2012.

[18] D. de Klerk, D. J. Rixen, and S. N. Voormeeren, "General framework for dynamic substructuring: History, review, and classification of techniques," *AIAA Journal*, vol. 46, no. 5, pp. 1169–1181, 2008. Number: 5.

[19] W. C. Hurty, "Dynamic analysis of structural systems using component modes," *AIAA Journal*, vol. 3, pp. 678–685, Apr. 1965. Number: 4.

[20] R. R. J. Craig and M. C. C. Bampton, "Coupling of Substructures Using Component Mode Synthesis," *AIAA Journal*, vol. 6, no. 7, pp. 1313–1319, 1968. Number: 7.

[21] J. R. R. Craig and C.-J. Chang, "On the use of attachment modes in substructure coupling for dynamic analysis," in *18th Structural Dynamics and Materials Conference*, Structures, Structural Dynamics, and Materials and Co-located Conferences, American Institute of Aeronautics and Astronautics, 1977.

[22] R. H. MacNeal, "A hybrid method of component mode synthesis," *Computers & Structures*, vol. 1, no. 4, pp. 581–601, 1971. Number: 4.

[23] R. M. Hintz, "Analytical Methods in Component Modal Synthesis," *AIAA Journal*, vol. 13, pp. 1007–1016, Aug. 1975. Number: 8.

[24] S. Rubin, "Improved Component-Mode Representation for Structural Dynamic Analysis," *AIAA Journal*, vol. 13, pp. 995–1006, Aug. 1975. Number: 8.

[25] D. J. Segalman, "A Four-Parameter Iwan Model for Lap-Type Joints," *Journal of Applied Mechanics*, vol. 72, pp. 752–760, Sept. 2005. Number: 5.

[26] D. J. Segalman, "Modelling joint friction in structural dynamics," *Structural Control and Health Monitoring*, vol. 13, pp. 430–453, Jan. 2006. Number: 1.

[27] D. J. Segalman, D. L. Gregory, M. J. Starr, B. R. Resor, M. D. Jew, J. P. Lauffer, and N. M. Ames, "Handbook on Dynamics of Jointed Structures," tech. rep., Sandia National Laboratories, Albuquerque, NM 87185, 2009.

[28] W. D. Iwan, "ON DEFINING EQUIVALENT SYSTEMS FOR CERTAIN ORDINARY NONLINEAR DIFFERENTIAL EQUATIONS," *International Journal of Non-Linear Mechanics*, vol. 4, no. 4, pp. 325–334, 1969. Number: 4.

[29] M. Feldman, "Non-linear system vibration analysis using Hilbert transform–I. Free vibration analysis method 'Freevib'," *Mechanical Systems and Signal Processing*, vol. 8, no. 2, pp. 119–127, 1994. Number: 2.

[30] H. Festjens, G. Chevallier, and J.-L. Dion, "A numerical tool for the design of assembled structures under dynamic loads," *International Journal of Mechanical Sciences*, vol. 75, pp. 170–177, 2013.

[31] R. J. Kuether, P. B. Coffin, and A. R. Brink, "On Hurty/Craig-Bampton Substructuring With Interface Reduction on Contacting Surfaces," in *Proceedings of ASME 2017 International Design Engineering Technical Conferences and Computers and Information in Engineering Conference*, American Society of Mechanical Engineers Digital Collection, Nov. 2017.

[32] D. Krattiger, L. Wu, M. Zacharczuk, M. Buck, R. J. Kuether, M. S. Allen, P. Tiso,

and M. R. W. Brake, "Interface Reduction for Hurty/Craig-Bampton Substructured Models: Review and Improvement," *Mechanical Systems and Signal Processing*, vol. 114, pp. 579–605, Jan. 2019.

[33] SIERRA Solid Mechanics Team, "Sierra/SolidMechanics 4.56.2 User's Guide," Tech. Rep. SAND2020-5362, Sandia National Laboratories, Albuquerque, NM, May 2020.

[34] R. Lacayo, B. Deaner, and M. S. Allen, "A Numerical Study on the Limitations of Modal Iwan Models for Impulsive Excitations," *Journal of Sound and Vibration*, vol. 390, pp. 118–140, 2017.

[35] M. S. Allen, R. Lacayo, and M. R. Brake, "Quasi-static Modal Analysis based on Implicit Condensation for Structures with Nonlinear Joints," in *International Seminar on Modal Analysis (ISMA)*, (Leuven, Belgium), Sept. 2016.

[36] Mitchell P. Wall, Matthew S. Allen, and Robert J. Kuether, "Observations of Modal Coupling due to Bolted Joints in an Experimental Benchmark Structure," *Mechanical Systems and Signal Processing*, 2020.

[37] R. Waltz, J. Morales, J. Nocedal, and D. Orban, "An interior algorithm for nonlinear optimization that combines line search and trust region steps," *Mathematical Programming*, vol. 107, pp. 391–408, July 2006.

[38] R. H. Byrd, J. C. Gilbert, and J. Nocedal, "A trust region method based on interior point techniques for nonlinear programming," *Mathematical Programming*, vol. 89, pp. 149–185, Nov. 2000.

[39] Z. Ugray, L. Lasdon, J. Plummer, F. Glover, J. Kelly, and R. Martí, "Scatter Search and Local NLP Solvers: A Multistart Framework for Global Optimization," *INFORMS Journal on Computing*, vol. 19, pp. 328–340, July 2007. Publisher: INFORMS.

[40] B. Deaner, *Modeling the Nonlinear Damping of Jointed Structures Using Modal Models*. PhD thesis, University of Wisconsin-Madison, Madison, WI, May 2013.

[41] J. H. Porter, C. R. Little, N. N. Balaji, and M. R. W. Brake, "An Assessment of

the Applicability and Epistemic Uncertainties Inherent to Different Classes of Friction Models for Modeling Bolted Interfaces," in *Nonlinear Structures & Systems, Volume 1* (G. Kerschen, M. R. Brake, and L. Renson, eds.), Conference Proceedings of the Society for Experimental Mechanics Series, (Cham), pp. 291–294, Springer International Publishing, 2021.

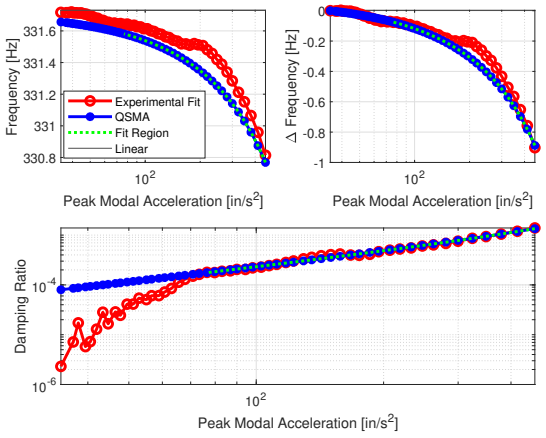

(a) Full - RBAR, Solution **A**

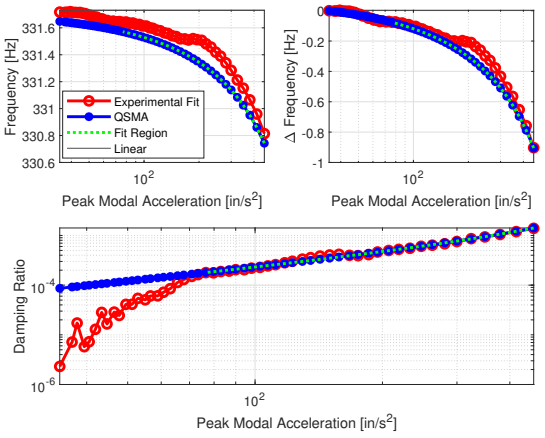

(b) Reduced - RBAR, Solution **B**

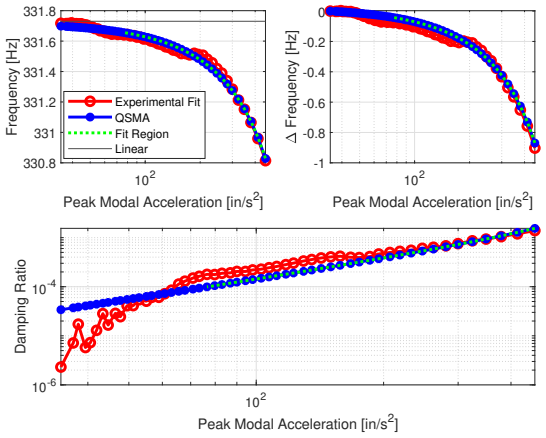

(c) Full - RBAR, Solution **C**

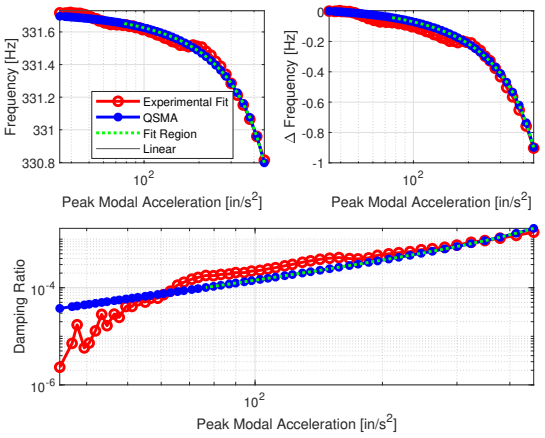

(d) Reduced - RBAR, Solution **D**

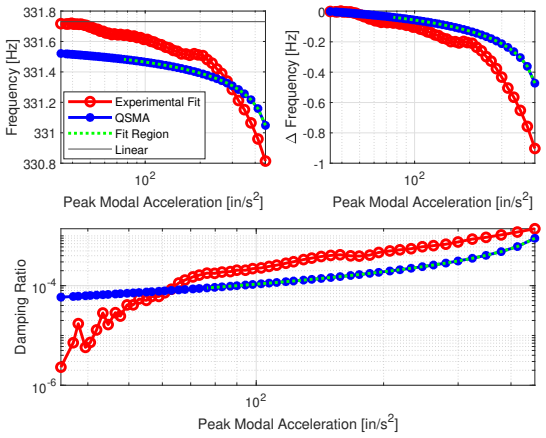

(e) Full - RBE3, Solution **E**

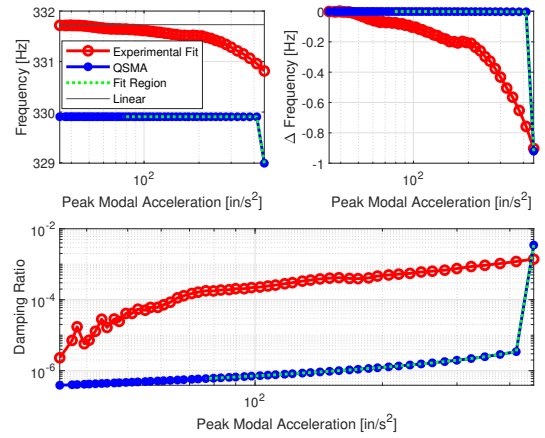

(f) Reduced - RBE3, Solution **F**

Figure 9: Quasi-static solutions compared to experiments at the six solution points in Fig. 8.

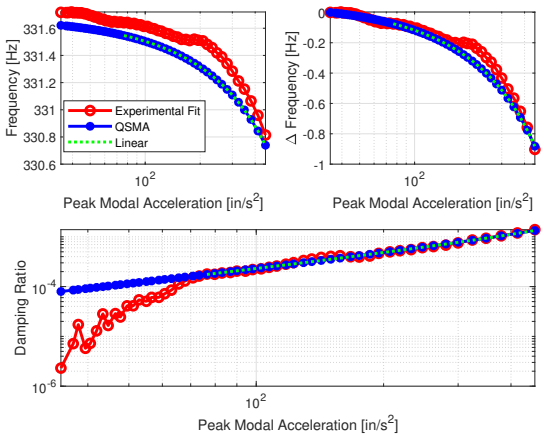

(a) Full - RBAR Model

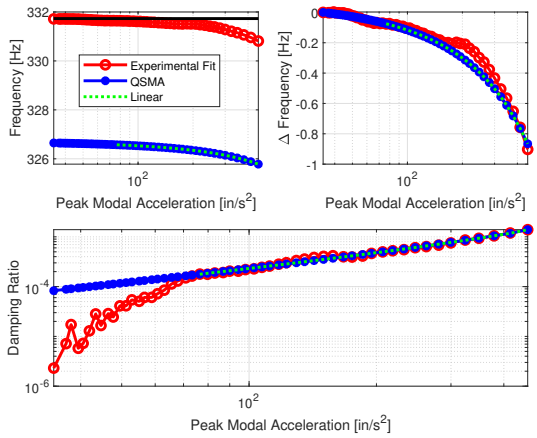

(b) Full - RBE3 Model

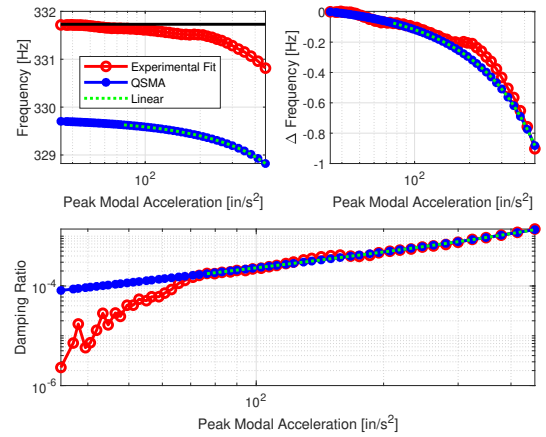

(c) Reduced - RBAR Model

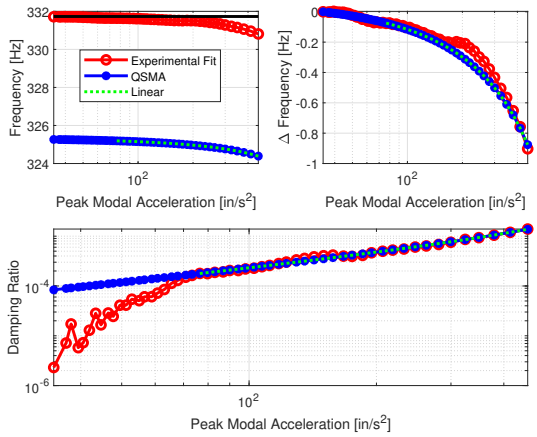

(d) Reduced - RBE3 Model

Figure 10: Global Search optimization for each candidate model where the tangential stiffness is allowed to vary.

Substructure Interface Reduction Techniques to Capture Nonlinearities in Bolted Structures

Aabhas Singh	University of Wisconsin - Madison
Matthew S. Allen	University of Wisconsin - Madison
Robert J. Kuether	Sandia National Laboratories

ABSTRACT

Structural dynamic finite element models typically use multi-point constraints (MPC) to condense the degrees of freedom (DOF) near bolted joints down to a single node, which can then be joined to neighboring structures with linear springs or nonlinear elements. Scalability becomes an issue when multiple joints are present in a system, because each requires its own model to capture the nonlinear behavior. While this increases the computational cost, the larger problem is that the parameters of the joint models are not known, and so one must solve a nonlinear model updating problem with potentially hundreds of unknown variables to fit the model to measurements. Furthermore, traditional MPC approaches are limited in how the flexibility of the interface is treated (i.e. with rigid bar elements the interface has no flexibility). To resolve this shortcoming, this work presents an alternative approach where the contact interface is reduced to a set of modal DOF which retain the flexibility of the interface and are capable of modeling multiple joints simultaneously. Specifically, system-level characteristic constraint (S-CC) reduction is used to reduce the motion at the contact interface to a small number of shapes. To capture the hysteresis and energy dissipation that is present during microslip of joints, a hysteretic element is applied to a small number of the S-CC Shapes. This method is compared against a traditional MPC method (using rigid bar elements) on a two-dimensional finite element model of a cantilever beam with a single joint near the free end. For all methods, a four-parameter Iwan element is applied to the interface DOF to capture how the amplitude dependent modal frequency and damping change with vibration amplitude.

1 INTRODUCTION

Large structural finite element models are typically composed of several sub-assemblies that are connected with joints. Nonlinearity and significant energy dissipation arise from the friction at the joint interfaces between these structures, which can be characterized in two regimes: microslip and macroslip. Microslip of a joint occurs when an applied load causes low pressure regions of the contact interface to slip while the majority of the joint remains stuck. These small regions of slip cause the effective modal damping and natural frequency to change with vibration amplitude, i.e. leading to weakly nonlinear behavior. As the joint is further loaded, macroslip occurs where the entire contact interface exhibits slip and the structure may exhibit more complicated phenomena such as modal coupling and multi-harmonic responses and even joint failure.

Although finite element software can solve contact problems with high fidelity using friction elements such as Coulomb friction to capture microslip behavior [1], the models must have highly refined meshes at the interfaces in order to obtain an accurate predictive model. Jewell, et al. [2] demonstrated this using a commercial finite element package (Abaqus®) where models with one or two joints were studied; her results showed showed that, in order to accurately simulate the static response, the mesh needed to be highly refined and much effort was needed to find an appropriate set of solver settings. This required tens of hours of simulation per iteration and considerable effort to obtain reasonable solutions. Extrapolating this method to realistic systems with 100s to 1000s of joints and to cases where the dynamic response must be computed over many cycles (whereas Jewell et al. modeled only a quarter vibration cycle), it is clear that modeling the contact in detail is not feasible.

In industry, the common approach to modeling joints is to spider each joint interface together using multi-point constraints (MPCs) [3] to reduce each contact surface down to a single point and apply either linear springs for a linear analysis or a combination of springs and hysteretic elements to capture nonlinear behavior [4, 5] as shown in Fig 1.

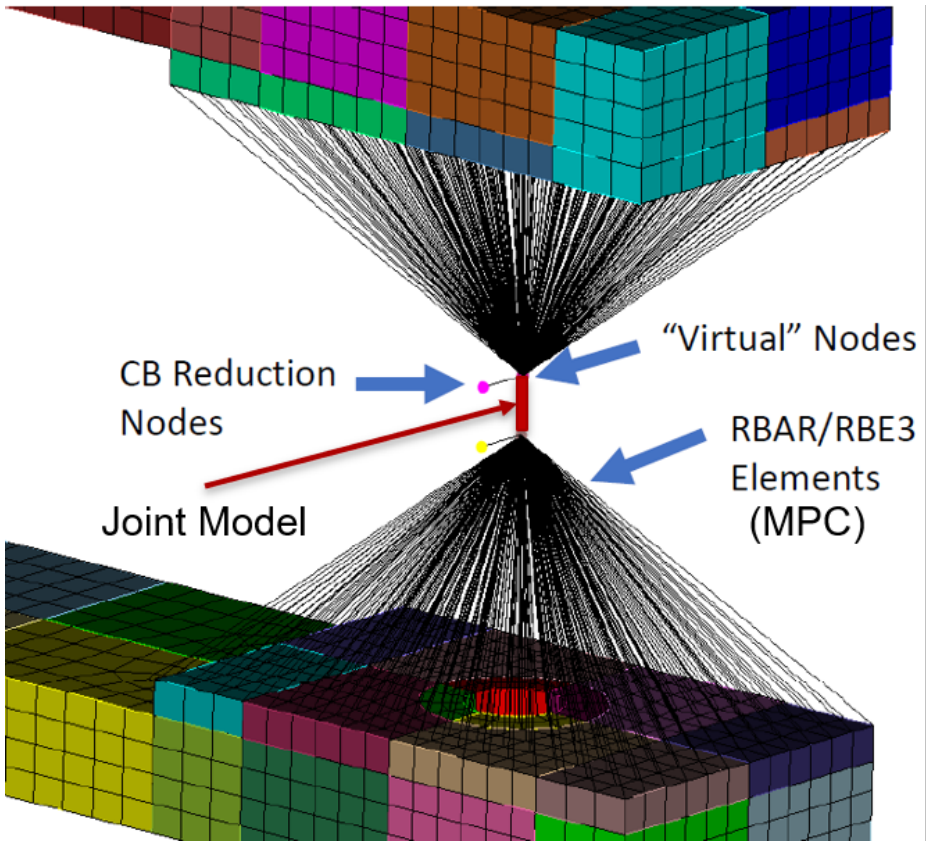

Figure 1: A schematic of a spidered joint where two interfaces are reduced to a single node and connected via a whole joint model [6]

These constraints are meant to approximate the actual contact, where in reality there are certain regions in the interface that have adequate pressure to remain fully in contact (i.e. stuck) while in other regions gaps may open up or the surfaces may be in contact but slide relative to one another as the structure vibrates. Lacayo and Allen [7] studied this using MPCs connected with Iwan elements (a whole joint hysteretic model) [8]. They used Quasi-Static Modal Analysis (QSMA) [9] to compute the change in the modal properties with vibration amplitude and iterated on the Iwan parameters until the properties of the model matched the measured variation in the natural frequency and damping with amplitude. They observed Pareto fronts in which there was a trade off where either the frequency error or

damping error could be minimized but not both. Singh et al. [6] showed that this spidering approach yields different results depending on whether the spiders were rigid (i.e. RBAR) or averaging type (i.e. RBE3) and depending on the size of the contact area. For the case study considered, the RBAR MPC was shown to be the most effective at matching the experimental data, but with the others it was impossible to obtain a good fit to measurements.

This work seeks to develop an alternative that transitions from the traditional MPC approach to a continuous flexible interface allowing one to extend linear interface reduction techniques to nonlinear problems. To do so, a full FEM is reduced down to the interface DOF using a Hurty/Craig Bampton (HCB) reduction to decrease the size of the model. Then a preload is applied using the penalty stiffness method in Abaqus [10, 11], and the result is a linear model with springs constraining motion in the normal and tangential directions that capture the response at low amplitudes when the joints are fully stuck. A second model is solved which is identical except that the friction force is set to zero, to represent the system when the joints are fully slipping yet still in contact. The nonlinear interface portion of these two models are then reduced using System Level Characteristic Constraint (S-CC) reduction to obtain a subset of interface deformation shapes [12]. In the reduced S-CC space, a physical Iwan element is added to each S-CC DOF to approximate the nonlinearity localized at the interface. This allows for the nonlinear hysteretic model to be applied in a decoupled coordinate space while potentially preserving the coupling between modes when the nonlinear interface forces are projected onto the structure's linearized modes. This method differs from a Modal Iwan approach [13] since a modal Iwan model assumes that the modes are uncoupled and has no mechanism to capture modal coupling.

This work evaluates the ability of this new S-CC method to capture the nonlinear behavior of various modes of a simple 2D beam structure. The model is intentionally created to be simple enough that the interface motions can be easily visualized and the dynamic and static response can be found relatively easily even when nonlinear contact with friction is

enabled. The performance of this approach is also compared to a traditional approach where the interface nodes are spidered using rigid bar elements (RBAR) and connected through an Iwan joint, as in [6, 7]. In all cases the reduced models are compared to the full-order model with Coulomb friction at the interface, which is considered to be the truth model.

THEORY AND METHODOLOGY

Hurty/Craig Bampton Reduction

Consider an undamped equation of motion for a multi degree of freedom system as given by Eq. 1, where $\mathbf{M}$ is the mass matrix, $\mathbf{K}$ is the stiffness matrix, F is the external forcing, $F_J(u, \theta)$ is the source of the nonlinearity, u is the physical displacement, and $\ddot{u}$ is the physical acceleration. If the nonlinear force is only applied to a boundary, a Reduced order model (ROM) can be used to approximate the full-order model at that set of reduction nodes [14]. Although many methods of model reduction exist, this paper will focus on the HCB method as discussed in [15].

$$\mathbf{M\ddot{u}} + \mathbf{Ku} + \mathbf{F}_J(\mathbf{u}, \theta) = \mathbf{F} \tag{1}$$

For the HCB method, the system is partitioned between the boundary and internal DOFs as

$$\begin{bmatrix} \mathbf{M}_{ii} & \mathbf{M}_{ib} \\ \mathbf{M}_{bi} & \mathbf{M}_{bb} \end{bmatrix} \begin{Bmatrix} \ddot{\mathbf{u}}_i \\ \ddot{\mathbf{u}}_b \end{Bmatrix} + \begin{bmatrix} \mathbf{K}_{ii} & \mathbf{K}_{ib} \\ \mathbf{K}_{bi} & \mathbf{K}_{bb} \end{bmatrix} \begin{Bmatrix} \mathbf{u}_i \\ \mathbf{u}_b \end{Bmatrix} + \begin{Bmatrix} 0 \\ \mathbf{F}_{j,b(\mathbf{u}_b)} \end{Bmatrix} = \begin{Bmatrix} 0 \\ \mathbf{F}_b \end{Bmatrix} \tag{2}$$

where subscripts b and i represent the boundary and interior DOF respectively. Note that only the boundary DOF are assumed to be forced either externally or internally through the joint. The interface is described by static constraint modes. The interior is described by vibration modes (fixed-interface modes) and the static constraint modes. These are combined to capture the dynamics of the assembled structure. As a result, a small number of fixed interface modes, Φ, are computed and that basis is augmented with constraint modes, Ψ, as detailed [16], to obtain the HCB transformation matrix,

$$\begin{Bmatrix} \mathbf{u}_i \\ \mathbf{u}_b \end{Bmatrix} = \mathbf{T}^{\mathrm{HCB}} \begin{Bmatrix} \mathbf{q}_i \\ \mathbf{u}_b \end{Bmatrix} = \begin{bmatrix} \boldsymbol{\Phi} & \boldsymbol{\Psi} \\ \mathbf{0} & \mathbf{I} \end{bmatrix} \begin{Bmatrix} \mathbf{q}_i \\ \mathbf{u}_b \end{Bmatrix} \tag{3}$$

This transformation then reduces the equations of motion to the following where the bar above the mass and stiffness terms indicates the transformed HCB model,

$$\begin{bmatrix} \mathbf{I} & \bar{\mathbf{M}}_{ib} \\ \bar{\mathbf{M}}_{bi} & \bar{\mathbf{M}}_{bb} \end{bmatrix} \begin{Bmatrix} \ddot{\mathbf{q}}_i \\ \ddot{\mathbf{u}}_b \end{Bmatrix} + \begin{bmatrix} \Lambda_{ii} & \mathbf{0} \\ \mathbf{0} & \bar{\mathbf{K}}_{bb} \end{bmatrix} \begin{Bmatrix} \mathbf{q}_i \\ \mathbf{u}_b \end{Bmatrix} + \begin{Bmatrix} 0 \\ \mathbf{F}_{j,b}(\mathbf{u}_b) \end{Bmatrix} = \begin{Bmatrix} 0 \\ \mathbf{F}_b \end{Bmatrix} \tag{4}$$

The ROM can be used to analyze the dynamic response of a structure more efficiently than the full finite element model, depending on the number of boundary DOF that must be retained in the nonlinear internal force vector. The quasi-static HCB model is solved for the preloaded equilibrium state as,

$$\begin{bmatrix} \Lambda_{ii} & \mathbf{0} \\ \mathbf{0} & \bar{\mathbf{K}}_{bb} \end{bmatrix} \begin{Bmatrix} q_i \\ u_{pre} \end{Bmatrix} + \begin{Bmatrix} 0 \\ \mathbf{F}_{j,b}(\mathbf{u}_{pre}) \end{Bmatrix} = \begin{Bmatrix} 0 \\ \mathbf{F}_{pre} \end{Bmatrix} \tag{5}$$

The joint force, $\mathbf{F}_{j,b}(\mathbf{u}_{pre})$, is modeled here using the node-to-node penalty stiffness method using either normal gap elements or triaxial gap elements. The former only applies penalty stiffness in the direction normal to the contact surface, whereas the triaxial spring applies additional in-plane stiffness when a contact gap closes. Consider the jth node pair, such that the normal gap is computed as,

$$g^j = (Z_2^j - \Delta Z_2^j) - (Z_1^j - \Delta Z_1^j) \tag{6}$$

where Z is the undeformed normal coordinate of each and ΔZ is the relative normal displacement. ΔZ is the amount of displacement present during the preload step. The penalty spring method defines the normal contact force for the jth node pair as,

$$F_Z^j = \begin{cases} k_z g^j & g^j < 0 \\ 0 & g^j \geq 0 \end{cases} \tag{7}$$

The normal penalty spring stiffness is denoted as k_z. For the triaxial penalty spring, an in-plane stiffness term is included, with in-plane penalty stiffnesses k_x and k_y,

$$F_X^j = \begin{cases} k_x \Delta X^j & g^j < 0 \\ 0 & g^j \geq 0 \end{cases} \tag{8}$$

$$F_Y^j = \begin{cases} k_y \Delta Y^j & g^j < 0 \\ 0 & g^j \geq 0 \end{cases} \tag{9}$$

The joint force, $\mathbf{F_J}(\mathbf{u})$ is created by assembling the F_X, F_Y, F_Z for all of the nodes at the interface. This is done in lieu of a friction element, such as a Coulomb or Jenkins element, for the in-plane directions. This avoids having to compute stick/slip states for closed elements, and is a simplified contact element that can be used to capture the approximate contact area in the joint, but can't necessarily capture the frictional damping. Following the quasi-static preload analysis of the model in Eq. 4, the model is linearized about this equilibrium state yielding,

$$\begin{bmatrix} \mathbf{I} & \bar{\mathbf{M}}_{ib} \\ \bar{\mathbf{M}}_{bi} & \bar{\mathbf{M}}_{bb} \end{bmatrix} \begin{Bmatrix} \ddot{q}_i \\ \ddot{u}_b \end{Bmatrix} + \begin{bmatrix} \Lambda_{ii} & \mathbf{0} \\ \mathbf{0} & \bar{\mathbf{K}}_{bb} + \left.\frac{\partial \mathbf{F_j}}{\partial \mathbf{u_b}}\right|_{\mathbf{u_{pre}}} \end{bmatrix} \begin{Bmatrix} q_i \\ u_b \end{Bmatrix} = \begin{Bmatrix} 0 \\ \mathbf{F}_b \end{Bmatrix} \tag{10}$$

The partial derivative of the nonlinear force added to the HCB stiffness matrix at the boundary DOF represents the stiffness of the joint in either a fully stuck state in the case of the

triaxial penalty spring, or a fully slipped state for the normal penalty springs.

1.1 RBAR MPC Reduced Model

The MPC/RBAR method requires that the two substructures be completely uncoupled to one-another, each with their own mass and stiffness matrix. To obtain the mass and stiffness matrix of each structure at the interface, a rigid body transformation applied to the HCB reduced matrices is required as given by Eq. 11 - 13 where T_{RBAR} is the transformation matrix from the interface DOF to the reduced RBAR DOF, Ψ are the rigid body unit deformation shapes, and M/K_{RBAR} are the resulting RBAR mass and stiffness matrices.

$$\mathbf{T_{RBAR}} = \begin{bmatrix} I & 0 & 0 \\ 0 & \Psi_{RBAR,substr_1} & 0 \\ 0 & 0 & \Psi_{RBAR,substr_2} \end{bmatrix} \tag{11}$$

$$[\mathbf{M_{RBAR}}] = [\mathbf{T_{RBAR}}]^{\mathbf{T}}[\mathbf{M_{HCB}}][\mathbf{T_{RBAR}}] \tag{12}$$

$$[\mathbf{K_{RBAR}}] = [\mathbf{T_{RBAR}}]^{\mathbf{T}}[\mathbf{K_{HCB}}][\mathbf{T_{RBAR}}] \tag{13}$$

Ψ is generated for the interface DOF for each substructure by applying a unit deflection of the interface rigidly in the in-plane direction, the normal direction, and the rotation direction. The latter was calculated using $\Psi_{Rotation} = (x_{DOF} - x_c)\theta$ where x_{DOF} is the location of all in-plane nodes, x_c is the centroid of the interface, and θ is a unit rotation. This yields a Ψ matrix of size n interface DOF for the top and bottom beams by two rigid body displacements and one rotation for each interface (total 6).

System Level Characteristic Constraint Reduction (S-CC)

The application of the System Level Characteristic Constraint (S-CC) interface reduction further decreases the number of DOF in the Hurty/Craig-Bampton ROM in Eq. 10. This approach computes the eigenvectors from the boundary partition of the linearized HCB model and uses a truncated set of the S-CC modes as a basis for the reduction [12, 16]. The modes are computed about the linearized state, and the subscript CC denotes characteristic constraint modes,

$$\left(\mathbf{K}_{bb} + \left.\frac{\partial \mathbf{F}_j}{\partial \mathbf{u}_b}\right|_{\mathbf{u_{pre}}} - \omega_{cc}^2 \mathbf{M}_{bb}\right) \Phi_{cc} = \mathbf{0} \tag{14}$$

Depending on the type of penalty springs used to linearize the system, this equation produces either the fully stuck or fully slipping S-CC modes. A truncated subset of the S-CC modes is used to further reduce the HCB mass and stiffness matrices using the transformation matrix,

$$\mathbf{T}_{SCC} = \begin{bmatrix} \mathbf{I} & \mathbf{0} \\ \mathbf{0} & \Phi_{cc} \end{bmatrix} \tag{15}$$

$$\mathbf{M}_{SCC} = (\mathbf{T}_{SCC})^T \begin{bmatrix} \mathbf{I} & \bar{\mathbf{M}}_{ib} \\ \bar{\mathbf{M}}_{bi} & \bar{\mathbf{M}}_{bb} \end{bmatrix} \mathbf{T}_{SCC} \tag{16}$$

$$\mathbf{K}_{SCC} = (\mathbf{T}_{SCC})^T \begin{bmatrix} \Lambda_{ii} & \mathbf{0} \\ \mathbf{0} & \bar{\mathbf{K}}_{bb} + \left.\frac{\partial F_j}{\partial u_b}\right|_{u_{pre}} \end{bmatrix} \mathbf{T}_{SCC} \tag{17}$$

If all CC modes are kept in the reduction, the S-CC model is identical to the HCB reduced model. This reduction method captures both the motion of the boundary and the global dynamics of the structure, reducing the size of the HCB model. Utilizing the linearized

EOM from the preloaded state in Eq. 10, the EOM for the S-CC reduced model about the nonlinear preloaded state is,

$$\begin{bmatrix} \mathbf{I} & \bar{\mathbf{M}}_{ic} \\ \bar{\mathbf{M}}_{ci} & \mathbf{I} \end{bmatrix} \begin{Bmatrix} \ddot{q}_i \\ \ddot{q}_{cc} \end{Bmatrix} + \begin{bmatrix} \Lambda_{ii} & \mathbf{0} \\ \mathbf{0} & \Lambda_{cc} \end{bmatrix} \begin{Bmatrix} q_i \\ q_{cc} \end{Bmatrix} = \bar{\mathbf{f}}(\mathbf{t}) \tag{18}$$

where the c subscript indicates the reduction using CC modes. The stiffness matrix is completely decoupled with Λ_{cc}, a diagonal matrix with the ω_{cc}^2 values. All coupling is through the mass matrix off-diagonal terms, $\mathbf{M}_{ic}$ and $\mathbf{M}_{ci}$.

Adding the S-CC Iwan Element

A traditional interface reduction has a set of vectors describing the motion of a top surface and a second set for the bottom surface. The S-CC model presented here is different in that it is a reduction applied after assembly. The motions captured by $\mathbf{q}_i$ involve motion of nodes away from the interface with the interface remaining fixed, whereas the coordinates $\mathbf{q}_c c$ capture motions where the interface can move as well as the rest of the structure. Hence, one can capture friction in the joint by applying a 4-parameter Iwan element between each $\mathbf{q}_c c$ coordinate and ground in Eq. 18. In this way the joint is inactive if the structure vibrates in a fixed-interface mode (with no deformation of the interface) and is activated when the interface deforms.

In the case where the joint is modeled using only normal penalty springs (i.e. fully slipping in the lateral directions), the bolts are the only source of in-plane stiffness, and the linearized natural frequency for the ith S-CC mode shape is denoted as $\omega_{cc,i,\infty}^2$ which are the values on the diagonal of Λ_{cc} in Eq. 18. Conversely, when the interface is fully stuck, the linearized frequency is $\omega_{cc,i}^2$. The relationship between these two models can be explicitly shown with the EOM for the S-CC coordinates. An Iwan element is appended to the ith S-CC coordinate, after which the quasi-static terms in Eq. 18 can be written as,

$$\omega_{cc,i,\infty}^2 q_{cc,i} + \bar{f}_{cc,i}(q_{cc,i}) = \bar{f}_i(t) \tag{19}$$

where $\bar{f}_{cc,i}(q_{cc,i})$ is the force from the nonlinear joint model applied to the ith S-CC coordinate. The Iwan joint has a linearized stiffness associated with it, termed K_T, which can be chosen such that $\Lambda_{cc}|_i = \omega_{cc,i,\infty}^2 + K_T$. This constraint is placed on the selection such that the modes 1.) converge to the fully stuck solution at low response amplitudes, and 2.) converge to the fully slipped solution at high response amplitude as the stiffness of the Iwan element goes to zero. It is important to note that the slipped and stuck models have different S-CC shapes and so this method does not ensure a perfect match between the two models, but in the examples studied to date it has worked quite well. The resulting nonlinear equations-of-motion with grounded S-CC modal Iwan elements becomes,

$$\begin{bmatrix} \mathbf{I} & \bar{\mathbf{M}}_{\mathbf{ic}} \\ \bar{\mathbf{M}}_{\mathbf{ci}} & \bar{\mathbf{M}}_{\mathbf{cc}} \end{bmatrix} \begin{Bmatrix} \ddot{\mathbf{q}}_{\mathbf{i}} \\ \ddot{\mathbf{q}}_{\mathbf{cc}} \end{Bmatrix} + \begin{bmatrix} \Lambda_{ii} & \mathbf{0} \\ \mathbf{0} & \Lambda_{cc,\infty} \end{bmatrix} \begin{Bmatrix} \mathbf{q}_{\mathbf{i}} \\ \mathbf{q}_{\mathbf{cc}} \end{Bmatrix} + \begin{Bmatrix} \mathbf{0} \\ \bar{\mathbf{f}}_{\mathbf{cc}}(\mathbf{q}_{\mathbf{cc}}) \end{Bmatrix} = \bar{\mathbf{f}}(\mathbf{t}) \tag{20}$$

For this paper, the S-CC model with a nonlinear joint is referred to as an nSCC model.

Whole Joint Models

Segalman's 4-parameter Iwan element considered both analytical solutions for contact and empirical evidence that showed that joints exhibit power-law energy dissipation versus force (or vibration amplitude) [17]. An Iwan element is a collection of slider or Jenkins elements in parallel, in which the slip force[1]for each slider is governed by several parameters, i.e. the friction coefficient, normal force, etc.... Segalman's model recognizes that the net effect of all of these parameters must be to produce power-law dissipation versus vibration amplitude, which is now governed by only two of the four parameters in the Iwan model. The other two parameters control the transition to macroslip when the joint slips completely.

Macroslip is typically not observed in engineered joints if they are tightened properly, except perhaps under extreme loading.

The four parameter Iwan model can be represented by the parameters: F_s,K_T,χ,and β, given in Table 1. For an in-depth discussion of the Iwan element, refer to Segalman's original paper on Iwan elements [17] and Deaner's paper on the modal Iwan model [18].

Table 1: Definition of Iwan Parameters (Physical Description)

F_S	The force necessary to cause macroslip
K_T	The tangential stiffness of the Jenkins elements (i.e. the joint stiffness when no slip occurs)
χ	The exponent that describes the slope of the energy dissipation curve
β	The ratio of the number of Jenkins elements that slip before microslip and then at macroslip

This element is general in that it can be applied physically between two interfaces for the RBAR method or between an S-CC shape and ground in the case of the nSCC ROM. The same equations are used in either case and only the interpretation of the displacement and forces changes (i.e. physical or modal). This enables the model to capture the hysteresis in the joint when the surface slips and generate curves that depict the amplitude dependent trends of the natural frequency and damping for each global mode. For this paper, the

[1]If all sliders have the same friction coefficient then the slip force is defined by the normal force for each slider.

quasi-static method is utilized to generate these curves. In the case of the nSCC ROM, it is important to note that adding these elements to S-CC shapes allows the modes of the system to retain some level of coupling. The reduced S-CC shapes are uncoupled, but allow coupling between different physical modes because each S-CC shape may be active in the response of multiple modes.

Quasi-static Modal Analysis

The goal is to understand how each mode responds (decay and frequency of oscillation) during free vibration after a large initial force/displacement. This would require simulating the dynamic response and decomposing that into modes. However, that is computationally expensive [2]. The Quasi-static modal analysis method is used in lieu of a dynamic analysis to generate the hysteresis curve depicting the dependency of the modal frequency and damping ratio on amplitude. The method used is a variation to the one developed by Festjens et. al. [9] which was extended to whole joint models by Lacayo and Allen [7]. Festjens et. al. solved the quasi-static problem in which a distributed load in the shape of the vibrational mode of interest is applied on a structure at various amplitude levels. Together with Masing's rules, the load–displacement hysteresis curve can be used to obtain an estimate of the dynamic response of the system. A brief overview of the method is presented here. See [7, 19, 20] for additional details and limitations. Utilizing the undamped MDOF equation of motion given in Eq. 1, at low amplitudes, the joint force $\mathbf{F}_J(\mathbf{u})$ can be replaced by a low amplitude stiffness at the equilibrium position given by

$$\mathbf{K}_T = \left.\frac{\partial \mathbf{F}_J}{\partial \mathbf{u}}\right|_{\mathbf{u}_0} \tag{21}$$

The modes of the linearized system about the equilibrium point are found by solving the linearized eigenvalue problem about the preloaded state,

$$(\mathbf{K} + \mathbf{K}_T - \omega_{0,r}^2 \mathbf{M})\Phi = 0 \tag{22}$$

Applying a force in the shape of the mode $\mathbf{F} = \mathbf{M}\phi_i$ where ϕ_i is the mode of interest, results in the following quasi-static problem where α are the different load levels. The acceleration term is removed since the system is solved statically.

$$\mathbf{K}\mathbf{u} - \mathbf{F}_J(\mathbf{u}) = \mathbf{M}\phi_i\alpha \tag{23}$$

In this work, the nonlinear joint force comes from the Iwan element and is a function of the displacements, $\mathbf{u}$. After solving Eq. 23, one obtains the static response, $\mathbf{u}(\alpha)$, from which the modal amplitude, natural frequency, and damping ratio can be written as function of α as shown in Eq. 12-17 in [7]. The damping ratio is obtained by summing up the energy dissipated by friction from each Iwan joint in the system. Given that all three variables are functions of amplitude, the damping and natural frequency can be plotted in terms of modal amplitude and this is the convention that will be used in this work.

LINEAR REDUCTION TECHNIQUES

Structure of Interest

This work applies the S-CC Iwan reduction methodology to a 2D structure built in Abaqus, and contrasts the method using traditional MPC methods with RBAR-type elements connected with a physical four-parameter Iwan element. The 2D cantilever beam is made of steel with the properties shown in Table 2. The 2D Abaqus mesh and a diagram showing the bolt section, where a preload is applied to the top and bottom surface, and the resulting contact patch (where the nodes come into contact) is shown in Fig. 2. The beam has fixed boundary conditions on the left end.

Table 2: Material Properties and Dimensions for the 2D Abaqus Model

Property	Value (SI)	Value (Imperial)
Length	20.32 cm	8.00 in
Cross-Section	1.27 cm square	0.50 in square
Density	7.84e-3 kg/cm^3	7.34e-4 $slinches/in^3$
Elastic Modulus	200 GPa	2.9e7 psi
Poisson Ratio	0.29	0.29

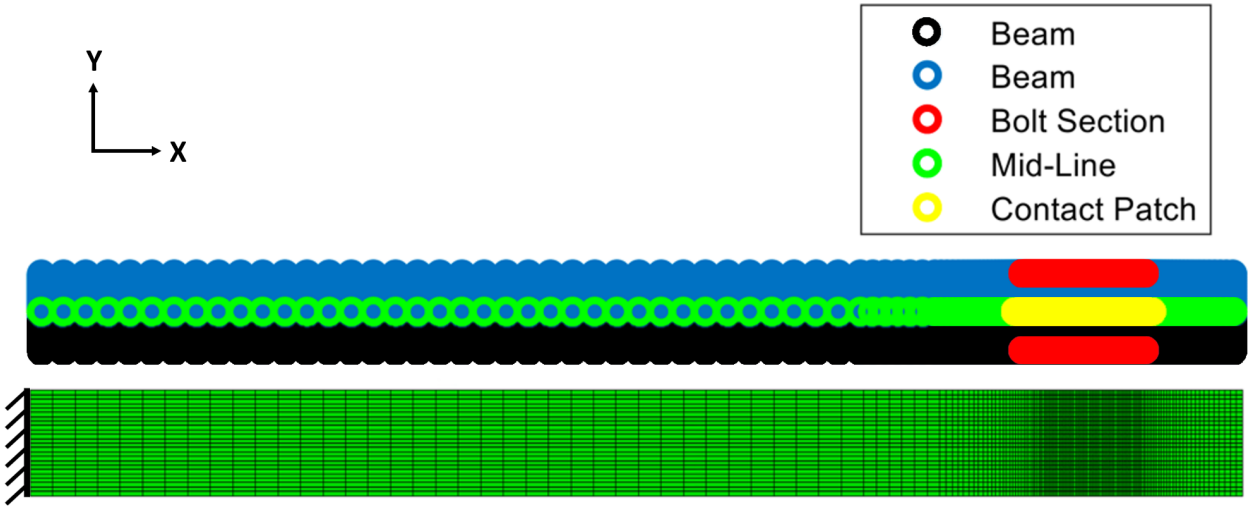

Figure 2: (Top) Node diagram of the beam, (Bottom) Abaqus beam model

The model has two beams of half the total height sandwiched to one another along the

mid-line where contact occurs. A preload distributed force is applied to the outer surfaces of the bolt section (red) and a contact simulation is done to retrieve the first six modes of the structure after preload. The resulting nodes in contact from Abaqus after preload are shown in yellow. The y direction displacement after the preload step from Abaqus is scaled for visualization and shown in Fig. 3.

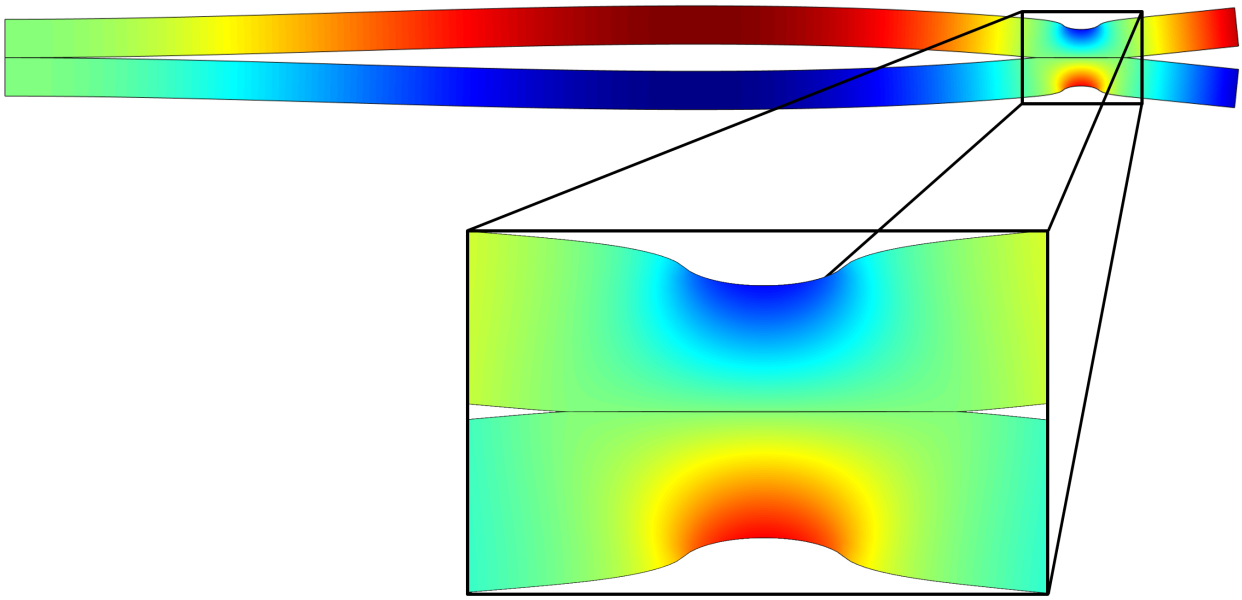

Figure 3: 500 scaled Y displacement of the beam after the preload step

The amplitude dependent frequency and damping curves are generated from a quasi-static analysis in Abaqus for three modes of interest: Mode 1 (first order bending), Mode 2 (second order bending), and Mode 4 (third order bending). The deformation shapes for the modes of interest are depicted in Figure 4. The mode shapes scale is exaggerated to show the shape clearly and colored by the deformation in the in-plane (x) direction, to give an indication of each mode's propensity to shear the joint. The third mode involved opening and closing of the joint and no shear and hence could be well approximated as linear and was not considered here.

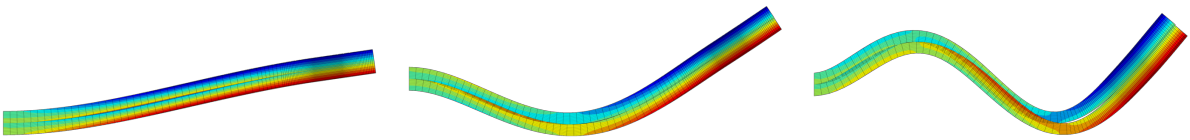

(a) Mode Shape 1 **(b)** Mode Shape 2 **(c)** Mode Shape 4

Figure 4: Stuck mode shapes of the cantilever beam for the first three modes of interest

To evaluate the effectiveness of the ROM methods, each was implemented in Matlab. While it was possible to solve for the contact with and without friction in Abaqus, it was apparently not possible to export a stiffness matrix from Abaqus that included the stiffness of any penalty springs used when solving the contact problem. So, the mass and stiffness matrices from Abaqus were exported to MATLAB for a case where the beams were not in contact. Then, in order to obtain the stiffness matrices including the penalty springs, springs were added in Matlab between all pairs of nodes that Abaqus found to be in contact, and the spring constants were adjusted until the natural frequencies obtained in Matlab matched those obtained by Abaqus. Then, the models that included the penalty stiffnesses were reduced to RBAR and nSCC NLROMs, as described in the previous section. Two models were created in Matlab: The slipped model only had penalty springs in the normal direction, whereas the stuck model had a the same normal spring constant and an in-plane spring to account for friction. The nodes in contact were determined from the Abaqus preload solution with friction. The resulting normal stiffness was 1.01e6 lb/in (1.77e8 N/m) and the in-plane stiffness was 488.72 lb/in (8.56e4 N/m). With these stiffnesses, the maximum error in any natural frequency (comparing the Matlab model to the natural frequencies computed by Abaqus for the corresponding case) was 0.002%. The first six linear frequencies for the penalty stiffness model for the slipped and stuck models are given in Tab. 3. Error between the Abaqus frequencies and the penalty stiffness frequencies could be attributed to the stress straining affects present in the Abaqus solver which could perturb the results. However, these effects are apparently small because the Matlab models agrees well with the

Abaqus predictions, and are suitable for developing the ROMs.

Table 3: Linear Frequencies for the MATLAB Slipped and Stuck Penalty Stiffness Models and Error when Compared to Abaqus

Mode	Slipped Model		Stuck Model	
	Freq. [Hz]	Error	Freq. [Hz]	Error
1	139.09	0.001%	198.23	0.00%
2	861.5	0.00%	1035.8	-0.002%
3	1157.4	0.002%	1157.4	0.002%
4	2366.1	-0.002%	2531.6	0.001%
5	3177.7	-0.002%	3177.7	-0.002%
6	4571.9	0.00%	4713.6	0.001%

Linear Reduction

The full model containing 8684 DOF was reduced down to a HCB ROM that retained 260 interface DOF (Static Constraint Modes) and 20 Fixed Interface Modes while maintaining a maximum frequency error of 0.002% for the first 10 modes in either case. This HCB model was then further reduced using the MPC/RBAR method and S-CC Reduction. The natural freuqencies of these models were compared to examined their effectiveness in modeling the linear dynamics with a smaller set of DOF. For the RBAR model, the mass and stiffness matrices include 20 Fixed Interface Modes, 3 DOF for the top beam (x, y, and rotation), and 3 DOF for the bottom beam. Springs were added between each of the three DOF from

the top and bottom halves of the beam to calibrate to the HCB model. Since the full/HCB models were generated with normal and in-plane springs, the slipped model was used with the expectation that a negative spring constant would be possible for the normal direction in the RBAR model to counter this constraint. Using the direct search optimization method [21] to minimize frequency error between HCB and RBAR, the following spring constants were used: $k_x = 1.95e7\ lb/in$, $k_y = -7.88e7\ lb/in$, and $k_\theta = -7.78e7\ lb/in$ ($3.42e9$, $-1.38e9$, $-1.36e9\ N/m$). The resulting frequencies are compared to those of the stuck model in Tab. 4.

Table 4: Linear Frequencies for the Slipped Model for the HCB, RBAR, and S-CC Cases

Mode	HCB Model	RBAR Model	S-CC Model
	Freq. [Hz]	Freq. Error (%)	Freq. Error (%)
1	198.23	-0.02	0.00
2	1035.6	-0.03	0.00
3	1157.4	0.2	0.00
4	2531.6	0.08	-0.001
5	3177.8	-0.18	-0.005
6	4717.2	0.30	-0.002

Similar to the RBAR/MPC method, the S-CC method required 6 S-CC Shapes to correlate to the HCB reduced Model for both the slipped and stuck cases. These S-CC shapes

of the stuck case are given in Fig. 5 with the color gradient describing displacement in the x direction. The resulting frequencies for the first six modes and errors are given in Tab. 4.

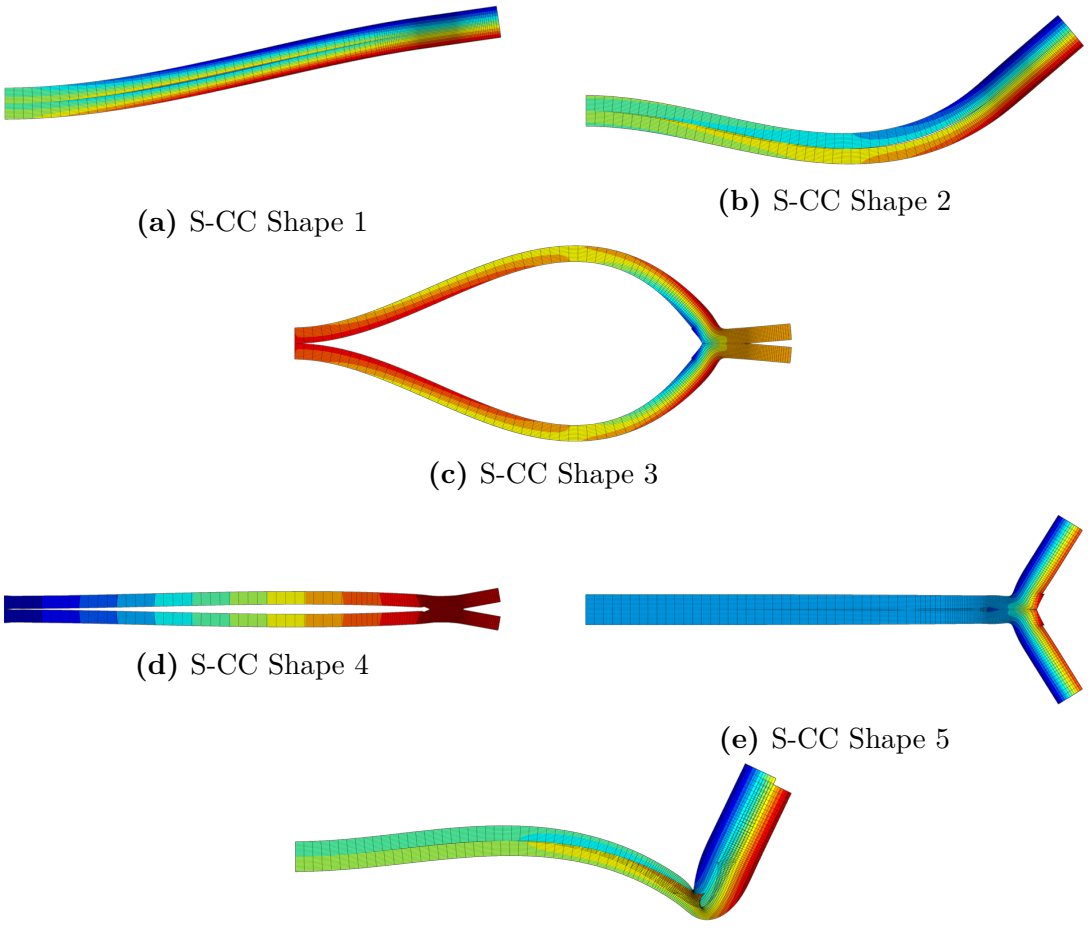

(a) S-CC Shape 1

(b) S-CC Shape 2

(c) S-CC Shape 3

(d) S-CC Shape 4

(e) S-CC Shape 5

(f) S-CC Shape 6

Figure 5: S-CC Deformation Shapes

The first few S-CC mode shapes look very similar to the first few global mode shapes of the structure. In essence, the S-CC mode shapes are the modes of a model for the complete structure after statically reducing the assembled model to the interface. However, it is also important to note that all interface DOF are free to move in the S-CC modes, so they can capture relative slip between the surfaces, as is visible in some of the higher S-CC modes. In Fig. 5, the S-CC shapes are transformed back to the full DOF space to show how the rest of

the beam deforms in each S-CC shape. In all 6 modes, the S-CC Reduced model produces negligible errors in the assembled natural frequencies; much lower than those for the RBAR reduced model. The mode shapes were also compared (not shown) and also found to be very similar.

NONLINEAR REDUCTION TECHNIQUES

Nonlinear Extension of RBAR MPC Reduction

For linear analysis, three linear springs were placed between the two halves of the beams at each DOF for the RBAR approach. This is then extended to the nonlinear regime by replacing the spring in the slip direction (x-direction) with an Iwan element to capture micro-slip while retaining the linear springs in the other directions to keep the joint from opening. This is done with the goal to compute the amplitude dependent frequency and damping curves (see Figs. 7,8) for the ROMs and compare against those obtained from Abaqus. A 100,000 iteration Monte-Carlo study was conducted randomly varying F_S, γ, χ, and β, where γ allows one to perturb the linear tangential stiffness slightly from the value K_T found by comparing the stuck and slipped S-CC stiffness matrices as described earlier. Hence, the stiffness value used for the Iwan element was defined as $K_{T,Scaled} = \gamma K_T$ where γ was forced to remain near unity.

Additionally, Singh et al. [6] found that when using the RBAR method it was often necessary to use a larger contact area than that of the actual contact in order to obtain a nonlinear model whose QS curves match those from measurements. To explore this in the context of this study, the contact area was adjusted between 0.75 and 1.5 times the nominal contact area from Abaqus. The results of the Monte-Carlo study on the three contact areas are shown in Fig. 6 for Mode 1, which depicts the RMS frequency percent error and RMS damping percent error between the RBAR nonlinear model and the Abaqus full model. The RMS error is calculated by computing the difference between the two models over

the entire amplitude range used for each mode. In order to illustrate some typical results, three solutions are examined: (1) the optimal solution for the nominal contact area that minimizes frequency and damping error, (2) the solution for the larger contact area that minimizes frequency error, and (3) the solution for the larger contact area that minimizes the damping error.

The frequency and damping curves for these solutions are shown Fig. 7 and 8 with the corresponding Iwan parameters in Tab. 5. It is important to note that, in contrast to our prior study, in this study the tangential stiffness scaling was limited to ±2% to maintain accuracy in the linear regime. If the linear frequency error was disregarded, a better solution would be possible.

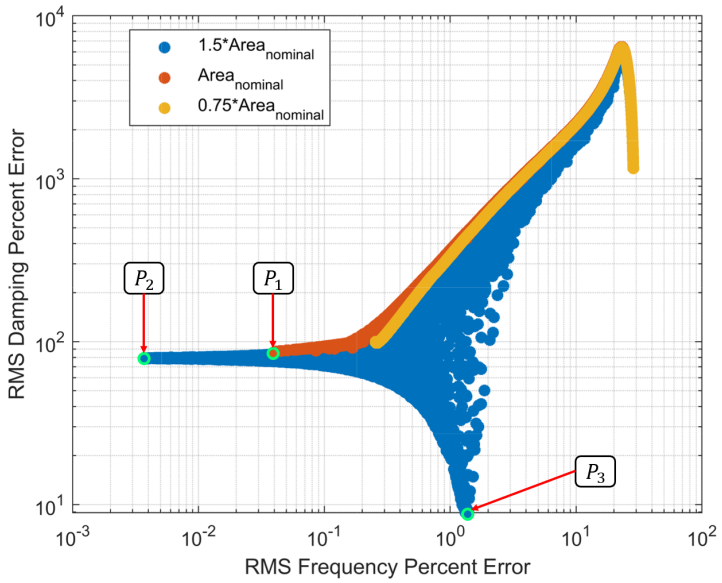

Figure 6: Mode 1 RMS frequency and damping error for a 100,000 iteration Monte-Carlo for different contact areas

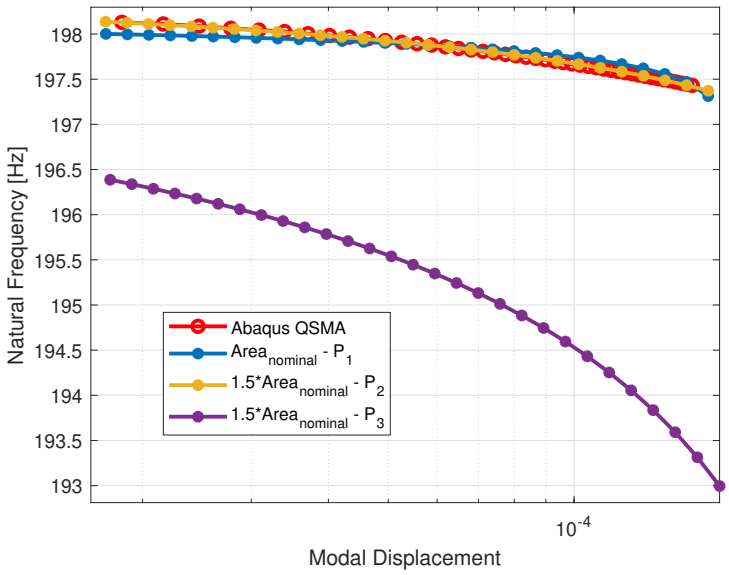

Figure 7: Mode 1 frequency vs. amplitude curve for the RBAR model vs. Abaqus

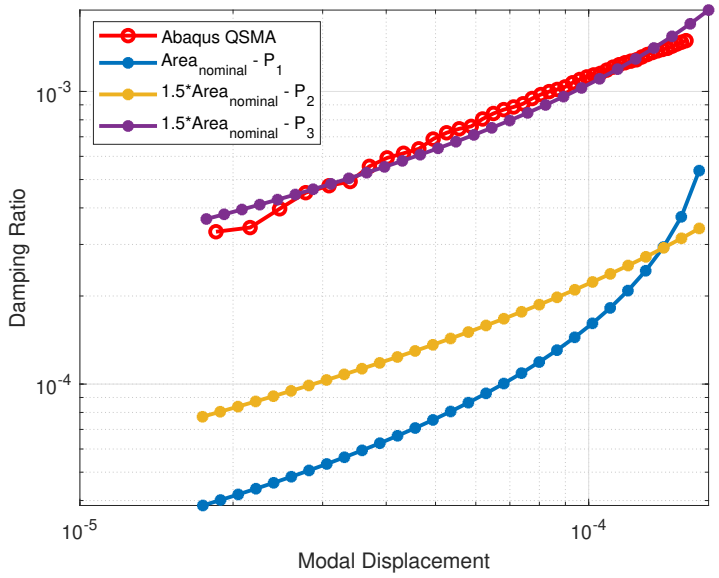

Figure 8: Mode 1 damping vs. amplitude curve for the RBAR model vs. Abaqus

Table 5: Iwan parameters for Mode 1 in the X - direction for the RBAR model

Point	$F_S[lbf]$	γ	χ	β
P_1	90.32	1.0136	-0.892	0.01
P_2	111.17	1.0072	-0.693	0.585
P_3	118.68	1.0011	-0.8953	0.045

Increasing the contact area yielded much better results for either the frequency or damping curves, but only a small improvement in both simultaneously. The percent frequency and damping errors for the three points are shown in Table 6 clearly show that only one modal parameter can be optimized for a given contact area within the current parameter space.

Table 6: Percent Errors for the RBAR Model against Abaqus QSMA

Point	Contact Area	Frequency Error	Damping Error
P_1	Nominal	0.04%	86.27%
P_2	1.5*Nominal	0.003%	78.90%
P_3	1.5*Nominal	1.39%	8.89%

Extending the range of the F_s from 1 to 50,000 did not result in curves with a lower

frequency or damping error. Modes 2 and 4 could not be correlated to the Abaqus results either and, for brevity, are not shown here. In our past works we encountered similar cases, where no set of model parameters would produce a spidered model that correlated well with measurements, without sacrificing the accuracy of the linear fit, i.e. significantly changing K_T such that there was large percent error in the linear frequency. although the agreement here is worse than in any of our prior works [6].

Proposed nSCC Method

Whereas nonlinear joint analysis in the physical domain places a hysteretic (Iwan) model between the reduced joint interfaces, this approach places an Iwan element between the ground and an S-CC modal coordinate, $\mathbf{q}_{cc}$, to capture the slip at the joint when the structure deforms in the shape of the S-CC shape in question. The eigenvectors of the S-CC reduced mass and stiffness matrices can provide insight into the contribution of each S-CC Shape on the mode of interest. Table 7 shows the percent contribution of each S-CC Shape and the sum of the contributions of the 20 fixed interface modes to the three modes of interest.

Table 7: S-CC Shape Percent Contributions to the Modes of Interest

	Mode 1	**Mode 2**	**Mode 4**
Fixed Interface Modes	2.05	46.26	62.73
S-CC Shape 1	97.93	17.86	10.63
S-CC Shape 2	0.02	30.84	26.39
S-CC Shape 3	0.00	0.00	0.00
S-CC Shape 4	0.00	0.00	0.00
S-CC Shape 5	0.00	0.00	0.00
S-CC Shape 6	0.00	0.04	0.25

The results show that Mode 1 is only influenced by S-CC Shape 1, and so any nonlinearity in Mode 1 will be governed by the Iwan joint connected to S-CC Shape 1. Hence, the

parameters for that Iwan joint can be determined using Mode 1 alone. In contrast, both Modes 2 and 4 are affected by S-CC Shapes 1 and 2, and so, while one might obtain initial estimates for the Iwan elements to apply at each S-CC shape using the individual modes, in the end Modes 2 and 4 must be considered simultaneously. The K_T value for each S-CC shape has already been determined as explained previously, and so this was not allowed to vary by more than 2% so as to not degrade the linear performance of the model. Similar to the RBAR model, this is done by adjusting the K_T value with the scale factor, γ. Placing a 4 Parameter Iwan element at S-CC Shape 1 and updating each parameters separately until the curves overlaid, returned the following amplitude dependent frequency and damping curves for Mode 1 after the model is solved using QSMA.

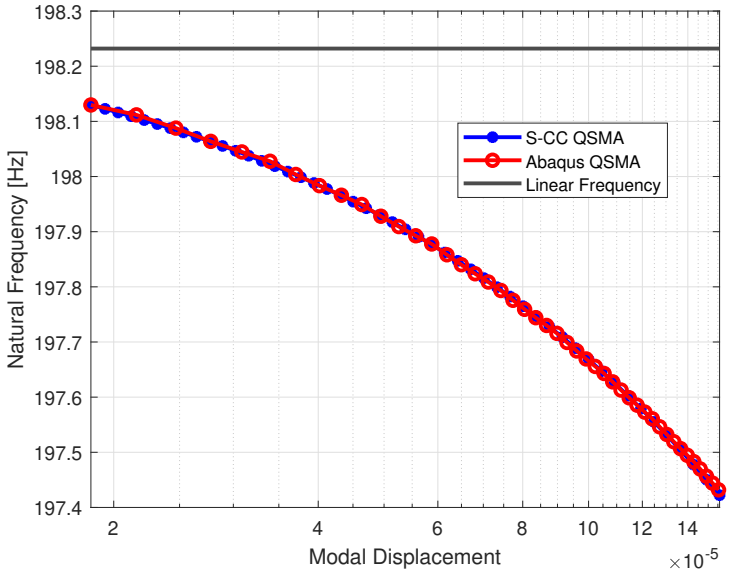

Figure 9: Mode 1 Amplitude Dependent Natural Frequency

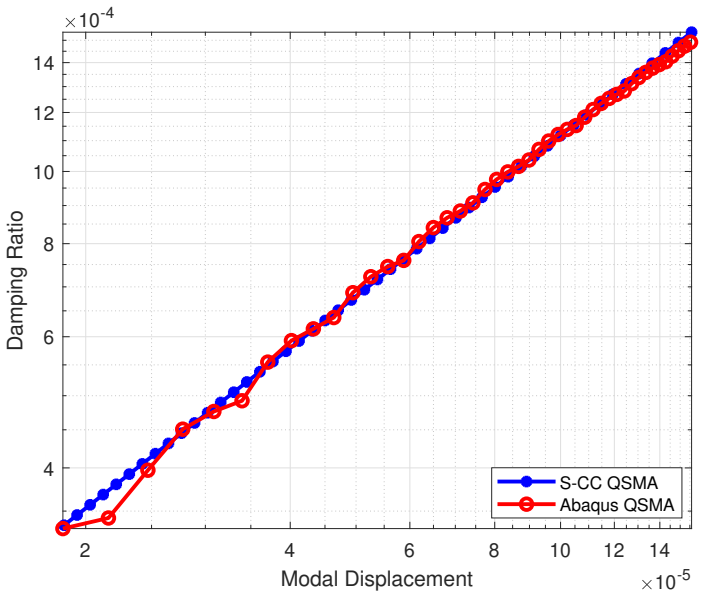

Figure 10: Mode 1 Amplitude Dependent Damping Ratio

The nSCC model can accurately capture the frequency and damping behavior of QSMA for Mode 1 with Abaqus to within 0.007% and 2.99% respectively. An exceptionally good model for the freuqency and damping of Mode 1 was obtained in this case, in contrast to the RBAR model which could fit one or the other, but not both. The larger error in damping is attributed to fitting the entire modal displacement range of the Abaqus model which does not purely exhibit power law behavior. Mode 1 can be tuned with ease since it is primarily dependent on Shape 1; however, Modes 2 and 4 require S-CC Shape 2 to be tuned to minimize the error between the S-CC and Abaqus quasi-static curves for both modes. For the purpose of the study, Modes 1 and 2, and Modes 1 and 4 were fit by fixing the parameters for S-CC Shape 1 and tuning the parameters for S-CC shape 2 (or shape 4). The parameters obtained are given in Table 8 each nSCC NLROM, one for Modes 1 and 2 ($\text{nSCC}_{1,2}$), and the other for Modes 1 and 4 ($\text{nSCC}_{1,4}$). Both nSCC NLROMs preserve the quasi-static response for Mode 1 and fit the other mode very well.

Table 8: Iwan Parameters for the two nSCC NLROMs

Iwan Parameters			
	S-CC Shape 1 (M_1)	**S-CC Shape 2** ($M_1 + M_2$)	**S-CC Shape 2** ($M_1 + M_4$)
F_S	5150	23481	16013
γ	1.0019	1.0013	1.0000
χ	-0.287	-0.232	-0.015
β	0.7602	0.9344	0.12648

The results so far show that it is quite simple to determine the parameters for the Iwan element connected to a particular S-CC shape in order to very accurately replicate the behavior of a particular mode. However, it is usually desired to have a single NLROM to capture all of the nonlinear modes of interest. Given that both Mode 2 and 4 are dependent on Shape 2, a Monte - Carlo simulation was conducted with 100,000 iterations randomly varying F_S, γ, and χ for Shape 2. These parameters were bounded between the values required to calibrate $\text{nSCC}_{1,2}$ and $\text{nSCC}_{1,4}$. β was not varied as it was the same for both models. The error metric used to find the optimal solution of the Monte - Carlo simulation is given by Eq. 24. The total error is a sum of the errors of each mode (denoted by the subscript i) which is found using a weighted sum of the squares of the damping and frequency errors defined by Eq. 25. Each mode can be weighted separately (W_i) as well as the damping and frequency (W_ω, W_ζ). The symbols ω and ζ refer to the damping and frequency points

from QSMA respectively, and the subscript *ref* refers to the reference data, in this case the points from the Abaqus quasi-static curves. The norm of these error vectors are calculated in Eq. 26 such that they can be used in subsequent equations as scalars.

$$E_{total} = (\sum E_i^2)^{1/2} \tag{24}$$

$$E_i = W_i \cdot \frac{(W_{\omega,i}^2 \cdot E_{\omega,i}^2 + W_{\zeta,i}^2 \cdot E_{\zeta,i}^2)}{\sqrt{(W_{\omega,i}^2 + W_{\zeta,i}^2)}} \tag{25}$$

$$E_{\omega,i} = \|((\omega_i - \omega_{ref,i})/\omega_{ref,i})\|\,, \qquad E_{\zeta,i} = \|((\zeta_i - \zeta_{ref,i})/\zeta_{ref,i})\| \tag{26}$$

The optimal solution from the Monte Carlo simulation generated a single $\text{nSCC}_{1,2,4}$ ROM that can closely reproduce the frequency and damping versus amplitude for all three modes of the Abaqus truth model. Although, the curves do not overlay completely with those from Abaqus, the frequency and damping are within 0.02% and 8% of the Abaqus QSMA curves respectively for both modes. The resulting parameters for this NLROM are given in Table 9.

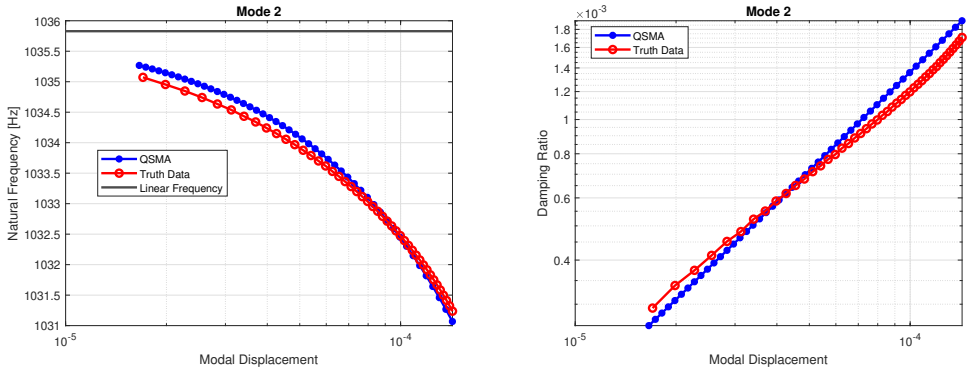

(a) **(b)**

Figure 11: Mode 2 Amplitude Dependent Natural Frequency (a) and Damping (b) using nSCC $ROM_{1,2,4}$

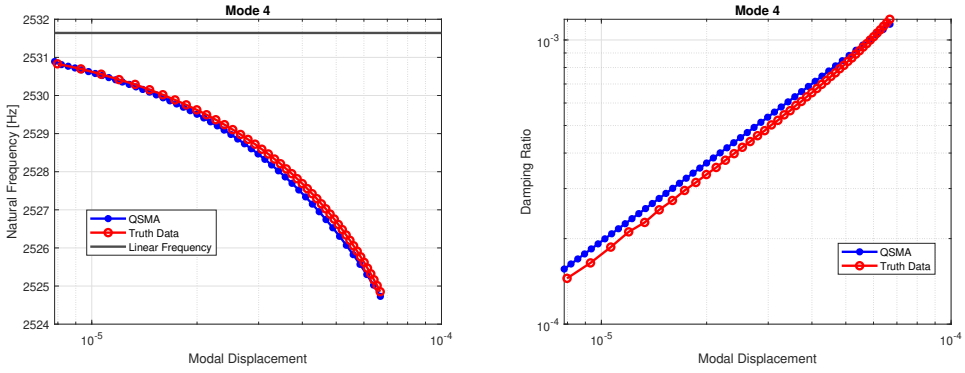

(a) **(b)**

Figure 12: Mode 4 Amplitude Dependent Natural Frequency (a) and Damping (b) using nSCC $ROM_{1,2,4}$

Table 9: Iwan Parameters for the single nSCC $ROM_{1,2,4}$

Iwan Parameters		
	Shape 1	**Shape 2**
	(Mode 1)	**(Mode 1 + Mode 2 + Mode 4)**
F_S	5150	19079
γ	1.0019	1.0011
χ	-0.287	-0.0927
β	0.7602	0.1026

A frequency weighting factor $W_\omega = 1e8$ and Mode 4 weighting factor $W_4 = 100$ were used leaving W_ζ and W_2 at unity. The model often chose parameters resembling those for $nSCC_{1,2}$ therefore requiring a larger weight on the error from the Mode 4 calibration. Since the damping length scale is much smaller than frequency, it is susceptible to higher errors, thus requiring a frequency weighting factor to ensure the errors are around the same order of magnitude.

CONCLUSION

This paper explored the extension of linear S-CC reduction to nonlinear analyses, creating what are here dubbed nSCC ROMs, and which were compared to the traditional spidering approach with RBAR MPCs. This was done on a 2D Beam whose nonlinear frequency and damping behavior could be computed directly, in order to gauge the effectiveness of these

NLROMs at recreating these curves from a high-fidelity model. The RBAR model used rigid bar constraints to reduce each interface to a single point by enforcing the same deformation, whereas S-CC reduction maintains some flexibility in the interface, depending on how many S-CC shapes are retained. The viability of both methods was evaluated by comparing their ability to reproduce the linear natural frequencies of the beam, as well as the amplitude dependent frequency and damping curves, which were estimated using QSMA.

The S-CC and RBAR and reduced models were able to accurately capture the linear natural frequencies of the first 6 modes of the HCB model within 0.5%. The S-CC model had errors significantly below those for RBAR. Both models needed 20 Fixed Interface Modes and 6 DOF to capture the linear dynamics by reducing the 8684 DOF in the FEM by a factor of 1000.

Iwan elements were then inserted into both models to capture the nonlinearity in the structure due to the joint. The accuracy of the models was evaluated by comparing the effective natural frequency and damping as a function of amplitude, which indicates the model's ability to more accurately predict the vibration level (and stresses) at high amplitudes when the joints are dissipating significant energy. The RBAR model was able to reproduce the frequency or damping curves for Mode 1, but not both, and the results for Modes 2 and 4 were also poor even after a thorough exploration of the parameter space. The optimization required to explore such a broad parameter space was daunting, similar to our experience in applying this method to other systems. In contrast, the extension of S-CC to nonlinear (nSCC) allowed for relatively intuitive tuning of the Iwan parameters for each mode separately, and this provided initial estimates about which to center the optimization, making it far simpler. In the end, excellent correlation was obtained for the 3 modes of interest. Although Mode 3 did not exhibit nonlinearity, this model is able to capture the linear modal parameters of Mode 3. With Mode 1 dependent on Iwan parameters for S-CC Shape 1, there was a much simpler optimization problem to solve to capture the nonlinear

effects of Modes 2 and 4 through S-CC Shape 2.

The S-CC reduction method performed efficiently enough on the 2D Abaqus beam to be viable for multi-joint structures. In future work we will apply the S-CC method to other models and explore whether this method can capture coupling between the modes due to the nonlinearity. The hope is that the inherent flexibility and more intuitive updating of this method will make it easier to capture the nonlinear dynamics in larger systems that exhibit more complicated phenomenon.

ACKNOWLEDGEMENTS

The views expressed in the article do not necessarily represent the views of the U.S. Department of Energy or the United States Government. Sandia National Laboratories is a multimission laboratory managed and operated by National Technology & Engineering Solutions of Sandia, LLC, a wholly owned subsidiary of Honeywell International Inc., for the U.S. Department of Energy's National Nuclear Security Administration under contract DE-NA0003525. SAND2020-5174 C

REFERENCES

[1] "Abaqus analysis user's guide," 2014.

[2] E. Jewell, M. S. Allen, and R. Lacayo, "Predicting damping of a cantilever beam with a bolted joint using quasi-static modal analysis," Aug. 2017.

[3] MSC.Software, "MSC Nastran 2013 Quick Reference Guide," June 2013.

[4] M. Griebel, J. Wilson, A. Johnson, B. Erickson, A. Doan, C. Flanigan, P. Bremner, J. Sills, and E. Bruno, "Orion E-STA Nonlinear Dynamic Correlation and Coupled Loads Analysis," (El Segundo, CA), June 2019. Matt Griebel, Jesse Wilson, Adam Johnson, Brent Erickson, Andrew Doan, and Chris Flanigan, Quartus Engineering, Inc., Paul Bremner, AeroHydroPLUS, Joel Sills, NASA Engineering Safety Center, Erica Bruno,

Analytical Mechanics Associates, In.

[5] M. S. Allen, J. D. Schoneman, W. Scott, and J. Sills, "Leveraging Quasi-Static Modal Analysis for Nonlinear Transient Dynamics," (El Segundo, CA), June 2019.

[6] A. Singh, M. Wall, M. S. Allen, and R. J. Kuether, "Spider Configurations for Models with Discrete Iwan Elements," in *Nonlinear Structures and Systems, Volume 1* (G. Kerschen, M. R. W. Brake, and L. Renson, eds.), Conference Proceedings of the Society for Experimental Mechanics Series, (Cham), pp. 25–38, Springer International Publishing, 2020.

[7] R. M. Lacayo and M. S. Allen, "Updating Structural Models Containing Nonlinear Iwan Joints Using Quasi-Static Modal Analysis," *Mechanical Systems and Signal Processing*, vol. 118, no. 1 March 2019, pp. 133–157, 2019. Number: 1 March 2019.

[8] D. J. Segalman, "Model reduction of systems with localized nonlinearities," *Transactions of ASME. Journal of Computational and Nonlinear Dynamics*, vol. 2, no. 3, pp. 249–66, 2007. Number: 3.

[9] H. Festjens, G. Chevallier, and J.-L. Dion, "A numerical tool for the design of assembled structures under dynamic loads," *International Journal of Mechanical Sciences*, vol. 75, pp. 170–177, 2013.

[10] P. Wriggers, *Computational Contact Mechanics*. Berlin Heidelberg: Springer-Verlag, 2 ed., 2006.

[11] Patrick J Hughes, Wensi Wu, and Wesley E Scott, "Interface Reduction on Hurty/Craig-Bampton Substructures with Frictionless Contact," in *Nonlinear Dynamics*, vol. 1, (Orlando, FL), pp. 1–16, Springer, June 2018.

[12] M. P. Castanier, Y. C. Tan, and C. Pierre, "Characteristic constraint modes for component mode synthesis," *AIAA Journal*, vol. 39, no. 6, pp. 1182–1187, 2001. Number: 6.

[13] B. Deaner, M. S. Allen, M. J. Starr, D. J. Segalman, and H. Sumali, "Application of

Viscous and Iwan Modal Damping Models to Experimental Measurements From Bolted Structures," *ASME Journal of Vibrations and Acoustics*, vol. 137, p. 12, 2015.

[14] R. J. Kuether, P. B. Coffin, and A. R. Brink, "ON HURTY/CRAIG-BAMPTON SUBSTRUCTURING WITH INTERFACE REDUCTION ON CONTACTING SURFACES," in *International Design Engineering Technical Conferences*, (Cleveland, Ohio), 2017.

[15] R. R. J. Craig and M. C. C. Bampton, "Coupling of Substructures Using Component Mode Synthesis," *AIAA Journal*, vol. 6, no. 7, pp. 1313–1319, 1968. Number: 7.

[16] D. Krattiger, L. Wu, M. Zacharczuk, M. Buck, R. J. Kuether, M. S. Allen, P. Tiso, and M. R. W. Brake, "Interface Reduction for Hurty/Craig-Bampton Substructured Models: Review and Improvement," *Mechanical Systems and Signal Processing*, vol. 114, pp. 579–605, Jan. 2019.

[17] D. J. Segalman, "A Four-Parameter Iwan Model for Lap-Type Joints," *Journal of Applied Mechanics*, vol. 72, pp. 752–760, Sept. 2005. Number: 5.

[18] B. Deaner, M. S. Allen, M. J. Starr, and D. J. Segalman, "Investigation of Modal Iwan Models for Structures with Bolted Joints," Feb. 2013.

[19] M. S. Allen, R. Lacayo, and M. R. Brake, "Quasi-static Modal Analysis based on Implicit Condensation for Structures with Nonlinear Joints," Sept. 2016.

[20] R. Lacayo, B. Deaner, and M. S. Allen, "A Numerical Study on the Limitations of Modal Iwan Models for Impulsive Excitations," *Journal of Sound and Vibration*, vol. 390, pp. 118–140, 2017.

[21] J. Lagarias, J. Reeds, M. Wright, and P. Wright, "Convergence Properties of the Nelder–Mead Simplex Method in Low Dimensions," *SIAM Journal on Optimization*, vol. 9, pp. 112–147, Dec. 1998.

Multi-mode Quasi-static Excitation for Systems with Nonlinear Joints

Aabhas Singh — University of Wisconsin - Madison

Matthew S. Allen — University of Wisconsin - Madison

Robert J. Kuether — Sandia National Laboratories

ABSTRACT

Finite element models can be used to model and predict the hysteresis and energy dissipation exhibited by nonlinear joints in structures. As a result of the nonlinearity, the frequency and damping of a mode is dependent on excitation amplitude, and when the modes remain uncoupled, quasi-static modal analysis has been shown to efficiently predict this behavior. However, in some cases the modes have been observed to couple such that the frequency and damping of one mode is dependent on the amplitude of other modes. To model the interactions between modes, one must integrate the dynamic equations in time, which is several orders of magnitude more expensive than quasi-static analysis. This work explores an alternative where quasi-static forces are applied in the shapes of two or more modes of vibration simultaneously, and the resulting load-displacement curves are used to deduce the effect of other modes on the effective frequency and damping of the mode in question. This methodology is demonstrated on a simple 2D cantilever beam structure with a single bolted joint which exhibits micro-slip nonlinearity over a range of vibration amplitudes. The predicted frequency and damping are compared with those extracted from a few expensive dynamic simulations of the structure, showing that the quasi-static approach produces reasonable albeit highly conservative bounds on the observed dynamics. This framework is also demonstrated on a 3D structure where dynamic simulations are infeasible.

1 INTRODUCTION

Finite element analysis (FEA) is foundational when modeling the behavior of structures, and while it produces highly accurate results for a single elastic part, significant challenges arise when trying to capture the effects of frictional contact at the interfaces between parts [1, 2]. When joints are preloaded the contact pressure is typically greatest near the bolt and decreases away from the bolt (see, e.g. [3, 4]). Part of the contact patch can slip when the structure is loaded, causing energy dissipation. A joint is in the microslip regime when slip occurs at the extremities of the contact patch and the remainder of the patch remains stuck. In this regime the nonlinearity tends to be weak and the response is typically quasi-linear and yet significant energy can be dissipated causing the effective modal damping and the modal natural frequency to change with vibration amplitude [5–7]. In contrast, as the load on the structure is increased, macroslip may occur in which the joint loses in-plane stiffness and the entire interface slips. If the slip in the joints is large enough, complicated phenomena such as multi-harmonic responses, modal coupling and even quasi-periodic responses or chaos can occur. However, in most cases the joint is considered to have failed if macroslip is reached so this work focuses on modeling joints in the microslip regime.

To solve these contact problems, significant mesh refinement is necessary at the contact interfaces to capture the localized slip [4, 8, 9]. As the number of joints increases, high-resolution modeling of these interfaces becomes computationally expensive or even infeasible. This was illustrated by Jewel et al. [4] who demonstrated that when the mesh was adequately refined and the solver (Abaqus) was tuned to accurately solve the contact mechanics problem, tens of hours were required to obtain accurate solutions for the static response of a structure with only two joints. Dynamic analysis of the same jointed structure could take days to weeks for a few cycles of loading, and thousands of cycles would be needed if one wished to model a time response similar to what might be recorded in an experiment. To mitigate the computational costs of time integration, various alternative methods have been developed.

A few different classes of methods have been proposed that can extend the concept of a mode to nonlinear systems, and hence describe phenomena such as the amplitude dependent frequency and damping that are observed in structures with bolted joints. One of the most well known is the nonlinear normal mode (NNM) definition of Vakakis & Kerschen [10–12], which defines an NNM as a periodic response of a conservative nonlinear system. This has proven quite effective for understanding the dynamics of conservative nonlinear systems such as structures exhibiting geometric nonlinearity [13]. Krack extended this concept to damped systems by adding an artificial negative damping term to counter-act the actual damping in the system, calling the resulting method the extended periodic motion concept (EPMC) [14]. Using this method, one can extend existing methods for computing NNMs [12] to damped systems. Other methods such as numerical continuation, shooting methods, and manifold methods [15–18] can also be applied to damped systems. Shooting methods typically integrate the equations of motion over one vibration cycle and iterate on the initial conditions until the steady-state response has been obtained [12]. In contrast, Harmonic Balance (HB) methods, which have been extended to address systems with frictional contact, [9,19,20], represent the response as a Fourier series and solve a nonlinear system of algebraic equations to obtain the Fourier Coefficients at each frequency/amplitude.

The methods developed in this work are related to the averaging method [21], which integrates the nonlinear equations over one cycle of vibration to find the quasi-linear system that best approximates the nonlinear response [22]. A quasi-linear system is a linear system whose parameters, i.e. natural frequency and damping, are amplitude dependent; at a fixed amplitude the response is assumed to be well approximated as linear. Within this framework, methods [23–25] have recently been developed that can compute the frequency and damping of a structure as a function of vibration amplitude from a single quasi-static load-displacement curve. Festjens et al. [23] introduced a quasi-static framework for jointed systems where a structure is forced to the shape of a mode of interest and the elastic energy

and energy dissipated are used to compute the effective frequency and damping. A variant of this method, called quasi-static modal analysis (QSMA), was introduced by Allen and Lacayo [24] which simplified the approach in [23] slightly and uses the static load-displacement curve in modal coordinates to compute the effective natural frequency and damping ratio, allowing one to more easily diagnose problems with the contact simulations. It has been shown that QSMA can accurately compute the nonlinear frequency and damping of simple joined structures on a mode-by-mode basis in orders of magnitude less time than would be required to compute the dynamic response [24] and the method has subsequently been applied to various systems [4, 26, 27]. For example, in one case study for a structure with 350,000 elements and two contact interfaces, the modal behavior was extracted using QSMA in 8 to 48 hours; the authors judged dynamic analysis to be infeasible, although Najera-Flores and Kuether [28] later performed a 1.0 second dynamic analysis on a similar model, requiring 20 days on 112 processors.

For a linear system, the modes of a structure are independent of amplitude and a modal filter [29] can be used to separate a multi-modal response into the contributions from the individual modes. If the modal frequencies are sufficiently distinct then a temporal filter could be used instead. For a weakly nonlinear response, it is often observed that the nonlinearity primarily affects damping and does not alter the mode shapes significantly; thus, the linear modes are assumed to remain uncoupled and can be used to decouple the nonlinear system, as long as the criteria outlined by Eriten et al. [22] are satisfied (e.g. modal frequencies are not integer multiples of one another). However, the modes may not always satisfy these conditions. Coupling occurs when the excitation of one mode causes a transfer of energy that perturbs another mode [30]. Recent studies on experimental structures have shown that the interactions between modes are not always negligible and hence one may obtain large errors in the predicted damping if they are not considered [31–33].

Many works have studied nonlinearity and the coupling that it can induce between modes.

For example, the NNM framework in [11, 34] captures internal resonance branches, which are a manifestation of coupling in an undamped nonlinear system. Vakakis has studied this extensively in the context of vibration absorbers and the one-way transfer of energy (see, e.g. [35]) and the International Conference on Nonlinear Vibrations, Localization and Energy Transfer is dedicated, in part, to this topic. Most works on modal interactions focus on cases in which the frequencies of the two modes in question are integer multiples of one another, in which case a super-harmonic resonance can occur and modal coupling is known to be significant [21]. This work is concerned with a different phenomenon, in which the a typically weaker nonlinearity causes coupling between two modes whose frequencies are not integer related, such that the effective frequency and damping of one mode is influenced by the other mode. Such was the case for the measurements done by Wall et al. [33].

While experimentally capturing modal coupling is feasible, numerically modeling the coupling is computationally expensive, especially when seeking to model the contact between the structures in detail as is the focus of this work. A dynamic transient analysis can produce a response that is consistent with the mesh and the friction law that was assumed at the interface, but this comes at a large computational cost. On the other hand, the QSMA method in [24] is computationally efficient, but require that the joints remain weakly nonlinear such that modal coupling is negligible. This work seeks to extend the quasi-static framework in [24] to predict modal coupling without having to run a dynamic analysis. Termed Multi-Mode QSMA (MM-QSMA), the method proposed in this work statically loads the structure in the shape of two or more modes simultaneously. The loading is defined such that other modes are excited in addition to the mode of interest, whose motion is suspected to change the response of the mode of interest.

The proposed MM-QSMA method is demonstrated on Abaqus finite element models of a 2D beam structure [4] and the S4 Beam [3, 33]. The MM-QSMA procedure is applied with various relative amplitudes and phasing between the modes to establish bounds on the

coupling in a response. This is contrasted with a single mode excitation baseline (i.e., using the standard QSMA procedure), and a few expensive dynamic responses are used to validate the procedure. The comparison shows that the MM-QSMA procedure does well to predict the bounds on the effective natural frequency and damping that are observed in the dynamic response and the single mode quasi-static response, although the predictions are somewhat over-conservative.

2 THEORY

2.1 Multi-Mode Quasi-Static Modal Analysis (MM-QSMA)

A brief overview of the QSMA approach by Lacayo and Allen [24] is detailed below. Refer to [4,24,31,36] for additional details and limitations. The FE discretized equations of motion for an undamped multi-degree of freedom (MDOF) system are given by Eq. 1, where $\mathbf{M}$ is the mass matrix, $\mathbf{K}$ is the stiffness matrix, $\mathbf{F}_{ext}$ is the external forcing, $\mathbf{F}_J(\mathbf{u}, \boldsymbol{\theta})$ is the force localized at the joint, which is a function of the preload applied to the joint, and $\mathbf{u}$ is the physical displacement. To determine whether the nodes of the joint are slipping or stuck, an internal variable, $\boldsymbol{\theta}$, is used to track the state of the slider elements the comprise the joint model in the previous timestep to determine the force and displacement of the nodes at the next timestep.

$$\mathbf{M}\ddot{\mathbf{u}} + \mathbf{K}\mathbf{u} + \mathbf{F}_J(\mathbf{u}, \boldsymbol{\theta}) = \mathbf{F}_{ext} \tag{1}$$

If the displacements are small relative to an equilibrium position, the joint force can be linearized about the equilibrium state by computing the Jacobian of the force with respect to each coordinate of $\mathbf{u}$. This is often done when a preload or clamping force is applied to the system prior to dynamic loading, resulting in the following tangent stiffness matrix for

the joint forces.

$$\mathbf{K}_0 = \left.\frac{\partial \mathbf{F}_J}{\partial \mathbf{u}}\right|_{\mathbf{u}_0} \tag{2}$$

The linearized modes of vibration can be computed about this equilibrium by solving the following eigenvalue problem where ω_r and $\boldsymbol{\phi}_r$ are the respective eigenvalue and eigenvector for the rth mode.

$$\left(\mathbf{K} + \mathbf{K}_0 - \omega_r^2 \mathbf{M}\right) \boldsymbol{\phi}_r = \mathbf{0} \tag{3}$$

A quasi-static distributed force is then applied such that replicates the inertial loading experienced during vibration in the rth mode. The following equation is then solved statically

$$\mathbf{K}\mathbf{u} + \mathbf{F}_J(\mathbf{u}, \boldsymbol{\theta}) = \mathbf{M}\boldsymbol{\phi}_r \alpha \tag{4}$$

where α represents a scalar amplitude for the applied body load. For the purposes of this paper, α is linearly increased from 0 to a maximum amplitude level of interest. The maximum value of alpha is determined by Eq. 5 where ω_r is the natural frequency of the rth mode, h is the thickness of the structure, γ is a scale factor, and ϕ_{max} is the absolute maximum of the rth mode shape.

$$\alpha_{max} = \frac{\gamma \omega_r^2 \mathrm{sgn}(\phi_{r,max}) h}{\phi_{max}} \tag{5}$$

It is important to note that the loading does not account for changes in the mode shapes, but the resulting static response may depend on all of the modes, i.e., modes other than the mode in question may be statically excited. After solving Eq. 4 one obtains the static response as a function of the scalar amplitude levels, $\mathbf{u}(\alpha)$, from which the modal amplitude, natural frequency ($\omega(\alpha)$), and damping ratio ($\zeta(\alpha)$) can be written as function of α as shown in Eq. 12-17 in [24]. Once these are obtained, one can plot the frequency and damping as a function of modal amplitude as shown in subsequent figures (e.g. Fig. 3). Note that one can compute the amplitude of every mode from $\mathbf{u}(\alpha)$, and this has been used to detect modal coupling in previous works, but the response is typically dominated by the mode that is excited (i.e., mode r in Eq. 4).

Multi-Mode QSMA extends the Eq. 4 framework by quasi-statically exciting multiple modes so that the right hand side of the quasi-static problem changes and the following equation is solved for $\mathbf{u}$

$$\mathbf{K}\mathbf{u} + \mathbf{F}_J(\mathbf{u}, \boldsymbol{\theta}) = \mathbf{M} \sum_{n=1}^{N} \boldsymbol{\phi}_{\boldsymbol{i}} \alpha_i \tag{6}$$

The response $\mathbf{u}(\alpha)$ is dependent on the force amplitudes α_i of all modes that are excited. Similar to QSMA, each α_i is applied linearly from 0 to some $\alpha_{i,max}$ simultaneously. To obtain the response of each mode, a modal filter is used as given in Eq. 7, where $q_r(\alpha)$ is the modal response of the rth mode.

$$q_r(\alpha) = \boldsymbol{\phi}_r^{\mathrm{T}} \mathbf{M} \mathbf{u}(\alpha) \tag{7}$$

Since the quasi-static load is intended to only excite the rth mode, the purposeful addition of other modes will allow one to evaluate whether those modes are statically coupled to the

rth mode, and to quantify the coupling by computing how much the frequency and damping curves deviate from an uncoupled case, i.e. those computed using **u** from Eq. 4.

It is important to note that the signs on the loads applied in Eq. 6 can be important. Suppose that two modes of interest have the same sign at some point on the structure. If the signs on forces α_i are the same then we can think of the modes as being in phase. Specifically, the quasi-static response represents a case in which the structure is vibrating such that these two modes are in phase and have the same natural frequency. The two modes would each achieve their maximum displacements at the same instant. Conversely, if the signs on α_i are opposite then this represents a case where the modes vibrate out of phase. (These cases are illustrated in Fig. 4, which will be discussed later.) In almost all cases of interest the two modes in question will not have the same natural frequency, neither will they have natural frequencies that are integer related, so the phasing between the modes can be expected to be changing continuously during a dynamic response. The hypothesis behind MM-QSMA is that the in-phase (IP) and out-of-phase (OOP) static loadings are extreme cases that can provide a bounding box for the actual dynamic response. Hence one must perform a pair of MM-QSMA for each pair of modes of interest, and the frequency and damping estimated from the IP and OOP loadings will provide upper and lower bounds. The examples presented in the following section support this hypothesis.

2.2 Direct Time Fitting Dynamic Responses

To evaluate the efficacy of MM-QSMA, a dynamic transient simulation of the finite element model is used. The nonlinear static response is found using Eq. 6, i.e., when a force is applied that is the sum of the desired mode shapes. It is important to use this as the initial condition, rather than a prescribed displacement into the shape of two modes, because the latter would not allow the quasi-static relaxation that occurs near the joint in a real structure [4]. Let the displacement at the end of the quasi-static analysis be denoted

$\boldsymbol{u}_0$. This becomes the initial condition for the equation of motion in Eq. 1, which is then integrated in time implicitly to calculate the physical response at each node in the FEM, $\mathbf{u}(t)$ for the desired loading case. The modal filter in Eq. 7 is then used to decompose this into the response of each mode of interest, $q_1, q_2, ...$ One can then compute the effective natural frequency and damping ratio for each mode as a function of time. Whereas the phasing of the modes is constant throughout the quasi-static response, the phasing of the modes varies throughout time for the dynamic response.

In prior works, the frequency and damping curves for each mode were obtained using the Hilbert Transform [37]. That method typically fits each mode separately [37], and one would have to match the results in time to compare the amplitudes of the various modes. Furthermore, because the Hilbert transform is based on an FFT, the algorithm sometimes has difficulty when the transient response does not ring down to near zero amplitude, often introducing leakage that can contaminate the estimate of frequency and damping. In this work a new direct time fitting method is utilized instead. The method is presented in detail in Moldenhauer et al. [38]. In summary, the direct time fitting method is an extension of that presented by Goyder et. al [39] where the multi-harmonic time response is discretized into smaller time segments where the natural frequency is expected to be constant. For each segment, a damped sine is fit such that the error, defined as E is minimized as shown in Eq. 8 where A and B are amplitudes, α and β are two parameters that are found during the optimization, and H(t) is the Heaviside function, which limits the time window to $t_2 < t < t_1$.

$$y_{fit}(t, t_1, t_2) = \exp(-\beta t)(A\cos\alpha t - B\sin\alpha t) * [H(t - t_1) - H(t - t_2)] \tag{8}$$

$$E = y(t, t_1, t_2) - y_{fit}(t, t_1, t_2) \tag{9}$$

The parameters α and β are found during a single objective optimization and the amplitudes A and B are found using a least squares procedure. Each mode is fit simultaneously to ensure any interactions and influences between modes are captured. The instantaneous damping and frequency can be computed for each mode at each time segment using the equations below.

$$\omega_n = \sqrt{\alpha^2 + \beta^2} \tag{10}$$

$$\zeta = \frac{\beta}{\sqrt{\alpha^2 + \beta^2}} \tag{11}$$

The frequency and damping is found at the midpoint of the time segments, i.e. $t_m = \frac{(t_1+t_2)}{2}$.

3 SINGLE MODE EXCITATION FOR A 2D CANTILEVER BEAM

A 2D structure built in Abaqus is used to to demonstrate the MM-QSMA methodology, but prior to that, a baseline is formed with single mode excitation. The 2D structure is comprised of two cantilever beams made of steel with the properties shown in Table 1, and plane strain is applied so this represents a structure of unit depth with uniform properties through the depth. Figure 1 shows the Abaqus mesh and a diagram depicting the two beams, the sections where a preload is applied to the top and bottom surface (blue), and the region of contact. The contact surface has been modeled with element-to-element Coulomb friction elements. To obtain an accurate analysis of the energy dissipation due to the joint, the mesh has been refined towards the bolt section for a total of 8684 elements.

A preload pressure of 17.55 MPa (2546 psi) was applied to both the top and bottom of the bolt section and the linearized modes of vibration and frequency were obtained from

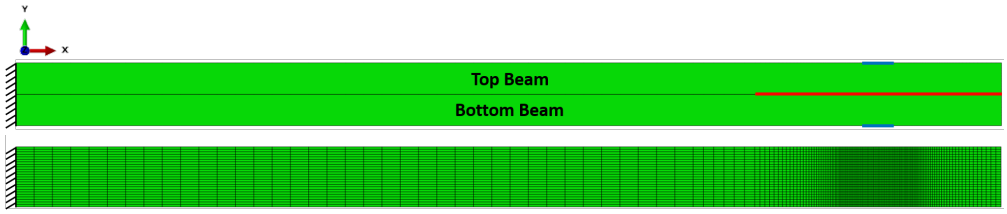

Figure 1: (Top) 2D Beam FE Model composed of a top beam, bottom beam, regions where the preload is applied (blue), and region of contact that is solved (red), (Bottom) A mesh of the 2D Beam from [4]

Table 1: Material properties and dimensions for the 2D Abaqus Model

Property	Value (SI)	Value (Imperial)
Length	20.32 cm	8.00 in
Height	1.27 cm	0.50 in
Density	7.84e-3 kg/cm^3	7.34e-4 $slinches/in^3$
Elastic Modulus	200 GPa	2.9e7 psi
Poisson's Ratio	0.29	0.29
Static Friction Coefficient	0.60	0.60

a linear analysis in Abaqus using the Lanczos Method [40]. Figure 2 shows the first two modes of interest and their respective natural frequencies. The modes are contoured by the magnitude of the displacement and scaled for visualization. In the following we apply the single mode QSMA approach to understand how each mode behaves in isolation then then we use the MM-QSMA approach to understand how these modes couple due to the nonlinear forces in the joint.

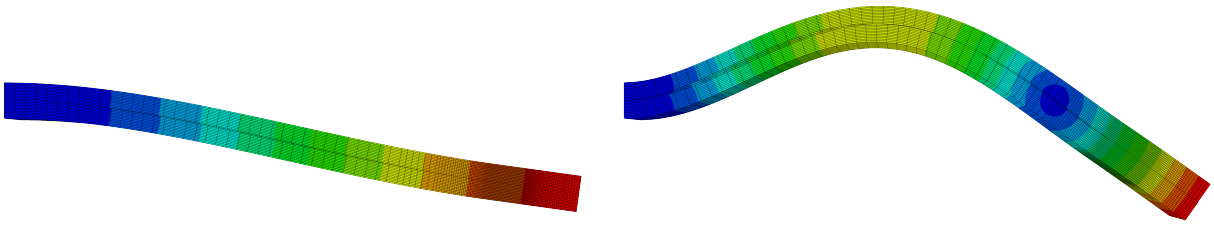

(a) **(b)**

Figure 2: (a) Mode 1 at 198 Hz, (b) Mode 2 at 1036 Hz

The natural frequency and damping predicted by single mode QSMA are compared to those estimated from an implicit dynamic transient solution in Fig. 3 for Modes 1 and 2. The QSMA predictions were obtained using Eq. 12-17 in [24] and the frequency and damping were extracted from the dynamic response by fitting the signals using Eqs. 7-10 in Section 2.2. Implicit dynamic analysis was performed in Abaqus using the Hilbert-Hughes-Taylor method for time integration [40], with the α parameter set to 0 to set the numerical damping to zero. However, the algorithm was found to still introduce spurious damping that appeared to be linear with respect to amplitude and dependent on the timestep, specifically the ratio of timestep to vibration frequency. For all dynamic responses, the integrator utilized an adaptive time step with a minimum step size of 5e-10 and a maximum step size of 1e-6. The numerical damping was found to increase if larger timesteps were used. It was judged impractical to reduce the step size further; with these settings $\sim$26 hours were required to integrate the response over 0.3 seconds. And so, the difference between the dynamic and quasi-static solutions was taken to be the numerical damping and it was assumed to be constant so long as the time step was not changed, specifically, the numerical damping ratios were found to be $\zeta_{\text{num},1} = 0.025\%$ and $\zeta_{\text{num},2} = 0.136\%$ for Modes 1 and 2, respectively. These values were subtracted from the damping obtained in the dynamic responses in the following section to facilitate those comparisons as well.

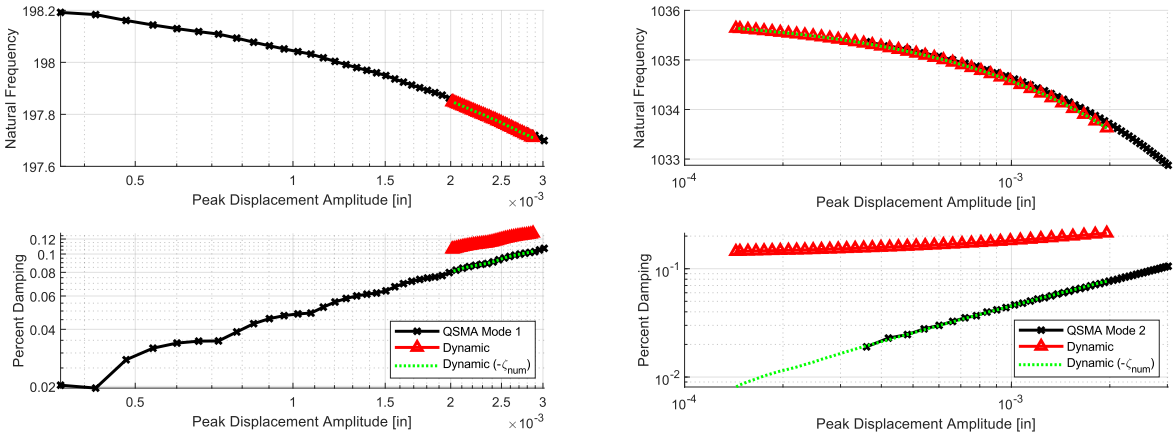

(a) **(b)**

Figure 3: (a) Mode 1 (b) Mode 2 dynamic response compared to the quasi-static response. The green dashed lines show the frequency and damping estimated from the dynamic response after subtracting off the numerical damping, ζ_{num}.

4 MULTI-MODE EXCITATION FOR A 2D CANTILEVER BEAM

As explained in Sec. 2.1, two multi-mode loads were applied: (1) in phase (IP) excitation, where the two modes in Fig. 2 are forced such that they have the same sign, and (2) out-of-phase (OOP) excitation where the modes have opposing signs. Since the sign on a mode is arbitrary, the modes were first made to have the same sign in the y - direction at the tip of the beam, prior to setting the signs for IP and OOP excitation. Figure 4 illustrates the two methods on the 2D structure where the red and yellow distributed loads are the two mode shapes of interest, and the superposition of these two loads is shown in blue.

In order to quantify how the relative strength of the modes affects the coupling, MM-QSMA was applied with various relative strengths of the modes, defined by the peak modal displacement of each mode, defined as the maximum displacement that the linear structure would achieve in the mode in question if only that mode were applied. Then, the ratio between these peak modal displacements defines their relative strengths. Three peak modal displacement amplitude ratios were applied: ± 10 to 1 (10%), ± 2 to 1 (50%), and ± 1 to 1

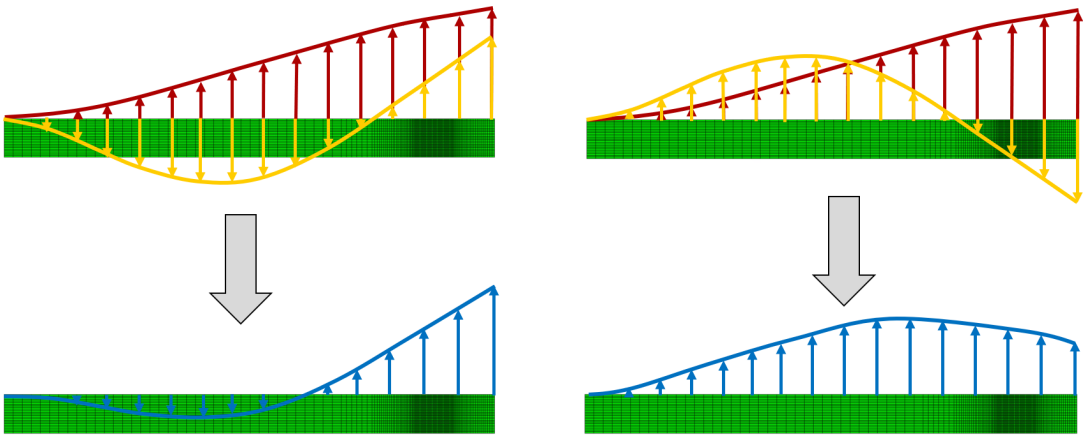

Figure 4: (a) In-Phase, (b) Out-of-Phase of Mode 1 and Mode 2 for the 2D beam and the resulting load curves in blue. Mode 1 and Mode 2 are arbitrarily scaled

(100%). The ratios, R, were determined by comparing the scale factor from Eq. 5 for the ith and jth modes as follows.

$$\mathrm{R}(\gamma) = \gamma_i/\gamma_j \tag{12}$$

The sign on the ratio defines the phasing of the load where a positive ratio indicates in-phase loading and a negative ratio indicates out-of-phase loading, and magnitude gives the relative strength of the mode in question, which is typically assumed to be the dominant mode, i.e. typically $R < 1$. For example, a -2 to 1 (or -2:1) ratio for Modes 1 and 2 would indicate that the force on Mode 1 is twice as large as that on Mode 2 and that the modes are out-of-phase.

To understand the coupling predicted by MM-QSMA, the frequency and damping predicted from the coupled responses are compared to single mode QSMA predictions (where minimal coupling exists) and to the frequency and damping extracted from dynamic transients. In the latter case the initial conditions for the dynamic transients were set by applying the same forces used in MM-QSMA, and then releasing the force and allowing the beam to

vibrate freely. In doing so, an in-phase excitation was used (i.e. +2 to 1 (in-phase) for whichever mode was of interest. This sets the initial condition for the transient response, and the phasing had little consequence because the frequencies of the modes are not commensurate (i.e. the ratio of the linearized frequencies of Modes 1 and 2 is 5.23) so the phase varied continuously throughout the response. (The structure was also given a -2 to 1 out-of-phase initial condition for the dynamic response, and the resulting frequency and damping versus time were found to be nearly identical and so these responses are not presented here.) It is also important to note that the modes also decay at different rates, with Mode 2 decaying much more quickly, and so the ratio of the amplitudes of Modes 1 and 2 varies throughout the response.

4.1 Mode 1 Dominant Excitation

Figures 5a and 5b show the frequency and damping curves for Mode 1 QSMA, when Mode 1 is the mode of interest and hence is thought to be dominant and Mode 2 is subdominant. Additionally, the frequency and damping from a transient response is also shown which initiated from the +2:1 static deflection. Each subsequent figure contains four types of results as follows: (1) single mode QSMA (black), (2) IP MM-QSMA (solid lines with round markers with one line for each ratio), (3) OOP MM-QSMA (dashed lines with one line for each ratio), and (4) the dynamic simulation after removing the numerical damping (red). For the dynamic analyses, the structure was allowed to ring out for 0.3 seconds. The dynamic response is also investigated in detail at 3 key points marked A, B, and C.

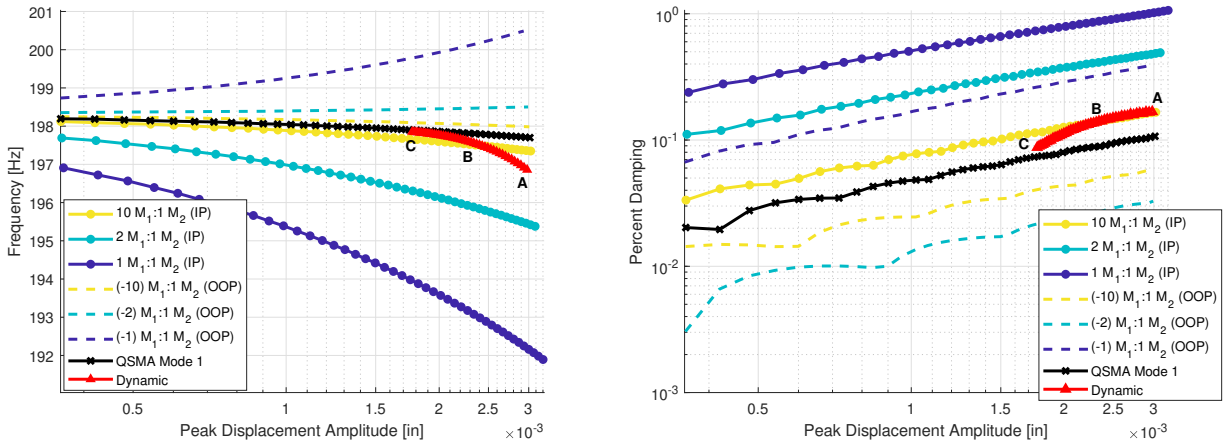

(a) **(b)**

Figure 5: (a) Frequency and (b) damping curves for Mode 1 QSMA, Mode 1 dominant MM-QSMA, and those obtained from a dynamic response

The dynamic response reveals the true changes that would occur in the frequency and damping of Mode 1 when Mode 2 is excited simultaneously. The true transient response, shown with red in Fig. 5a shows softening and an increase in damping compared to the damping that Mode 1 would have in isolation (black). The dynamic response shows larger deviations when the amplitude of Mode 2 was larger, i.e., earlier in the time history, and approaches the single mode quasi-static curve when Mode 2's relative amplitude decreases (later in the time history). This phenomenon can be quantified by examining the time responses from the fit as shown in Figure 6a, where the top sub-figure shows the the total response and fit and the two lower sub-figures show the fit for Mode 1 and Mode 2 respectively. This shows that Mode 2 damps out much more quickly than Mode 1, leading to a decrease in effect of Mode 2 on Mode 1. This can be further seen by examining Fig. 6b which shows the ratios of the amplitudes of Mode 1 to Mode 2, as obtained from the time fitting. As the simulation time increases, there is an increase in the ratio of Mode 1 to Mode 2, hence a reduction of the effect of Mode 2 on Mode 1. Specifically, early in the time history at point A, the ratio of Mode 1 to Mode 2 is almost exactly 2 to 1 as prescribed. At around

the midpoint at point B the ratio is approximately 9:1 and increases to 29:1 at the end of the time history. Due to the large presence of Mode 1 at the end of the time history at point C, the results appear to converge to the single mode QSMA backbone.

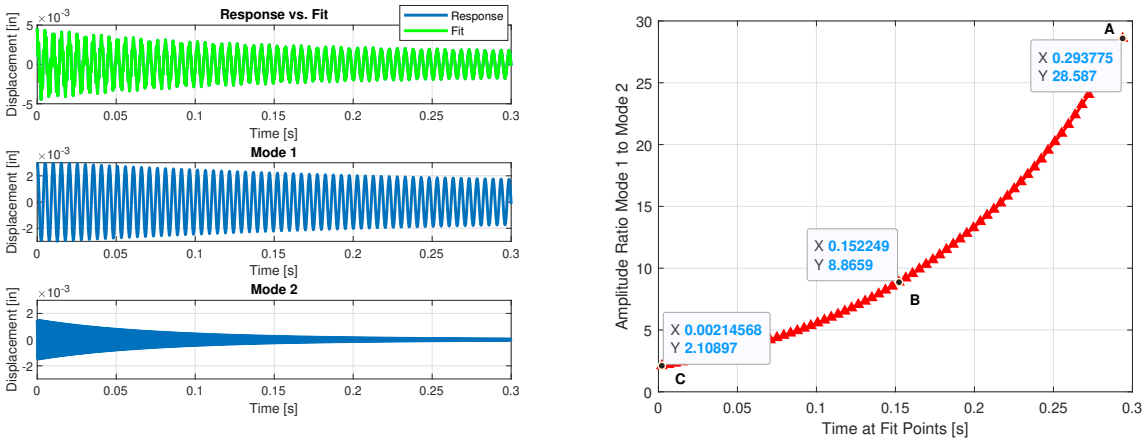

(a) **(b)**

Figure 6: (a) Fit of the multi-mode dynamic response using [38], (b) Amplitude ratio between Mode 1 and Mode 2 at fit points

The results show that MM-QSMA predicts an increase/decrease in the natural frequency for OOP/IP forcing, with the deviation in the frequency becoming larger as the amplitude ratio increases. Similarly, for the damping there is a decrease/increase for OOP/IP forcing, although there is one exception; the damping curve for the -1:1 case exhibits an increase in damping, whereas the -2:1 and -10:1 curves predict a decrease. The bounds predicted by MM-QSMA are generally quite a bit larger than that observed in the dynamic response. For example, at point A where the ratio Mode 1 to Mode 2 is 2:1, the QSMA bound predicts a frequency shift that is twice as large as what actually occurs, while at point B where the dynamic response shows a 9:1 ratio the actual frequency shift is about 30% of that predicted by the 10:1 MM-QSMA prediction. The response never shows the characteristics exhibited by the OOP MM-QSMA curves (increasing frequency and decreasing damping), so perhaps

there is no value to computing these, but one may not know a priori whether the IP or OOP case was more relevant.

To further investigate, the contact interfaces of the single mode QSMA and -1:1 MM-QSMA simulations for the last static load step are shown in Figs. 7a and 7b. Stuck and slipped elements are contoured as green and yellow respectively, and all remaining elements not in contact are shown in blue. The multi-mode response in Fig. 7b has a much larger area of the interface that is slipping, which explains the larger damping that is seen in this case.

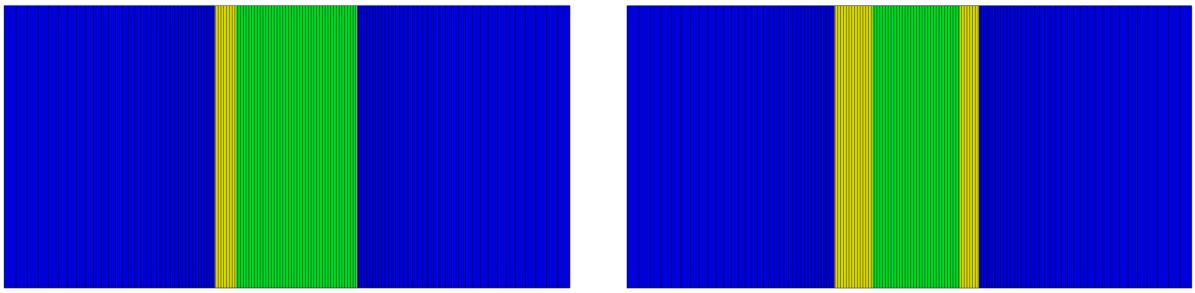

(a) **(b)**

Figure 7: Contact status of the interface of the 2D beam at the end of quasi-static loading for (a) Mode 1, and (b) -1:1 Mode 1 to Mode 2. The cantilevered end is left of the interface. The model is solved in plane strain and is shown with arbitrary width to aid in visualization

4.2 Mode 2 Dominant Excitation

The same analysis was repeated for the case where Mode 2 is dominant, and the results comparing MM-QSMA to the single mode backbone and dynamic response are shown in Figs. 8a and 8b, with the Mode 1 and Mode 2 time responses and amplitude ratios shown in Figs. 9a and 9b. Compared to the previous case, MM-QSMA predicts that Mode 1 would have a much smaller influence on the frequency and damping of Mode 2 than in the reverse case. Even when the modes are excited the same amount (i.e. with a 1:1 ratio), the frequency and damping are not predicted to change very much.

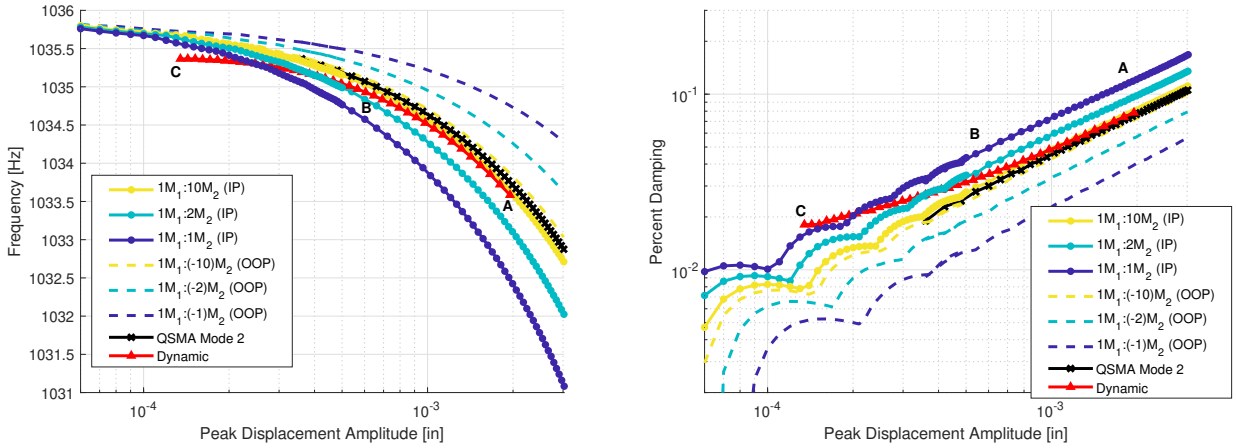

(a) **(b)**

Figure 8: (a) Frequency and (b) damping curves for Mode 2 QSMA, Mode 2 dominant MM-QSMA, and a fit of the dynamic response using [38]

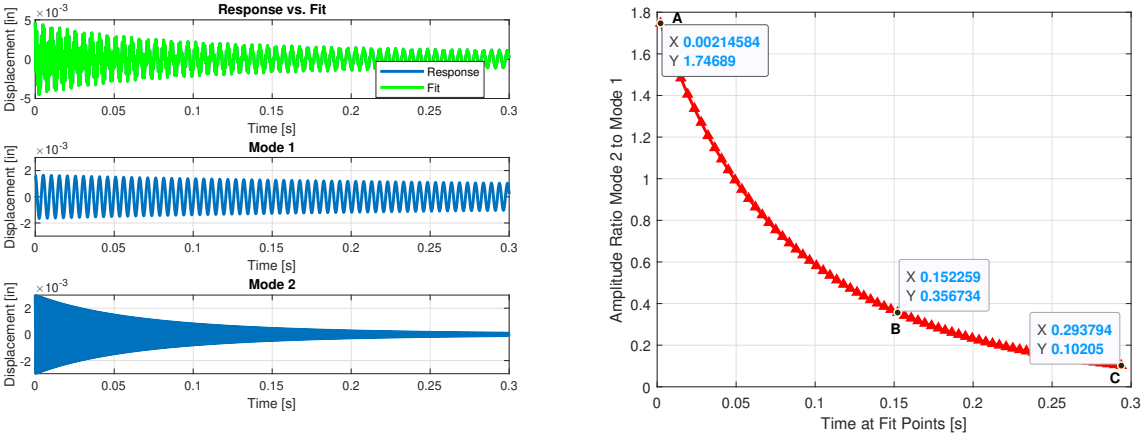

(a) **(b)**

Figure 9: (a) Fit of the multi-mode dynamic response using [38], (b) Amplitude ratio between Mode 2 and Mode 1 at fit points

Comparing the results with the dynamic response, an interesting phenomenon is observed. In this case the dynamic response was initiated with a 1 to 2 forcing for modes 2 and 1 respectively. Even though Mode 1 is twice as strong as Mode 2, the frequency and damping

in the dynamic response are only slightly perturbed from the values they would have when Mode 2 was excited in isolation; the MM-QSMA envelope for the 1:10 (Mode 1 to Mode 2) case nearly envelops this response even though the dynamic response amplitudes have a 1:2 ratio, five times lower. In this case the bound predicted by MM-QSMA is extremely over-conservative.

As the dynamic response evolves, Mode 1 becomes more and more dominant. Specifically, the ratios of the amplitudes of Mode 1 to Mode 2 early (A), mid (B), and late (C) in the time history are approximately 1:1.75, 2.80:1, and 9.80:1, respectively. At point B the dynamic response exceeds the bound predicted by MM-QSMA with a 1:10 ratio and is at about 25% of the bound predicted by MM-QSMA with a 1:1 ratio, which was the largest ratio that was used and is still 2.8 times smaller than the actual response ratio. Finally, at point C the frequency and damping exceed the bound from the 1:1 MM-QSMA prediction, but at this point the dynamic response of Mode 1 is 9.8 times greater than that of Mode 2. Hence, while MM-QSMA has proven qualitatively correct in that it predicted that Mode 1 would have a lesser effect on Mode 2 than vice versa, it is highly over-conservative in this second case. Even then, MM-QSMA may still prove advantageous if one considers that the MM-QSMA analysis can be done for this model in 3-5 minutes, whereas between 26-30 hours (1560 - 1800 minutes) were required to compute the one multi-mode dynamic response that was shown (on the same computer).

5 MULTI-MODE EXCITATION FOR A 3D BEAM MODEL

A second numerical study was performed on the unconstrained S4 Beam [4,33] to evaluate the efficacy of MM-QSMA on a more complicated 3D Model where. The S4 Beam features two C shaped beams that are connected on the ends with two steel bolts. A FE mesh of the beam is shown in Fig. 10. The model consists of 348,818 elements with a total of 14,794 elements at the interfaces [4]. The properties of the model are listed in Table 2. The

interfaces at the ends of the beam are nominally flat, although it has been shown that there is slight curvature at the interfaces [33]. For the purposes of this paper, only the model with the nominally flat interfaces is considered; work is ongoing to account for the curvature in the interfaces while still obtaining reasonable QSMA predictions [33]. While in this case it will not be possible to integrate the equation of motion to obtain the true modal coupling, this is more of a realistic case to demonstrate how one could use MM-QSMA on large FE models where time integration is extremely expensive if not infeasible.

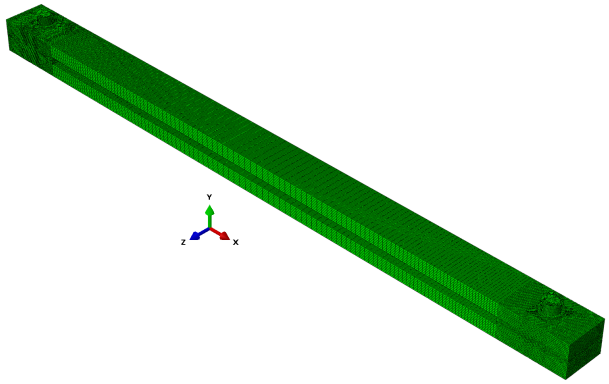

Figure 10: Finite element model of the S4 Beam built in Abaqus

Table 2: Material properties and dimensions for the 3D S4 Beam Model

Property	Value (SI)	Value (Imperial)
Length	50.80 cm	20.00 in
Width	3.18 cm	1.25 in
Density	8.01e-3 kg/cm^3	7.49e-4 $slinches/in^3$
Elastic Modulus	194 GPa	2.81e7 psi
Poisson Ratio	0.29	0.29
Static Friction Coefficient	0.60	0.60

A preload force of 21.2 kN (4766 lbf) is applied to both beams in Abaqus and an eigen-

analysis was performed to compute the linearized modes of the structure. For this study, Modes 2 and 8 are used which are the most analogous modes to the two in the 2D Beam case study, although there are many other pairs of modes that may also be of interest for the S4 Beam. The modes and their respective natural frequencies are shown in Figs. 11a and 11b. The figures show a contour of nodal displacement amplitudes for the two modes, both of which are in-phase, symmetric bending modes; this type of deformation induces shearing at the interfaces.

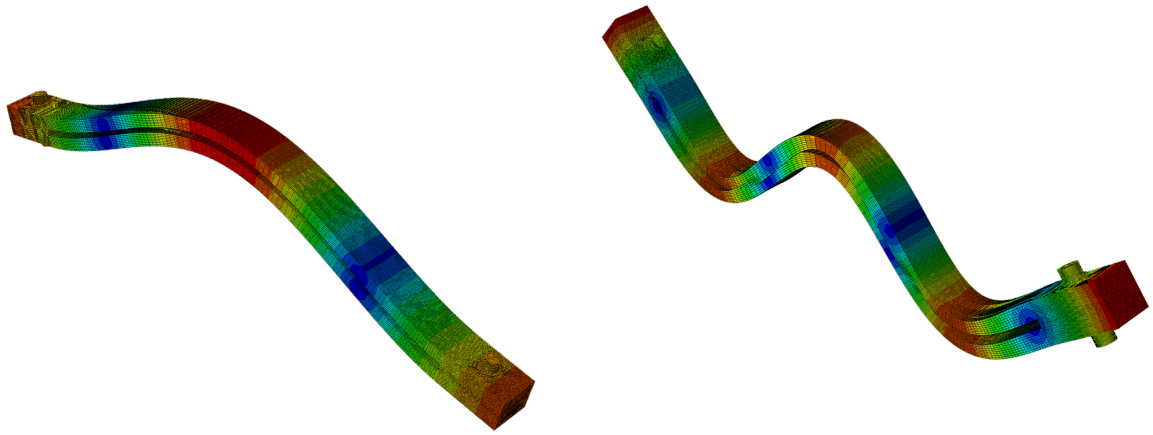

(a) **(b)**

Figure 11: (a) Mode 2 at 333 Hz , (b) Mode 8 at 1274 Hz

MM-QSMA was performed at modal amplitude ratios of ±1:1, ±2:1, and ±1:2 for Mode 2 and Mode 8, and contrasted against the single mode excitation backbone of each mode and the result is shown in Fig. 12. Figs. 12a and 12b show Mode 2 dominance for frequency and damping, and Figs. 12c and 12d show Mode 8 dominance for frequency and damping.

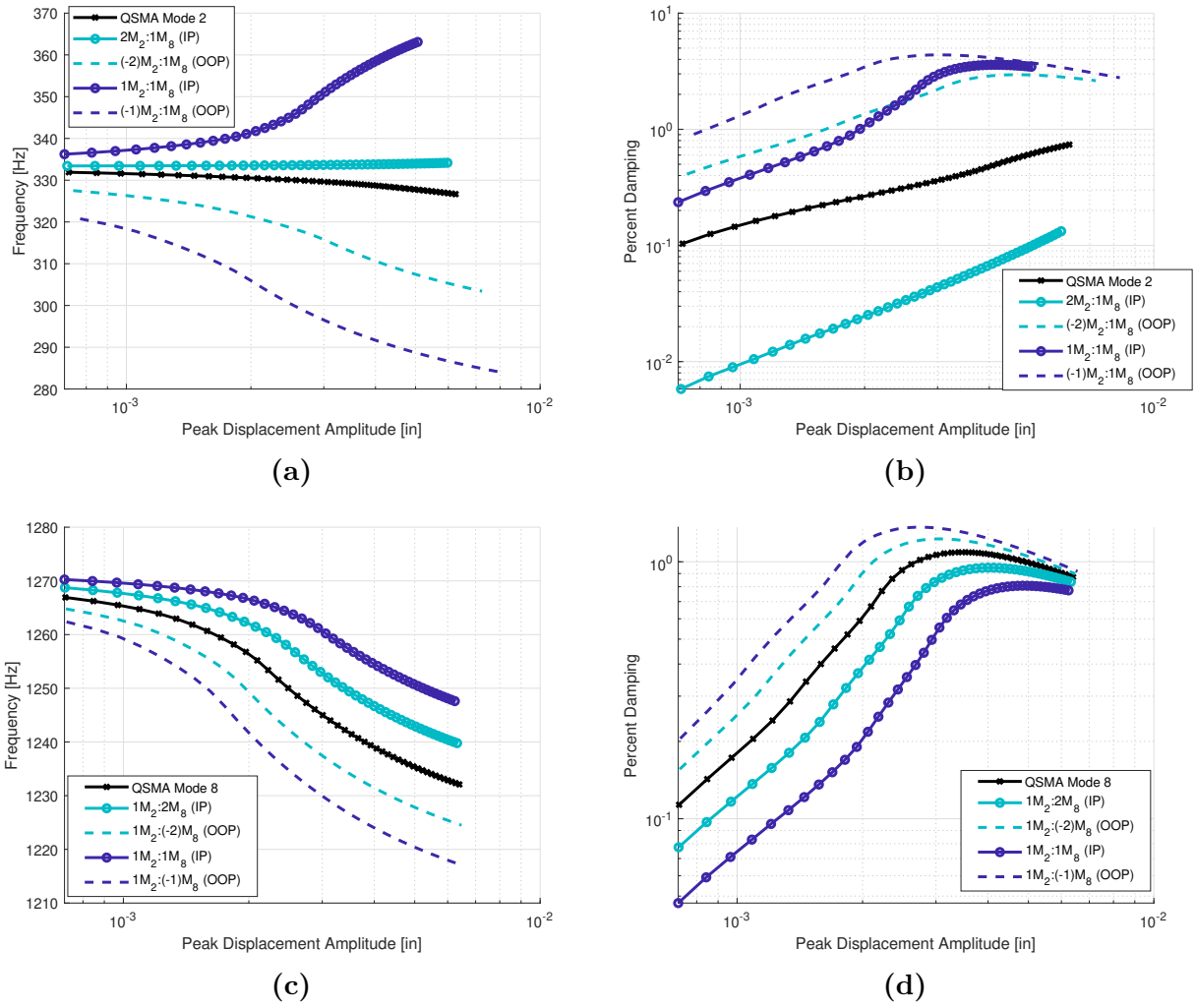

Figure 12: MM-QSMA frequency and damping curves of Mode 2 to Mode 8 for (a-b) Mode 2 dominance and (c-d) Mode 8 dominance

The IP and OOP MM-QSMA curves show similar behavior to those seen for the 2D beam, fully bounding both the frequency backbones for Modes 2 and 8. The damping curves also show the same trends, and once again the 1:1 case with Mode 2 dominant does not bound the damping backbone but instead shows an increase in damping. In this case the OOP curves are probably the relevant ones, as they show a decrease in stiffness and increase in damping when the modes are excited simultaneously; presumably this occurs because OOP motions of the global structure cause increased slip at the joints for this 3D model,

while for the 2D model and with the way the signs were set for the two modes, IP motions caused increased slip for that model.

The effect of the modes can be further understood by examining the contact status in the interfaces during quasi-static loading. Figure 13 shows the contact status of the left interface during loading where the rows correspond to loading for Mode 2 alone, Mode 8 alone, and Mode 2/Mode 8 1:1 in phase and -1:1 out-of-phase respectively. Each column represents the solution at load steps 6 (low), 18 (mid), 36 (mid), and 48 (high), where the force and the quasi-static with increasing load step. The contact status is contoured green for in-contact and stuck, yellow for in-contact but slipping, and blue for nodes that are not in contact. The slip evolves much more quickly for OOP MM-QSMA -1:1, revealing that this is the case which puts the greatest stress on the joint. Increased slip at the interfaces likely leads to increased energy dissipation, causing the damping to increase when both modes are excited out-of-phase. At the end of the quasi-static loading, all of the interfaces appear to be in a state of macroslip, and so these simulations likely span the range of meaningful loads.

As was observed in the 2D Beam, the Mode 8 MM-QSMA curves have a tighter bound on the backbone, indicating that Mode 8 is less affected by Mode 2 than vice versa. Furthermore, Mode 2 of the S4 Beam is affected quite significantly by Mode 8; at high amplitudes MM-QSMA predicts a frequency shift of greater than 10% for Mode 2 and an increase in damping of about an order of magnitude. The ratio of the linear natural frequencies of Modes 2 and 8 is once again not an integer (3.82), so the phase would again change continuously. Considering this and our experience with the 2D beam, we would expect these bands to be conservative, but in this case we do not have validation data to test this hypothesis. For the S4 Beam a quasi-static solution takes 6-8 hours, whereas a dynamic transient simulation would take more than a day for a single cycle, and likely weeks to months to obtain meaningful data.

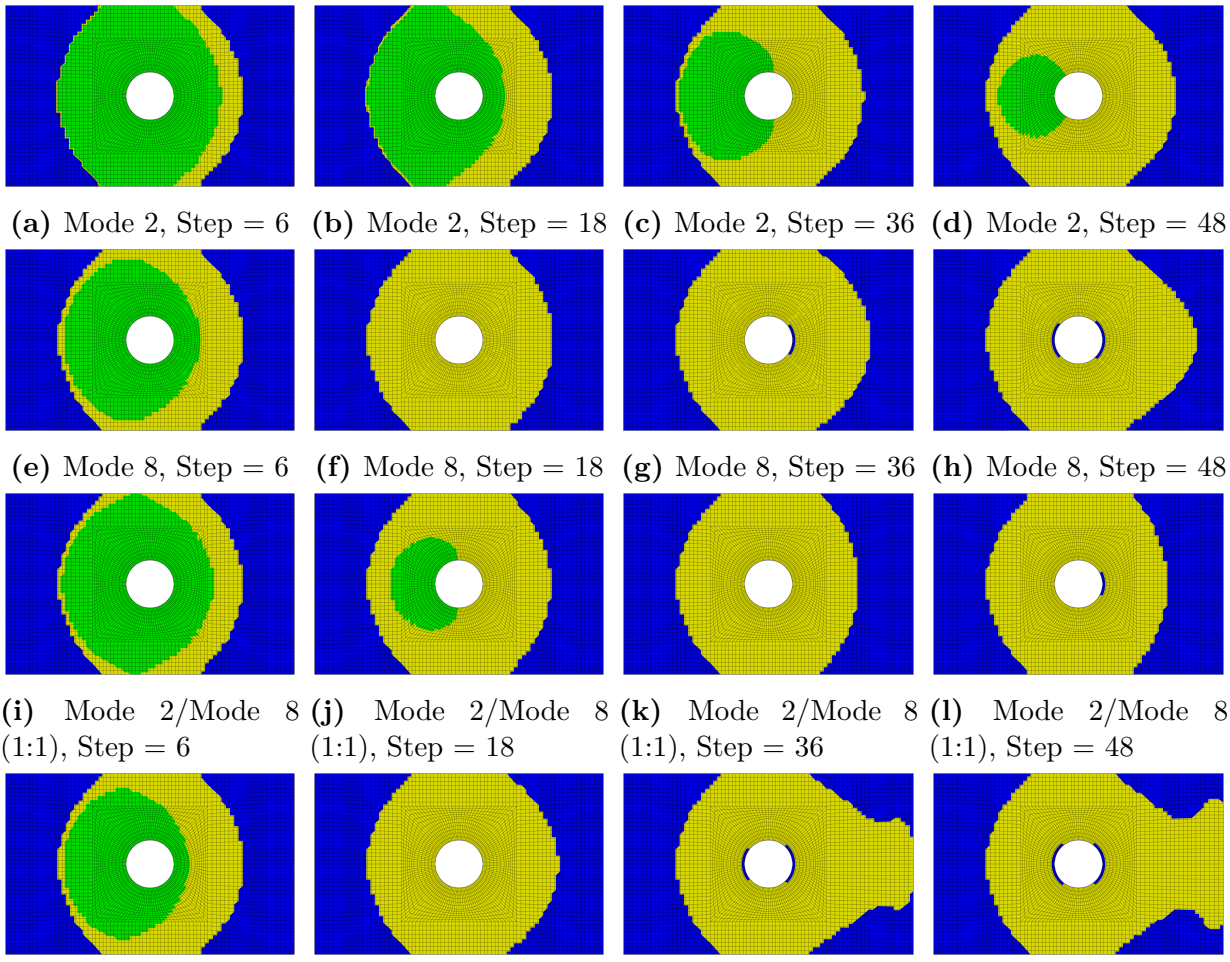

(a) Mode 2, Step = 6 **(b)** Mode 2, Step = 18 **(c)** Mode 2, Step = 36 **(d)** Mode 2, Step = 48

(e) Mode 8, Step = 6 **(f)** Mode 8, Step = 18 **(g)** Mode 8, Step = 36 **(h)** Mode 8, Step = 48

(i) Mode 2/Mode 8 (1:1), Step = 6 **(j)** Mode 2/Mode 8 (1:1), Step = 18 **(k)** Mode 2/Mode 8 (1:1), Step = 36 **(l)** Mode 2/Mode 8 (1:1), Step = 48

(m) Mode 2/Mode 8 (-1:1), Step = 6 **(n)** Mode 2/Mode 8 (-1:1), Step = 18 **(o)** Mode 2/Mode 8 (-1:1), Step = 36 **(p)** Mode 2/Mode 8 (-1:1), Step = 48

Figure 13: Quasi-static load steps for (a-d) QSMA Mode 2, (e-h) QSMA Mode 8, (i-l) IP MM-QSMA 1:1, (m-p) OOP MM-QSMA -1:1. There are at the left interface of the bottom beam. i.e the S4 Beam is right of this interface.

6 CONCLUSION

This paper explored a new method for evaluating the effect of mode coupling on the natural frequency and damping that is observed in each mode in a structure with nonlinearities due to a bolted joint. In contrast to prior works, in this paper the structure was excited quasi-statically in the shape of two modes simultaneously. The viability of this approach was first studied on a 2D beam structure, quantifying the static coupling between the modes

and comparing it to the coupling observed in a few dynamic responses. Then this approach was examined on a 3D structure to statically quantify modal coupling where a dynamic response was impractical. The slip induced at the interfaces was examined in both cases to understand the effect that simultaneously exciting two modes has on the interface.

For the 2D cantilever beam model, the two modes in question were forced with positive and negative phase, and the results were found to form conservative (sometimes highly conservative) bounds on the damping and effective natural frequency that were observed in the dynamic response. In a dynamic response, the phase of the modes would change continuously with time unless their natural frequencies were integer multiples. In this work the ratio of the mode frequencies was 5.23, so the relative phase changes quickly in a dynamic response, perhaps explaining why the dynamic response was so different from the IP and OOP static responses. Nevertheless, considering the huge difference in the cost of MM-QSMA versus the dynamic response, the bounding boxes are still highly useful even if they are sometimes overly conservative.

In the case study of the 3D model of the S4 Beam, both modes of interest displayed effects of coupling when the sub-dominant mode was introduced into the static response. Not only did the response change, the contact interface changed with coupling to the extent where there was a significant increase of slip for all solutions. The modes investigated were similar to those studied for the 2D Beam, and the frequency and damping responses depicted similar trends. Another interesting feature observed in both structures is that the modal coupling was not symmetric i.e., the effect of one mode on the other was clearly not the same in reverse. Recent experiments on the S4Beam [33] showed a similar phenomenon where the out-of-phase Mode 1 was completely unaffected by vibration of the in-phase Mode 2, and yet Mode 2 was strongly affected by Mode 1. Unfortunately, to date no model exists that can capture those experiments, and so we cannot yet validate MM-QSMA against that experimental data, yet we believe that the MM-QSMA method might still be a uesful

tool when seeking to evaluate modal coupling. Due to the complexity of modal coupling, additional work is needed to understand the relation between various sets of modes and develop models that can capture it.

In future works this method will be applied to more complicated structures with more joints and modes that load the joints in multiple directions. For example, the method is being applied to various reduced order models to seek to understand the extent to which they capture mode coupling. Furthermore, this framework will be repeated on future versions of the S4Beam model that will be better tuned (i.e. including the surface topology) to hopefully reproduce the experimental data more accurately. This should allow prediction of modal coupling in the simulation model and this could be compared to the experimental measurements of mode coupling that were presented in [33]. Additionally, it may be necessary to study coupling between more than two modes at once, so the phasing between all of the modes will need to be considered. The hope is that this method can be used to identify cases when modal coupling is likely to be important and to provide a conservative estimate of the effect that it will have on a structure's dynamic response, in a small fraction of the time required to integrate the dynamic equations. Designers could then use these bounds to speed up design and to screen models. Perhaps with time and experience they can learn when these bounds are overly conservative and to adjust expectations accordingly.

ACKNOWLEDGEMENTS

The views expressed in the article do not necessarily represent the views of the U.S. Department of Energy or the United States Government. Sandia National Laboratories is a multi-mission laboratory managed and operated by National Technology & Engineering Solutions of Sandia, LLC, a wholly owned subsidiary of Honeywell International Inc., for the U.S. Department of Energy's National Nuclear Security Administration under contract DE-NA0003525.

REFERENCES

[1] A. A. Ferri. Friction damping and isolation systems. *Journal of Mechanical Design, Transactions of the ASME*, 117 B:196–206, 1995.

[2] Matthew R. W. Brake, editor. *The Mechanics of Jointed Structures: Recent Research and Open Challenges for Developing Predictive Models for Structural Dynamics*. Springer International Publishing, 2018.

[3] Aabhas Singh, Matteo Scapolan, Yuta Saito, Matthew S. Allen, Daniel Roettgen, Ben Pacini, and Robert J. Kuether. Experimental Characterization of a New Benchmark Structure for Prediction of Damping Nonlinearity. In Gaetan Kerschen, editor, *Nonlinear Dynamics, Volume 1*, Conference Proceedings of the Society for Experimental Mechanics Series, pages 57–78, Cham, 2019. Springer International Publishing.

[4] Emily Jewell, Matthew S. Allen, Iman Zare, and Mitchell Wall. Application of Quasi-Static Modal Analysis to a Finite Element Model and Experimental Correlation. *Journal of Sound and Vibration*, 479(4 August):115376, 2020. Number: 4 August.

[5] R. A. Ibrahim and C. L. Pettit. Uncertainties and dynamic problems of bolted joints and other fasteners. *Journal of Sound and Vibration*, 279(3-5):857–936, 2005. Number: 3-5.

[6] Brandon Deaner, Matthew S. Allen, Michael J. Starr, D. J. Segalman, and Hartono Sumali. Application of Viscous and Iwan Modal Damping Models to Experimental Measurements From Bolted Structures. *ASME Journal of Vibrations and Acoustics*, 137:12, 2015.

[7] Daniel R. Roettgen and Matthew S. Allen. Experimental Dynamic Substructuring of a Catalytic Converter System using the Transmission Simulator Method. 2015.

[8] D. J. Segalman, D. L. Gregory, Michael J. Starr, Brian R. Resor, Micheal D. Jew, James P. Lauffer, and Nicoli M. Ames. Handbook on Dynamics of Jointed Structures. Technical report, Sandia National Laboratories, Albuquerque, NM 87185, 2009.

[9] E. P. Petrov and D. J. Ewins. Analytical Formulation of Friction Interface Elements for Analysis of Nonlinear Multi-Harmonic Vibrations of Bladed Disks. *Journal of Turbomachinery*, 125(2):364–371, 2003. Number: 2.

[10] R. M. Rosenberg. Normal modes of nonlinear dual-mode systems. *Journal of Applied Mechanics*, 27:263–268, 1960.

[11] G. Kerschen, M. Peeters, J. C. Golinval, and A. F. Vakakis. Nonlinear normal modes. Part I. A useful framework for the structural dynamicist. *Mechanical Systems and Signal Processing*, 23(1):170–94, 2009. Number: 1.

[12] M. Peeters, R. Viguié, G. Sérandour, G. Kerschen, and J. C. Golinval. Nonlinear normal modes, Part II: Toward a practical computation using numerical continuation techniques. *Mechanical Systems and Signal Processing*, 23(1):195–216, 2009. Number: 1.

[13] Robert J. Kuether, M. R. Brake, and Matthew S. Allen. Evaluating Convergence of Reduced Order Models Using Nonlinear Normal Modes. February 2014.

[14] Malte Krack. Nonlinear modal analysis of nonconservative systems: Extension of the periodic motion concept. *Computers & Structures*, 154:59–71, July 2015.

[15] L. Renson, G. Kerschen, and B. Cochelin. Numerical computation of nonlinear normal modes in mechanical engineering. *Journal of Sound and Vibration*, 364:177–206, March 2016.

[16] Gaetan Kerschen. Computation of Nonlinear Normal Modes through Shooting and Pseudo-Arclength Computation. In Gaetan Kerschen, editor, *Modal Analysis of Nonlinear Mechanical Systems*, CISM International Centre for Mechanical Sciences, pages 215–250. Springer, Vienna, 2014.

[17] Remi Arquier, Sergio Bellizzi, Robert Bouc, and Bruno Cochelin. Two methods for the computation of nonlinear modes of vibrating systems at large amplitudes. *Computers and Structures*, 84(24-25):1565–1576, 2006. Number: 24-25.

[18] George Haller and Sten Ponsioen. Nonlinear normal modes and spectral submanifolds:

existence, uniqueness and use in model reduction. *Nonlinear Dynamics*, 86(3):1493–1534, November 2016.

[19] Malte Krack and Johann Groß. *Harmonic Balance for Nonlinear Vibration Problems*. Mathematical Engineering. Springer International Publishing, 2019.

[20] C. W. Schwingshackl, D. Di Maio, I. Sever, and J. S. Green. Modeling and validation of the nonlinear dynamic behavior of bolted flange joints. *Journal of Engineering for Gas Turbines and Power*, 135(12), 2013. Number: 12.

[21] Ali Hasan Nayfeh. *Introduction to perturbation techniques*. Wiley, New York, 1981.

[22] Melih Eriten, Mehmet Kurt, Guanyang Luo, D. Michael McFarland, Lawrence A. Bergman, and Alexander F. Vakakis. Nonlinear system identification of frictional effects in a beam with a bolted joint connection. *Mechanical Systems and Signal Processing*, 39(1-2):245–264, 2013. Number: 1-2.

[23] Hugo Festjens, Gael Chevallier, and Jean-Luc Dion. A numerical tool for the design of assembled structures under dynamic loads. *International Journal of Mechanical Sciences*, 75:170–177, 2013.

[24] Robert M. Lacayo and Matthew S. Allen. Updating Structural Models Containing Nonlinear Iwan Joints Using Quasi-Static Modal Analysis. *Mechanical Systems and Signal Processing*, 118(1 March 2019):133–157, 2019. Number: 1 March 2019.

[25] Nidish Narayanaa Balaji and Matthew R. W. Brake. A quasi-static non-linear modal analysis procedure extending Rayleigh quotient stationarity for non-conservative dynamical systems. *Computers & Structures*, 230:106184, April 2020.

[26] Aabhas Singh, Mitchell Wall, Matthew S. Allen, and Robert J. Kuether. Spider Configurations for Models with Discrete Iwan Elements. In *Nonlinear Structures and Systems, Volume 1*, Conference Proceedings of the Society for Experimental Mechanics Series, pages 25–38, Orlando, FL, January 2019. Springer International Publishing.

[27] Iman Zare and Matthew S. Allen. Adapting a contact-mechanics algorithm to predict

damping in bolted joints using quasi-static modal analysis. *International Journal of Mechanical Sciences*, 189, January 2021.

[28] David A. Najera-Flores and Robert J. Kuether. A Study of Whole Joint Model Calibration Using Quasi-Static Modal Analysis. *Journal of Vibration and Acoustics*, 142(051109), June 2020.

[29] Q. Zhang, Randall J. Allemang, and D. L. Brown. Modal Filter: Concept and Applications. pages 487–496, 1990.

[30] Allen Mathis and D. Quinn. Analysis of Systems with Generalized Light Damping with Emphasis on Mode Coupling. In *Proceedings of the ASME 2017 International Design Engineering Technical Conferences & Computers and Information in Engineering Conference IDETC/CIE 2017*, Cleveland, Ohio, August 2017.

[31] Robert Lacayo, Brandon Deaner, and Matthew S. Allen. A Numerical Study on the Limitations of Modal Iwan Models for Impulsive Excitations. *Journal of Sound and Vibration*, 390:118–140, 2017.

[32] Benjamin J. Moldenhauer, Aabhas Singh, Phil Thoenen, Daniel R. Roettgen, Benjamin R. Pacini, Robert J. Kuether, and Matthew S. Allen. Influences of Modal Coupling on Experimentally Extracted Nonlinear Modal Models. In Gaetan Kerschen, M. R. W. Brake, and Ludovic Renson, editors, *Nonlinear Structures and Systems, Volume 1*, Conference Proceedings of the Society for Experimental Mechanics Series, pages 189–204, Orlando, FL, January 2019. Springer International Publishing.

[33] Mitchell P. Wall, Matthew S. Allen, and Robert J. Kuether. Observations of Modal Coupling due to Bolted Joints in an Experimental Benchmark Structure. *Mechanical Systems and Signal Processing*, 2020.

[34] Robert J. Kuether, Ludovic Renson, Thibaut Detroux, Chiara Grappasonni, Gaetan Kerschen, and Matthew S. Allen. Nonlinear Normal Modes, Modal Interactions and Isolated Resonance Curves. *Journal of Sound and Vibration*, 351(299-310), 2015. Num-

ber: 299-310.

[35] Alexander F. Vakakis, D. Michael McFarland, Lawrence Bergman, Leonid I. Manevitch, and Oleg Gendelman. Isolated Resonance Captures and Resonance Capture Cascades Leading to Single- or Multi-Mode Passive Energy Pumping in Damped Coupled Oscillators. *Journal of Vibration and Acoustics*, 126(2):235–244, 2004. Number: 2.

[36] Matthew S. Allen, Robert Lacayo, and Matthew R.W. Brake. Quasi-static Modal Analysis based on Implicit Condensation for Structures with Nonlinear Joints. In *International Seminar on Modal Analysis (ISMA)*, Leuven, Belgium, September 2016.

[37] M. Feldman. Hilbert transform in vibration analysis. *Mechanical Systems and Signal Processing*, 25(3):735–802, 2011. Number: 3.

[38] Benjamin Moldenhauer, Aabhas Singh, Matthew S. Allen, and Daniel Roettgen. Extensions to a method for characterizing instantaneous frequency and damping of nonlinear systems. In *Proceedings of 39th International Modal Analysis Conference (XXXIX)*, Orlando, FL, February 2021.

[39] Hugh G. D. Goyder and Damien P. T. Lancereau. Methods for the Measurement of Non-Linear Damping and Frequency in Built-Up Structures. American Society of Mechanical Engineers Digital Collection, November 2017.

[40] Dassault Systèmes. Abaqus Analysis User's Manual Version 6.14, 2014.